IMPERIAL COLLEGE OF SCIENCE
TECHNOLOGY AND MEDICINE

DEPARTMENT OF BIOENGINEERING

P H D T H E S I S

submitted for the

**Degree of Doctor of Philosophy
of Imperial College London**

Defended by

Alice Boo

MEng, Imperial College London (2017)

Towards Engineering Microbial Consortia Using RNA-Based Genetic Controllers

prepared at Imperial College London, Centre for Synthetic Biology

submitted on January 13, 2022

Supervisors :	Guy-Bart Stan	-	Imperial College London
	Rodrigo Ledesma-Amaro	-	Imperial College London
Examiners :	Karen Polizzi	-	Imperial College London
	Chris Barnes	-	University College London

Towards Engineering Microbial Consortia Using RNA-Based Genetic Controllers

Abstract:

In nature, quorum sensing is a mechanism used by microbes to communicate and coordinate behaviours at the population level. Over the last two decades, synthetic biologists have used the unique property of quorum sensing to sense population density for coordinating cellular behaviours of single and mixed cultures. This gave rise to the development of multicellular biosynthesis systems for metabolic engineering and of spatially distributed systems for synthetic biology. However, robustly controlling the composition of multicellular systems remains a challenge and limits its wide adoption by the metabolic engineering community. Current strategies for controlling synthetic microbial communities vastly rely on engineering metabolic dependencies between microbial species in a process called syntrophy. While syntrophy guarantees the survival of all strains in the coculture, it does not provide a way to control community composition. Existing genetic circuits that can dynamically control community composition often impose too much burden on their hosts for division of labour to be a viable solution to improve yields and titers of valuable metabolic products. Here we investigate the potential of using RNA-based gene circuits to reduce the cost of expressing heterologous genes for the control of community composition in a two-member *E. coli* coculture. In this work, we present the development of three genetic modules that rely on RNA species to detect changes in population density and to regulate growth rate when community composition becomes unstable. Together, the modules work in concert to stabilise community composition around a ratio set by the intrinsic properties of the circuit's genetic components. We identify the key parameters of the circuits that enable tuning of the composition ratio. We characterise the cost of expressing each module of the genetic controller by measuring its impact on the host growth rate and on consumption of free cellular resources. Together these findings highlight the importance of developing host-aware circuits to control community composition so as to enable their wide adoption by metabolic engineers.

Keywords: Synthetic biology, microbial consortia, regulatory RNAs, quorum sensing, genetic circuits.

Declaration

I hereby certify that everything included in this thesis is my own work, and in the instances where work has been used from other sources, it is acknowledged appropriately.

The copyright of this thesis rests with the author. Unless otherwise indicated, its contents are licensed under a Creative Commons Attribution-Non Commercial 4.0 International Licence (CC BY-NC). Under this licence, you may copy and redistribute the material in any medium or format. You may also create and distribute modified versions of the work. This is on the condition that: you credit the author and do not use it, or any derivative works, for a commercial purpose. When reusing or sharing this work, ensure you make the licence terms clear to others by naming the licence and linking to the licence text. Where a work has been adapted, you should indicate that the work has been changed and describe those changes. Please seek permission from the copyright holder for uses of this work that are not included in this licence or permitted under UK Copyright Law.

Acknowledgments

First, I am very grateful to my supervisors Guy-Bart Stan and Rodrigo Ledesma Amaro for all the support and encouragement they have given me throughout my PhD project, and especially for keeping me on track whenever I lost sight of the bigger picture. I will always admire Guy's readiness to help even when it comes to soldering broken turbidostat. I would also like to thank all the PIs of the Synthetic Biology Centre for providing a unique environment that fosters friendships and mutual assistance.

I would like to thank to all the members of the Centre for Synthetic Biology that make this place special and have supported me throughout my time in the lab: Jane, Anastasiya, Wei, Huadong, Alicia G., Amrit, Linda, Lara, Rochelle, Kealan and so many others. A special thanks to Edina, Song and Nana, who have always worked to make everything in the Centre runs as smoothly as possible.

I huge thank you to all the wonderful members of the Stan lab and the RLA lab, both past and present, who have made this journey such an enriching experience. Thank you to all the Potatoes of the B603 lab, Alicia a.k.a. Electropotato, Andreas a.k.a. Optopotato, Albert a.k.a. Nitropotato, Gediz a.k.a. Protopotato (whenever she uses the ice machine), Javier and Ismael for all your support throughout all my ups and lows and for always filling the lab with happy tunes. Thank you to Olivier Borkowski for being a great mentor when I first started in the lab and always taking the time to look for the answers to all my questions. Thank you Francesca Ceroni for all your great discussions about burden and giving me such great advice for preparing presentations. Thank you to Harrison Steel for his continuous support and input on getting the Chi.bios running. Thank you Wooli Bae for introducing me to the NUPACK world and your support for designing RNAs. Thank you Tigran for your continuous scientific support and for getting me to start engineering genomes with the λ-red system. Thank you Nicolas for your stimulating scientific debates. Thank you Ari and Ciáran for your helpful discussions about sRNAs. Thank you Marios and Zoltan for going through all the stages of setting up the turbidostats in the lab, through floods and all. Thank you Eszter for our conversations about the latest synbio papers, I will be missing them a lot. Thank you Duncan for your continuous support and friendship on our 4-year PhD journey in the GBS lab. Thank you Alicia C. for always helping me gain perspective on things and for keeping me going at my lowest point. Thank you Davina for all your help with the flow cytometer and for always making people smile, everyday. Thank you to the Local Aptamer for supporting me through this journey and for always taking the time to listen. Thank you to the old Ellis gang - Charlie, Will, Glen and Marcus for welcoming me to the Centre at the beginning of my project.

Thank you to all my amazing friends and housemates, and especially Smitha, Alice, Liam, Gilda, Abhinav and Cecilia who have been so supportive throughout this journey and have suffered through listening me talk about my bacteria one too many times.

Last but not least, I would like to thank my parents and my brother who have supported me through these four years. I could not have made it through without you.

Contents

List of Acronyms **xiii**

1 Introduction **1**

1.1 Summary . . . 2

1.2 Limitations of monocultures . . . 3

1.2.1 Monoculture limitations for synthetic biology . . . 3

1.2.2 Monoculture limitations for metabolic engineering . . . 6

1.2.3 Challenges of engineering cocultures . . . 10

1.3 Engineering bottom-up cocultures for composition control . . . 11

1.3.1 Design and simulation of microbial cocultures . . . 12

1.3.2 Communication tools for the design of microbial consortia . . . 13

1.3.3 Examples of coculture composition control mechanisms based on quorum sensing . . . 16

1.4 Designing a host-aware coculture composition controller . . . 22

1.4.1 Using RNA-based repressors to control coculture composition . . . 22

1.4.2 Using an RNA-based activator to control coculture composition . . . 25

1.4.3 Summary of host-aware strategies to control coculture composition . . . 27

1.5 Aims and objectives . . . 28

1.6 Publications resulting from this work . . . 30

2 Engineering a RNA-based Comparator **31**

2.1 Introduction . . . 31

2.2 Results and discussion . . . 32

2.2.1 Choosing the Optimal STAR sequence . . . 32

2.2.2 Building the first STAR-based comparator . . . 35

2.2.3 Optimising the fold repression of the STAR-based comparator . . . 40

2.2.4 Characterisation the final STAR-based comparator design . . . 50

2.3 Conclusions . . . 57

3 Engineering Cell-Cell Communication 59

3.1 Introduction . . . 59

3.2 Results and Discusssion . . . 60

3.2.1 Selection of the lux and rpa systems . . . 60

3.2.2 Characterisation of the transcriptional input-output response of the lux promoter . . . 66

3.2.3 Building the lux and rpa comparators . . . 72

3.2.4 Engineering strains to produce C6-HSL and pC-HSL . . . 76

3.2.5 Linking the comparator and the communication modules . . . 82

3.3 Conclusions . . . 85

4 Controlling Growth Rate Using RNA-based Regulators 87

4.1 Introduction . . . 87

4.2 Results and discussion . . . 88

4.2.1 Implementing reversible auxotrophy using CRISPRi . . . 88

4.2.2 Regulating growth rate using sRNA . . . 101

4.2.3 Regulating growth rate through expression burden and STAR . . . 107

4.3 Conclusions . . . 114

5 Bottom-Up Engineering of an *E.coli*-*E.coli* Coculture 117

5.1 Introduction . . . 117

5.2 Results and discussion . . . 119

5.2.1 Building the open-loop co-culture . . . 119

5.2.2 Validation of the pC-HSL communication channel for coculture regulation 122

5.2.3 Validation of the C6-HSL communication channel for coculture regulation 126

5.2.4 Ratio stabilisation in a 2-way-communicating co-culture . . . 130

5.2.5 The co-culture under turbidostat conditions . . . 139

5.3 Conclusions . . . 143

6 Discussion 145

6.1 Summary . . . 145

6.2 A tool-set for building burden-driven cocultures . . . 146

6.2.1 A new platform to study the benefit of division of labor 146
6.2.2 Optimisation of the coculture platform 148
6.2.3 Further applications of the coculture platform 155
6.3 Conclusions 161

7 Materials and Methods 163
7.1 Materials 164
7.1.1 *E. coli* strains 164
7.1.2 Antibiotics 166
7.1.3 Inducers and dyes 166
7.1.4 Media and Buffers 167
7.1.5 Amino Acids 168
7.2 Molecular Biology Methods 169
7.2.1 Culturing 169
7.2.2 Competent cells preparation and transformation 169
7.3 General DNA Manipulation 172
7.3.1 Around-the-world PCR 172
7.3.2 START/STOP Assembly 173
7.3.3 Gibson Assembly 173
7.4 Genomic integration 173
7.4.1 CRIM integration 173
7.4.2 λ-Red integration 176
7.5 Data collection and analysis 178
7.5.1 Plate-reader timecourse assays 178
7.5.2 Flow cytometry measurements 181
7.5.3 Quorum sensing sender-receiver assay 182
7.5.4 Coculture assay 183
7.5.5 β-Carotene assay 183
7.5.6 Chi.bio turbidostat assay 184
7.6 DNA parts and Plasmids 186
7.6.1 DNA Parts 186

7.6.2 Plasmids 200

8 Appendix **219**

8.1 STAR sequences 219

8.2 STAR Target sequences 220

8.3 Anti-STAR sequences 220

8.4 STAR and anti-STAR RNA structures 221

8.5 Comparator buffer sequences 223

8.6 Deactivation of the LLL and LRR STAR-based comparators 224

8.7 AHL-producing strains 225

8.8 Growth of quorum sender strains 226

8.9 GFP expression of inducible systems 227

8.9.1 Comparison of the LLL quorum sensing, araBAD and rhaBAD inducible systems 227

8.9.2 rhaBAD and araBAD promoter characterisation 227

8.10 Mutations in gRNA targeting the native LeuLp promoter 228

8.11 Targeting the LeuLp and HisLp promoters with CRISPRi 229

8.12 Continuous coculture 230

8.13 Muconic acid production modules 230

Bibliography **231**

List of Figures

1 Current challenges leading to the development of host-aware constructs in synthetic biology . . . 3
2 Division of labour to reduce burden and stress . . . 7
3 Coculture prevents crosstalks through compartmentalisation . . . 8
4 Coculture outcompetition by the fastest growing strain . . . 10
5 Bottom-up engineering of microbial consortia for composition control . . . 12
6 Quorum sensing for the coordination of microbial behaviour . . . 14
7 Circuits that use one-way quorum sensing to control population composition in bacterial cocultures . . . 17
8 Circuits that use two-way quorum sensing to control population composition in bacterial cocultures . . . 19
9 CRISPRi and sRNA repression mechanisms . . . 23
10 STAR Mechanism . . . 26
11 Strategies for building a host-aware coculture composition controller . . . 27
12 Proposed two-member coculture architecture for controlling community composition . . . 29

13 Testing the different STAR sequences from the Lucks Lab in DH10B-GFP . . . 33
14 Total mRFP yield obtained when using the STAR 5 and STAR 6 . . . 35
15 Characterisation of the first comparator design . . . 37
16 Characterisation of the first J23100 comparator design in DH10B and BW25113 39
17 Designing deoptimised STAR targets . . . 41
18 Effect of the deoptimised STAR targets on the comparator OFF state . . . 42
19 Effect of STAR-double-target . . . 44
20 STAR-based comparator toehold library . . . 46
21 Characterisation of the pBAD and pLux inducible promoters . . . 47
22 Inducible expression of STAR in the STAR-based comparator reveals a leakage of anti-STAR production . . . 49

23 Buffer Library to reduce RNAP read-through from the STAR transcriptional cassette to the anti-STAR transcriptional cassette . . . 51
24 Characterisation of the final inducible STAR-based comparator . . . 52
25 Characterisation of the STAR-based comparator with and without toehold . . 53
26 Burden characterisation of the STAR-based comparator with and without toehold . . . 54
27 Behaviour of the STAR-based comparator in a chemostat-type environment . 56

28 Homoserine lactones orthogonality . . . 62
29 Differences of promoter strength of the tra, rpa and lux systems . . . 63
30 Orthogonality of the lux and rpa systems . . . 64
31 Changing the regulator protein copy number to tune lux promoter properties 65
32 Structure of F30-2x-dBroccoli . . . 67
33 Effect of DFHBI-1T dye concentration on dBroccoli signal strength . . . 69
34 Plasmid- and genome-based production of HSL regulator protein . . . 70
35 Response of the lux and rpa systems to HSL gradients . . . 71
36 STAR-based comparator sensing C6-HSL and pC-HSL . . . 73
37 Modulation of the LuxR-Comparator behaviour . . . 75
38 Biosynthesis pathway of C6-HSL . . . 76
39 Biosynthesis pathway of pC-HSL . . . 77
40 Engineering C6-HSL and pC-HSL producing strains . . . 78
41 HSL-producing strains quantification workflow . . . 78
42 Characterising C6-HSL and pC-HSL producing strains . . . 79
43 dBroccoli expression increases with sender strain growth . . . 81
44 Response of the LuxR-Comparators to C6-HSL produced by the sender strains 83
45 Response of the RpaR-Comparators to pC-HSL produced by the sender strains 84

46 Growth rate modulation via reversible auxotrophy . . . 89
47 Growth rate modulation via external chemical control . . . 90
48 Designing a gRNA to target the LeuLp promoter . . . 91
49 Using CRISPRi to knockdown the LeuLp promoter . . . 92
50 Building gene knockdowns with CRISPRi . . . 94

51 CRISPRi knockdown creates population heterogeneity 96
52 Using CRISPRi to knockdown the leucine operon 98
53 Connecting the comparator to the CRISPRi module 100
54 Concept of a sRNA-based essential gene knockdown 102
55 Using sRNA to reduce maximum carrying capacity 103
56 Using interfering sRNA to down-regulate and rescue growth 106
57 Growth regulation module using expression burden 108
58 Controlling growth rate using VioB-mCherry expression 109
59 A burden approach to the STAR-based comparator controlling growth rate through VioB-mCherry expression 110
60 Controlling VioB-mCherry expressing with a comparator with or without toehold 111
61 A burden approach to the STAR-based comparator controlling growth rate through β-carotene production 113

62 A burden-based circuit for coculture composition regulation 118
63 Building coculture strains with different burden 120
64 Open-loop coculture expressing VioB-YFP and VioB-CFP 122
65 Detection of pC-HSL by the VioB-CFP producing strain 123
66 Effect of pC-HSL production on coculture composition. 125
67 Detection of C6-HSL by the VioB-YFP producing strain 127
68 Effect of C6-HSL production of coculture composition. 129
69 Two-way communication coculture stabilises coculture composition 132
70 C6-HSL and STAR expression tunes coculture composition 134
71 pC-HSL and STAR expression tunes coculture composition 136
72 Stabilisation of coculture composition for 2:3 inoculation ratio 138
73 Chi.bio turbidostat setup 140
74 Coculture behaviour in continuous culture 142

75 *In vitro* evolution of RNA for *in vivo* regulation and selection 149
76 A minimal circuit for stabilising coculture composition 152
77 *In vitro* evolution of N1 sRNA for growth regulation 153
78 Coculture for the production of muconic acid 156

79 Design of an *in vivo* burden and STAR AND gate 159

80 CRIM integration 174
81 λ-Red integration strategy for building C6-HSL producing BW25113 177

82 Secondary RNA structure of STAR and anti-STAR without toehold 221
83 Secondary RNA structure of STAR and anti-STAR with Toehold 0 221
84 Secondary RNA structure of STAR and anti-STAR with Toehold 1 222
85 Secondary RNA structure of STAR and anti-STAR with Toehold 2 222
86 Secondary RNA structure of STAR and anti-STAR with Toehold 3 222
87 Secondary RNA structure of STAR and anti-STAR with Toehold 4 223
88 Secondary RNA structure of STAR and anti-STAR with Toehold 5 223
89 Deactivation of the LLL and LRR STAR-based comparator 224
90 Growth of quorum-sensing-producer strains 226
91 Comparison of the LLL, araBAD and rhaBAD inducible systems 227
92 Characterisation of the araBAD and rhaBAD inducible promoters 228
93 Mutations in gRNA targeting LeuLp promoter 228
94 Targeting the LeuLp and HisLp promoters with CRISPRi 229
95 Coculture behaviour in continuous culture 230
96 Expression of the muconic acid production modules 230

List of Acronyms

ABS	Absorbance
AHL	N-Acyl homoserine lactones
Ara	L-arabinose
AU	Arbitrary units
bp	Base pair
CDS	Coding sequence
CRIM	Conditional-replication, integration, and modular plasmid
CRISPR	Clustered regularly interspaced short palindromic repeats
CRISPRi	CRISPR interference
DAPG	2,4-diacetylphophloroglucinol
DBTL	Design-Build-Test-Learn cycle
DNA	Deoxyribonucleic acid
EtOH	Ethanol
FU	Fluorescence units
GOI	Gene of interest
gRNA	Guide RNA
HDV	Hepatitis delta virus ribozyme
Hfq	Host factor-1
HH	Hammerhead ribozyme
HSL	Homoserine lactones
I/O	Input-Output
IPTG	isopropyl β-d-1-thiogalactopyranoside
kb	Kilo base pair
LB	Luria-Bertani
mCherry	Monomeric cherry fluorescent protein
mRNA	Messenger RNA
mScarlet-I	Monomeric scarlet fluorescent protein
OD	Optical Density
ORF	Open reading frame
Ori	Origin of replication
pC-HSL	P-Coumaroyl-homoserine lactone
PCR	Polymerase Chain Reaction
PBS	Phosphate Buffer Saline
Pir	Replication initiation protein
Rha	L-rhamnose
RBS	Ribosome Binding Site
RNA	Ribonucleic acid
RNAi	RNA interference
RNAP	RNA polymerase
RNAse E	Ribonuclease E
s.d.	Standard deviation
sfCFP	Superfolder cyan fluorescent protein
sfGFP	Superfolder green fluorescent protein
sfYFP	Superfolder yellow fluorescent protein
sRNA	Small non-coding RNA
STAR	Small Transcriptional Activating RNA
TF	Transcription factor
TSS buffer	Transformation and storage solution buffer
3OC6-HSL	3-oxohexanoyl-homoserine lactone

Chapter 1

Introduction

Contents

1.1 Summary **2**

1.2 Limitations of monocultures **3**

1.2.1 Monoculture limitations for synthetic biology 3

1.2.2 Monoculture limitations for metabolic engineering 6

1.2.3 Challenges of engineering cocultures 10

1.3 Engineering bottom-up cocultures for composition control **11**

1.3.1 Design and simulation of microbial cocultures 12

1.3.2 Communication tools for the design of microbial consortia 13

1.3.3 Examples of coculture composition control mechanisms based on quorum sensing 16

1.4 Designing a host-aware coculture composition controller **22**

1.4.1 Using RNA-based repressors to control coculture composition 22

1.4.2 Using an RNA-based activator to control coculture composition 25

1.4.3 Summary of host-aware strategies to control coculture composition . . . 27

1.5 Aims and objectives **28**

1.6 Publications resulting from this work **30**

1.1 Summary

Microbial biotechnology is bringing us one step closer to fighting the realities of climate change, pandemics, social inequalities and food shortages amongst many other challenges affecting our planet. Novel technologies developed in the last two decades have permitted the development and commercialisation of biotechnological products, which many of us would have been treated with, eaten, used or even worn [1, 2, 3]. The global market for synthetic biology in 2021 was evaluated to 9.5 billion USD and it is predicted to reach 30.7 billion USD in 2026 [4]. As products diversify and complexify, there is a need to develop novel strategies in which microbes work together to achieve a common goal. Our planet Earth is a microbial planet, made up of a vast diversity of microorganisms, which together sustain our biosphere. They cooperate, trade and exchange metabolites to achieve specialised tasks, which in concert form complex functions in different ecological niches. We can gather inspiration from nature, so that in the future, products are no longer produced from single strains, but instead are produced by small ecological systems in which strains can convert agricultural waste into energy for biofactories, fix nitrogen for agricultural plants, or grow functionalised self-healing materials. However, building microbial consortia remains a challenge, slowing down advances in the field of engineering multicellular systems. A number of studies have recently demonstrated the benefits from implementing division of labour across different microbial species to improve product yields. A commonly used approach to optimising yields from microbial consortia, is to vary inoculation ratios. However, there are few other tools that allow to dynamically tune, whether it be *in silico* or *in vivo*, the properties of microbial cocultures. Genetic controllers represent a possible solution to regulating coculture composition, thus providing a novel tool to optimise yields at the multicellular level. In this section, I discuss the field of engineered microbial consortia and the emergence of genetic controllers to control their temporal, spatial and composition properties, as well as their limitations, and possible solutions.

1.2 Limitations of monocultures

1.2.1 Monoculture limitations for synthetic biology

Monocultures are still the predominant production method in synthetic biology. However, overexpression of heterologous genes can impact the growth of their host, thus causing an unwanted reduction in yield and titer of the product of interest [5, 6, 7]. In this section I will discuss the limitation of monocultures for the production of metabolic products as well as for the construction of complex genetic circuits.

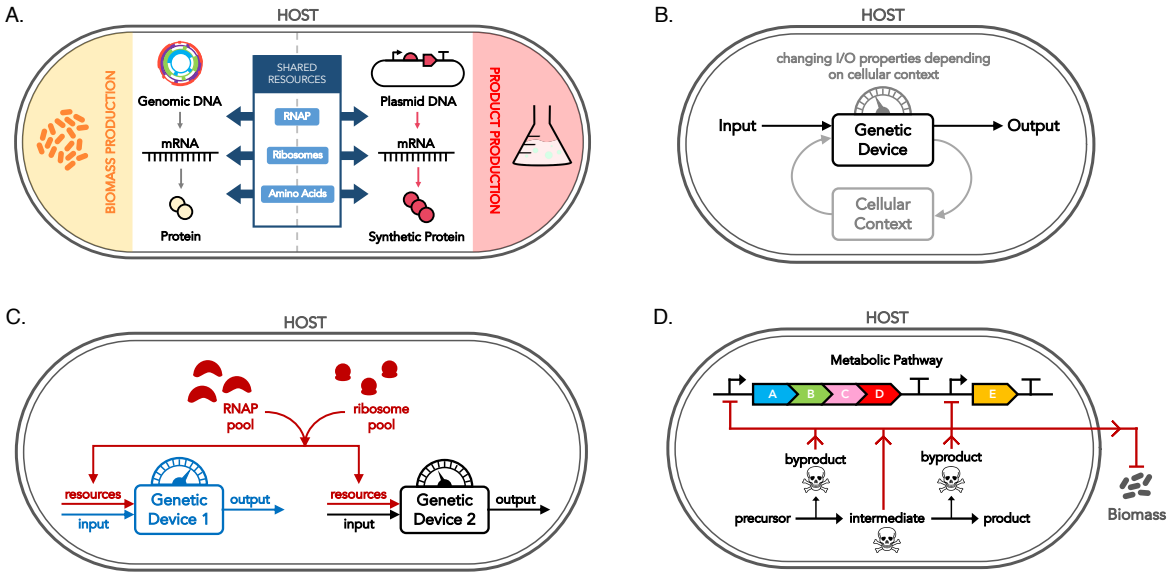


Figure 1: Current challenges leading to the development of host-aware constructs in synthetic biology. (A) Resource competition between the host cell and the synthetic constructs leads to growth rate reduction and poor system modularity, performance and robustness. (B) Input/output property fluctuations caused by variations of the host cellular context hamper the construction of modular constructs, that is, constructs whose operational behaviours do not change in the presence of other constructs. (C) Resource-induced cross-talks appear due to the fact that genetic constructs not only compete for resources with the host cell but also with one another. (D) Toxicity arising from the expression of heterologous pathways in a host cell also leads to poor productivity and poor cell growth. Figure and caption from [7]

First, heterologous gene expression redirects host cellular resources from native processes in a process called burden (Figure 1.A). As a result, the pool of cellular resources that was utilised for the accumulation of biomass is sparser and growth rate decreases [8]. As bacterial

growth is exponential, it negatively impacts the production of the gene of interest. Previous studies showed that the availability of free ribosomes, or ribosomal capacity, was the major bottleneck for heterologous gene expression [9, 8, 10].

Sharing resources between the genetic circuit and the host does not only impact yields and titers of the products of interest. It also affects the behaviour and predictability of genetic circuits, whether its function is to produce high-value products, to sense metabolites or to record cellular events for example (Figure 1.B). Indeed, the pool of available cellular resources varies based on the metabolic state of the cell and its environmental context, which in turn affects the input-output properties of the circuit [11, 12, 13].

Because heterologous gene expression uses the same pools of cellular resources as natural cellular processes, multiple genetic circuits can inhibit each other's behaviour in a phenomenon called retroactivity (Figure 1.C) [14, 15, 16, 17, 18]. In a tug-of-war manner, the different genetic constructs compete for the same resources. As the strength of expression of a first genetic device increases, this will cause a decrease in expression in other genetic devices.

Beyond the cost of heterologous gene expression, expressed heterologous proteins themselves can be harmful to the cell. Bactericidal proteins such as toxins (e.g. CcdB, Gp2) or antimicrobial peptides (e.g. bacteriocins, nisin) are toxic at high concentrations and are thus often used to build growth control mechanisms [19, 20, 21, 22, 23]. Expression of metabolic pathways can also lead to build up of toxic byproducts and final metabolic products. For example salicylic acid becomes toxic at high concentrations [24] or, in the production of amorphadiene, accumulation of the intermediate farnesyl pyrophosphate (FPP) is toxic and causes a reduction in the final yield of amorphadiene [25].

Both *in vivo* and *in silico* tools have been developed in order to measure, quantify, predict and mitigate the cost of heterologous gene expression on its host. The "capacity monitor" was developed to assess the reduction in free cellular resources caused by expressing heterologous expression [8]. It consists of a simple genetic device integrated into the genome and constitutively expressing superfolder GFP (sfGFP). When a genetic construct in expressed, it pulls away cellular resources otherwise used for sfGFP production. Thus, by quantifying the decrease in sfGFP expression, the user can infer the cost of expressing their genetic

circuits on the host cell. Beyond using fluorescent protein reporters, RNA-seq and Ribo-seq methods have also been developed to more quantitatively measure the impact of genetic constructs expression on their host [26]. These sequencing techniques allow to precisely quantify the flux of RNA polymerases (RNAP) and ribosomes for each heterologous gene, thus highlighting their specific demand in cellular resources. Other tools have also proved helpful to predict and quantify the burden caused by heterologous expression. For example, Borkowski et al. used cell-free lysates to measure the cellular resources consumption of different genetic constructs [27] . By integrating these *in vitro* measurements into a minimal model of translation, the authors were able to accurately predict the burden that these genetic circuits would cause to their host *in vivo*. Minimal mathematical models capturing coarse cellular processes have also been a good ally to foresee the cost of heterologous gene expression [9]. By modelling changes in pools of cellular resources, they can predict host-circuit interactions [9, 28, 29] and predict genetic failure caused by the emergence of deleterious mutations [30].

There have been several studies looking at mitigating the burden and toxicity caused by the expression of genetic devices and metabolic pathways. As translation was shown to be the major bottleneck for microbial gene expression, some studies have looked into creating orthogonal ribosome pools to insulate engineered genetic devices from native host processes [31, 32]. The genetic devices were programmed to only use a specifically allocated pool of ribosomes, whose size would vary depending on the state of the native pool of ribosomes. This would ensure that the host always has access to a large enough fraction of ribosomes to mitigate the effects of the synthetic genetic device on the host. Other studies have build negative feedback based on either stress-responsive promoters or promoters sensing specific metabolites to reduce expression of the heterologous genes or to express enzymes degrading the toxic intermediates [33, 25, 34, 35]. The MazF ribonuclease was used to target and degrade either synthetic mRNA or native mRNA in strains with codon-optimised mRNA. As a result, upon induction of MazF, the host translational resources can be entirely redirected for synthetic gene expression. Finally, feedback mechanisms relying on protein-based sequestration or RNA-based sequestration were built to decrease gene coupling between two genetic devices by reducing gene expression of one device when its resource consumption is

impacting the second device [17, 18]. Another method to reduce burden is to reduce the number of gene copies coding for the genetic devices of interest. Plasmid-based constructs can also lead to instability and cell-to-cell variability and integrating them into the genome has been shown to produce high titers almost comparable to plasmid-based production systems even though utilising far less cellular resources [36, 37, 38, 39].

Though all these studies report solutions to reduce burden, toxicity and retroactivity caused by expressing metabolic pathways and genetic devices, these solutions also require a significant fraction of the available cellular resources to function [18, 35, 40]. Though migrating from plasmid-based systems to genome-based genetic devices will certainly improve circuit-host interactions and the number of genes and genetic devices that can be expressed in a single cell, there will always be a limit on the number of heterologous genes that can be expressed. Using multicellular systems, combined with the existing host-aware genetic tools, will allow users to scale up the number of heterologous genes that a microbial culture can express. As a result, cocultures will be able to perform more complex biocomputing, to sense more metabolites, and to respond to more intracellular or extracellular stimuli [41]. They will also be able to produce more complex metabolic products through the expression of longer, more complex metabolic pathways.

1.2.2 Monoculture limitations for metabolic engineering

So far most methods of bioproduction have focused on engineering a single strain to produce high-value compounds. However, too often titer and yields are too low to envision a viable commercialisation of the products. Microbial cocultures have several properties that make them particularly interesting for tackling the challenges of monocultures for the production of metabolic products [42, 43, 44, 45, 46, 47].

First, splitting metabolic pathways across multiple microbial species contributes to reducing the burden caused by the expression of heterologous enzymes in the host. As seen in the section above, metabolic pathways can slow down biomass accumulation by rewiring cellular resources for their own expression. Using coculture is a mean to express more genes, thus more complex pathways, without impacting cell growth as much. For

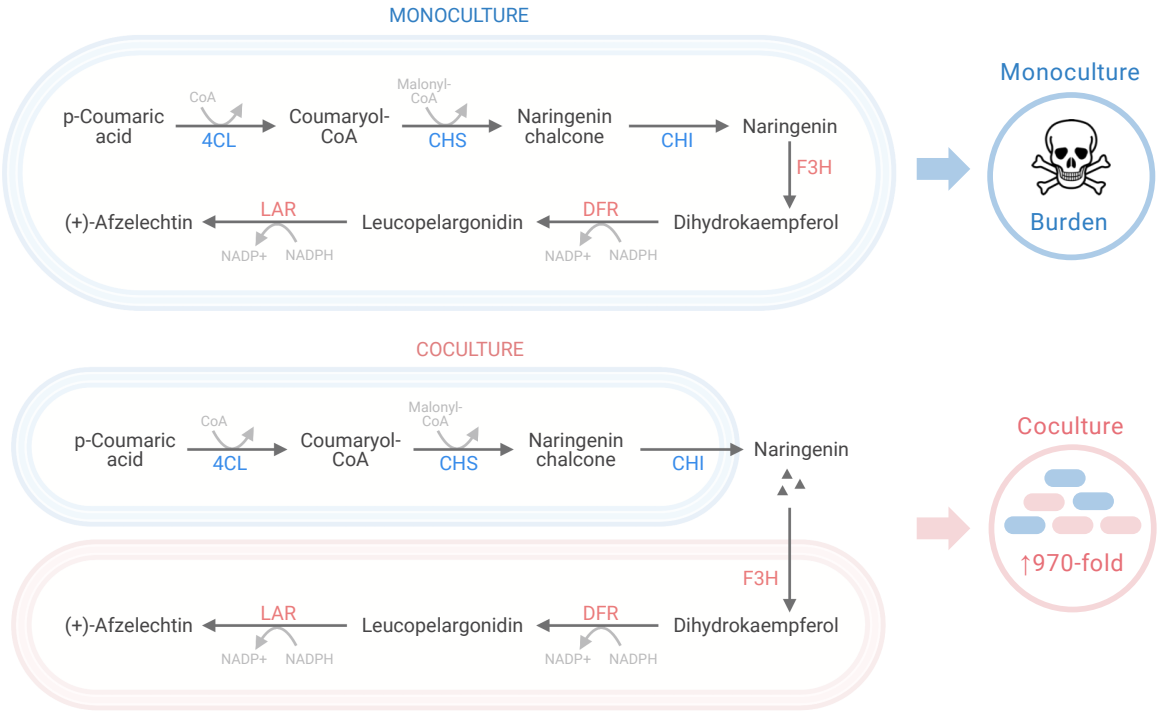


Figure 2: Division of labour to reduce burden and stress. In their work, Jones et al. splits a burdensome six-enzyme metabolic pathway into two *E. coli* strains for the production of (+)-afzelechtin, a flavan-3-ol [48]. The first strain is optimised to catalyse reactions using the malonyl-CoA cofactor. First, p-coumaric acid is converted to coumaryol-CoA by 4-coumaroyl-CoA ligase (4CL). Chalcone synthase (CHS) then converts it to naringenin chalcone before chalcone isomerase (CHI) converts it to naringenin. The second strain is optimised to catalyse reactions using the NADPH co-factor. It uses naringenin as a precursor to convert naringenin to dihydrokaempferol to leucopelargonidin to (+)-afzelechtin through the expression of the three enzymes: flavanone 3β-hydroxylase (F3H), dihydroflavonol 4-reductase (DFR) and leucoanthocyanidin reductase (LAR).

example, in their work, Jones et al. engineered an *E. coli*-based coculture for the optimised production of flavonoids (Figure 2) [48]. They found that overexpressing the six-enzyme pathway necessary for the production of (+)-afzelechtin caused cells to grow poorly. In order to reduce the metabolic burden caused by the overexpression of the enzymes, they decided to split the pathway in two, at a strategic splitting point, to optimise the fluxes of the divided pathways. As a result, the upstream pathway was designed to convert p-coumaric acid into naringenin through the expression of three enzymes, and the downstream pathway was designed to convert naringenin into (+)-afzelechtin through the expression of another three enzymes. Reactions in the upstream strain were dependent on the malonyl-CoA

cofactor, while they were dependent on NADPH in the downstream strain. Thus, designing strains to push the carbon flux towards specific co-factors and substrates of interest allows to separately optimise the different parts of a metabolic pathway. Overall, they were able to achieve a 970-fold improvement of (+)-afzelechtin titer compared to previously published monocultures. So cocultures not only are a mean to decrease metabolic burden to improve growth and titer, they also provide the opportunity to set the genetic context of the different strains to optimise the metabolic fluxes of the different parts of the pathway.

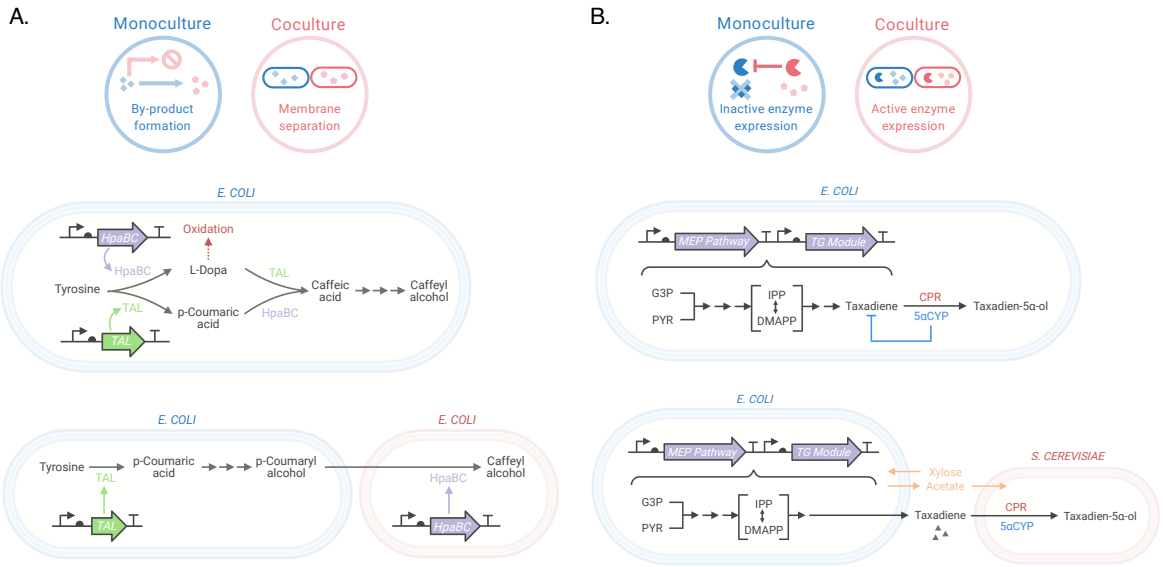


Figure 3: Coculture prevents crosstalks through compartmentalisation. (A) Coculture compartmentalisation reduces by-product formation during caffeic acid biosynthesis. In their work, Chen et al. built a coculture to physically separate the TAL and HpaBC enzymes that convert tyrosine to caffeyl alcohol [49]. Tyrosine is converted to p-coumaric acid by tyrosine ammonia lyase (TAL) and then to caffeic acid by 4-hydroxypropanoic acid 3-hydroxylase (HpaBC). But tyrosine can also be converted to the unwanted by-product L-Dopa by HpaBC. As HpaBC hydroxylation activity is much higher towards p-coumaryl alcohol than for tyrosine or p-coumaric acid, in the coculture HpaBC was compartmentalised to transform p-coumaryl alcohol into caffeyl alcohol. (B) Coculture compartmentalisation reduces enzymatic crosstalks. In their work, Zhou et al. found that expression of the cytochrome P450s (CYPs) enzymes, for oxygenation of taxanes, inhibited enzymes essential for the synthesis of taxadiene [50]. Compartmentalisation of taxadiene synthesis in *E. coli* and taxane oxygenation in *S. cerevisiae* improved oxygenated taxanes yields [51, 50].

Cocultures are also a means to prevent crosstalks between different stages of a metabolic pathway (Figure 3). Crosstalks can occur at different levels of a metabolic pathway but

also involve different kinds of interactions between enzymes and metabolites. In their study, Chen et al., highlighted the benefits of using coculture to prevent the production of unwanted side products (Figure 3.A) [49]. They aimed to produce caffeyl alcohol, which is converted from caffeic acid through the expression of three enzymes. However, the production of caffeic acid itself requires the expression of two enzymes. Tyrosine ammonia lyase (TAL) converts tyrosine into p-coumaric acid which is then converted into caffeic acid by 4-hydroxypropanoic acid 3-hydroxylase (HpaBC). However HpaBC can also convert tyrosine into L-Dopa which quickly oxidises and causes oxidative stress [52]. To prevent the production of the unwanted L-Dopa by-product, enzymatic assays were performed to determine the specific activity of HpaBC towards tyrosine, p-coumaric acid and p-coumaryl alcohol. HpaBC activity was much higher for p-coumaryl alcohol than for the other substrates. It was found that using a coculture significantly reduced HpaBC access to tyrosine, thus decreasing the production of the L-Dopa unwanted by-product. As a result, the final titer of caffeyl alcohol was improved by 12 fold compared to the monoculture strain. This demonstrated that coculture could inhibit unwanted enzymatic activity to reduce the production of unwanted side products by physically separating segments of a metabolic pathway.

Finally, crosstalks can also occur from the interaction between different enzyme expressed from a metabolic pathway. As a result, an enzyme can become inactive in the presence of an antagonist enzyme. For example, Ajikumar et al. reported that expressing cytochrome P450 taxadiene 5α-hydroxylase (5αCYP), necessary for the production of oxygenated taxanes in *E. coli*, inhibited taxadiene production [51]. They showed that 5αCYP prevented the functional expression of the enzymes responsible for taxadiene production. As a result, in their later work, Zhou et al., compartmentalised taxadiene production in *E. coli* and oxygenation of taxadiene into oxygenated taxanes in *S. cerevisiae* (Figure 3.B) [50]. This solution prevented 5αCYP from impacting the activity of the enzymes involved in taxadiene production in *E. coli*. In addition, it allowed to select the best chassis to express the different part of the pathway, thus providing a new way to optimise metabolic fluxes compared to monocultures.

In this section, we saw how cocultures can address monoculure limitations such as burden,

product toxicity, by-product synthesis, enzymatic crosstalks and chassis optimisation for different fragments of metabolic pathways. Division of labour improves the efficiency of bioproduction processes and cell viability. It provides a new way to scale up the number of genetic constructs that can be expressed by a microbial culture, thus opening the field to the design of more complex genetic devices and metabolic pathways.

1.2.3 Challenges of engineering cocultures

Despite all the benefits of cocultures that we have just examined, their widespread adoption is still limited by the lack of control that we have over their behaviours [53]. Comparable to the competition of genetic constructs for their host cellular resources, strains grown in a coculture compete for the same pool of energy and metabolites present in their culturing environment. But in the case of the coculture, due to the nature of exponential growth, the fastest growing strain will quickly take over the other strain(s) (Figure 4).

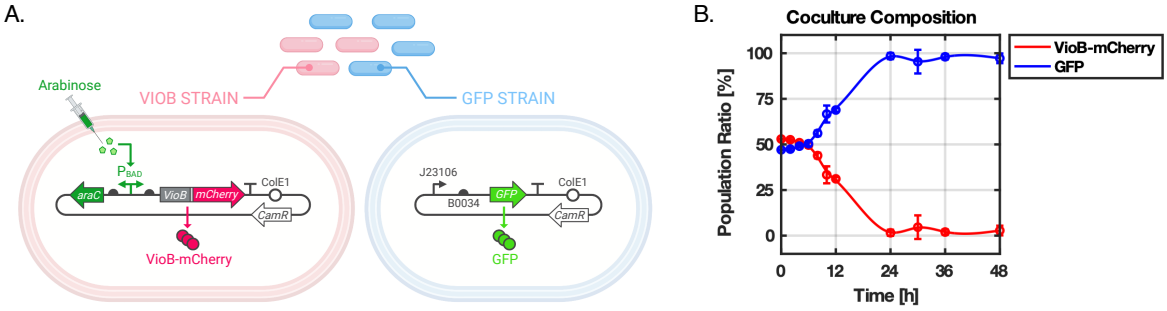


Figure 4: Coculture outcompetition by the fastest growing strain. (A) A coculture is composed of a first *E. coli* strain transformed with L-arabinose inducible VioB-mCherry construct and a second *E. coli* strain transformed with a construct constitutively expressing GFPmut3. (B) Coculture composition measured over time. Experiment was done in BW25113. Population ratio was measured through flow cytometry. Error bars represent the mean of 3 biological replicates.

Inspired from nature, syntrophs and auxotrophs enable the design of mutualistic relationships between the different species grown together [54, 55, 56]. As a result, coculture species cooperate by trading essential metabolites and amino acids to guarantee their survival. These mutualistic cocultures have the benefit of using multiple strains to create small ecological niches [57, 58, 59]. However, a drawback of this approach is that coculture com-

position is not tunable and fluctuates over time, which limits its use for some applications. Kerner et al. attempted to address these limitations by designing a system that tunes expression of the YddG tyrosine transporter [60]. As a result, the authors were able to control the ratio between two *E. coli* strains. But the burden due to the expression of the genetic circuit controlling population ratio was too high for division of labour to be an advantageous solution over a monoculture. Mutualistic relationships also favour the emergence of cheaters which benefit from the cross-feeding interactions between the cooperating species without contributing to it [61, 62].

Oscillatory mechanisms such as the famous predator-prey topology have also been developed to control coculture composition [63, 64, 65, 66]. A famous example of the application of oscillatory circuit is for the delivery of anti-cancer treatment to the core of a cancerous tumour [67, 68]. Oscillatory cocultures can release multiple cargos, such as anti-cancerous drugs, given a specific timing for more efficient treatments [69]. Though their oscillatory nature prevents them from being applied to a wide range of applications, especially for metabolic engineering, they are a great fit for *in vivo* therapeutic applications [70].

So, robustly controlling coculture composition is still a challenge, especially for applications to metabolic engineering. In the following section I will aim at presenting recent works aiming at controlling coculture composition to highlight the current gaps and challenges that remain for cocultures to be widely adopted for next-generation bioproduction processes.

1.3 Engineering bottom-up cocultures for composition control

In this section, I will examine the current progress and tools available for the bottom-up construction of microbial consortia, whose behaviour can be robustly controlled. The Design-Build-Test-Learn (DBTL) cycle is used in synthetic biology to provide a systematic and efficient approach to building genetic devices. The DBTL cycle can also be applied for the design of microbial consortia (Figure 5).

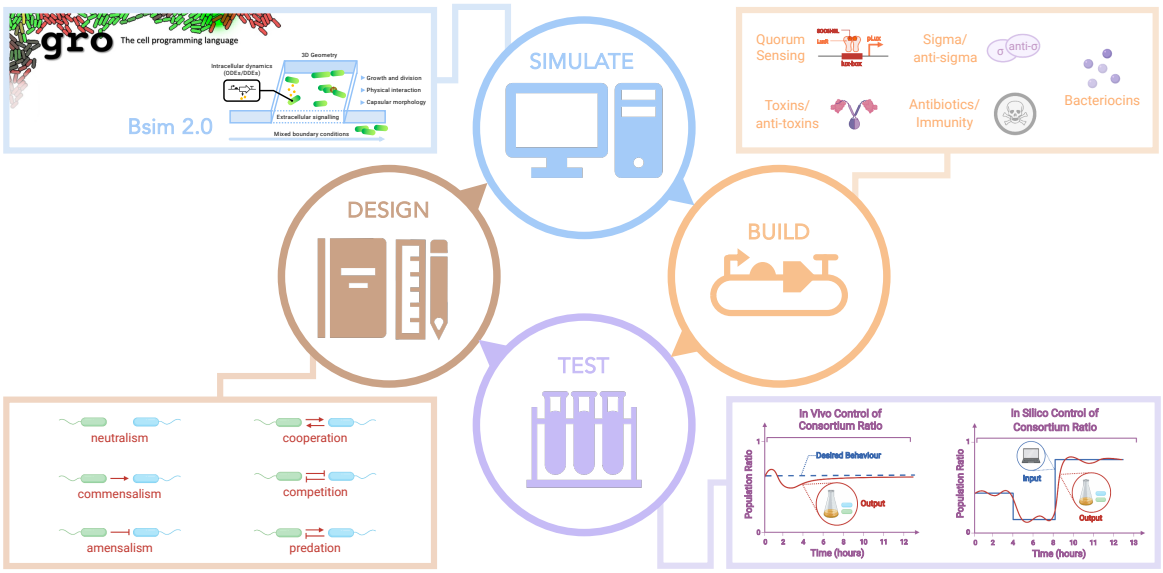


Figure 5: Bottom-up engineering of microbial consortia for composition control. The Design-Build-Test-Learn synthetic biology cycle can be applied for building microbial consortia displaying a specific behaviour such as population ratio control.

1.3.1 Design and simulation of microbial cocultures

Most natural systems rely on cooperation between strains, as is the case of auxotrophic systems [54]. However, auxotrophic pairs can only achieve a set ratio that is dependent on the specific metabolites that are being exchanged and that is not stable over time [57]. So despite the vast amount of available of auxotrophic pairs, new types of interactions have been developed since then. Six different types of interactions have thus been designed between any two species present in a microbial consortia (Figure 5) [71, 22]. First, neutralism occurs when no interaction can take place between the two species. Commensalism and amensalism are a one-way only positive or negative interaction between the two species. Finally, cooperation, competition and predation involve a two-way interaction between the two strains. These new interactions allow consortia designers to expand the engineerable properties to control microbial consortia behaviour.

Computational approaches have also been a tremendous asset for the construction of microbial consortia (Figure 5)[72]. Deterministic modelling and more specifically coarse-grain models describe the fundamental cell-cell interactions and well as circuit-host interactions.

They are a way to predict under which conditions and sets of parameters a microbial consortia will behave as expected [22, 73]. They can also be used to predict the benefits of using division of labour over monocultures by assessing the burden caused by the metabolic pathway of interest and the cost of dividing it across different cell types [74]. So deterministic models can be integrated within the DBLT cycle to predict whether a specific topology will be able to behave as expected and guide which parameters will need to be tuned to achieve this behaviour.

Agent-based models also rely on the use of minimal model. But instead of predicting population level behaviour, they follow the behaviour of each cell, or agent, in the consortia. This is particularly useful to predict coculture behaviour in small environments such as microfluidic chambers, where changes in environment topology and diffusion rates can have a large impact on the small amount of cells present in the chamber [75, 76, 77]. Agent-based modelling frameworks include Gro which is based on the C++ programming language [78, 79, 80] and Bsim/Bsim 2.0 based on Java [81, 82]. Agent-based models typically feature the 3D characteristics of the growth chamber, the morphology and growth of the cells, and the physical and molecular interactions between the cells and the environmental conditions.

Other types of mathematical models have also been developed to incorporate uncertainty into the interactions between the different players. Game theory was used to explore and understand the emergence of metabolic dependencies between auxotrophic *E. coli* strains [55]. Reinforcement learning was used to predict coculture behaviour in bioreactors [83], while Bayesian computation was used to identify circuit topologies that would provide stability and tunability of coculture composition [84].

1.3.2 Communication tools for the design of microbial consortia

Building cocultures with the desired behaviour requires a set of genetic parts and tools that enable communication between the different cell types and control of the community composition. First, engineering cell-to-cell communication is necessary to guarantee the robust coexistence of all strains in the coculture. Communication can either be a one-way or two-way mechanism. One-way mechanisms are particularly interesting for engineering existing microbial consortia *in situ* such as the gut microbiome [85]. Antimicrobial peptides such as bacteriocins and microcins can be used to design such one-way interaction by targeting

more or less specific gram-negative bacteria [86, 87], while Type VI Secretion System can be programmed to inhibit growth of a specific microbial target [88, 89].

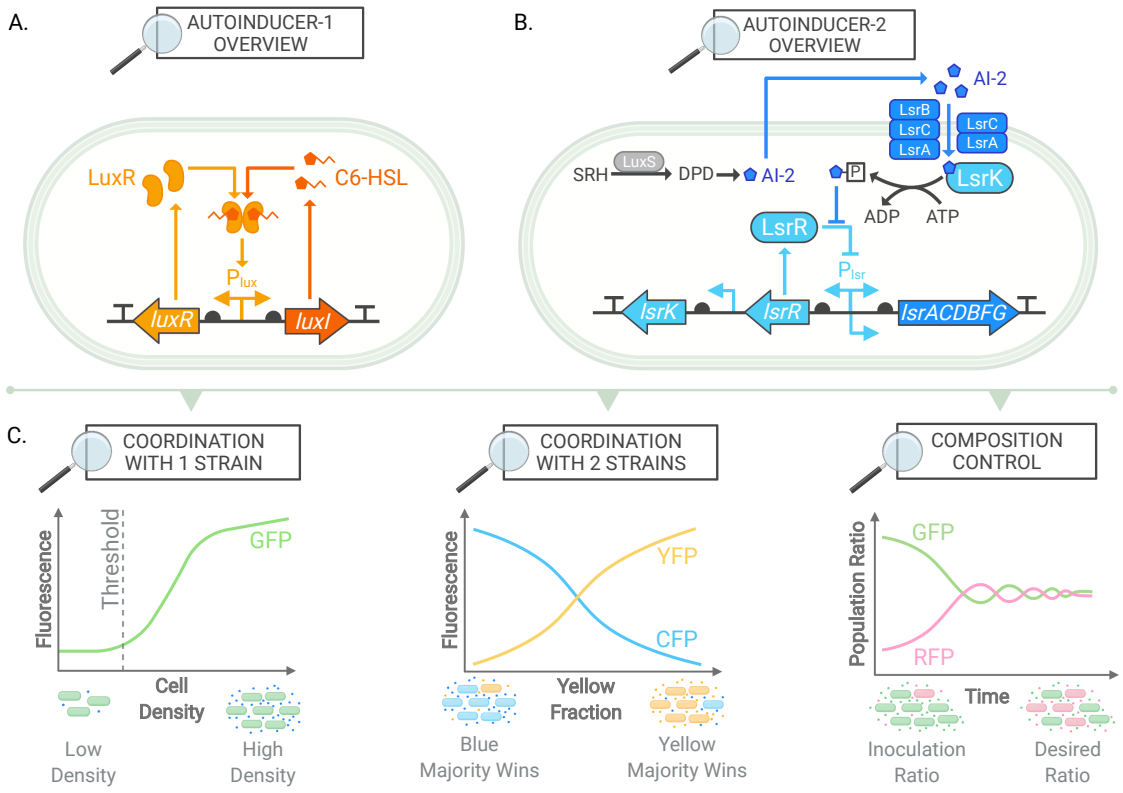


Figure 6: Quorum sensing for the coordination of microbial behaviour. (A) Components involved in the production and sensing of autoinducer-1 in *E. coli*. (B) Components involved in the production and sensing of autoinducer-2 in *E. coli*. (C) An overview of the recent efforts to engineer cell–cell communication for the coordination of population behaviour. Figure and caption from [90]

Two-way communication has been widely implemented using quorum sensing systems (Figure 6.A-B). Quorum sensing is a mechanism that enables a bacterial population to collectively respond to changes in cell density of its own population or of another bacterial population present in its environment. Quorum sensing molecules have first been discovered in the 1980s, in the marine bacterium *Vibrio fischeri* to control activation of bioluminescence when enough bacteria were in close proximity [91, 92, 93]. Since then, homologues of the 3OC6-HSL quorum sensing molecule, also called autoinducer-1 (AI-1), were discovered in bacteria from varied habitats such as soil or gut bacteria [94, 95, 96]. Later it was found that *Vibrio harveyi*, which was also a bioluminescent marine bacterium close to *Vibrio fis-*

cheri, expressed not one but three different types of quorum sensing systems, which together have been found to regulate the expression of more than 600 genes [97, 98]. One of them, 3OH-C4-HSL, is homologous to the one found in *Vibrio fischeri* and allows for intra-species communication [99]. The second, autoinducer-2 (AI-2) was found in more than 500 different gram-negative and gram-positive bacteria, which makes it the most widely used quorum sensing molecule in nature, and thus enables inter-species communication [100, 101, 102]. The third, (Z)-3-aminoundec-2-en-4-one is part of a third class of autoinducers first discovered in *Vibrio cholerae*, and named cholera autoinducer-1 (CAI-1) [103]. CAI-1 is used for intra-*Vibrio* communication. This demonstrates that cells can harbor different types of mechanisms to communicate with different potential microbial agents around them.

Both AI-1 and AI-2 quorum sensing systems have since then been widely used for coordinating cellular behaviour at the population level [104, 105, 90]. In *Vibrio fischeri*, the AI-1 mechanism is driven by a three component system (Figure 6.A). The LuxI synthase catalyses the production of 3OC6-HSL which binds to the LuxR transciptional activator. The dimerised complex binds to the *lux* promoter to activate expression of LuxI, LuxR and the luminescence operon luxCDABE. At low bacterial densities there is not enough 3OC6-HSL/LuxR complex to activate bioluminescence. But as cell density increases, more 3OC6-HSL/LuxR complex is produced, which in turn causes its own positive regulation, and bioluminescence production is activated. The structure of the AI-2 mechanism is more complex: AI-2 molecules cannot freely diffuse across cellular membranes, and thus require the expression of transporters (Figure 6.B) [106]. The *lsr* promoter of the AI-2 system was also relatively weak which prevented its broad application in synthetic biology. Studies have since then discovered ways to amplify the output signal of the *lsr* promoter using T7 polymerase and directed evolution [107, 108, 109]. They also circumvented the challenge of using AI-2 in the presence of glucose by using $\Delta ptsH$ and $\Delta luxS$ gene knockouts [110]. There are still few studies using AI-2 to engineer microbial consortia. However, as AI-1 quorum sensing has few fully orthogonal pairs, I envision that the optimised AI-2 system will be used in combination with AI-1 systems to design microbial consortia of more than two bacterial species [111, 112].

Quorum sensing has been used to coordinate population behaviour in single-strain and

dual-strain cultures (Figure 6.C). In monocultures, quorum sensing has been used to coordinate gene expression to build delay mechanisms to activate the expression of specific genes only when the culture has reached a high enough population density [113, 114, 115]. Control of gene expression based on population density has also been demonstrated in dual-strain *E. coli* cultures. For example, Kim et al. build a circuit to propagate a quorum sensing signal across long microfluidic chambers to coordinate oscillation across the entire chamber [73]. Alnahhas et al. demonstrated they could use quorum sensing to detect the majority strain and minority strain of the coculture to turn gene expression ON or OFF in the different fractions [116]. So quorum sensing is a versatile tool that can be used to coordinate gene expression across microbial cultures. In the next section, I specifically focus on how quorum sensing can be used to coordinate gene expression to control coculture composition.

1.3.3 Examples of coculture composition control mechanisms based on quorum sensing

There are a number of reviews on tools to engineer microbial consortia [117, 105, 90, 53, 47]. However, here I will focus on recent efforts to control coculture composition using quorum sensing to mediate population density information propagation in the coculture. I will first have a look at genetic designs that have implemented community control by engineering only one of the two strains. Then I will examine designs in which both strains have been engineered to control coculture behaviour.

In the first circuit I describe, Dinh et al. engineered only one strain to self-regulate its population density for the production of naringenin (Figure 7.A) [118]. The engineered strain carried the upstream half of the naringenin biosynthesis pathway. By expressing TAL, this half of the pathway catalysed the production of p-coumaric acid from L-tyrosine. At low cell density, the engineered strain produces p-coumaric and its growth is not affected. But at high cell density, it enters a new regime in which enough 3OC6-HSL/LuxR complex has accumulated to produce SspB, which recrutes the ClpXP proteases for the degradation of Pfk, an essential enzyme for the control of glucose assimilation. As a result, at high density, the engineered strain auto-downregulates its own growth, which gives the opportunity to the

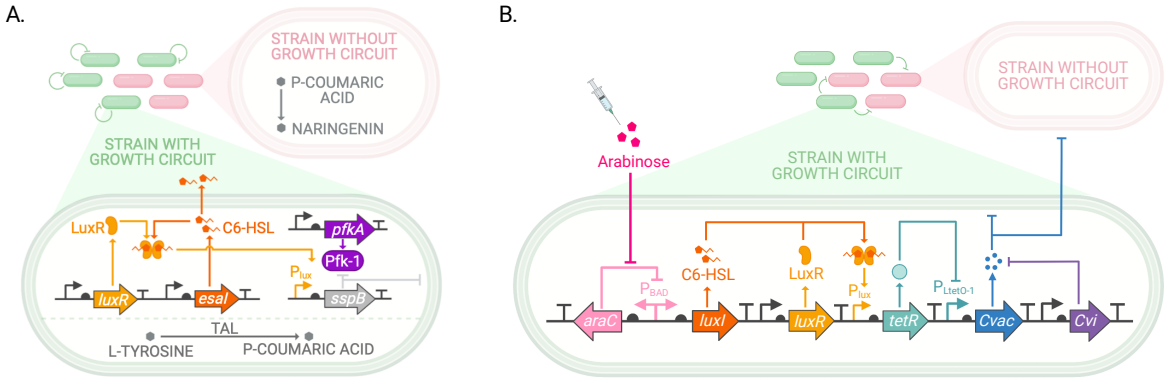


Figure 7: Circuits that use one-way quorum sensing to control population composition in bacterial cocultures. (A) A single-strain quorum sensing-based growth controller used to build an *E. coli–E. coli* coculture for the production of naringenin [118]. Pfk, an enzyme controlling the glycolytic flux of the cell, is tagged with a SspB-dependent degradation tag and is constitutively expressed in the cell. Self-produced 3OC6-HSL drives the expression of *sspB*, which mediates the degradation of Pfk, hence downregulating the overall growth rate of the cell when AHL levels increase. The strain equipped with the growth controller is engineered to produce the p-coumaric acid precursor. The unregulated strain then converts this precursor into naringenin. Figure and Caption from [90]. (B) A single-strain quorum sensing-based growth controller to modulate composition ratio in batch and continuous cultures [87]. The system is composed of an engineered strain that produces 3OC6-HSL and a wild-type strain. At high population density and in the presence of L-arabinose, the 3OC6-HSL/LuxR complex drives expression of TetR which represses expression of the growth inhibiting bacteriocin encoded by *CvaC*. As a result, the wild-type strain is able to grow when the competitor strain density is high and is killed by bacteriocins when the competitor strain density is low. *Cvi* is the immunity gene, which preserves the engineered strain from the effects of the bacteriocin.

second strain to utilise p-coumaric acid as a precursor for the second half of the naringenin biosynthesis pathway. Varying the strength of production of 3OC6-HSL gave the authors the ability to modulate the time at which the first strain would stop growing to let the second strain convert p-coumaric into naringenin. As a result, they were able to find a balance between the timing and cell density of each strain that lead to the best final naringenin titer. In the end, they were able to improve naringenin titer by about 60% compared to a coculture system in which their was no growth control and the titer was optimised by varying the inoculation ratios. This circuit demonstrates how quorum sensing can be used for division of labour to activate or deactivate the expression of the different segments of a metabolic pathway. This circuit gives the opportunity to vary the proportion of two producing strain not only using different inoculation ratios, but also by providing a temporal switch to control community composition.

In the second circuit, Fedorec et al. also implemented a circuit in which only one strain regulates the coculture composition (Figure 7.B) [87]. In this circuit, the strain carrying the community control mechanism does not use quorum sensing to self-regulate its own population density. Instead, it controls the population density of a wild-type strain based on its own population density. At high cell density, the engineered strain produces high amounts of 3OC6-HSL/LuxR complex that enables the production of the TetR repressor. As a result, bacteriocin production is inhibited and the wild-type strain can grow with no constraints. However, at low cell density, intracellular levels of 3OC6-HSL/LuxR decrease such that the *LtetO-1* promoter is derepressed and produces bacteriocins that inhibit the growth of the wild-type strain. The engineered strain is protected from bacteriocin growth inhibition through the expression of the *Cvi* gene conferring bacteriocin immunity to the strain. By varying the concentration of L-arabinose that is externally added to the culture, the authors were able to stabilise community composition at varying ratios both in batch and continuous culturing environments. The authors anticipate this circuit to be particularly useful for engineering existing microbial niches as their system does not require to engineer the targeted strain for growth regulation. Again, this circuit demonstrates the use of quorum sensing to stabilise community composition based on sensing cell the density of only one strain.

Next, I examine circuits that have enabled the control of community composition by engineering both strains of a two-member microbial consortium. Toxin-based systems offer a great diversity of tools to downregulate cell growth [120]. Most existing circuits control community composition by downregulating growth rate using toxins or lysis proteins. The first two-member coculture design using quorum sensing to control coculture composition was published by Balagaddé et al. (Figure 8.A) [63]. The predator-prey circuit engineered quorum sensing production in both strains to control the expression of CcdA antitoxin production in the predator strain and CcdB toxin production in both strains. The predator could only survive when the cell density of the prey was high enough, and the prey could only survive when the predator density was low enough. As a result, the coculture composition oscillated between high density of predator or high density of prey. The CcdA/CcdB toxin-antitoxin system was later employed to design a coculture that would stabilise community composition

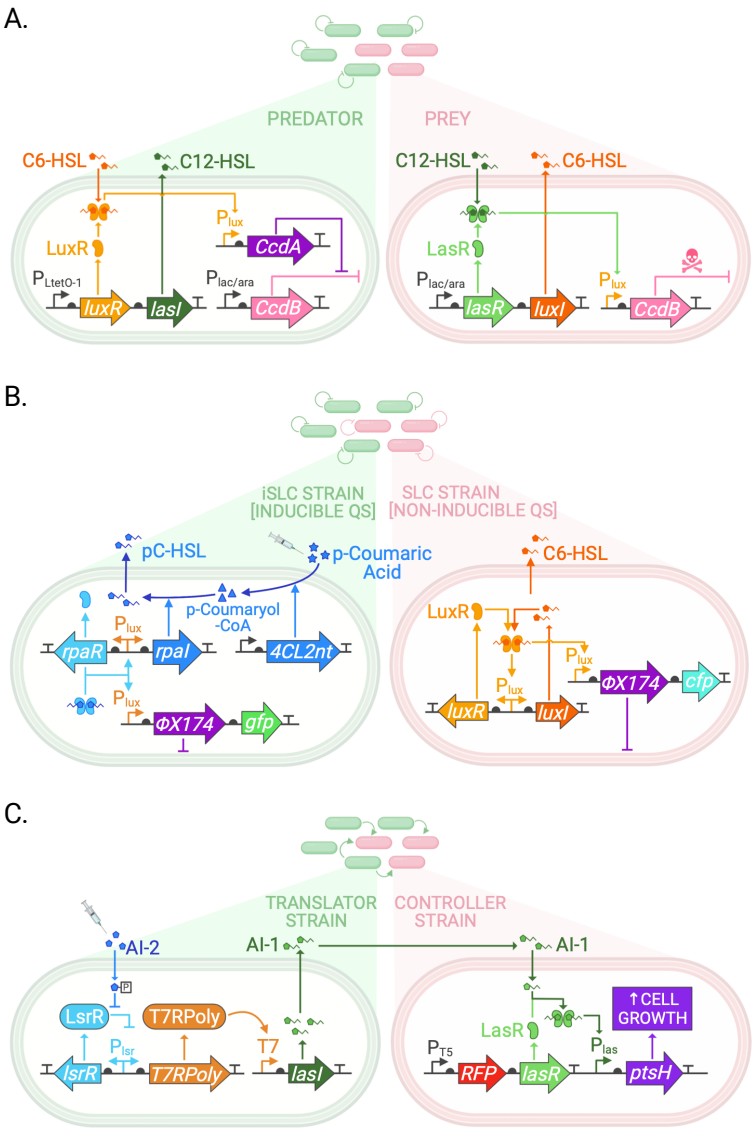


Figure 8: Circuits that use quorum sensing to control population composition in bacterial cocultures. (A) A predator-prey circuit to enable the oscillatory coexistence of both *E. coli* strains [63]. In the predator strain, CcdB toxin is controlled by the *lac/ara-1* promoter and CcdA antitoxin that inhibits CcdB is controlled by the *lux* promoter. The predator strain produces 3OC12-HSL which is detected by the prey to activate CcdB production. Because the las and lux systems are semi-orthogonal, CcdB produced in the prey is only activated by 3OC12-HSL and not by the self-produced 3OC6-HSL [111]. So by producing 3OC6-HSL, the prey enables the survival of the predator by activating expression of the antitoxin. (B) A circuit using inducible quorum sensing (iQS) to control the composition and cargo release of a two-strain E. coli coculture [69]. In the inducible quorum-sensing strain (iSLC strain), the concentration of produced pC-HSL is controlled by external addition of p-coumaric acid. pC-HSL binds to the RpaR regulator to trigger cell lysis and expression of the GOI. In the non-inducible quorum-sensing strain (SLC strain), the production of LuxR/3OC6-HSL is autonomous and cannot be controlled by an external input. LuxR/3OC6-HSL triggers cell lysis and GOI expression in the SLC strain. AHL, acyl-homoserine lactone; GOI, gene of interest. (C) A genetic circuit of a coculture responding to environmental levels of AI-2 to modulate culture composition [119]. The translator strain detects media levels of AI-2 by alleviating the repression of the *lsr* promoter caused by the LsrR repressor. The lsr promoter drives the expression of T7 RNA polymerase to amplify the AI-2 signal and produce 3OC12-HSL from the T7 promoter. In the controller strain, detection of 3OC12-HSL via binding to the LasR regulator upregulates expression of the PtsH sugar transporter, which, in turn, upregulates the growth rate of the controller strain. Panels B-C from [90].

at a set ratio and control the upper limit of coculture density [121, 122]. However, the authors highlighted that their circuit could currently control the maximum cell density of the coculture but that further tuning of AI-1 degradation was needed to control community composition.

Miano et al. also developed an oscillatory coculture by engineering a two-way quorum sensing communication system (Figure 8.B) [69]. However, in their case oscillations were sustained via the production of a lysis protein encoded by the $\Phi X174$ gene. Each strain produces a distinct quorum sensing molecule that will autoregulate lysis of their own population. However in the inducible quorum-sensing strain (iSLC strain), pC-HSL production is controlled through the external addition of p-coumaric acid, while in the non-inducible quorum-sensing strain (SLC strain), C6-HSL is produced constitutively. Different behaviours are obtained for different levels of p-coumaric acid induction. At low p-coumaric acid concentrations, the iSLC strain takes over the coculture as its lysis gene expression is low. At high p-coumaric acid concentrations, it is the SLC strain takes over the coculture as the rate of lysis of the iSLC strain will be too high for it to persist in the coculture. Finally, for medium-range p-coumaric acid concentrations, the iSLC and SLC will both stably coexist in an oscillatory coculture. The use of the lysis gene has been further used to design three-member coculture consortia. These consortia utilised three different toxin-antitoxin systems (colicin E3, colicin E7 and colicin V) to control community composition with or without the use of quorum sensing [65, 66]. In these systems each strain is able to kill another strain and to be killed by a different one. Theoretically this architecture can be expanded to as many strains as there are toxin and immunity gene pairs available. The architecture was also shown to increase the time to apparition of deleterious mutations, thus improving the genetic stability of the coculture. These studies have focused on controlling coculture composition by down-regulating growth.

In their work, Stephens et al. proposed a circuit that can control coculture composition by up-regulating growth instead. They engineered a two-member *E. coli* coculture that can increase growth rate of one of the strains based on the cell density of another (Figure 8.C) [119]. The first strain, called the translator strain, senses externally added AI-2 to produce its own AI-1 quorum sensing signal, 3OC12-HSL. The second strain is able to sense the AI-1 signal when 3OC12-HSL binds to the LasR transcriptional activator. The 3OC12-HSL/LasR

complex controls the expression of the PtsH sugar transporter, whose upregulation increases cell growth rate. Thus, at high density of the translator strain, the growth rate of the controller strain will increase. This system does not autonomously stabilise the population ratio as it requires the addition of an external input, however this external input gives the possibility to the user to adjust the population ratio of the coculture. This design is one of the rare circuit that enables growth rate upregulation to control community composition, which may improve the genetic stability over coculture designs that downregulate growth rate through toxin expression.

These current approaches demonstrate why quorum sensing is a great asset for the construction of community composition controllers. It provides a way to link information about population density to growth regulation mechanisms so as to control coculture behaviour. As a result, community composition can be designed to oscillate, to stabilise at different ratio or to be capped under a specific cell density threshold. Most studies implemented growth regulation through the expression of toxins, while few studies have looked at up-regulating growth rate to achieve control of community composition. Most studies, including the one using growth upregulation, have highlighted that expressing the genetic machinery of the community composition controller imposed a consequent burden, slowing down the growth rate of the strains. This may reduce the advantage of using cocultures to implement division of labour, and reduce their genetic stability, thus preventing the wide option of these circuits for metabolic engineering applications [74]. Though oscillatory cocultures have been shown to be genetically stable over long periods of times and have increased resistance to deleterious mutations, their oscillatory nature limits the realm of applications they can be used for. For example, they are extremely interesting for the production and delivery of therapies *in situ*, but less so for bioreactor production processes in the context of metabolic engineering. So there is currently a gap in understanding how to build host-aware community composition controllers for metabolic engineering that do not impact the advantage of implementing division of labour over using monoculture strategies.

1.4 Designing a host-aware coculture composition controller

In this thesis, I discuss the construction of a host-aware composition controller to stabilise the ratio of a two-member *E. coli* coculture suitable for metabolic engineering applications. That is, I aim to investigate strategies that will cause the least burden to our strains and to carefully quantify their cost for evaluating their potential in the application of division of labour for the production of high values products.

As I discussed earlier, previous studies have demonstrated that shared utilisation of the free ribosome pool is the key factor inhibiting host growth and processes [9, 8, 15, 10, 16]. So, methods expressing a protein for growth rate regulation (e.g. toxin, lysis protein, membrane transporter) would inevitably tap into the pool of free ribosomes. This would add to the burden of expressing the biosynthesis pathway for the production of the compound of interest. Instead of using protein-based regulators, I decided to investigate the use of RNA-based regulators to achieve coculture composition control. I hypothesised that expressing RNA-based devices would only tap into the transcriptional pool of cellular resources, thus minimising the utilisation of the ribosomal pool by our circuit such that the host sustains minimal burden.

1.4.1 Using RNA-based repressors to control coculture composition

Over the years, synthetic biologists have developed multiple RNA-based tools to control gene circuit behaviour [123, 124, 125]. RNA-based genetic circuits can activate or repress different gene expression processes such as transcription, translation or degradation. They have been used for a wide variety of applications ranging from the detection of viruses [126, 127, 128, 129] to the design of logic gates [130] and finally for screening best genetic designs and knockdown targets for metabolic engineering [131, 132]. Their diversity offers a large range of potential mechanisms to both control coculture growth rates and build the logic circuits needed to adjust coculture composition.

Specifically, CRISPR interference (CRISPRi) and small RNA (sRNA) are well known repressors of transcription and translation respectively. Their mode of action is briefly described in Figure 9. CRISPRi acts as an inhibitor of transcription initiation or elongation

(Figure 9.A) [133, 134]. CRISPRi is a two component system that uses a deactivated version of the Cas9 protein and a guide RNA (gRNA) to target a specific DNA sequence. By binding to a promoter region, the CRISPRi complex prevents RNA Polymerase (RNAP) from binding to the DNA, thus inhibiting transcription initiation. If the CRISPRi complex is designed to target a coding sequence (CDS), the tight binding of the CRISPRi complex to the DNA prevents RNAP from sliding along the DNA, thus blocking transcription elongation.

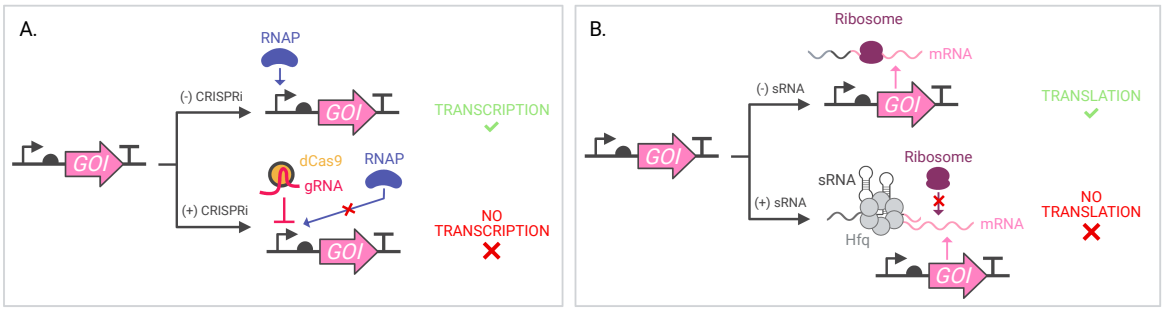


Figure 9: CRISPR interference (CRISPRi) and small RNA (sRNA) repression mechanisms. (A) CRISPRi transcription regulation mechanism. In the absence of the CRISPRi complex, RNA Polymerase (RNAP) is free to transcribe the gene of interest (GOI). The CRISPRi complex is formed in the presence of both deactivated Cas9 (dCas9) and a guide RNA (gRNA) targeting a sequence of interest, here the promoter driving expression of the GOI. Once bound to its target, the CRISPRi prevent transcription initiation, thus turning OFF the expression of the GOI. (B) sRNA translation repression mechanism. In the absence of a trans-encoded sRNA, ribosomes are able to initiate translation. However, in the presence of sRNA, the Hfq chaperone blocks translation initiation and promotes degradation of the targeted mRNA, thus turning OFF expression of the GOI.

CRISPRi has been used for applications in synthetic biology to build nucleic acid controllers such as oscillators and toggle-switches [135, 125]. Recently, a new version of the repressilator was implemented using CRISPRi [136]. CRISPRi repression strength can be regulated by the expression of an antisense RNA that would bind the spacer sequence of the gRNA [137]. CRISPRi has also been used in metabolic engineering to identify and repress multiple potential gene targets to optimise the carbon fluxes for the production of various metabolic products [138, 139, 140, 141]. For example, Kim et al. improved lycopene production by 9-fold when using CRISPRi to balance gene expression from the *crtEI* operon and the MVA pathway [142]. Despite the recent computation advances predicting gRNA targeting efficiency, it is still challenging to design gRNAs for use with CRISPRi and even

more challenging to titrate their repressive effects [143, 144]. This is partly due to the design constraints caused by the availability and position of PAM sequences in the target gene of interest. This probably explain the emergence of pooled CRISPRi screens to identify gRNA sequences that are able to knockdown gene expression in organisms of interest. As a result, several pooled CRISPRi screen studies have identified various essential genes in several organisms including *E. coli*, *B. subtilis*, or *V. natriegens* [145, 146, 147, 148, 149]. In their work, Hawkins et al. introduced mismatches into a pool of gRNA to identify the expression-fitness of essential genes in both *E. coli* and *B. subtilis* [150]. Using mismatches is a way to identify the expression level of essential genes and to find the right amount of repression needed to obtained a desired phenotype [151, 143, 152]. CRISPRi has not only been shown to down-regulate growth. Sanders et al. showed that by targeting *E. coli*'s ArgR repressor involved in arginine production with CRISPRi, they could upregulate the growth rate of their strain [153]. So CRISPRi can be used to dynamically control expression of essential genes to either down- or upregulate cellular growth rate.

CRISPRi is often considered not to be a dynamic system as it tighly binds to its target DNA. The rare dissociation events that occur between the target DNA and the CRISPRi complex, through either spontaneous dissociation or during replication, happen over timescales that are too short to derepress the target gene. However, gRNA mismatches provide a way to adjust the unbinding kinetics of dCas9 to its DNA target by RNAP [154]. As a result, they can potentially alleviate CRISPRi repression over time.

A final point to address is the potential burden of expressing dCas9. As previously mentioned, I am looking to design a circuit with minimal footprint to avoid slowing down the growth rate of its host. It has been shown that overexpression of dCas9 is toxic for the cell [155]. However, expressing small amounts of dCas9 does not cause cell growth defects while preserving the repressive function of CRISPRi [156]. Decreasing concentration of dCas9 in the cell also contributes to avoid saturating the target DNA site such that mismatched gRNA can play a role in the detachment of dCas9 from the target DNA [154]. So CRISPRi appears to be a good candidate for titrating essential gene expression for the control of cell growth rate. It does not cause burden as it is expressed at very low levels, and has the

potential to dynamically control gene expression when playing with the complementary of the gRNA spacer to the target DNA sequence.

Another kind of non-toxic RNA-based repressors are small RNAs (sRNAs) (Figure 9.B). Upon expression sRNAs bind to the native Hfq chaperone and form a complex that binds to the 5' untranslated region (UTR) of the target mRNA [157, 158]. The bound complex prevents ribosomes from binding to the Shine–Dalgarno (SD) sequence, thus inhibiting translation initiation. The Hfq chaperone also promotes the degradation of the sRNA/target mRNA complex by RNAse E. The advantage of this system is that it has a fast turnover rate, so it enables the design of fast dynamical systems. It also does not require the expression of a heterologous protein, like dCas9 for CRISPRi, as the Hfq is already natively expressed in *E. coli* [159]. Small RNAs have been used for applications in metabolic engineering, for example to optimise the production of tyrosine [131], riboflavin [160] or β-carotene [161]. They have also been used for constructing gene control circuits such as negative feedback loops [162] and XNOR logic gates [161]. Small RNAs have first relied on the construction of sRNA pools to identify the best sequence for targeting and down-regulation the mRNA of interest [163]. However, to improve the modularity and reusability of sRNA designs, a couple of studies designed adaptor sequences that can be added upstream of the gene of interest such that reusable sRNA/adaptor pairs can be used orthogonally in different contexts [161, 164].

Similar to genome-wide CRISPRi studies, Meng et al. performed a genome-wide sRNA screening study to uncover essential genes in *E. coli* [165]. Randomised sRNA pools were also used to identify growth inhibiting phenotypes in *Escherichia coli* and *Salmonella enterica* [166, 167]. In particular, the sRNA designs from Kawano et al. could tune *E. coli* growth rate without inducing a long lag phase as seen in CRISPRi studies [167]. So sRNA is an interesting candidate for controlling cell growth without requiring the expression of any heterologous proteins.

1.4.2 Using an RNA-based activator to control coculture composition

In their work, Chappell et al. designed a new kind of regulatory RNA: Small Transcriptional Activating RNA (STAR). Until then, to our knowledge, there was no transcriptional activating RNA mechanism available from either nature or the synthetic biology toolbox

[123, 124, 168]. The STAR mechanism is described in Figure 10.

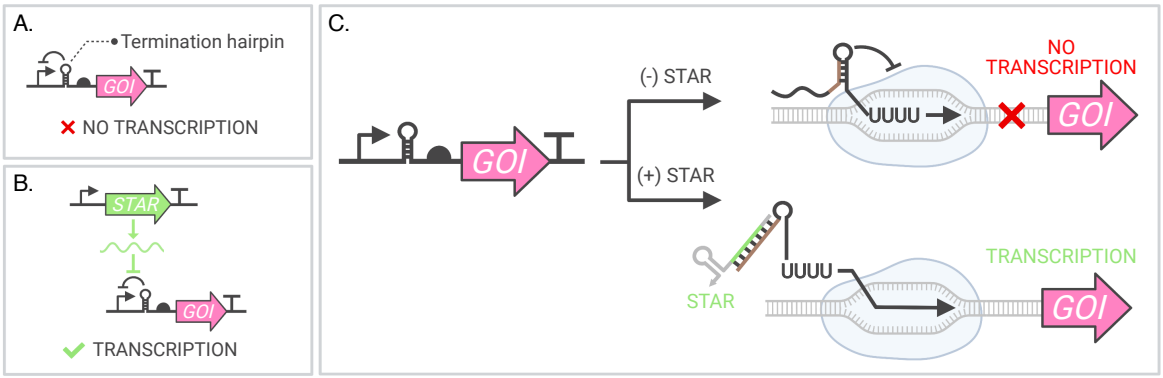


Figure 10: STAR Mechanism. Small transcription activating RNAs (STARs) are a new synthetic biology tool to activate gene transcription. (A) The STAR target is designed to express a strong termination hairpin that blocks transcriptional elongation of the downstream gene. (B) STAR inhibits termination hairpin formation to allow transcription of the gene of interest. (C) When transcribed, STAR binds to the hairpin to prevent formation of the terminator loop, thus allowing RNA Polymerase (RNAP) to transcribe the downstream gene of interest. Figure is adapted from [124]

STAR is a cis-acting RNA mechanism that works by placing a termination hairpin sequence upstream of the gene of interest. As the hairpin sequence is transcribed, it folds into a terminator structure that prevents transcription elongation. When STAR, a short RNA sequence is expressed, it binds to the termination hairpin, preventing formation of the terminator, thus allowing for the downstream gene to be transcribed. STAR has been improved by predicting the link between STAR sequence and function to improve its fold-activation range as well as designing orthogonal STAR-Target pairs as the RNA-RNA interaction of STAR is entirely sequence specific [168, 169, 130, 170].

STAR has since been used to build incoherent feedforward control loops [171]. It has also been used to modulate the strength of stress responsive promoters [172]. Finally it was used in combination with sRNAs to modulate the expression of a downstream gene [173]. In this design, STAR was sequestered by an antisense RNA to deactivate GOI expression, while another antisense RNA targeting the GOI further turned OFF GOI expression.

1.4.3 Summary of host-aware strategies to control coculture composition

Previous work by Gupta et al. has shown that the AI-1 quorum sensing transcriptional activators are very sensitive to low concentrations of AI-1 molecules [113]. As a result, they were able to integrate the different quorum sensing components into the genome, such that their expression did not cause cellular burden and slowed down the growth rate of their strain. So, I decided to use quorum sensing to convey information about strain densities and use this information to compute coculture ratio *in vivo* without causing substantial burden to the host (Figure 11).

While communication between strains can be implemented using quorum sensing without causing a lot of burden, the difference between those quorum sensing signals can also be computed without using proteins. A STAR-based sequestration mechanism can be used

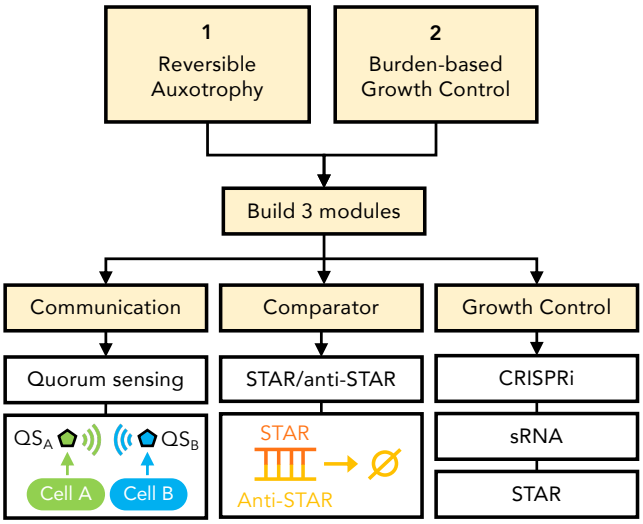


Figure 11: Strategies for building a host-aware coculture composition controller. Approaches for building a composition controller rely on two growth regulation mechanisms: (1) reversible auxotrophy and a (2) burden-based approach. Both approaches rely on building three essential modules: the communication, the comparator and the growth control modules. In the communication module, quorum sensing will convey information to all agents about the population size of each strain grown in the coculture. In the comparator module, STAR and anti-STAR will be used to measure the difference of population density between the different coculture species and activate the growth control module as needed to stabilise composition. With the reversible auxotrophy strategy, the comparator will express RNA-based repressors to down-regulate amino acid production. With the burden-based growth control strategy, the comparator controls expression of the GOI and its burden to modulate cell growth.

to measure the difference between the two quorum sensing signals, thus comparing the population sizes of both *E. coli* populations (Figure 11).

Based on the above sections, I also identified two approaches to control cellular growth rates using RNA-based regulators. First, RNA-based repressors could be used to reduce growth rate by creating essential gene knockdowns. For example, they could downregulate the expression of a gene essential for the production of amino acids, thus causing a reduction in growth rate. The second approach would rely on directly modulating the expression of the GOI or metabolic pathway producing the compound of interest. Varying gene expression will pull and free cellular resources that are essential for cell growth, thus providing a way to up- or down-regulate the host growth rate (Figure 11).

1.5 Aims and objectives

Microbial consortia present themselves as a promising production platform for synthetic biology and metabolic engineering to reduce burden on the hosts and focus on engineering specialised species working together to produce high-value products. Syntrophy remains the gold standard for building microbial consortia. While in syntrophic relationships, coculture composition is set by the inherent properties of the cross-feeding involved, controlling coculture composition using genetic circuits is still a challenge. The circuits often cause too much burden to enable their wide adoption for implementing division of labour strategies. The aim of this PhD project was, therefore, to rationally design a microbial consortia that could maintain its composition over time while minimising the impact of the controller on its hosts by using RNA-based circuits in *E. coli*.

Objective 1: Design a novel STAR-based comparator that computes the difference between two input signals. Show that the comparator can compare bacterial population density to an inducible reference signal to produce an activating signal that will subsequently be used to control the cell density of each strain. Explore the tunability of the comparator and its impact on its host in a context of building host-aware genetic circuits.

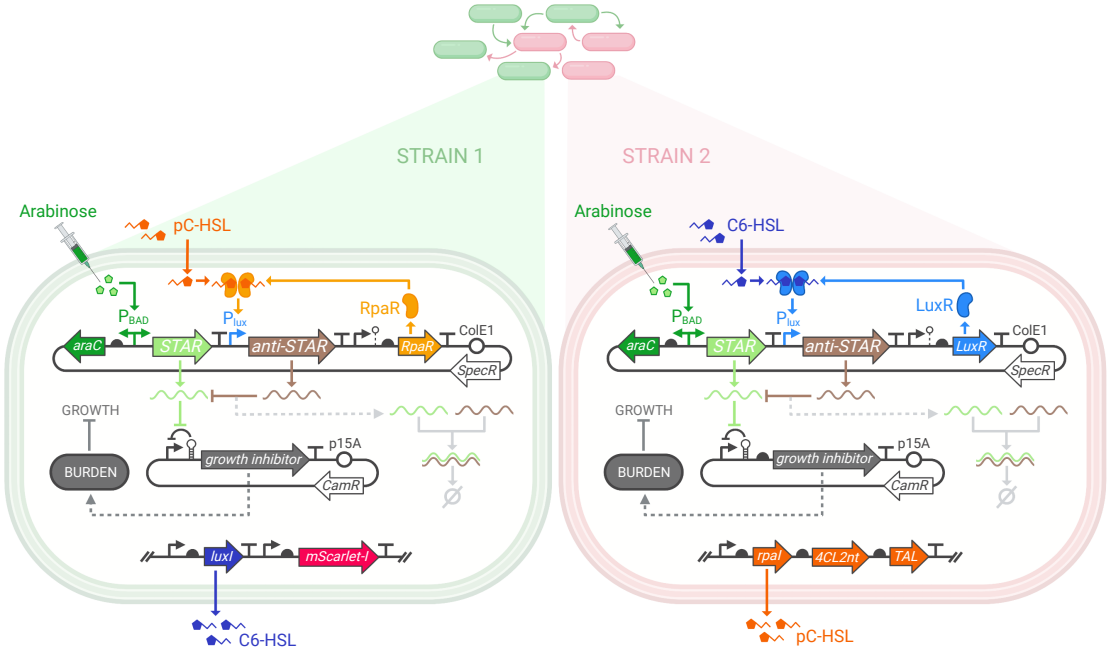


Figure 12: Proposed two-member coculture architecture for controlling community composition. The different versions of our growth control circuits are composed of three modules. (1) First, each bacterial population produces a different quorum sensing molecule (e.g. C6-HSL, pC-HSL) that reflects populations densities and that can be detected by the other population. (2) A synthetic RNA (anti-STAR) is produced upon detection of quorum molecules in each population and is compared to a reference signal (STAR) that is the same in both populations. STAR and anti-STAR preferably form an inactive complex, however if there is more STAR than anti-STAR, then STAR will activate a growth module that slows down cell growth.

Objective 2: Establish a modular two-way communication channel between two *E. coli* strains. For this, design a library of quorum sensing producing strains and comparator plasmids that, in different combination, can modulate the signal that is then given to the STAR-based comparator system to estimate the difference between population sizes. Characterise the transcriptional expression profile of the quorum sensing systems for use in combination with the RNA-based comparator.

Objective 3: Link the output of the STAR-based comparator to a growth module that controls bacterial growth rate. The growth regulation mechanism should use a minimal amount of host resources and be easily tunable through sensing quorum sensing gradients.

Objective 4: Combine the three modules built throughout the previous objectives: the communication, comparator and growth modules to stabilise the ratio of a two-*E. coli* strain coculture (Figure 12). Explore the parameters that can tune coculture composition, and test coculture behaviour in batch and continuous cultures.

1.6 Publications resulting from this work

- Alice Boo, Rodrigo Ledesma Amaro and Guy-Bart Stan."Burden-driven multicellular control for microbial consortia", Manuscript in preparation, 2022.
- Eliza Atkinson, Huadong Peng, Alice Boo, Guy-Bart Stan and Rodrigo Ledesma-Amaro. "Principles, Tools and Applications of Synthetic Consortia towards Microbiome Engineering.", To appear in *Principles in Microbiome Engineering*, 1st ed. Matthew Chang, Ed. Weinheim: Wiley-VCH, 2022.
- Alice Boo, Rodrigo Ledesma Amaro and Guy-Bart Stan. "Quorum sensing in synthetic biology: A review", *Current Opinion in Systems Biology*, vol. 28, p. 100378, 2021.
- Alice Boo, Tom Ellis and Guy-Bart Stan. "Host-aware synthetic biology", *Current Opinion in Systems Biology*, vol. 14, p. 66–72, 2019.

Chapter 2

Engineering a RNA-based Comparator

Contents

2.1 Introduction 31

2.2 Results and discussion 32

2.2.1 Choosing the Optimal STAR sequence 32

2.2.2 Building the first STAR-based comparator 35

2.2.3 Optimising the fold repression of the STAR-based comparator 40

2.2.4 Characterisation the final STAR-based comparator design 50

2.3 Conclusions 57

2.1 Introduction

In the introduction (Section 1.5), I have proposed a circuit that enables the stabilisation of the ratio between two bacterial species grown together in a co-culture. The design relies on the use of a "comparator" that allows each strain to compare its competitor strain density to a reference signal. If the ratio between the strain density signal and the reference signal is less than 1, that is if the strain density signal is less than the reference signal, then an output signal needs to actuate a downstream regulation cascade to re-balance the co-culture composition. The strength of that output signal will vary depending of the ratio between the signal of interest and the reference signal. This logic module is the core of the circuit, linking information about population density to a growth regulation mechanism that will balance the composition of the co-culture over time. As this module is essential to bringing

all the aspects our genetic design together, I present its development in this chapter.

As I wanted to design a system that would use the least amount of cellular resources, I chose to build the comparator module with RNA elements as their expression would minimise pulling away translation resources from the host, and thus causing burden [8]. The easiest implementation of a comparator is through a sequestration-based mechanism. The STAR (Small Transcriptional Activating RNA) system from Chappell et al. is able to achieve over 900-fold activation, much higher than any other RNA-based regulation mechanism described in the literature [130]. The large fold activation property of the system made it very attractive to use in the implementation of a activating sequestration-based mechanism.

In this chapter, I investigate how to build a STAR-based sequestration mechanism to implement the comparator module. First, I investigate how to build a STAR sequestration mechanism while not severely impacting the fold activation of the STAR mechanism. I also explore how to reduce the leakiness of the comparator using toehold domains for strand displacement. Finally, I examine how to tune the sensitivity of the comparator module to match different quorum sensing inputs. Looking into these different properties allowed us to evaluate the modularity of the design for future use in different circuits, genetic contexts and culture conditions.

2.2 Results and discussion

2.2.1 Choosing the Optimal STAR sequence

Before exploring strategies to build a STAR-based comparator, I needed to verify that the new STAR designs from Chappell et al. were working in our strain [130]. I also decided to verify the impact of STAR expression on cell growth and on cell capacity. To do so, I used the DH10B-GFP capacity monitor strain ("WT" in Figure 13.A) from Ceroni et al. to measure the rate of production of GFP per cell, a measure reflecting the resource availability of the cell at a given time [8].

I decided to test three STAR sequences from Chappell et al. [130]. In their paper, they

described STAR 5 as a low-strength activating RNA, STAR 8 as a medium-strength activating RNA and finally STAR 6 as a high-strength activating RNA. All the STAR sequences used in this project are reported in Appendix 8.1. All the STAR sequences are paired

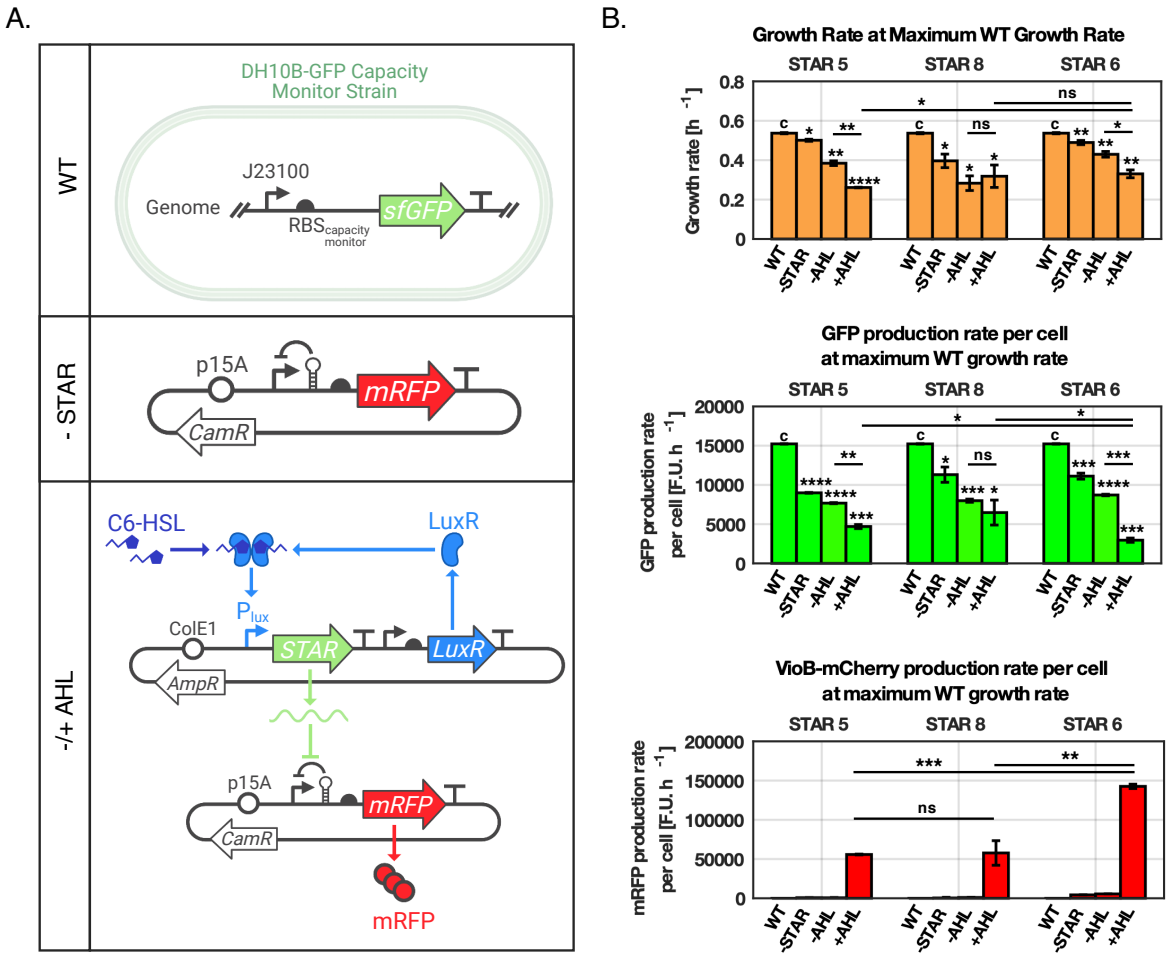


Figure 13: Testing the different STAR sequences from the Lucks Lab in DH10B-GFP. (A) Graphical representation of the different genetic circuits and conditions used in (B). The DH10B-GFP capacity monitor strains is used to evaluate the burden caused by the expression of the different STAR designs. The different STAR designs are under the control of the *lux* promoter activated in the presence of LuxR and C6-HSL. STARs bind to their cognate STAR target to activate expression of mRFP. (B) Bar graphs of the growth rate, GFP production rate per cell and mRFP production rate per cell taken at the time of maximum growth rate of the WT for the different STAR/STAR target pairs from Chappell et al. [130]. "-AHL" and "+AHL" refer to the external addition of 0 M and $10^{-}7$ M of C6-HSL inducer respectively. Experiments were carried in in DH10B-GFP. Data in represent the mean values of n = 3 biological replicates ± s.d. Statistically significant differences were determined against the wild-type (WT) control using two-tailed Student's t-test (**** represents p<0.0001, *** represents p<0.001, ** represents p<0.01, * represents p<0.1, ns represents not significant).

with a STAR target sequence, which once transcribed forms a termination hairpin in the absence of STAR. All anti-STAR sequences used in this project are reported in Appendix 8.2.

The WT capacity monitor strain (Figure 13.A) was chosen to represent the maximum capacity of the system, that is the maximum amount of resources that the cell can offer for expressing a gene in the absence of any heterologous gene circuit. The WT capacity monitor strain also sets the maximum growth rate achievable by the strain, as the absence of gene circuit signifies that all of the cell's resources can be dedicated to the production of biomass. The STAR system requires the expression of the STAR sequence from a high-copy plasmid. The target STAR sequence followed by the gene of interest should be placed on a medium-copy plasmid or lower to provide the best fold activation as possible [130]. I tested three STAR/STAR target designs from Chappell et al. to confirm that they could activate gene expression in our DH10B-GFP capacity monitor strain (Figure 13) [130]. The different STAR sequences were expressed in the presence of both LuxR, constitutively expressed from the P_{tet} promoter, and C6-HSL. First, I only transformed the STAR target plasmids in DH10B-GFP ("-STAR" in Figure 13.A). I found that though mRFP expression was not activated as no cognate STAR was present, GFP capacity of the cell was reduced up to 50% for the STAR 5 target plasmid. I will be discussing the impact of the STAR system on cell viability later in Section 2.2.4.2. By co-transforming each STAR plasmid with its corresponding STAR target mRFP plasmid, I confirmed that STAR 6 provided the highest level of mRFP expression (Figure 13.B) as described by Chappell et al. [130]. Despite producing mRFP at the highest rate, the fold change between non-induction (-AHL) and induction (+AHL) with 3OC6-HSL was lower with STAR 6 than with STAR 5 or 8: the fold change in mRFP production rate per cell of STAR 6 being 25-fold against 86-fold for STAR 5 and 56-fold for STAR 8.

I compared the total amount of mRFP produced after 10 hours of both STAR 5 and STAR 6 which exhibited the best and the worst fold change in mRFP production rate per cell out of the three STAR sequences tested (Figure 14). The total amount of mRFP produced using the STAR 6 sequence (Figure 14.B) was more than 3-times higher than that produced using STAR 5 (Figure 14.A). Despite STAR 6 having the lowest fold change in mRFP production rate per cell, it produced a higher yield of gene of interest (GOI) than the other 2 sequences.

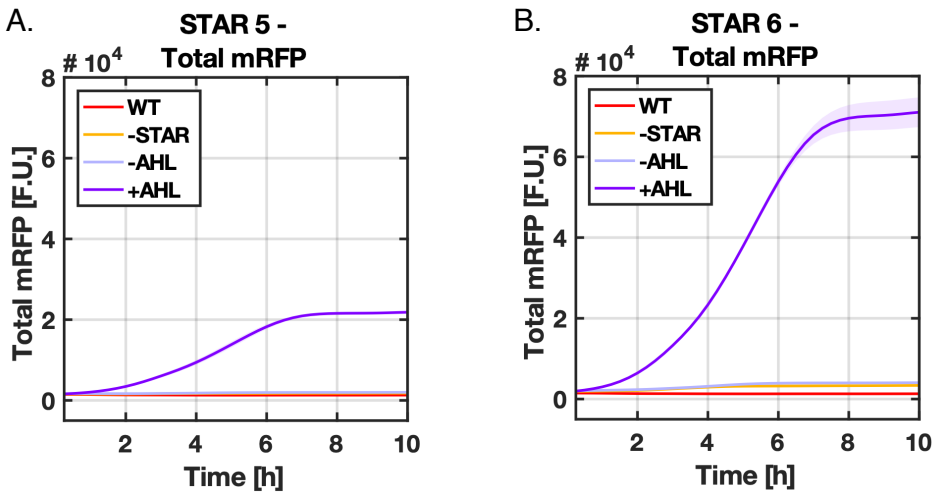


Figure 14: Total mRFP yield obtained when using the STAR 5 and STAR 6 STAR/STAR target sequences. (A) Total mRFP measured per well over time when mRFP is controlled by the STAR/STAR target 5 pair. (B) Total mRFP measured per well over time when mRFP is controlled by the STAR/STAR target 6 pair. Experiments were carried in in DH10B-GFP. Data represent the mean values of n = 3 biological replicates ± s.d.

As the goal was to build a coculture suitable for metabolic engineering applications, the STAR 6 design was selected for its high yield property to build a universal comparator aimed at regulating the expression of a burdensome heterologous protein. If yield would not be the main focus of the co-culture, STAR 5 could provide a tighter regulating option, perhaps for the expression of a species imposing high burden or toxicity.

2.2.2 Building the first STAR-based comparator

Using the STAR 6 design selected in the previous section for its high ON state property, I designed a sequestration mechanism to determine whether STAR 6 could be sequestered to stop transcription of a target gene.

One way to sequester STAR 6 is through the expression of its complementary sequence, which I call anti-STAR. If STAR and anti-STAR are bound into a double stranded RNA complex, STAR would have limited capacity to bind to its cognate STAR target. However, the hybridisation energy between STAR 6 and the STAR 6 Target was -121.2 kcal/mol while that of STAR 6 and anti-STAR was -120.6 kcal/mol (Table 2.1). As the hybridisation ener-

gies between the two complexes were very similar, I decided to use a toehold to favour the formation of the STAR:anti-STAR complex over the formation of the STAR:STAR-target complex. Toeholds have also been used *in vivo* to trigger RNA-RNA strand displacement reactions [174]. Placing a toehold domain on STAR and anti-STAR could trigger the displacement of STAR by anti-STAR when STAR is bound to the linear region on the STAR target. The strand displacement reaction would as a result act in favour of the formation of the STAR:anti-STAR complex over STAR:STAR-target complex. The toehold, referred as "Toehold 0", was selected based on the AND gate design of Chappell et al. such that the difference of hybridisation energy between the STAR:anti-STAR complex and the STAR:STAR-target complex was 28.6 kcal/mol in favour of the STAR:anti-STAR complex (Table 2.1) [130].

Table 2.1: Hydridisation energies of the original comparator design. Hybridisation energies were calculated with the IntaRNA software [175]

STAR	**Anti-STAR**	**STAR Target**	**Hybridisation Energy**
STAR6	anti-STAR6	—	-120.6 kcal/mol
STAR6	—	STAR Target 6	-121.2 kcal/mol
STAR6_toehold0	anti-STAR6_toehold0	—	-150.4 kcal/mol
STAR6_toehold0	—	STAR Target 6	-121.8 kcal/mol

First, in Figure 15.A, I tested that STAR followed by Toehold 0 could still activate mRFP expression. I placed the new STAR design with Toehold 0 under the control of the inducible pLux promoter and varied the concentration of 3OC6-HSL. The fold activation of the system was 15-fold, compared to 25-fold in Figure 13.B. Despite a 40% decrease in fold activation, STAR 6 with Toehold 0 could still activate mRFP production in DH10B-GFP. I then verified that anti-STAR cannot interact with the STAR target to cause activation of downstream gene transcription. For this, I placed anti-STAR under the control of pLux and varied its expression level by supplementing the media with a range of 3OC6-HSL concentrations. As expected, anti-STAR could not activate mRFP production (Figure 15.B). Finally, by placing both STAR and anti-STAR under the same inducible promoter, I characterised the leakage of mRFP production due to unsequestered STAR in the system (Figure 15.C). Though mRFP production could not be completely inhibited by anti-STAR expression, it was significantly reduced from 15-fold to 2.6-fold activation. I thus verified that it is possible to control the expression of a gene of interest, here mRFP, by sequestration

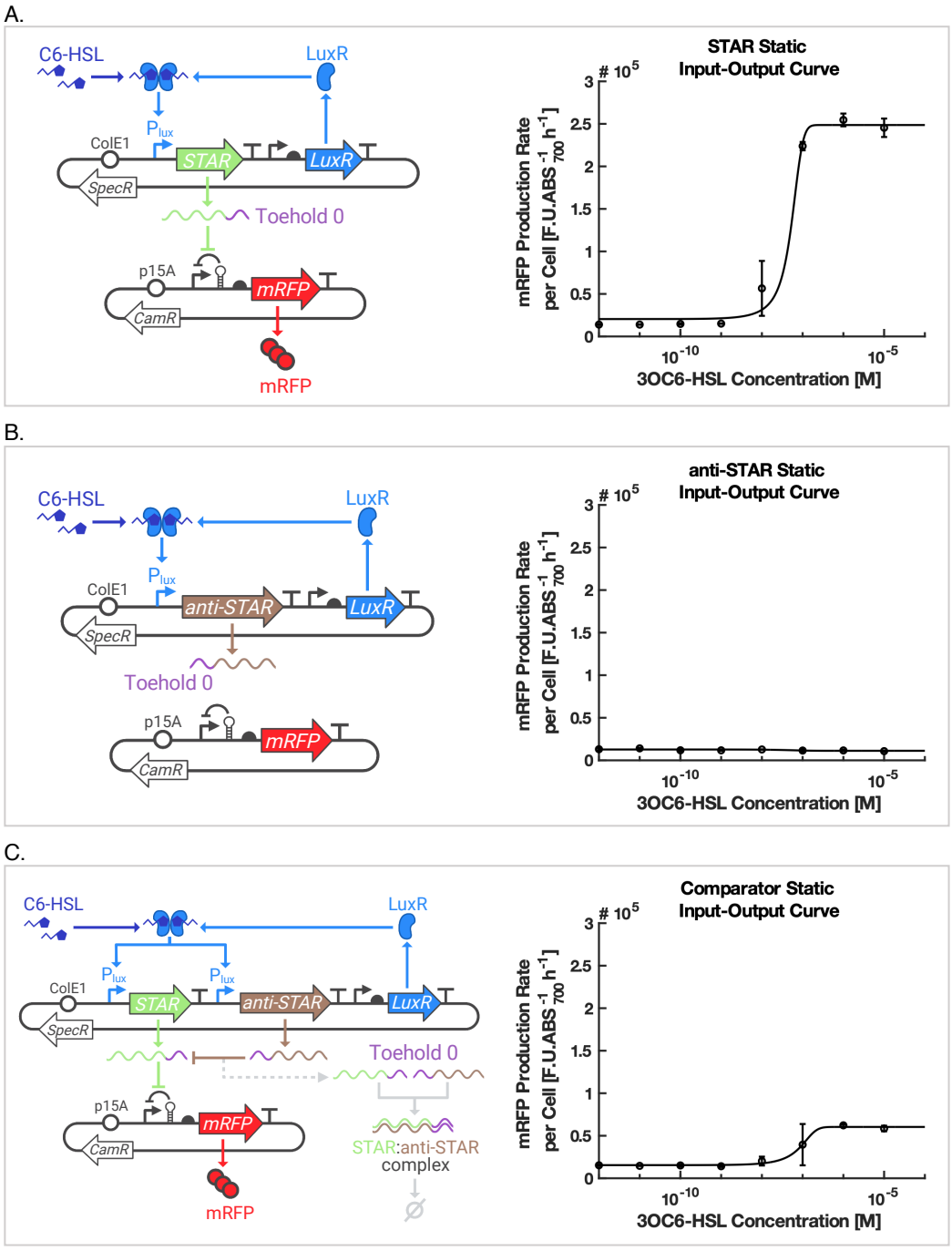


Figure 15: Characterisation of the first comparator design. (A) Activation of mRFP production by STAR as a function of 3OC6-HSL concentration. As 3OC6-HSL concentration increases, more STAR is produced leading to an increase of mRFP production rate per cell. (B) Control circuit checking that anti-STAR does not activate mRFP production as 3OC6-HSL concentration increases. (C) STAR:Anti-STAR sequestration efficiency to downregulated mRFP production rate per cell when 3OC6-HSL concentration increases. Experiments were carried in in DH10B-GFP. Data represent the mean values of n = 3 biological replicates ± s.d. Curves were fitted using MATLAB four-parameter nonlinear regression fit.

of two RNA inputs based on the STAR design presented in Figure 15.C.

To compare the strength of two different input signals, I designed a system (Figure 16.A) in which STAR was placed under a constitutive promoter such that a constant amount of STAR would be produced into the system, activating the expression of mRFP. Anti-STAR on the other hand is placed under the control of the inducible quorum-sensing promoter pLux. As the strength of the quorum sensing signal increases, a larger portion of STAR is sequestered, hence the subtraction of both signals leads to a change in the output expression of STAR. As more anti-STAR is present in the system, the output will reflect the difference between the two signals. In Figure 16.C-D, I see that increasing 3OC6-HSL concentration leads to a greater sequestration of STAR, hence decreasing the mRFP output signal in two different *E. coli* strains.

Despite enabling an output change when the strength difference between two input signals increases, I notice that the comparator is not very efficient at turning down gene expression. In Figure 16.B, I compared the mRFP production rate per cell when STAR is expressed under the J23100 promoter or under the maximally induced pLux promoter. mRFP production rate per cell is significantly higher when STAR is expressed by pLux than by J23100. Hence in the comparator design, I would expect significantly more anti-STAR to be produced than STAR in the system when pLux is maximally induced. Despite the mRFP output signal decreasing by around 60% in both DH10B and BW25113, some mRFP is still produced when anti-STAR is maximally expressed under pLux. In the following sections, I will explore how to improve the fold deactivation of the comparator in order to build a more sensitive and modular comparator.

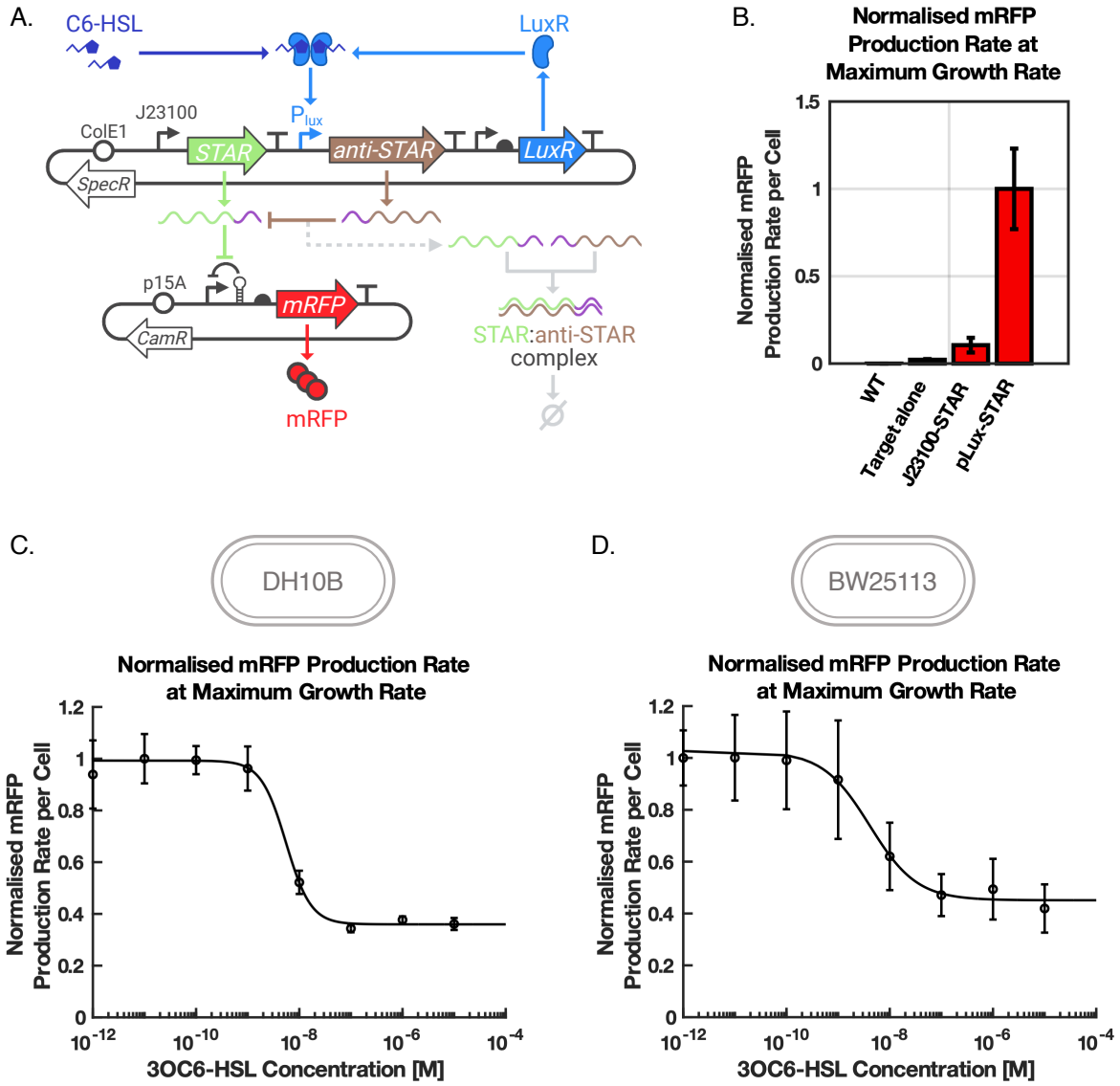


Figure 16: Characterisation of the first J23100 comparator design in DH10B and BW25113. (A) STAR is constitutively expressed under the strong J23100 promoter, while anti-STAR concentration depends on 3OC6-HSL concentration externally provided to the system. As anti-STAR concentration increases, more STAR is sequestered leading to the down-regulation of mRFP. (B) Bar graph represents the normalised mRFP production rate per cell of four conditions. (1) "WT": BW25113 not carrying either the STAR or the mRFP plasmid. (2) "Target alone": BW25113 carrying only the mRFP plasmid from Panel A. (3) "J23100-STAR": BW25113 carrying the mRFP plasmid as well as a plasmid expressing STAR under the J23100 promoter. (4) "pLux-STAR": BW25113 carrying the mRFP plasmid as well as a plasmid expressing STAR under the pLux promoter. Cells were induced with 10^{-7}M of 3OC6-HSL. (C) Characterisation of the J23100-pLux comparator in DH10B. (D) Characterisation of the J23100-pLux comparator in BW25113. Data represent the mean values of n = 3 biological replicates ± s.d. Curves were fitted using MATLAB four-parameter nonlinear regression fit.

2.2.3 Optimising the fold repression of the STAR-based comparator

I have shown that STAR and anti-STAR can be sequestered to report a change between two inputs' strength. I now explore different mechanisms to improve the STAR and anti-STAR binding dynamics.

2.2.3.1 STAR Target Deoptimisation

A first strategy to improve the sequestration of STAR by anti-STAR is to reduce the hybridisation energy between STAR and its target sequence compared than that of STAR and anti-STAR. As a result, STAR should preferentially bind to anti-STAR instead of its target, hence prioritising STAR deactivation by anti-STAR rather than STAR activation of the output gene. I hypothesised that prioritising the formation of the STAR:anti-STAR complex over the STAR:target complex would decrease the OFF state of the comparator.

To reduce the hybridisation energy of STAR to its STAR target, I rationally introduced mutations into the STAR target (Figure 17.A). The mutations were introduced to form a hairpin in the linear binding region of the target, which is the region where STAR binds to unfold the STAR target termination loop. The theoretical new hairpins were visualised using NUPACK [176] in Figure 17.B-D, and the hybridisation energy of the different complexes were calculated using IntaRNA [175] in Figure 17.E. According to the IntaRNA results, introducing the mutations in the target effectively reduced the hybridisation energy of STAR with the STAR target. To verify whether the mutated targets would still work and reduce the leakiness of the STAR comparator, I constructed plasmids carrying the two versions of the mutated STAR target and tested them with the J23100-pLux comparator from Figure 16.A.

Characterisation results of the different STAR Targets are shown in Figure 18.B. First, I observe that the deoptimised STAR Target v1 lost its termination functionality. The introduction of the hairpin in Target v1 appears to have disrupted the formation of the termination loop, leading to high and noisy expression of mRFP. Anti-STAR does not appear to have any effect on turning down mRFP expression in this system. On the other

A.

>Original STAR 6 Target

CCAGTCATCAAGTCAGTCCAGTCAAAGTTTCCGTCGTTCAGCGGGGAATGTATACAGTTCATGTATATATTCCCCGCTTTTTTTTT

>Deoptimised STAR 6 Target v1

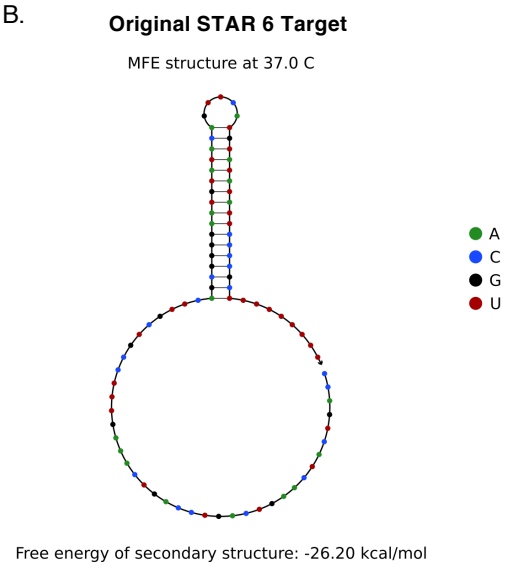
CCAGTCATCAAGTCAGTCCAGTCAAAGTTTCCGTGGTTCAGCGGGGAATGTATACAGTTCATGTATATATTCCCCGCTTTTTTTTT

>Deoptimised STAR 6 Target v2

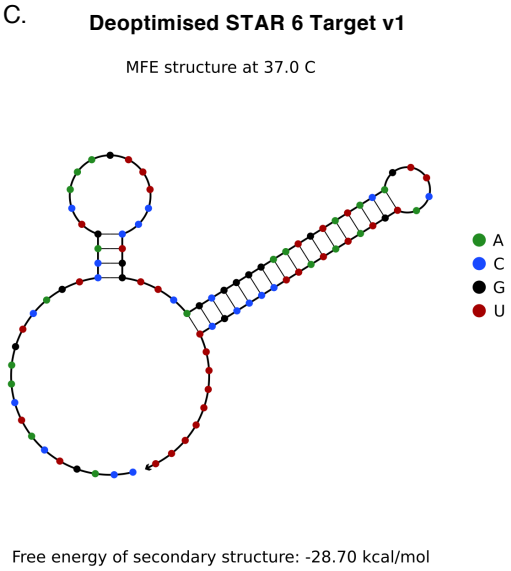
CCAGTCATCTGGTCAGTCCAGTCAAAGTTTCCGTCGTTCAGCGGGGAATGTATACAGTTCATGTATATATTCCCCGCTTTTTTTTT

Linear Binding Sequence | Mutation | Stem and Loop Binding Sequence | Loop | Target Loop

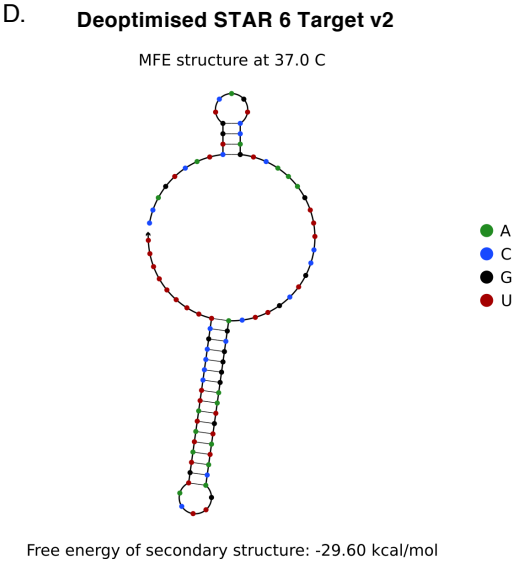
B.



C.



D.



E.

Complex		Hybridisation Energy (kcal/mol)
STAR 6	Original STAR 6 Target	-121.2
STAR 6	anti-STAR 6	-120.6
STAR 6 Toehold 0	Original STAR 6 Target	-121.8
STAR 6 Toehold 0	Deoptimised STAR 6 Target v1	-111.4
STAR 6 Toehold 0	Deoptimised STAR 6 Target v2	-116.4
STAR 6 Toehold 0	anti-STAR 6 Toehold 0	-150.4

Figure 17: Designing deoptimised STAR targets. (A) DNA sequences of the original STAR 6 Target and of the two deoptimised STAR 6 Targets. (B-D) STAR Target RNA structures generated with NUPACK [176]. (E) Hybridisation Energy of the different STAR:anti-STAR and STAR:target complexes calculated using the IntaRNA software [175].

hand, deoptimised STAR Target v2 appears to have retained its transcriptional termination property. In the ON state, both the original STAR target and deoptimised v2 STAR target have similar mRFP expression levels. However, deoptimisation of target v2 did not improve the OFF state of the system as the mRFP expression of the deoptimised v2 target was not significantly reduced compared to the original STAR target.

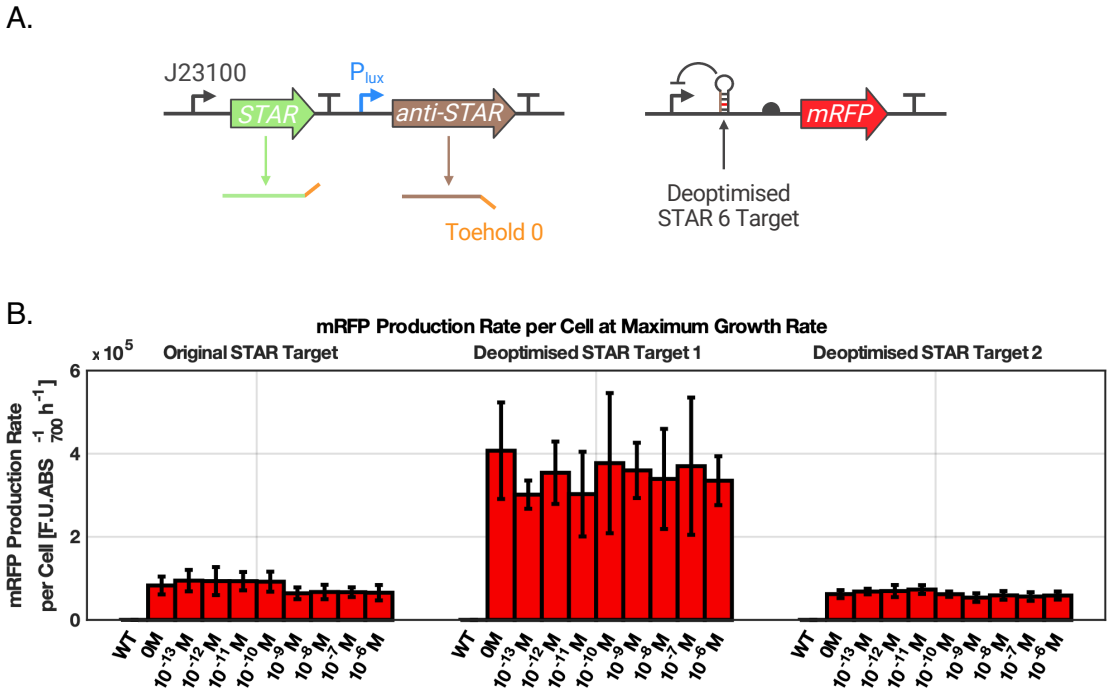


Figure 18: Effect of the deoptimised STAR targets on the comparator OFF state. (A) Diagram of the J23100-pLux comparator with the mRFP output plasmid carrying the mutated versions of the STAR Target. STAR and anti-STAR are both equipped with Toehold 0. (B) Bar graph showing the mRFP production rate per cell in BW25113 for the J23100-pLux comparator combined with the different STAR Targets for different concentrations of 3OC6-HSL. Data represent the mean values of n = 3 biological replicates ± s.d.

Introducing mutations in the STAR Target did not grant better OFF properties to the comparator design. Instead it destabilised the formation of the transcriptional termination loop that is required to ensure the well functioning of the STAR mechanism. Therefore, I will not be using deoptimisation of the STAR target as a strategy to further improve the dynamics of the STAR-based comparator.

2.2.3.2 STAR Target Doubling

Introducing mutations in the STAR target to reduce the hybridisation energy between STAR and the target did not have a significant effect on reducing the OFF state of the STAR-based comparator. Another strategy to reduce the leakiness level of the comparator is to put two STAR targets in series. Downstream gene expression can only occur if two STARs are bound to the two targets at the same time, acting similarly to a cooperative activation mechanism (Figures 19.A and C).

First I characterised the behaviour of the double-STAR target compared to the original system using only one STAR target. I placed STAR under the control of pLux and monitored the activation of mRFP expression controlled by either one or two STAR targets as the concentration of 3OC6-HSL increases (Figure 19.A). In Figure 19.B, I observe that the double STAR-target reduced both the basal expression and the maximum expression of mRFP compared to the single STAR target. At maximum growth rate, the fold activation of mRFP production rate per cell increased from 44-fold with the single STAR target to 254-fold with the double STAR target. Hence using two STAR target in series significantly reduces the basal expression of the STAR system.

I then tested the double STAR target system with the STAR-based comparator from Figure 16.A (Figure 19.C). I observe in Figure 19.D that the fold repression of the comparator with single STAR target is 0.95-fold while that of the double STAR target is 10-fold. Though the fold repression is significantly improved by the double STAR target, it is done at the cost of drastically reducing the maximum expression of mRFP. One of the aims of our coculture is to be applicable for metabolic engineering production purposes. This often requires high expression of a gene of interest, which will be difficult to achieve using the double STAR target. As a result, I will not be using the double STAR target design further as I would like our coculture to retain a high production capability. However, if the gene of interest is very toxic or very potent, thus requiring a tight regulation mechanism, then the double STAR target will likely be able to provide such a tight regulation property.

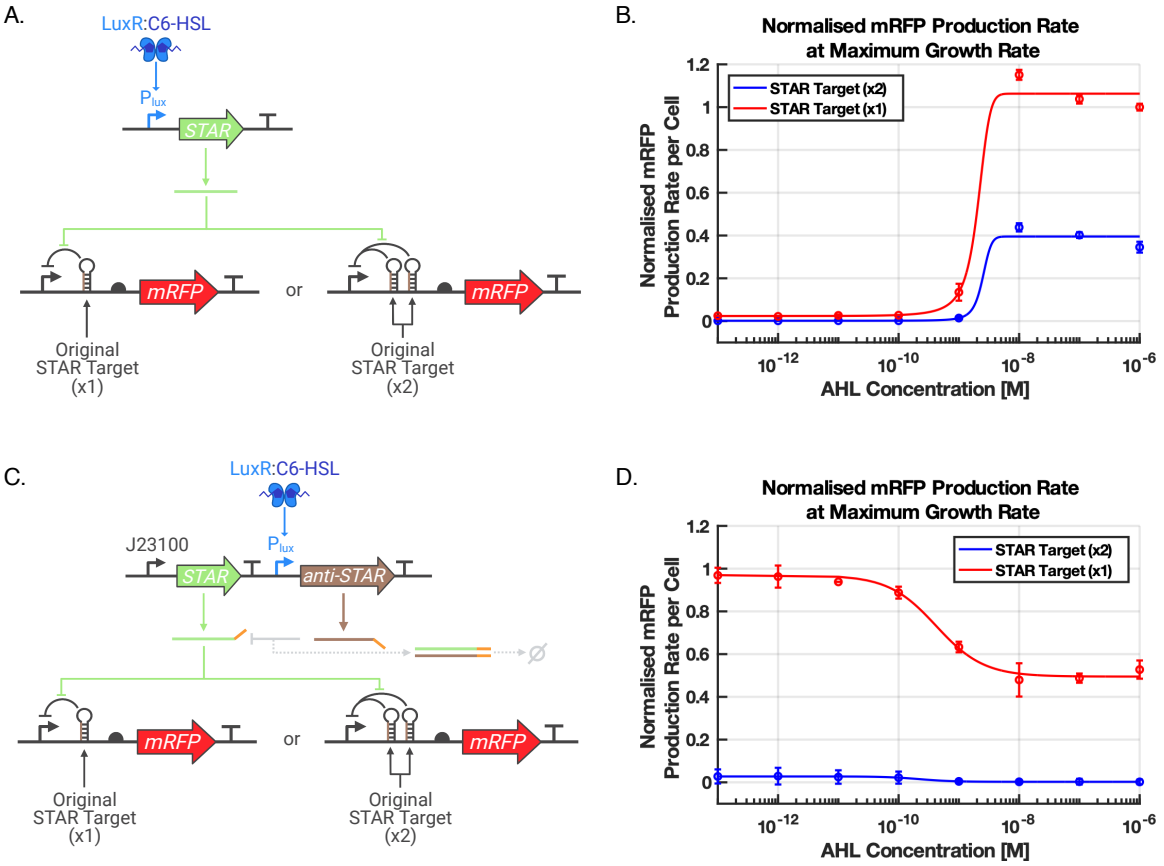


Figure 19: Effect of STAR-double-target. (A) Diagram of circuit used to characterise the effect of the STAR-double-target on mRFP expression. (B) Normalised mRFP production rate per cell as a function of 3OC6-HSL concentration when the gene of interest (*mRFP1*) is controlled by either a single-STAR target or a double STAR target. (C) Diagram of circuit used to characterise the effect of the STAR-double-target on the behaviour of the STAR-based comparator. (D) Normalised mRFP production rate per cell as a function of 3OC6-HSL concentration when the STAR-based comparator's gene of interest (*mRFP1*) is controlled by either a single-STAR target or a double-STAR target. Experiments were carried in BW25113. Data represent the mean values of n = 3 biological replicates ± s.d. Curves were fitted using MATLAB four-parameter nonlinear regression fit.

2.2.3.3 Toehold Library

I have shown that using two STAR targets in series improves fold repression at the cost of reducing the maximum production rate of a gene of interest. I now look at constructing a small toehold library to test whether different RNA toeholds can improve the fold deactivation of the STAR-based comparator without excessively compromising on its maximum production property. Toeholds would improve the fold deactivation of the comparator by mediating RNA-RNA strand displacement reactions between STAR and anti-STAR when STAR is bound to STAR target.

In Green et al., the authors forward engineered toehold switches and characterised their ON/OFF properties in *E. coli* [174]. I decided to use the toehold sequences of the five toehold switches with the best ON/OFF ratio from [174]. Using NUPACK, I verified that the addition of the toehold would not create one or multiple hairpins in the linear binding region of STAR, which would prevent STAR from binding properly to the STAR target and could cause a significant decrease of the maximum ON property of the comparator. NUPACK RNA folding predictions are available in Appendix 8.4.

I built new versions of STAR and anti-STAR carrying these toehold sequences (Figure 20.A). I compared the behaviour of the new STAR-based comparators to the original version carrying Toehold 0 (Figure 20.C-D). In Figure 20.B, I compared the effect of the different toehold sequences on the ON/OFF property of the comparators. Toehold 0 has 1-fold repression between the uninduced and induced AHL condition while Toehold 2 and 5 have a 2.5-fold and 2.2-fold repression respectively. I then mapped the response of both Toehold 0 and 2 to 3OC6-HSL concentration in Figure 20.C and that of Toehold 0 and 5 in Figure 20.D. The static input-output response curve of Toehold 2 comparator was more sensitive to 3OC6-HSL concentration than that of Toehold 5, making it a better candidate to sense smaller concentrations of quorum sensing molecules in the media.

Looking at the results presented in Figure 20, I conclude that toehold sequences are not only a way of modulating the ON/OFF properties of the STAR-based comparator, but also

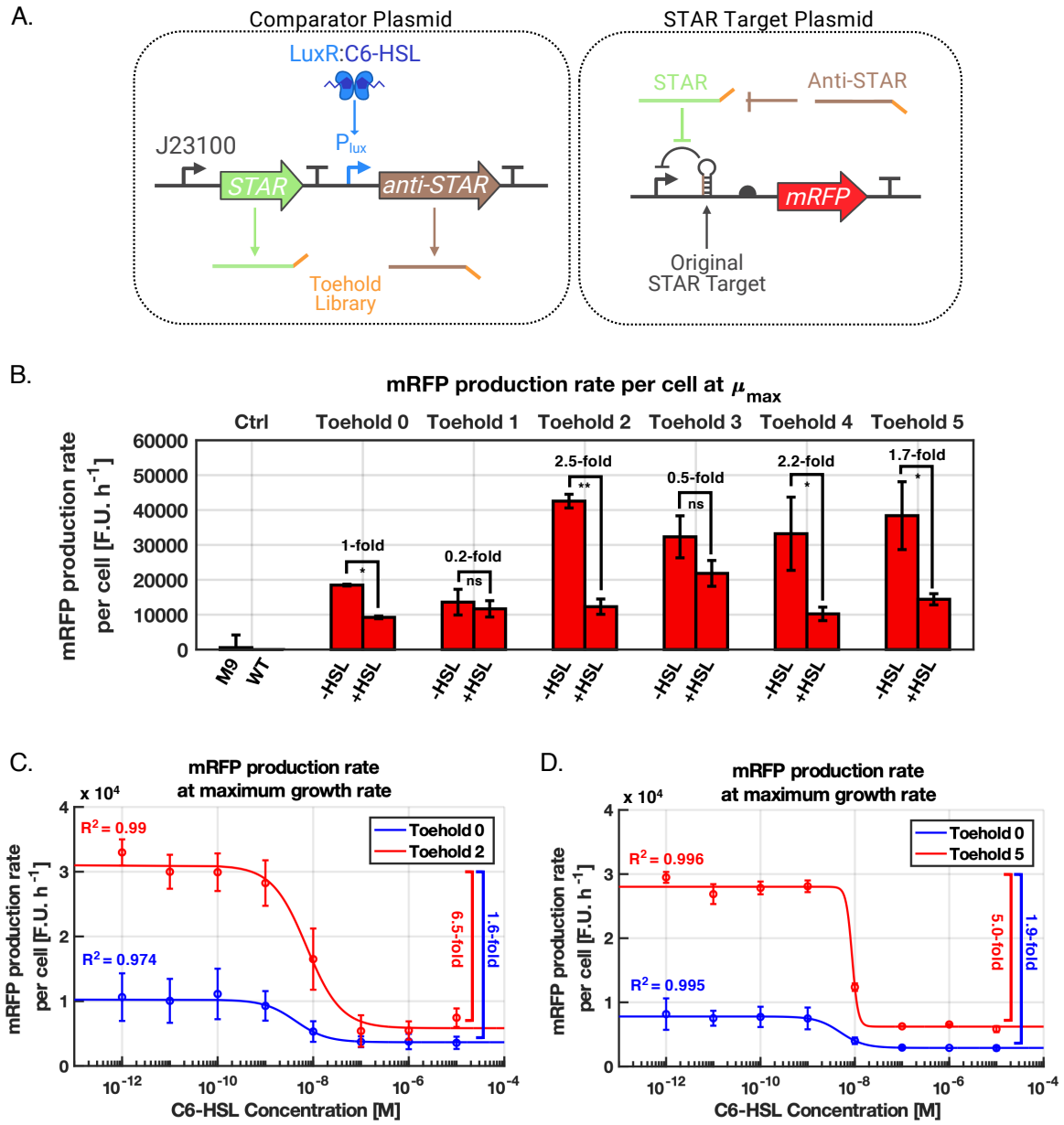


Figure 20: STAR-based comparator toehold library. (A) Diagram of the J23100-pLux STAR-based comparator with the toehold library. Target plasmid carries a single STAR target driving expression of mRFP. (B) Bar graph representing the mRFP production rate of the strains carrying the comparators with the different toeholds. "-AHL" represents a concentration of 0M while "+AHL" represents a concentration of 10^{-7}M of C6-HSL. (C) Toehold 0 and Toehold 2 comparators' normalised mRFP production rate per cell as a function of C6-HSL concentration. (D) Toehold 0 and Toehold 5 comparators' normalised mRFP production rate per cell as a function of C6-HSL concentration. Experiments were carried in BW25113. Data represent the mean values of n = 3 biological replicates ± s.d. Curves were fitted using MATLAB four-parameter nonlinear regression fit. Statistically significant differences were determined using two-tailed Student's t-test (**** represents p<0.0001, *** represents p<0.001, ** represents p<0.01, * represents p<0.1, ns represents not significant).

a way to modulate its sensitivity to an inducible input. So, I decided to further exploit the versatility of toehold domains in subsequent designs of the STAR-based comparator.

2.2.3.4 STAR Titration with inducible promoter

To demonstrate that the reference signal of the STAR-based comparator can be modulated to varying levels, I investigate the comparator's behaviour when STAR expression is driven by an inducible promoter. Changing the promoter driving STAR expression is also a way of reducing the basal and maximum expression of the comparator as less STAR is inherently present in the system to bind to the STAR Target.

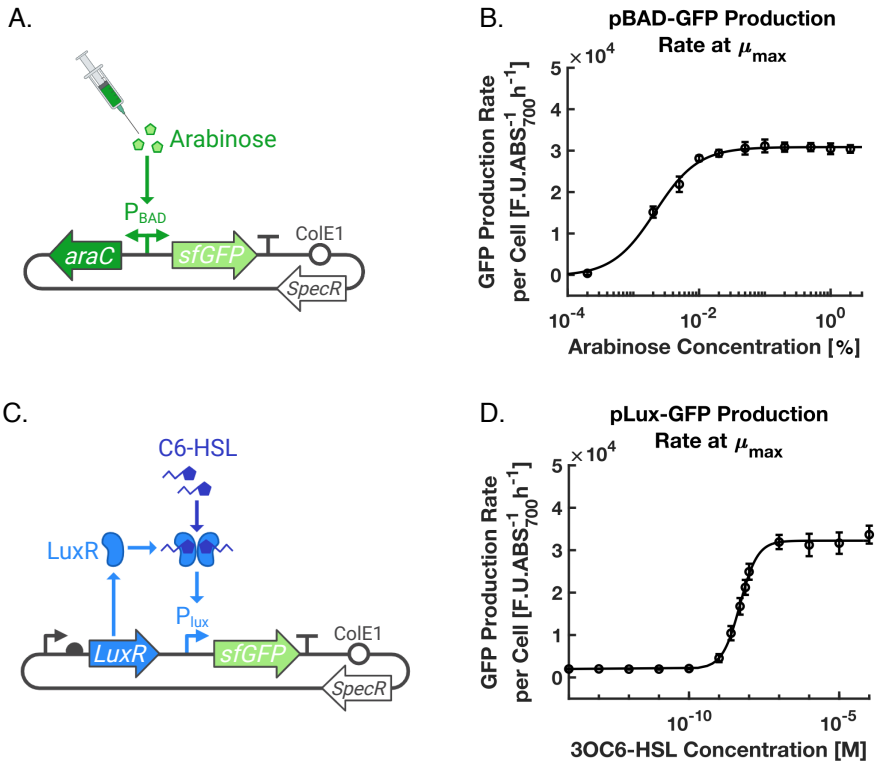


Figure 21: Characterisation of the pBAD and pLux inducible promoters. (A) Diagram of the plasmid used to test the strength of the pBAD promoter by induction with L-arabinose. (B) GFP production rate per cell driven by the pBAD promoter in response to L-arabinose concentration. (C) Diagram of the plasmid used to test the strength of the pLux promoter by induction with 3OC6-HSL. (D) GFP production rate per cell driven by the pLux promoter in response to 3OC6-HSL concentration. Experiment was done in BW25113. Data represent the mean values of n = 3 biological replicates ± s.d. Curves were fitted using MATLAB four-parameter nonlinear regression fit.

I chose two promoters of comparable strength (Figure 21), pBAD and pLux, which I tested using GFP and the same plasmid backbone as used for the comparator plasmid. In Figure 21.B and D I confirm that both promoters have similar basal and maximum GFP expression levels. Ideally, when STAR is maximally induced and anti-STAR is not induced, the comparator would produce its maximum output signal. When both STAR and anti-STAR are maximally induced, the comparator should produce its minimum output signal.

I built a new comparator with pBAD driving the expression of STAR and pLux driving the expression of anti-STAR (Figure 22.A). In Figure 22.B, I confirm that I can upregulate the expression of VioB-mCherry, the gene of interest, as I increase L-arabinose concentration. I will be using VioB-mCherry in Chapter 4 for regulating growth, but I are using it here to study the leakage of anti-STAR expression. VioB-mCherry is a 3.7kb fusion protein whose expression imposes a high expression burden on its host [8]. So as arabinose concentration increases, growth rate and GFP production rate per cell, which is an indicator of available resources in the host, should go down. This is indeed what I observed in Figure 22.A for the "STAR" condition. However, the "STAR" and "[-AHL]" conditions should give similar results as in both these conditions anti-STAR should not be expressed. Looking at the bar graphs, I observe that this is not the case. The "[-AHL]" and "[+AHL]" are a lot more similar to each other than "STAR" and "[-AHL]". I deduce that if growth rate, and GFP capacity increase when anti-STAR is present in the plasmid, it must be because anti-STAR is expressed. I hypothesise that this might be due to the fact that the t500 terminator and spacer that separates the STAR and the anti-STAR transcriptional cassettes are not enough to stop the read-through of RNAP between the two cassettes.

To reduce the read-through from the STAR transcriptional cassette to the anti-STAR transcriptional cassette, I tested two new spacer sequences. The original spacer was used as a comparison benchmark (Buffer 1 in Figure 23). The second spacer was built using a strong double terminator BBa_B1001 and a 306 bp non-coding region, which I obtained from the AND-gate design from Chappell et al., placed between the STAR and anti-STAR transcriptional units (Buffer 2 in Figure 23) [130]. The third spacer consisted of only adding

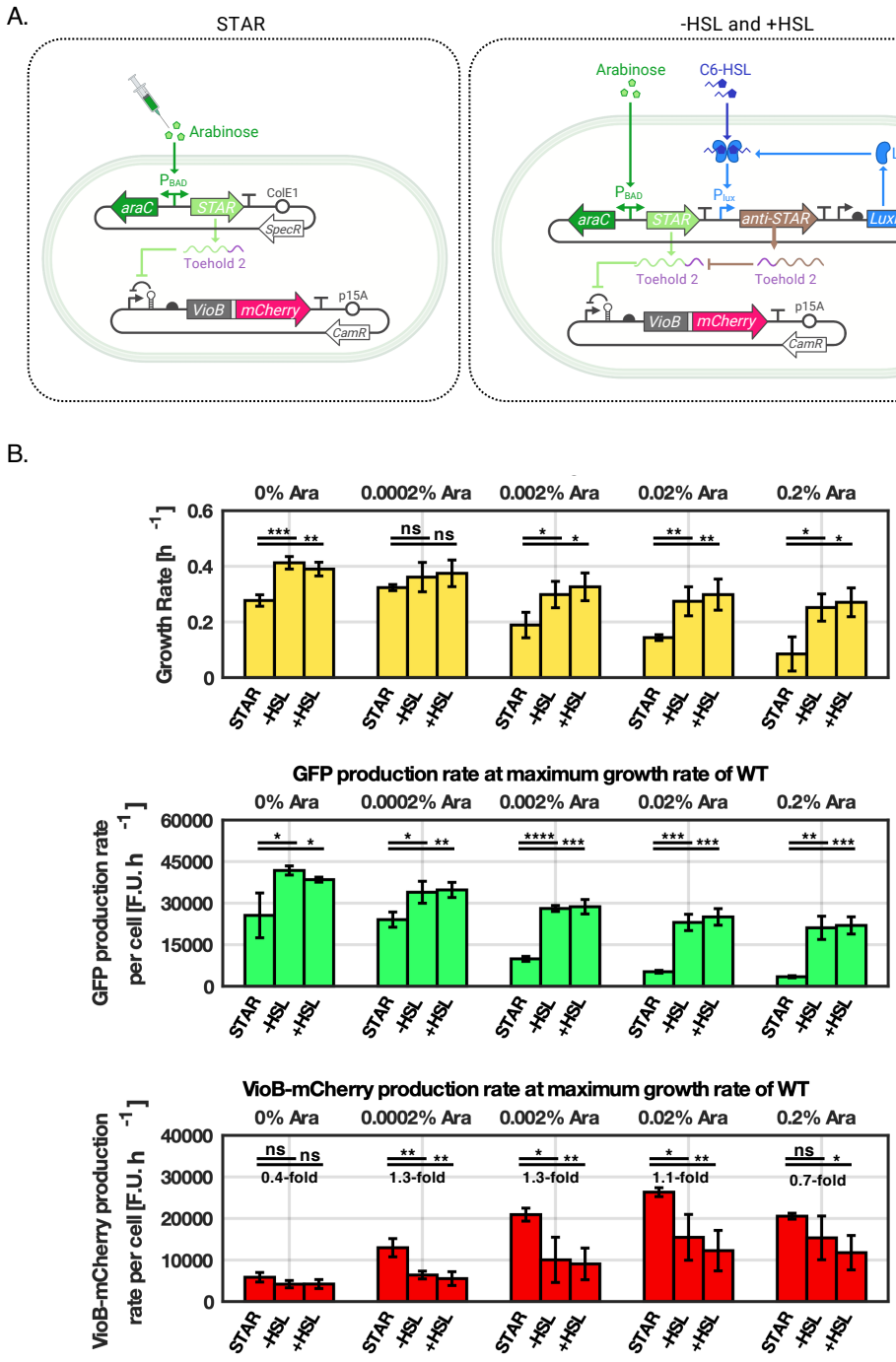


Figure 22: Inducible expression of STAR in the STAR-based comparator reveals a leakage of anti-STAR production. (A) In the "STAR" circuit, the expression of STAR 6 with Toehold 2 is induced in the presence of L-arabinose. STAR then binds to its target to activate production of VioB-mCherry. In the "-HSL" and "+HSL" circuits, mCherry expression is driven by the comparator plasmid. In the presence of L-arabinose, VioB-mCherry expression is turned ON. "-HSL" and "+HSL" denote the external addition of 3OC6-HSL, at 0 M and 10^{-7}M of C6-HSL respectively, to activate anti-STAR expression. (Caption continues on the next page).

Figure 22: (B) Bar graphs displaying the growth rate, GFP production rate per cell and VioB-mCherry production rate per cell of the circuits shown in B. "-HSL" represents a concentration of 0M of C6-HSL and "+HSL" represents a concentration of 10^{-7}M of C6-HSL. Experiment was carried in DH10B-GFP. Data represent the mean values of n = 3 biological replicates ± s.d. Statistically significant differences were determined using two-tailed Student's t-test (**** represents $p<0.0001$, *** represents $p<0.001$, ** represents $p<0.01$, * represents $p<0.1$, ns represents not significant).

the strong BBa_B1001 terminator between the two transcriptional units (Buffer 3 in Figure 23). The sequences of the DNA spacers are recorded in Appendix **??**. I characterised the change in fold repression of the comparator with the original spacer (Buffer 1) and the two new spacers (Buffers 2 and 3). In Figure 23.B, I observe that adding the B1001 double terminator with or without the non-coding region from the Lucks AND-gate improved the fold change significantly compared to the original spacer sequence.

Using buffer 3, which gave the best fold repression between the two conditions when anti-STAR was not produced and when it was, I mapped the comparator's response to increasing arabinose and 3OC6-HSL concentrations in Figure 24. At 0.2% and 0.002% L-arabinose, the output level was repressed 12-fold and 4-fold respectively. Also I observe that the STAR-based comparator is able to drive VioB-mCherry expression down to the same output expression level for different levels of induction with L-arabinose.

I have shown that RNAP read-through is a substantial issue when driving STAR expression with a strong promoter. To mitigate the read-through from the STAR transcriptional cassette to the anti-STAR cassette, it is necessary to use a stronger terminator than t500 used in the original STAR system. In subsequent comparator designs, I will be using the Buffer 3 DNA spacer to keep the STAR and anti-STAR transcriptional units isolated from one another.

2.2.4 Characterisation the final STAR-based comparator design

For our purpose, I needed a comparator with good ON/OFF properties, low OFF state and high ON state. Based on these requirements, I selected the best toehold, buffer and STAR target to meet those criteria. In this section, I show the final properties of our STAR-based comparator which I will be using in the following chapters to sense quorum sensing inputs produced by our co-culture strains, and to regulate their growth accordingly.

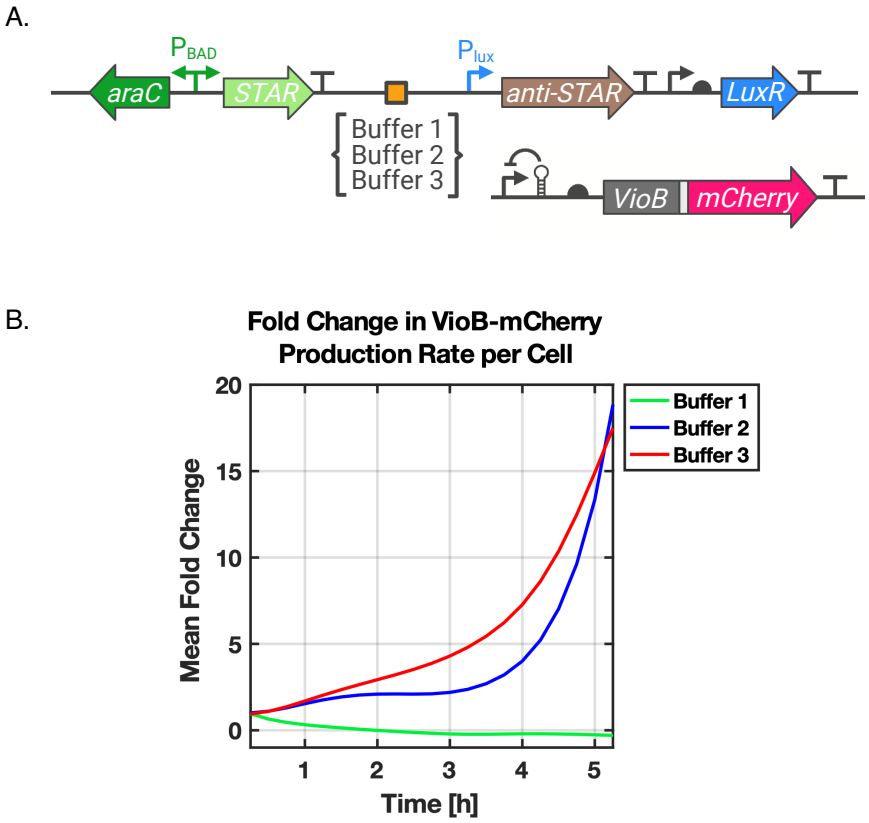


Figure 23: Buffer Library to reduce RNAP read-through from the STAR transcriptional cassette to the anti-STAR transcriptional cassette. (A) Diagram if the STAR-based comparator with the different buffer sequences. (B) Fold repression of VioB-mCherry over time when pBAD is maximally induced with 0.2% L-arabinose and pLux is maximally induced with 10^{-7}M of 3OC6-HSL. Experiment was carried in DH10B-GFP. Data represent the mean values of n = 3 biological replicates ± s.d.

2.2.4.1 Comparison of the no-toehold and toehold comparators.

I have seen that toeholds can affect the ON/OFF properties of the comparator. Here I characterise the behaviour of our insulated comparator with and without toehold.

In Figure 25.B, the comparator without toehold has a fold repression of 5.5-fold while the comparator with Toehold 2 has a fold repression of 3.8-fold. The toehold appears to decrease the maximum mRFP expression level of the system, but it also reduced its OFF state level. The bar graph in Figure 25.C confirms that there is now minimum leakage of anti-STAR in the system as the STAR Controls which lack the presence of anti-STAR on the plasmid have similar output levels as their cognate comparator design which carry both STAR and anti-

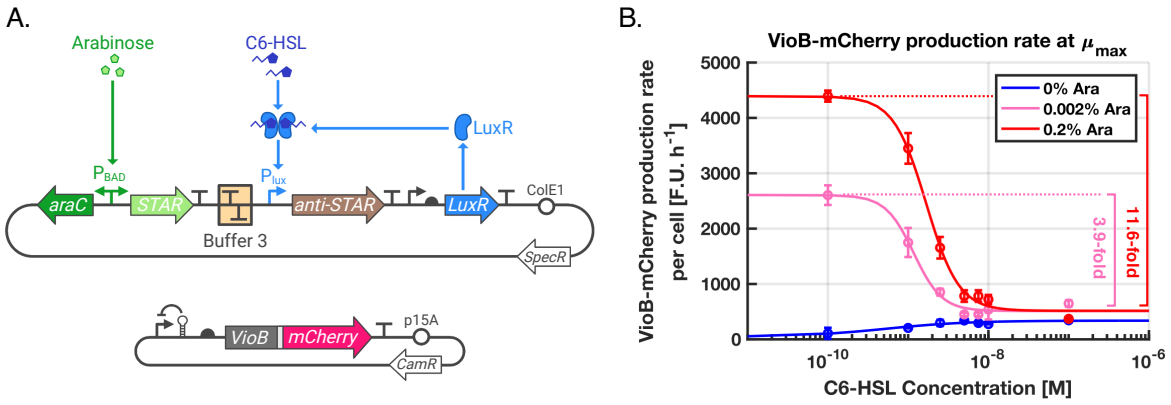


Figure 24: Characterisation of the final inducible STAR-based comparator. (A) Diagram of the final inducible STAR-based comparator expressing VioB-mCherry as an output. (B) VioB-mCherry production rate per cell at the time of maximum growth rate and as a function of C6-HSL concentration. Different curves represent the different levels of L-arabinose induction. Curves were fitted using MATLAB four-parameter nonlinear regression fit. Experiment was carried in DH10B-GFP. Data represent the mean values of n = 3 biological replicates ± s.d. Curves were fitted using MATLAB four-parameter nonlinear regression fit.

STAR on the comparator plasmid. However, some read-through might still be occurring in the case of the toehold comparator as mRFP expression from the Toehold 2 control is ∼25% higher than that of the Toehold 2 comparator in the presence of L-arabinose and absence of 3OC6-HSL. The two comparator designs with and without Toehold 2, thus provide different ON/OFF properties which I will be exploiting for the expression of burdensome proteins in Chapters 4 and 5.

2.2.4.2 STAR and anti-STAR Toxicity

I started designing a RNA-based comparator based on the hypothesis that RNA-based logic requires less cellular resources than protein-based logic as it only requires resources for transcription. The STAR-based comparator aimed to utilise as little host resources as possible. To study the impact of our STAR-based comparator on its host, I next characterised its effect on growth rate and GFP capacity.

To characterise the impact of the comparator on the host, I transformed the STAR-based comparator plasmid with and without toehold into the DH10B-GFP capacity monitor strain

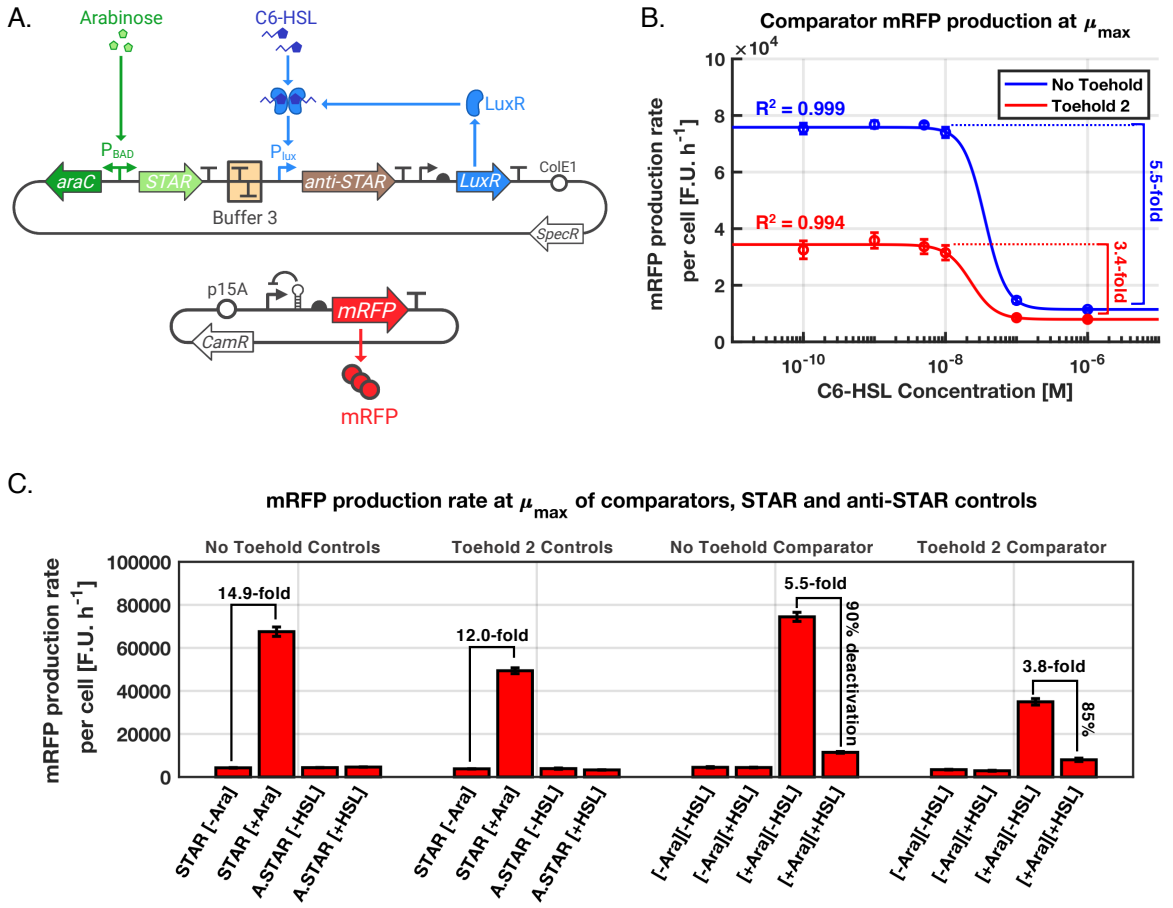


Figure 25: Characterisation of the STAR-based comparator with and without toehold. (A) Diagram of the circuit used to compare the STAR-based comparator with and without toehold. (B) No Toehold and Toehold 2 comparators' VioB-mCherry production rate per cell at the time of maximum growth rate and as a function of C6-HSL concentration. (C) Bar graph of mRFP production rate per cell. The STAR controls only carried STAR with or without toehold on the comparator plasmid and was induced by L-arabinose. The A.STAR controls only carried anti-STAR with or without toehold on the comparator plasmid and was induced by C6-HSL. Two concentrations of L-arabinose were used for induction: "[-Ara]" for 0% and "[+Ara]" for 0.2%. 2 concentrations of C6-HSL were used for induction: "[-HSL]" for 0M and "[+HSL]" for $10^{-6}M$. The deactivation percentage of the comparators was calculated as $(m\dot{R}FP_{[+Ara][-AHL]} - m\dot{R}FP_{[+Ara][+AHL]})/(m\dot{R}FP_{[+Ara][-AHL]} - m\dot{R}FP_{[-Ara][-AHL]})$, where $m\dot{R}FP$ is the mRFP production rate per cell. Experiment was carried in DH10B. Data represent the mean values of n = 3 biological replicates ± s.d. Curves were fitted using MATLAB four-parameter nonlinear regression fit.

(Figure 26.A). Any decrease in GFP will indicate how resource-greedy the comparators are on their host. In Figure 26.B-C, I report the growth rate and GFP production rate per cell of the capacity monitor strain when STAR and anti-STAR are expressed from the

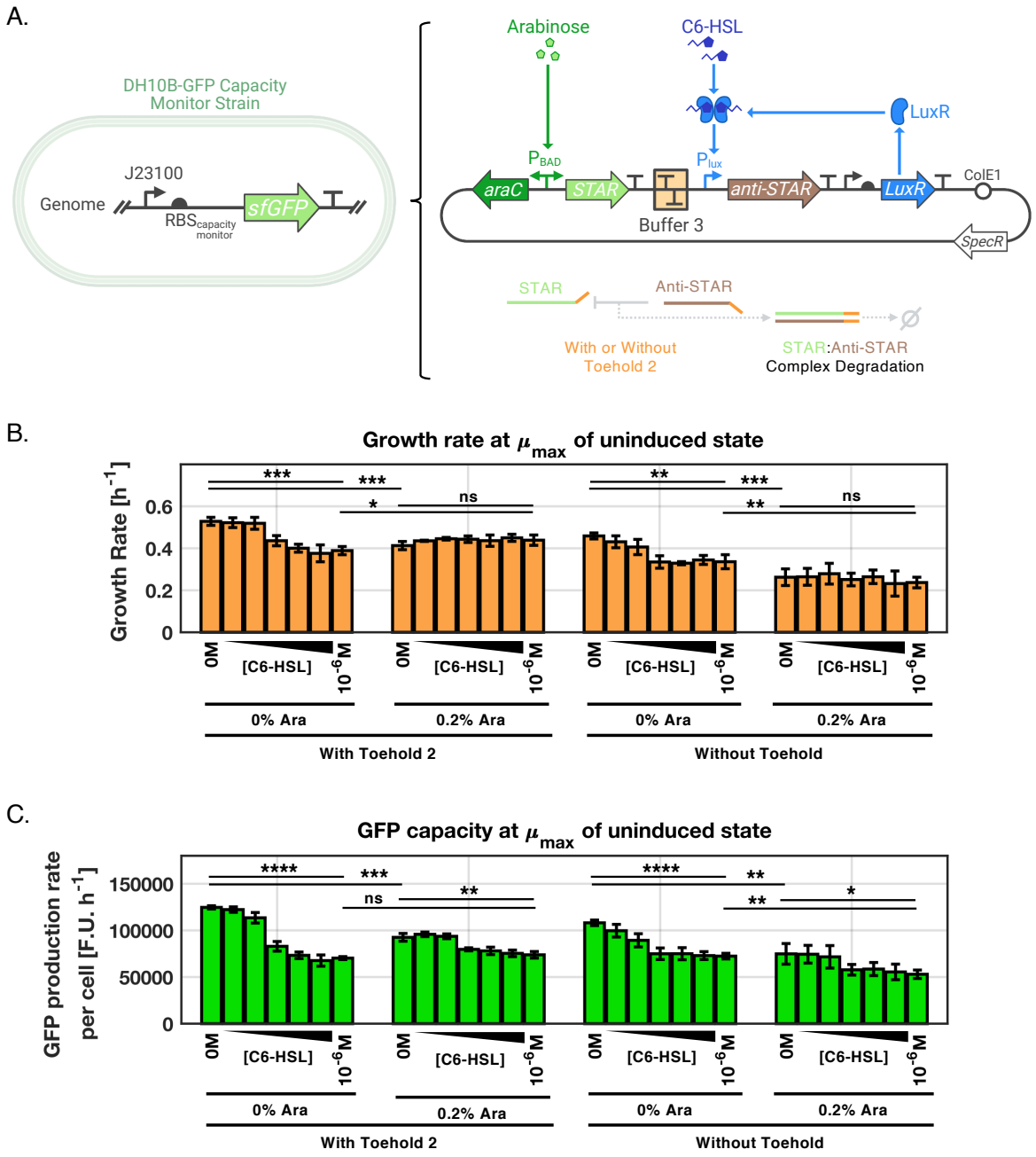


Figure 26: Burden characterisation of the STAR-based comparator with and without toehold. (A) Diagram of the comparator plasmid tested in the DH10B-GFP strain carrying the GFP capacity monitor to assess the burden caused by expression of STAR and anti-STAR. STAR expression is enabled by L-arabinose, while anti-STAR expression is enabled by C6-HSL. (B) Growth rate of the comparator plasmids with and without toehold. (C) GFP capacity measured as the GFP production rate per cell of DH10B-GFP capacity monitor strain transformed the comparator plasmids with and without toehold. Experiment was carried in DH10B-GFP. Two concentrations of L-arabinose were used: 0% and 0.2%. Concentrations of C6-HSL used are: 0M, 10^{-10}M, 10^{-9}M, 5×10^{-9}M, 10^{-8}M, 10^{-7}M, 10^{-6}M. Data represent the mean values of n = 3 biological replicates ± s.d. Statistically significant differences were determined using two-tailed Student's t-test (**** represents p<0.0001, *** represents p<0.001, ** represents p<0.01, * represents p<0.1, ns represents not significant).

different comparator plasmids. STAR is produced in the presence of L-arabinose, while anti-STAR is produced in presence of C6-HSL. First I observe that the comparator with Toehold 2 exhibited the best growth and GFP capacity out of the two comparators. I observe that in the case of the comparator with toehold, GFP capacity drops by 20% when STAR is produced and by 40% when anti-STAR is produced. While for the comparator without toehold, GFP capacity drops by 20% for both STAR and anti-STAR when they are expressed separately. However, STAR without toehold appears to be 20% more resource-greedy than STAR with toehold, while anti-STAR without toehold appears to be 20% less resource greedy than anti-STAR with toehold. Similarly, for the growth rate STAR and anti-STAR separate expression with or without toehold induces a 20-25% drop in growth rate. STAR and anti-STAR without toehold also have a larger impact on maximum growth rate than those with Toehold 2. Interestingly, STAR and anti-STAR sequestration seem to limit their impact on the host both at the growth and GFP capacity level.

This result suggests that STAR and anti-STAR when unbound may be interfering with other cell RNA species, which could explain why their impact on the host is improved when both are present in the system, hence bound into a complex sheltering cellular species from their interference. The impact on the host of the STAR-based comparator with a toehold is more limited than in the case of the comparator without toehold. As a result, I will use the toehold version of the comparator in the future chapters as I aim for the comparator layer to have a minimal impact on the host.

2.2.4.3 STAR-based comparator in chemostat

In an effort to demonstrate that the comparator can be used in different kinds of culture environments, I tested whether the STAR-based comparator with toehold also works in continuous culture. Continuous cultures such as chemostat environments, allow to study the dynamics of a system by keeping growth rate constant. Cells remain in a similar metabolic state and as a result, gene expression is stable unless external inputs or perturbations are applied on the system. Looking at co-culture dynamics under continuous conditions is particularly attractive as it enables the tracking of population dynamics over extended periods of time. Checking that the STAR-based comparator is able to compute the difference

between two input signals in a chemostat environment is a first step to building a circuit to control coculture composition in a continuous culture.

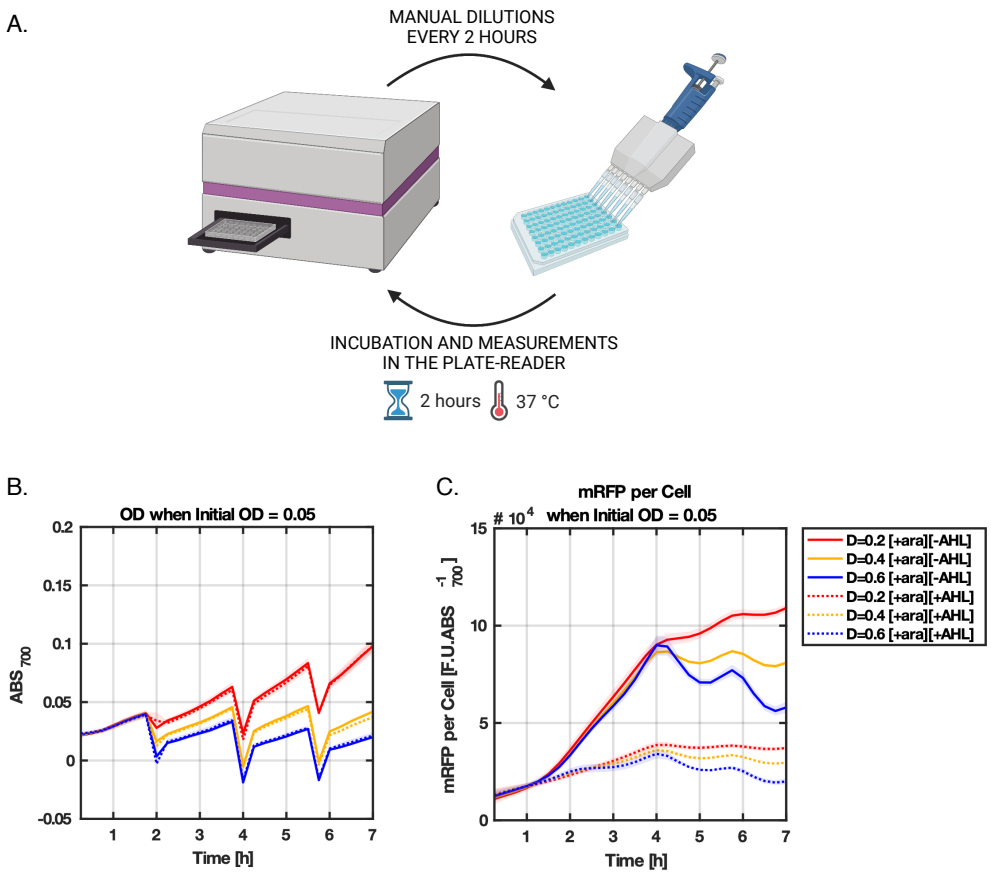


Figure 27: Behaviour of the STAR-based comparator in a chemostat-type environment. (A) STAR-based comparator was grown in a plate-reader and diluted every 2 hours to simulate growth in a chemostat environment. Three dilution volumes were chosen to approximate chemostat dilution rates. (B) Cell density over time for different dilution factors. L-arabinose drives STAR expression while 3OC6-HSL drives anti-STAR expression. STAR activates the production of mRFP. (C) Total mRFP per cell over time for different dilution factor. Experiment was carried in DH10B-GFP. Data represent the mean values of n = 3 biological replicates ± s.d.

I designed an experiment in which I incubated the cells carrying the comparator in the plate-reader. Every two hours I diluted the cultures with a set volume that mimics the dilution in a chemostat (Figure 27.A). Different volumes where chosen to determine the optimal dilution rate to keep growth rate constant. In Figure 27.B, the optimal dilution rate was 0.4 h^{-1}. If the dilution factor D was below 0.4 h^{-1}, cells grew faster than they were

diluted so after some time they would reach saturation. If D was above 0.4 h^{-1}, cells grew slower than they were diluted, leading to a loss of cells over time. In Figure 27.C, I confirm that by adding L-arabinose I activate mRFP expression which stabilises over time as the system enters its steady state. Furthermore, when adding 3OC6-HSL, mRFP expression is deactivated as I have seen in the previous sections carried in batch-cultures.

This small chemostat experiment shows that the comparator is able to integrate two chemical inputs in a chemostat-like environment. It would be interesting to carry chemostat experiments over longer periods of time to study the stability of the comparator over time. It would also allow to study the activation and deactivation of the system when the inputs' strength fluctuate over time. I can imagine placing anti-STAR under the control of a light inducible promoter and using a setting such as the Chi.bio to switch the light input ON and OFF to measure the time it takes for STAR to sequester STAR away from the system to repress the output gene expression [177].

2.3 Conclusions

In this chapter, I explored strategies to design a RNA-based comparator. As a starting point, I used Small Transcriptional Activating RNAs (STARs) and designed an RNA regulator, anti-STAR, to implement the transduction cascade that senses the difference between two input signals. As the STAR to anti-STAR ratio increases in the cell, the output signal increases. As a result, the output signal is titrated according to the ratio between the two input signals' strength. I then explored different RNA designs to tune the leakiness, sensitivity and dynamic range of the STAR-based comparator. Reducing the leakiness of the anti-STAR transcriptional cassette was critical to obtain a good dynamic range and maximum ON state. The final comparator design is able to integrate two inducible inputs both in batch and continuous cultures. Though the expression of the comparator species has an impact on cell growth, I was able to mitigate its effect by selecting a toehold combination with less interference on the host. I believe that the STAR-based comparator is modular and provides an effective sequestration mechanism that integrates input signals' strength over time. In the following chapters it will serve as the controller mechanism for balancing the ratio of our

co-culture strains.

Chapter 3

Engineering Cell-Cell Communication

Contents

3.1 Introduction 59

3.2 Results and Discusssion 60

3.2.1 Selection of the lux and rpa systems 60

3.2.2 Characterisation of the transcriptional input-output response of the lux promoter 66

3.2.3 Building the lux and rpa comparators 72

3.2.4 Engineering strains to produce C6-HSL and pC-HSL 76

3.2.5 Linking the comparator and the communication modules 82

3.3 Conclusions 85

3.1 Introduction

With the STAR-based comparator I have developed over the last chapter, I now have a module to compare two input signals. In the context of our coculture, I need to build two strains that produce a signal detectable by the other strain that will reflect their population density. As said in the introduction, quorum sensing molecules have been widely used in synthetic biology circuits to regulate gene expression depending on population density. By expressing two quorum sensing systems, each strain in our coculture will be able to sense population density of the other strain to regulate their ratio. However, for the coculture to be balanced, both comparators need to exhibit symmetrical behaviours in both strains. This means that the production and sensing of quorum sensing molecules needs to be tuned to

achieve comparable anti-STAR expression in both strains' comparators.

Production of quorum sensing molecules as well as the orthogonality between their different system parts: (1) promoter, (2) regulator protein and (3) ligand, has already been extensively characterised in *E. coli* [111, 178, 112]. However, the response of quorum sensing promoters varies widely depending on genetic context and background. This makes it difficult to choose existing quorum sensing systems that have similar properties: sensitivity, maximum output, tightness, dynamic range and operational range. Tuning these promoter properties would facilitate the use of those quorum sensing parts in synthetic biology circuits.

In this chapter, I build a set of quorum sensing producing strains and characterise their signal strength with a RNA-based fluorescent aptamer to gain understanding on the transcriptional expression profile of anti-STAR in the context of the STAR-based comparator. I use the constructed strains to study the impact of quorum sensing production on the comparator's response to increasing cell density. I also investigate how to tune the comparator's sensitivity and leakiness to achieve better symmetry between the two comparator versions that will be transformed in each of the coculture strains.

3.2 Results and Discusssion

3.2.1 Selection of the lux and rpa systems

The first use of quorum sensing to sense population density and regulate coculture composition accordingly was published nearly two decades ago by Balagaddé et al. [63]. Since then, both AHL and AI-2 quorum sensing systems have provided a means to regulate gene expression based on population density in synthetic biology circuits. They have not only been useful for the development of synthetic cocultures, but also to re-direct the flux of resources between biomass and compound production depending on the cell metabolic profile [113]. Despite the numerous accounts of quorum sensing use in the synthetic biology literature, it has not yet been investigated how to build symmetrical quorum-sensing-based systems, that is two (or more) circuits with similar input-output properties based on two different quorum sensing inputs [90].

In 2016, Scott et al. characterised all the potential cross-talks that could occur between the different parts of four homoserine lactones systems: lux, tra, las and rpa [111]. Since each quorum sensing system is made up of three parts: the promoter, the regulator protein and the ligand, they built 16 different circuits to study the cross-talk interactions between the different parts.

In Figure 28, I represented Scott & Hasty's experimental cross-talk results of the tra versus rpa systems (Figure 28.A) as well as the lux versus rpa systems (Figure 28.B) [111]. Their results show that the tra and the rpa systems are completely orthogonal such that the tra promoter can only be activated by the formed TraR and 3OC8-HSL complex, and the rpa promoter can only be activated by the RpaR and pC-HSL complex. These two systems would therefore be the best choice for building an orthogonal circuit based on two quorum sensing systems.

On the other hand, the comparison of the lux and rpa systems in Figure 28.B, revealed that the two systems are not completely orthogonal to each other, they are only signal orthogonal. This means that both the lux and rpa promoters can be activated by their own regulator protein and cognate ligand complex but also by the regulator protein and cognate ligand of the other system. However, if the regulator protein is not bound to its cognate ligand, for example LuxR and pC-HSL, neither promoters will be activated. This system could also be used to build an orthogonal circuit based on two quorum sensing systems. But to preserve the orthogonality of both systems, LuxR and RpaR will have to be physically separated. For example, this can be achieved by expressing LuxR and RpaR in different cells.

To further examine the suitability of using either the tra and rpa systems or the lux and rpa systems for building our coculture, I inspected their input-output response. To do so, I analysed the supplementary material given by Scott et al. in Figure 29. In Figure 29.A, I present the different quorum sensing systems I consider for comparison; and in Figure 29.B, I map their input-output response [111]. Each system is designed by three letters referring to each of the three parts of the quorum sensing systems. For example, "LLL" refers to the system using: (1) the lux promoter, (2) the LuxR regulator protein and (3) the lux ligand 3OC6-HSL. "L" means that the component belongs to the lux system,

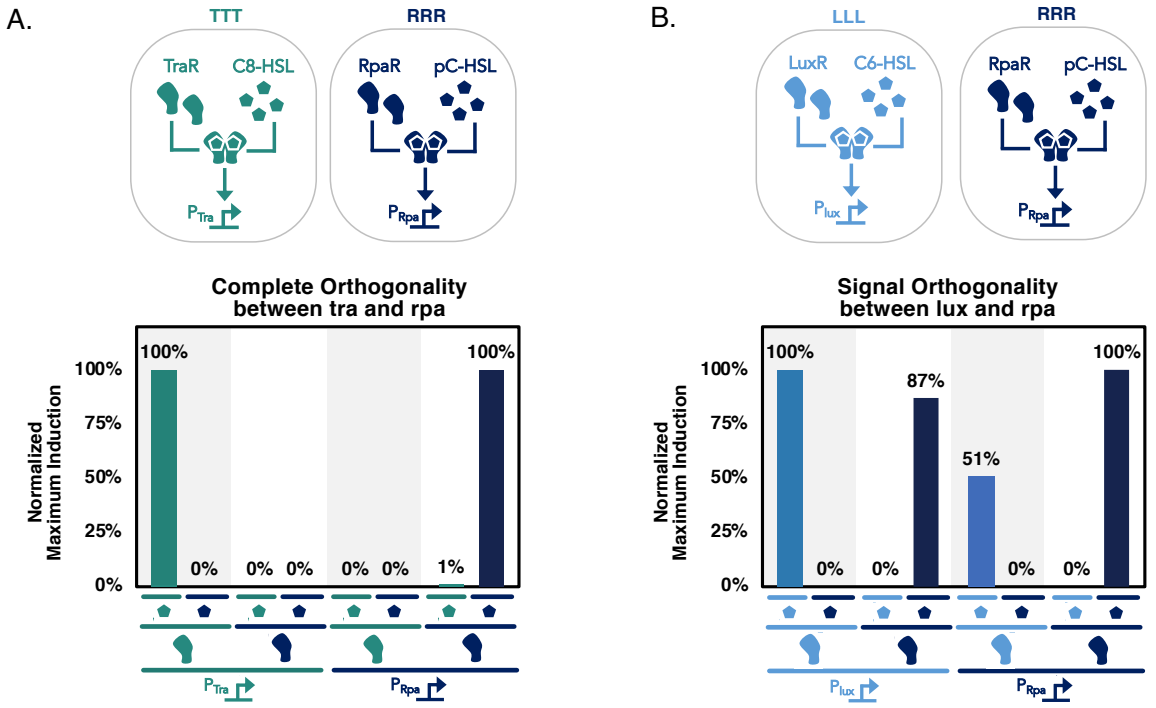


Figure 28: Homoserine lactones orthogonality. (A) The tra and rpa systems have complete promoter and signal orthogonality. The tra promoter can only be activated by the binding of the TraR regulator protein with its ligand 3OC8-HSL. Similarly the rpa promoter can only be activated by the binding of the RpaR regulator protein with its ligand pC-HSL. (B) The lux and rpa systems are completely signal orthogonal but not promoter orthogonal. Both promoters can only be activated by the regulator protein bound to its cognate ligand so when LuxR is bound to 3OC6-HSL and when RpaR is bound to pC-HSL. Figure is adapted from [111].

"T" to the tra system and "R" to the rpa system. In Figure 28.A, I saw that the tra (TTT) and rpa (RRR) systems were perfectly orthogonal. However, in Figure 29.B, their input-output response is very different. RRR has a much higher maximum output than TTT, it is leakier and has a larger operational range. Tuning the input-output properties of the two systems would require modifying the concentration of regulator protein in the cell as well as introducing mutations in the promoters to tune their sensitivities and hence adjust their operational range. The LLL and LRR systems however appear to have very similar input-output properties. Using the LLL and LRR systems would therefore save a lot of time as they would not require the same level of tuning as the TTT and RRR systems would require to build two comparators with similar input-output properties. Since both comparator circuits will be compartmentalised in each strain of the coculture,

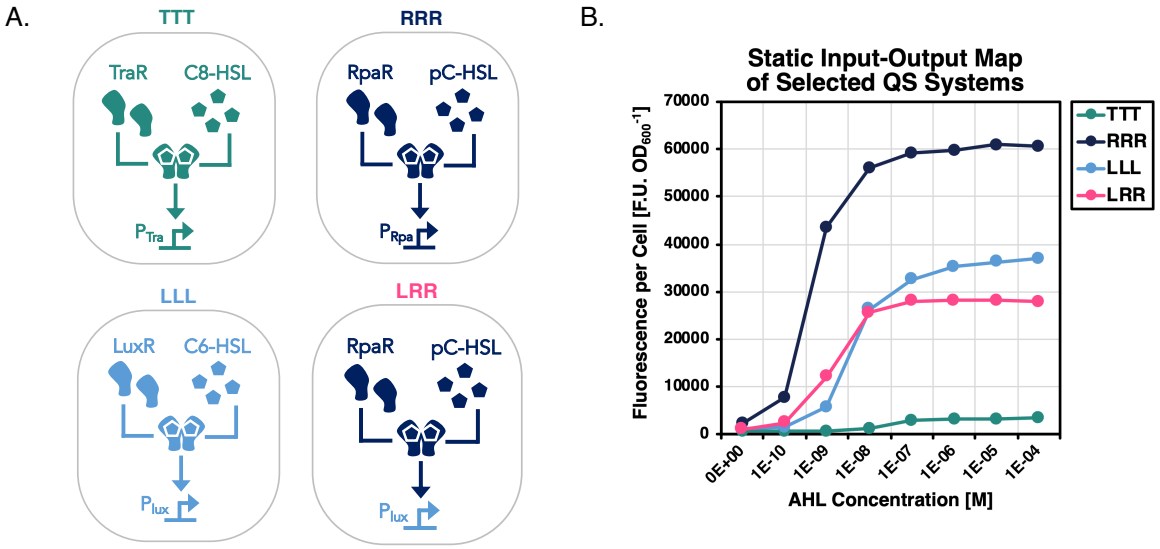


Figure 29: Differences of promoter strength of the tra, rpa and lux systems. (A) Diagram of the four quorum sensing systems considered in this system: the tra system (TTT), the rpa system (RRR), the lux system (LLL) and the mixed lux-rpa system (LRR). The first letter on the abbreviation corresponds to the promoter of the system used, the second letter corresponds to the regulator protein and the third letter to the ligand. (B) Fluorescence per cell of the four considered quorum sensing systems. GFP is expressed downstream of the quorum sensing promoter of each of the four systems. Figure represents data from the supplementary materials of [111].

the orthogonality of the LLL and LRR systems would preserved. Thus, I decided to use the LLL and LRR systems to build the two comparators needed to balance the coculture ratio.

To verify the orthogonality of the LLL and LRR systems in our hands, I build two plasmids each expressing sfGFP downstream of the lux promoter but each under the control of either the LuxR and RpaR regulator proteins (Figure 30). In Figure 30.A, I confirm that Strain A can only activate sfGFP expression when LuxR is forming a complex with its cognate ligand 3OC6-HSL. Similarly, in Strain B, sfGFP expression is only turned ON when RpaR binds to pC-HSL but not C6-HSL. The spatial separation of LuxR and RpaR maintains the orthogonality of the LLL and LRR system in Strain A and B. Having checked for the orthogonality of both systems, I now proceed to verifying that their input-output responses are similar in our strains as the ones of [111].

In Scott et al., the LLL and LRR systems displayed very similar input-output properties

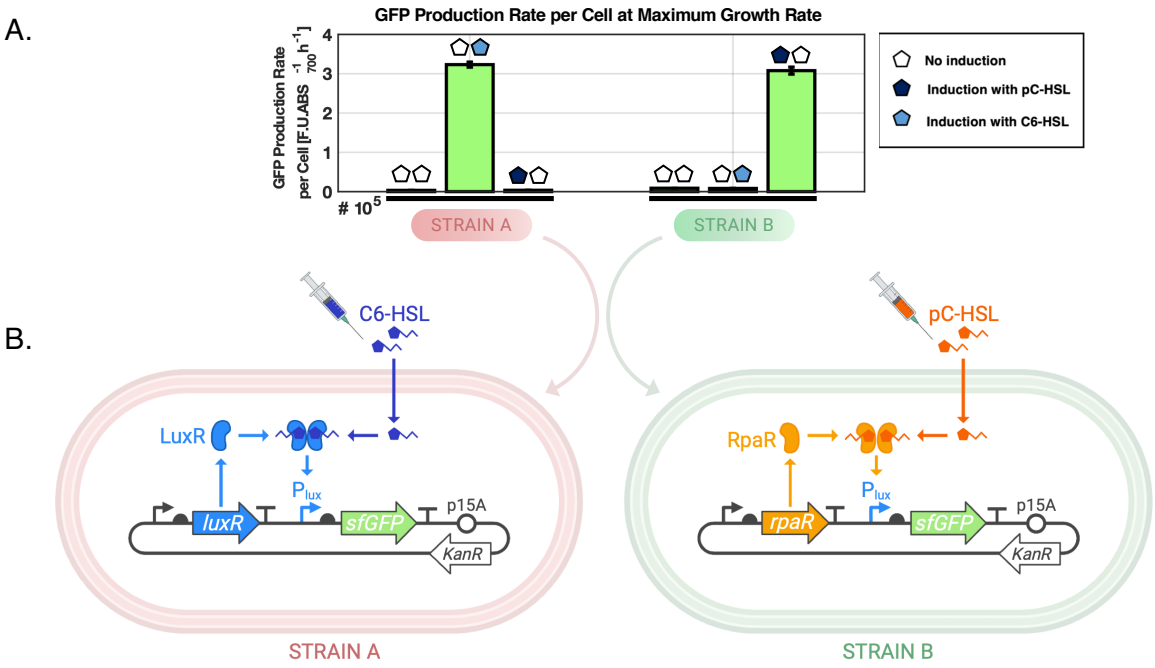


Figure 30: Orthogonality of the lux and rpa systems. (A) Strain A and B are induced with either no HSL, 10^{-7}M of C6-HSL or 10^{-7}M of pC-HSL. Strain A can only detect the presence of C6-HSL and not pC-HSL, while Strain B can only detect pC-HSL and not C6-HSL. (B) Genetic circuits of Strain A and Strain B. In Strain A, sfGFP is regulated by the LLL system; while in Strain B, sfGFP is regulated by the LRR system. Experiments was carried in BW25113. Fluorescence was monitored in a timecourse plate-reader assay. Data represent the mean values of n = 3 biological replicates ± s.d.

[111]. In Figure 31.A I built two plasmids carrying the lux promoter as well as either LuxR or RpaR to characterise the input-output response of the lux promoter to changing AHL concentrations. In Figure 31.B, I induced the LuxR and RpaR Receivers with 3OC6-HSL and pC-HSL respectively. I observed that the LuxR Receiver has a higher maximum GFP production rate per cell than the RpaR Receiver and the RpaR Receiver is also not as tight as the LuxR Receiver, as suggested by the previous data by [111]. To see whether reducing the copy number of the regulator proteins could improve the leakiness of both systems, but especially that of the LRR system, I integrated the LuxR and RpaR transcriptional units into the genome of the parent strains BW25113 (Figure 31.C). I then transformed both strains with the same plasmid carrying sfGFP downstream of the lux promoter acting as a reporter plasmid. The results, shown in Figure 31.D, point that reducing the copy number of the LuxR and especially of RpaR enhanced the tightness of the LRR system such that

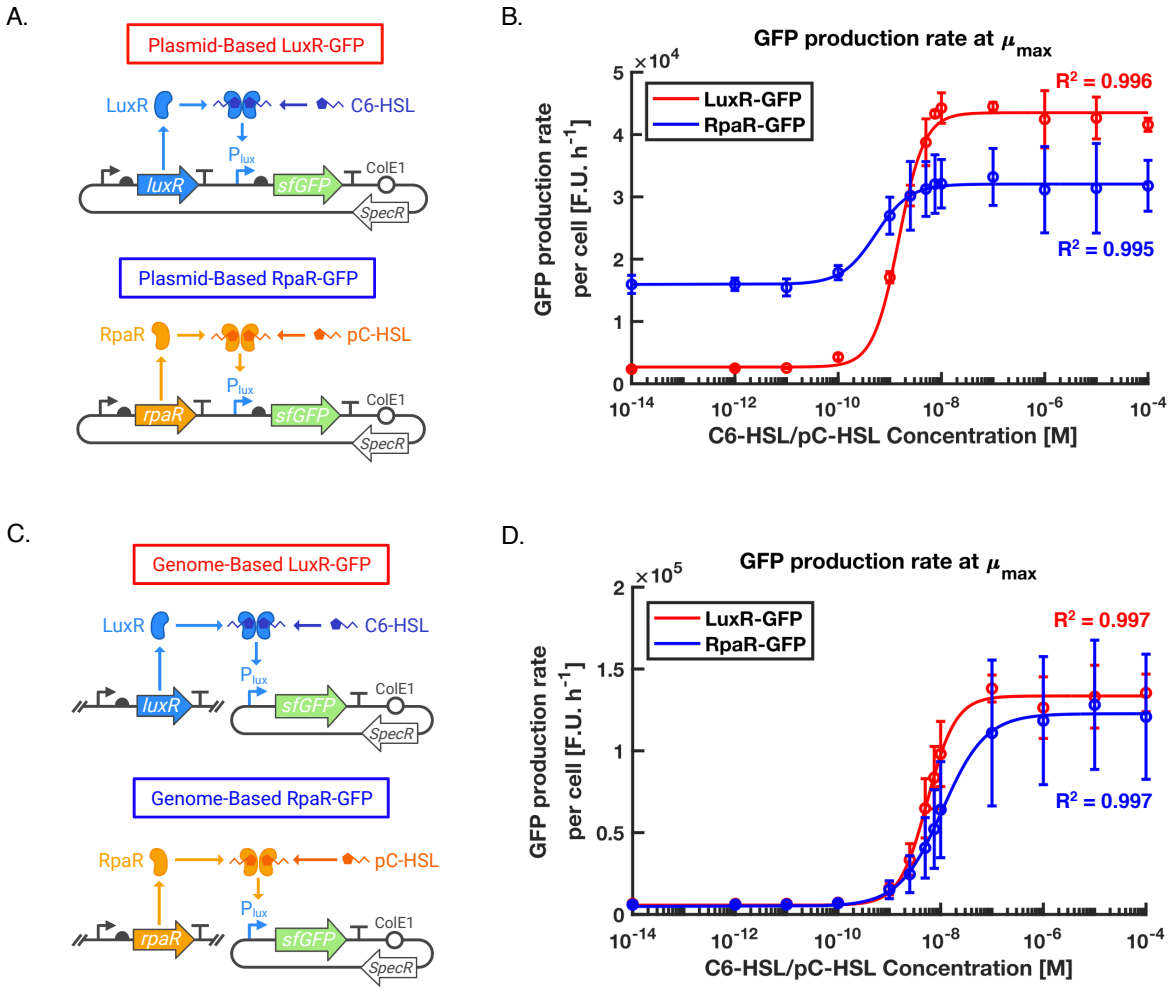


Figure 31: Changing the regulator protein copy number to tune lux promoter properties. (A) sfGFP is placed downstream of the lux promoter which is regulated by either LuxR in the case of the LuxR Receiver plasmid or by RpaR in the case of the RpaR Receiver plasmid. Both the sensor and the regulator protein are expressed from a ColE1 plasmid. (B) Input-Output responses of the plasmid-based LuxR and RpaR Receivers pictured in A. LuxR Receiver cells are induced with C6-HSL while RpaR Receiver cells are induced with pC-HSL. (C) sfGFP is placed downstream of the lux promoter which is regulated by either LuxR or RpaR. The regulator proteins LuxR and RpaR are integrated into the genome via CRIM integration while the lux promoter is on a ColE1 plasmid. (D) Input-Output responses of the genome-based LuxR and RpaR Receivers pictured in C. LuxR Receiver cells are induced with C6-HSL while RpaR Receiver cells are induced with pC-HSL. Experiments were carried in BW25113. Fluorescence was monitored in a timecourse plate-reader assay. Curves were fitted using MATLAB four-parameter nonlinear regression fit. Data represent the mean values of n = 3 biological replicates ± s.d.

the input-output responses of the LLL and LRR systems are now very similar.

I have shown that the LLL and LRR constitute a good basis to build our two symmetrical

STAR-based comparator circuits. Reducing the expression of RpaR by integrating it into the genome reduced the leakiness of the LRR quorum sensing system. As a result, both LLL and LRR exhibited similar input-output properties, laying a a solid corner stone for balancing anti-STAR production in the two version of the STAR-based comparator needed to balance coculture composition.

3.2.2 Characterisation of the transcriptional input-output response of the lux promoter

I have seen that the LLL and LRR quorum sensing systems have similar input-output properties. However, I have characterised this input-output response using a protein-based reporter: GFP. Though GFP is a standard way to characterise the input-output response of any given promoter, it does not provide a way to dissociate the transcriptional context from translational context. As the lux promoter is meant to drive expression of anti-STAR in our comparator circuits, I would like to characterise mRNA expression independently from translation.

Previously, Pothoulakis et al. developed a transcription characterisation tool for synthetic biology using the Spinach RNA fluorescent aptamer [179]. Using Spinach, they could characterise the strength of strong promoters without requiring the use of a fluorescent protein, hence without requiring translation. Their system however only worked when characterizing strong promoters such as the T7 and T5 promoters. However weaker promoters such as the araBAD promoter would not produce detectable levels of fluorescence. The poor fold activation of the tool made it difficult to read fluorescence values above background. To improve on the tool, I decided to use F30-2x-dBroccoli (Figure 32) instead of Spinach as a mRNA expression reporter [180]. Contrary to Spinach, F30-2x-dBroccoli was developed *in vivo* and exhibits higher fluorescence than either Spinach or Spinach 2. dBroccoli becomes fluorescent upon binding with the DFHBI dye, which is very similar to the GFP chromophore. To improve the signal-to-noise ratio of the RNA aptamer measurements, I decided to use DFHBI-1T dye, instead of DFHBI used in Pothoulakis et al. [179]. DFHBI-1T was reported to be 40% brighter than DFHBI and also have less background fluorescence.

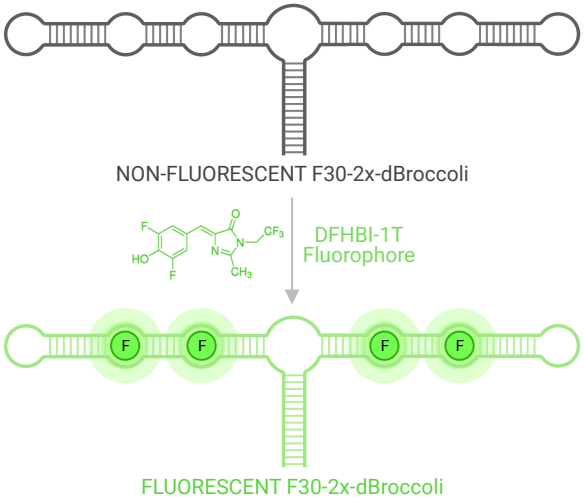


Figure 32: Structure of F30-2x-dBroccoli. F30-2x-dBroccoli is a tandem version of dBroccoli connected by the F30 junction. dBroccoli is a RNA aptamer that is fluorescent in the presence of DFHBI-1T dye.

I constructed a circuit in which dBroccoli is placed downstream of the lux promoter and the LuxR regulator protein (Figure 33.A). In Figure 33.B, I added 100μM of DFHBI-1T dye and 10^{-7}M of 3OC6-HSL to the cells carrying the dBroccoli LLL sensing plasmid and measured dBroccoli fluorescence over time in a plate-reader.

I observed that dBroccoli production rate per cell had two maximum peaks of expression over time. One coinciding with the maximum growth rate of the cells during exponential phase, and the second and largest during the entry of the cells into stationary phase. This differs from the expression of fluorescent proteins which only leads to a single peak of fluorescence production (Supplementary Figures of Appendix 8.9). mRNA has a faster turnover rate than fluorescent proteins, especially sfGFP-derived proteins which are exceptionally stable. This makes an RNA-based fluorescent reporter much more temporally precise than a protein-based reporter. This data suggest that anti-STAR might not be produced at high expression rates until entry of the cells into stationary phase.

I further explored the effect of DFHBI-1T on dBroccoli fluorescence (Figure 33.C). It appears that the range of DFHBI-1T concentrations tested is not enough to saturate the system at the second peak happening during the entry into stationary phase which I will call “Max dBroccoli Rate”. The concentration of dBroccoli in the cell is too high to achieve

saturation at Max dBroccoli Rate but is enough for the dBroccoli levels during maximum growth rate. Due to the high cost of DFHBI-1T dye, I decided to use 100μM of dye for further experiments. Though 100μM did not provide the maximum possible signal, it was well over 50% of the maximum fluorescent signal achievable, which was enough to provide a good fluorescence signal detectable by the plate-reader.

In Figure 33.D, I verified that dBroccoli expression did not impose too high a cost on the host. As the concentration of C6-HSL increases, dBroccoli expression increases. However, there is no impact on the growth rate of the cell. So dBroccoli makes a good transcriptional tool to characterise a promoter transcription profile with a high temporal resolution and without consuming much cellular resources.

Using our dBroccoli transcriptional characterisation tool, I now had the resources to compare the transcriptional behaviours of the LLL and LRR quorum sensing systems. I built two versions of the quorum sensing systems (Figure 34.A-B).

In the first version, all elements of the LLL and LRR systems were placed onto a single plasmid. While in the second version, the reporter plasmid only contained GFP placed downstream of the lux promoter. The regulator proteins LuxR and RpaR were integrated into the genome using CRIM integration. In Figure 34.B and Figure 34.C I compare the behaviour of the LRR systems when RpaR is expressed from the reporter plasmid ("Plasmid-Based") to the behaviour of the "Genome-Based" LRR system when RpaR is expressed from the DH10B genome. Figure 34.B shows the input-output behaviours of those two systems at first peak of dBroccoli expression at maximum growth rate, while Figure 34.C shows the input-output behaviours of the two systems at the second and highest peak of dBroccoli expression. Figures 34.B-C shows that when RpaR is expressed from the sensor plasmid, the input-output response is shifted to the left. This means that the system is more sensitive to pC-HSL concentration, which is expected as more RpaR is expressed and therefore available to form a complex with the pC-HSL ligand.

Similarly, in Figure 34.D, I constructed the equivalent plasmid-based and genome-based circuits of the LLL quorum sensing system. Figures 34.E and 34.F show the input-output response of the LLL systems when LuxR is either expressed from the reporter plasmid or from the genome at either the first peak of dBroccoli expression at maximum growth

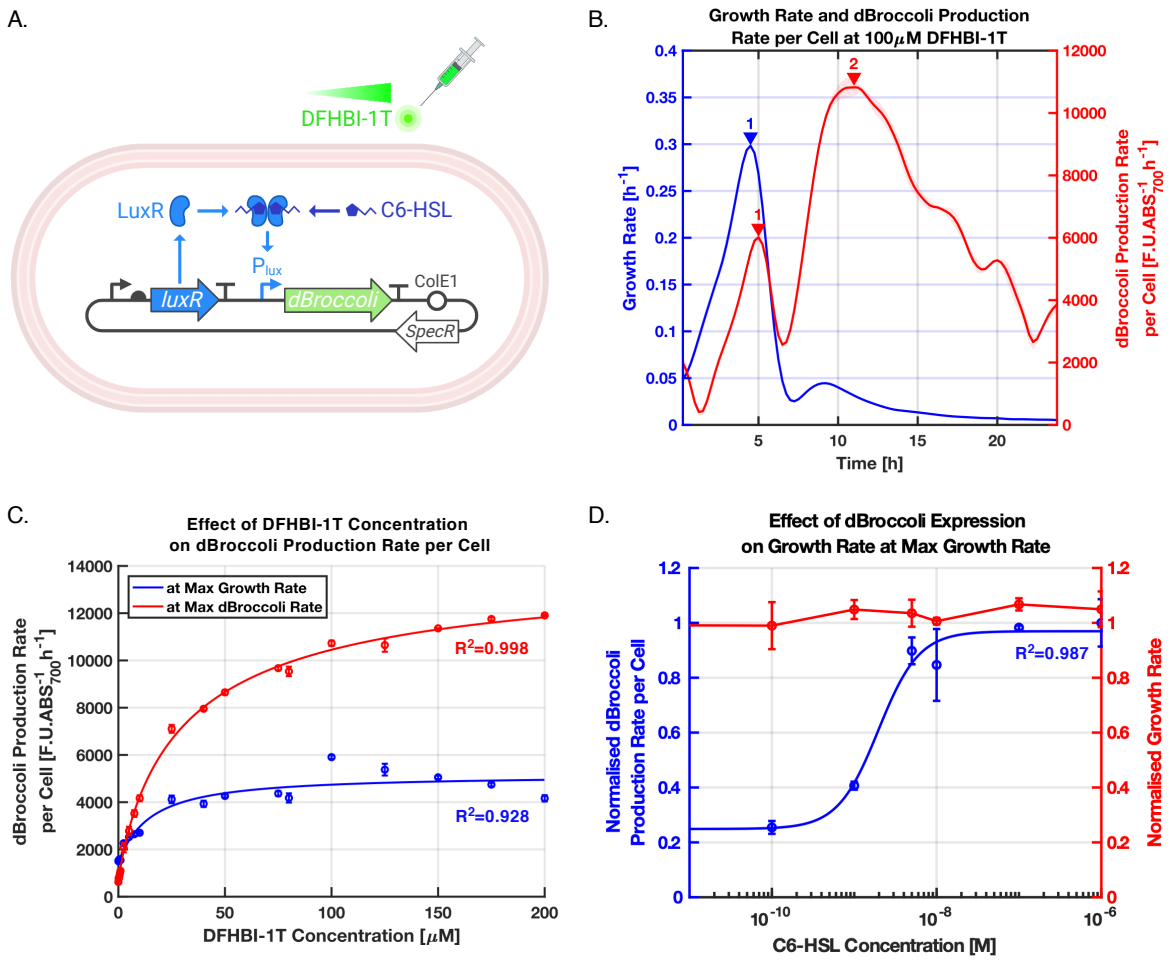


Figure 33: Effect of DFHBI-1T dye concentration on dBroccoli signal strength. (A) Different concentrations of DFHBI-1T dye are tested to study the impact of DFHBI-1T concentration on dBroccoli signal strength. dBroccoli is expressed under the LLL quorum sensing system, with 10^{-7}M of C6-HSL. (B) dBroccoli production rate per cell has two maxima: one coinciding with the maximum growth rate of the cells during exponential phase, and the other when the culture is in stationary phase. (C) Effect of DFHBI-1T dye concentration on dBroccoli production rate per cell both at both dBroccoli production maxima. Cells are induced with 10^{-7}M of C6-HSL. (D) Effect of dBroccoli expression on growth rate at the time of maximum growth rate. Cells are mixed with 100μM of DFHBI-1T dye. All experiments were carried in DH10B. Fluorescence was monitored in a timecourse plate-reader assay. Curves were fitted using MATLAB four-parameter nonlinear regression fit. Data represent the mean values of n = 3 biological replicates ± s.d.

rate or at the highest peak of dBroccoli expression respectively. Again, as I observed for the LRR system, the plasmid-based LLL system is more sensitive to C6-HSL ligand concentration than the genome-based LLL system. However, the maximum output of the LLL genome-based and plasmid-based system vary significantly over time. At maximum

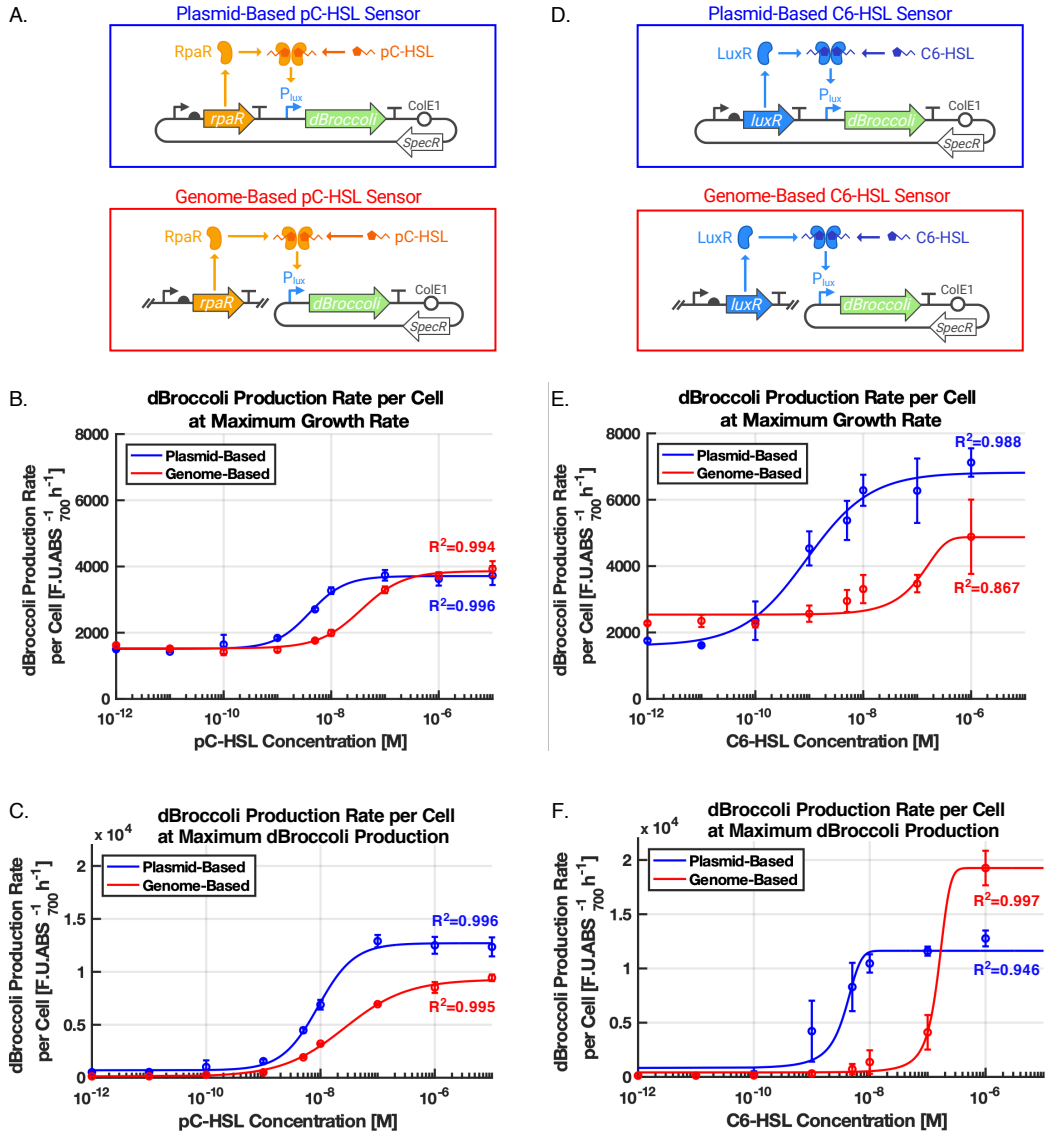


Figure 34: Plasmid- and genome-based production of HSL regulator protein. (A) Strains expressing the RpaR regulator protein either from the genome or from a plasmid. RpaR together with pC-HSL activates the plasmid-based lux promoter to produce dBroccoli. (B) dBroccoli production rate per cell at the time of maximum growth rate when the lux promoter is regulated by the RpaR and pC-HSL complex. (C) dBroccoli production rate per cell at the time of maximum dBroccoli production when the lux promoter is regulated by the RpaR and pC-HSL complex. (D) Strains expressing the LuxR regulator protein either from the genome or from a plasmid. LuxR together with C6-HSL activates the plasmid-based lux promoter to produce dBroccoli. (E) dBroccoli production rate per cell at the time of maximum growth rate when the lux promoter is regulated by the LuxR and C6-HSL complex. (F) dBroccoli production rate per cell at the time of maximum dBroccoli production when the lux promoter is regulated by the LuxR and C6-HSL complex. All experiments were carried in DH10B. Fluorescence was monitored in a timecourse plate-reader assay. Curves were fitted using MATLAB four-parameter nonlinear regression fit. Data represent the mean values of n = 3 biological replicates ± s.d.

growth rate, the maximum dBroccoli expression of plasmid-based LLL is higher than that of genome-based LLL. At maximum dBroccoli expression, when the cells are entering stationary phase, genome-based LLL expresses more dBroccoli that the plasmid-based system. I also observe that the operational range of the genome-based LLL system is reduced compared to all other systems.

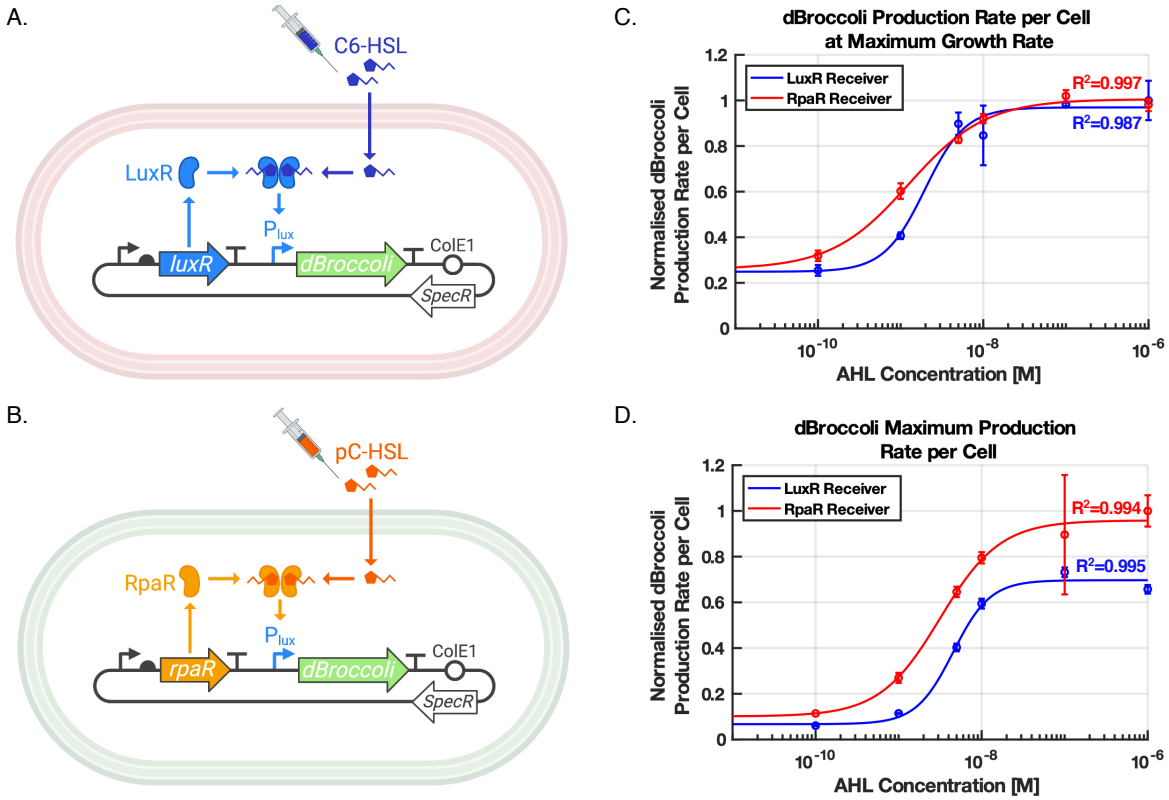


Figure 35: Response of the lux and rpa systems to HSL gradients. (A) The LuxR Receiver circuit is composed of the LLL driving expression of dBroccoli. (B) The RpaR Receiver is composed of the LRR system driving expression of dBroccoli. (C) dBroccoli production rate per cell at the time of maximum growth rate, for different concentrations of C6-HSL and pC-HSL added to the LuxR Receiver and the RpaR Receiver respectively.(D) dBroccoli production rate per cell at the time of maximum dBroccoli production, for different concentrations of C6-HSL and pC-HSL added to the LuxR Receiver and the RpaR Receiver respectively. All experiments were carried in DH10B. Fluorescence was monitored in a timecourse plate-reader assay. Curves were fitted using MATLAB four-parameter nonlinear regression fit. Data represent the mean values of n = 3 biological replicates ± s.d.

As the goal of this comparison is to find the most comparable LLL and LRR quorum sensing systems, I decided that the plasmid-based LLL and LRR systems were the most comparable, with similar sensitivities and operational ranges. This is surprising as it is not in

agreement with the results I previously found in Figure 31. Indeed, when I characterised the LLL and LRR systems with GFP, I previously found that using genome-based production of LuxR and RpaR provided the most similar static I/O curves. This highlights the need for characterising the quorum sensing system at the transcriptional level given that the results obtained with GFP and dBroccoli are very different, and that I am interested in expressing regulatory RNAs downstream of the LLL and LRR systems.

Therefore, I compare the input-output responses of the plasmid-based LLL and LRR systems in Figure 35. Both the LLL system (Figure 35.A) and the LRR system (Figure 35.B) were induced with a gradient of C6-HSL and pC-HSL respectively and dBroccoli measurements were taken in the plate-reader over time. I observe in Figure 35.D that at maximum growth rate, both LLL and LRR plasmid-based systems have very similar input-output properties. At both maximum growth rate and at maximum dBroccoli expression, the LRR system appears a little more sensitive than the LLL system and its maximum dBroccoli expression is 30% higher than that of LLL (Figure 35.D). The LRR system appears to also have a higher basal expression than the LLL system as its minimum output value is higher. Having looked into the transcriptional properties of the LLL and LRR systems, we know that the LRR system is slightly more sensitive than its LLL counterpart. This could affect the symmetrical behaviour of the lux and rpa comparators.

However understanding the differences between the transcriptional profile of both LLL and LRR will give us an understanding of why the two comparators are behaving differently. More importantly, it will give us clues on how to tune the comparator behaviours to make them more similar.

3.2.3 Building the lux and rpa comparators

Having deciphered the transcriptional behaviours of the LLL and LRR quorum sensing systems to produce an RNA output, I now investigate how the LLL and LRR systems behave when they are linked to the comparator module developed in Chapter 2. I also look at strategies to tune the behaviours of the newly built comparators.

To compare the input-output behaviours of the two STAR-based comparators, one ex-

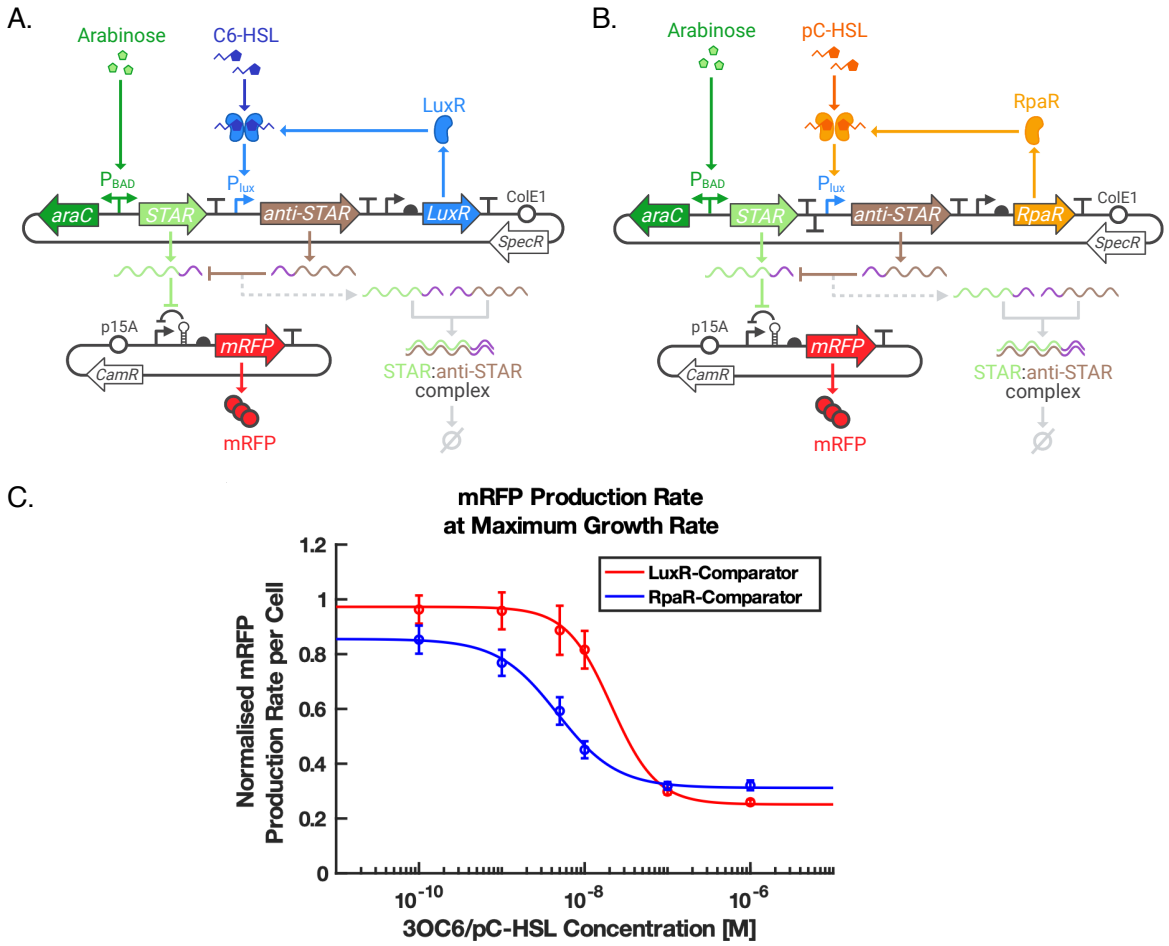


Figure 36: STAR-based comparator sensing C6-HSL and pC-HSL. (A) The STAR-based comparator comparing arabinose and C6-HSL input signals through the sequestration of STAR and anti-STAR with Toehold 2. (B) The STAR-based comparator comparing arabinose and pC-HSL input signals through the sequestration of STAR and anti-STAR with Toehold 2. (C) Input-output behaviour of the LuxR-Comparator and the RpaR-Comparator. mRFP production rate per cell is monitored in the plate-reader for a range of C6-HSL and pC-HSL concentrations. All experiments were carried in DH10B. Fluorescence was monitored in a timecourse plate-reader assay. Curves were fitted using MATLAB four-parameter nonlinear regression fit. Data represent the mean values of n = 3 biological replicates ± s.d.

pressing anti-STAR under the LLL quorum sensing system and the other under the RLL system, I built a new comparator based on the final STAR-based comparator design from Chapter 2 (Figure 25.A). I used Toehold 2 and replaced the LuxR transcriptional cassette with a RpaR transcriptional cassette on the comparator plasmid (Figure 36.B).

In Figure 36.C, I compare the input-output properties of both comparators. The RpaR-Comparator exhibits a lower maximum output than the LuxR-Comparator. It is also more

sensitive as the drop in mRFP production rate occurs at smaller pC-HSL concentrations than C6-HSL concentrations. These observations agree with the dBroccoli results from the above section. As LRR is more sensitive than LLL, more anti-STAR would be produced at lower concentrations of pC-HSL, hence making sequestration mechanism more effective for lower concentrations of HSL. Coupling the sensitivity difference with the small difference in the minimum output level between the two systems could also explain why the maximum output value of the RpaR-Comparator is lower than its counterpart.

The properties of the comparator will have to be adjusted depending on the need of the coculture and for its application. Perhaps some coculture designs would require more sensitivity to lower HSL concentrations, thus requiring a circuit that is more sensitive to low population numbers. Or on the contrary, the coculture may need to respond more dynamically when dealing with larger population densities. I want to keep the design of the comparator as flexible and modular as possible such that it can be adapted and used in different conditions. The comparators will also have to be adjusted for how much HSL each strain is producing. Being able to tune the input-output properties of the comparator will later allow to more easily select the right comparator design to match the HSL production levels of the quorum sensing producing strains.

In an effort to identify ways to construct more similar comparators, I studied different strategies that can tune different properties of the circuit to normalise their behaviours (Figure 37.A). For example, to increase the leakiness of the LuxR-comparator, we can increase the level of LuxR in the cell. We can increase LuxR levels by choosing a stronger RBS upstream of *luxR* or by stabilising *luxR* mRNA by placing the RiboJ insulator upstream of its RBS. RiboJ has been demonstrated to improve protein abundance two- to ten-fold in *E. coli* [181]. Meyer et al. designed two variants of the lux promoter, the LuxA and the LuxB promoters, to tune the Hill slope and minimum output level (Figure 37.B) [182].

In Figures 37.C-D, I show the input-output behaviours of selected new LuxR-Comparators with regard to the RpaR-Comparator of Figure 36. I observe that none of the tested strategies were able to improve the sensitivity of the LuxR-Comparator as none of the new input-output static curves have shifted significantly to the left. However, all strategies in Figure 37.C successfully decreased the maximum output value of the LuxR-Comparator.

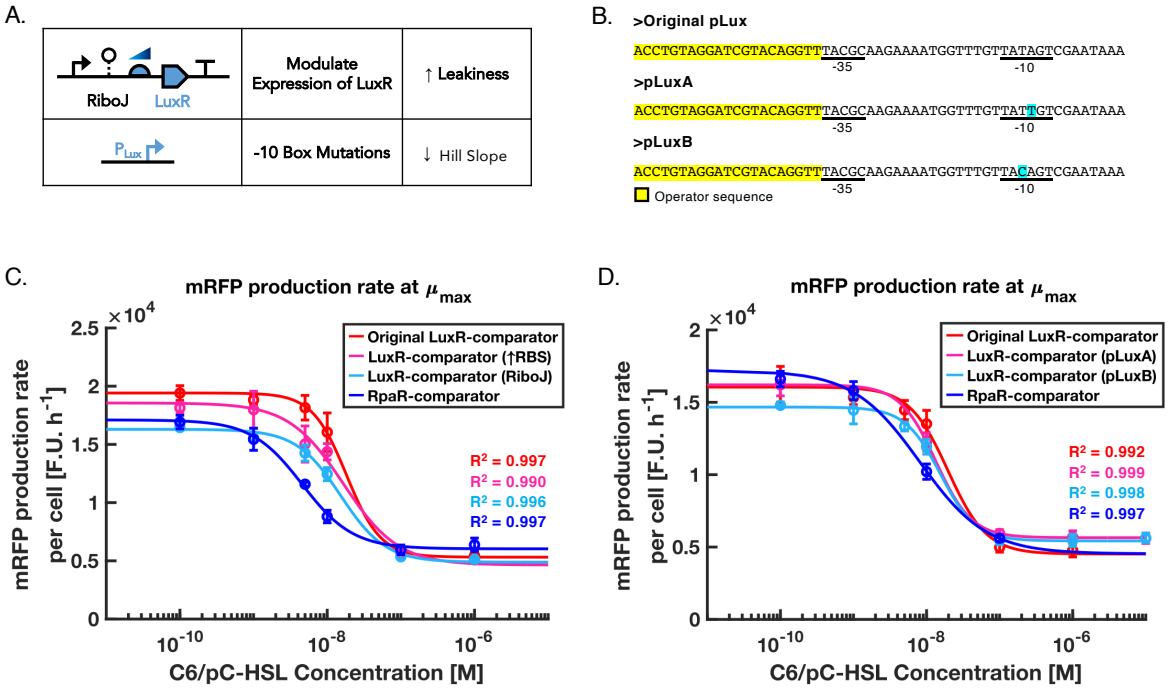


Figure 37: Modulation of the LuxR-Comparator behaviour. (A) The response of the STAR-based comparator to C6-HSL concentration can be tuned by varying LuxR expression or by introducing rational mutations in the lux promoter. (B) The response of the STAR-based comparator to C6-HSL concentration can be tuned by varying LuxR expression or by introducing rational mutations in the lux promoter. LuxA and LuxB promoters from Meyer et al. have mutations in the -10 site of the lux promoter [182]. (C) mRFP production rate per cell of different AHL sensing STAR-based comparators for a range of C6-HSL and pC-HSL concentrations. Behaviour of the LuxR-Comparator was tuned by either increasing the RBS strength of LuxR compared to the original LuxR-Comparator, or by increasing LuxR expression by placing RiboJ upstream of LuxR RBS. (D) Input-output behaviour of the LuxR-Comparators when the lux promoter contains -10 mutations. The comparators were induced with a range of C6-HSL and pC-HSL concentrations. All experiments were carried out in DH10B. Fluorescence was monitored in the plate-reader. Curves were fitted using MATLAB four-parameter nonlinear regression fit. Data represent the mean values of n = 3 biological replicates ± s.d.

The different lux promoters did not have much impact on the Hill slope of the input-output response, and thus failed at improving the operational range of the LuxR-Comparator. If needed, further mutations in the lux promoter could be tested both for the LuxR- and RpaR-Comparators to enhance the overlap of their operational ranges.

In this section I explored the input-output properties of the LuxR- and RpaR-Comparators. I observed that the RpaR-Comparator has a larger operational range than the LuxR-Comparator as well as a lower maximum output value. By increasing LuxR levels,

I obtained similar maximum output values for both the LuxR- and RpaR-Comparators. However, adding mutations in the -10 site of the lux promoter did not improve the operational range of the LuxR-Comparator by making it more sensitive to lower C6-HSL concentrations. Though more lux promoter versions could be tested, another way to compensate for the low sensitivity of the LuxR-Comparator is by engineering a strain that produces more C6-HSL compared to the strain producing pC-HSL. Since balancing quorum sensing production with the comparator input/output property is inevitable to assemble a working composition controller, I decided to link the existing comparators with the quorum sensing production modules before testing new versions of the *lux* promoter if needed.

3.2.4 Engineering strains to produce C6-HSL and pC-HSL

So far, I have explored how to tune the response of the receiver strains to an HSL input. To link the two strains in our consortia, I have to establish a two-way communication channel between them. Based on this flux of information, the strains will be able to self-adjust the composition of the coculture they are a part of. In this section I will look at building HSL sender strains producing different levels of C6-HSL and pC-HSL.

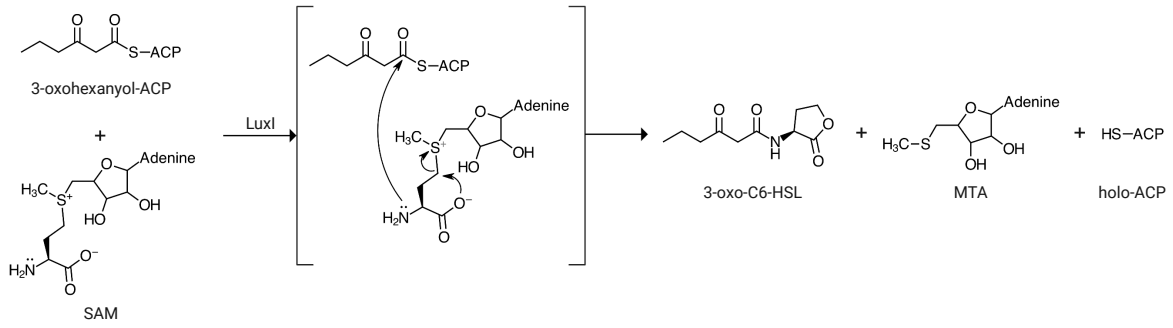


Figure 38: Biosynthesis pathway of C6-HSL. The synthase protein LuxI, from *Vibrio fischeri*, catalyses the formation the lactone ring from S-adenosyl methionine (SAM). LuxI also catalyses the acetylation from the 3-oxohexanyol-ACP donor to the lactone ring.

The biosynthesis pathways of C6-HSL and pC-HSL are depicted in Figures 38 and 39 respectively. C6-HSL is a 6-carbon N-acyl homoserine lactone. Its production is catalysed by the LuxI HSL synthase from *Vibrio fischeri* in the presence of S-adenosyl methionine (SAM) and 3-oxohexanyol-ACP donor species. As both donor species are

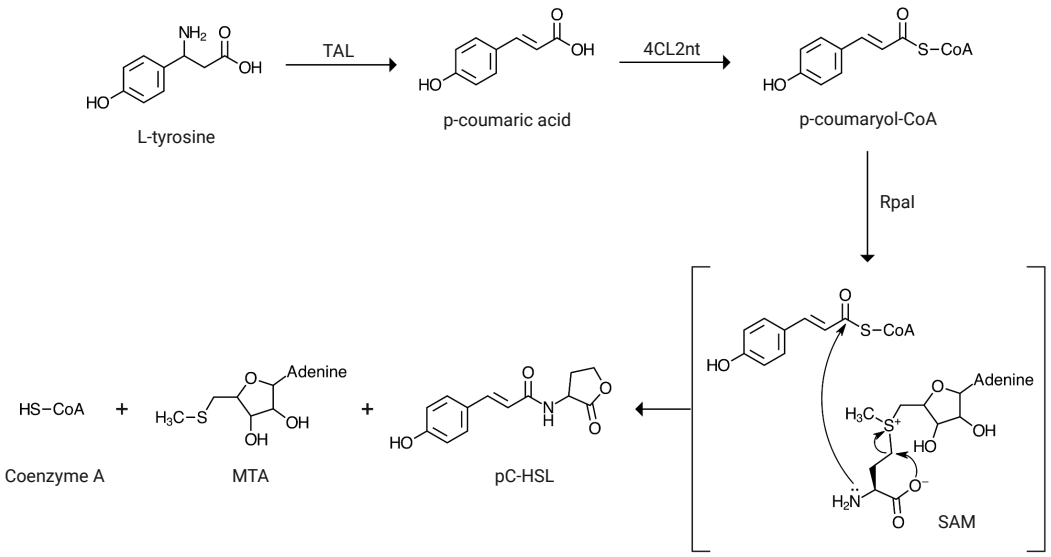


Figure 39: Biosynthesis pathway of pC-HSL. First, L-tyrosine is converted to p-coumaric acid by tyrosine ammonia lyase (TAL) from *Saccharothrix espanaensis*. p-coumaric acid is then converted to p-coumaryol-CoA by 4-coumarate-CoA ligase from *Nicotiana tabacum* (4CL2nt). HSL synthase RpaI, from *Rhodopseudomonas palustris*, finally catalises the formation of the HSL lactone ring from S-adenosyl methionine (SAM).

found in *E. coli*, producing C6-HSL only requires the expression of *luxI*. pC-HSL on the other hand requires more enzymes as it is derived from a coenzyme A (CoA) substrate not naturally found in E. coli: p-coumaroyl-CoA. p-coumaryol-CoA can be produced from L-tyrosine by expressing tyrosine ammonia lyase (TAL) that converts L-tyrosine into p-coumaric acid; and then by expressing 4-coumarate-CoA ligase from *Nicotiana tabacum* (4CL2nt) that converts p-coumaric acid to p-coumaryol-CoA. The RpaI HSL synthase is then able to convert p-coumaryol-CoA into pC-HSL. Thus, the expression of pC-HSL requires three genes. Previously, Du et al. expressed the pC-HSL pathway using an operon and achieved high pC-HSL yields. I therefore decided to assemble our three genes into the same operon organisation, with the HSL synthase in the first position in the operon [183].

I built 5 combinations of the LuxI transcriptional unit and 13 combinations of the rpa operon in DH10B, varying either the promoter or RBS strengths of the pathways. I integrated the different designs into *E. coli* by CRIM integration. I designed an experimental workflow to test the strength of the HSL production from the different strains (Figure 40). I decided

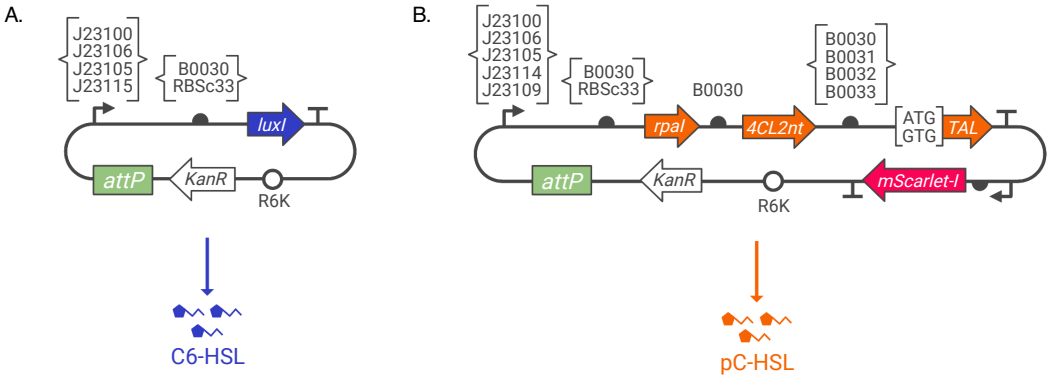


Figure 40: Engineering C6-HSL and pC-HSL producing strains. (A) CRIM integration plasmids used to build strains producing different levels of C6-HSL. (B) CRIM integration plasmids used to build strains producing various amounts of pC-HSL.

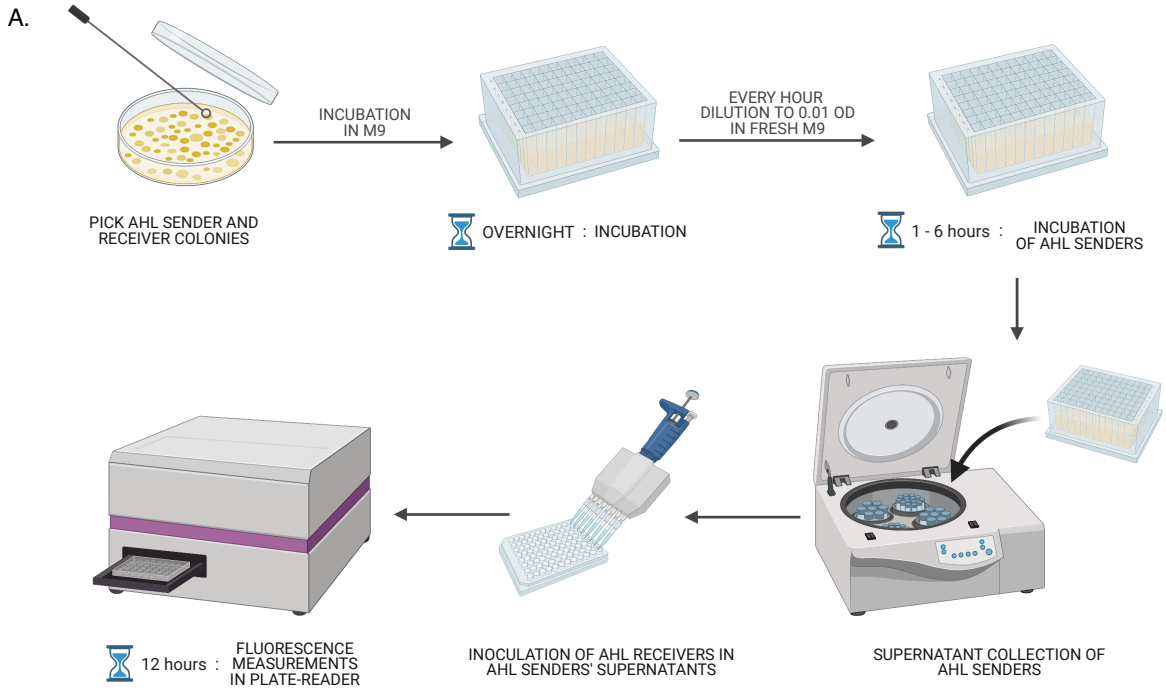


Figure 41: HSL-producing strains quantification workflow. (A) First set up overnight cultures of the quorum sensing sender and receiver strains. The sender strains produce either C6-HSL or pC-HSL. The receiver strains carry either the LuxR- or RpaR comparators. In the morning, overnight cultures are diluted and grown in M9. Every hour new cells are incubated such that at the end of the experiment, sender strains would have been incubated for various amounts of time. At the end, sender strains are centrifuged to collect the supernatant which will be diluted with half fresh M9 medium and used to grow the receiver strains into the plate-reader to measure fluorescence over time.

to culture the different sender strains for different amount of times to capture how much HSL is produced as a function of cell density (Figure 41). Sender and receiver strains were first picked and grown overnight. Senders were then diluted at different hours such that after X hours, Y sets of sender strains from Figure 40 of different cell densities were spun down to collect their supernatant, and hence the HSL they produced. Mixing the supernatant with the dBroccoli receiver strains allowed to measure the response of the receiver strains to the different amounts of HSL produced by the sender strains at different moments of their growth.

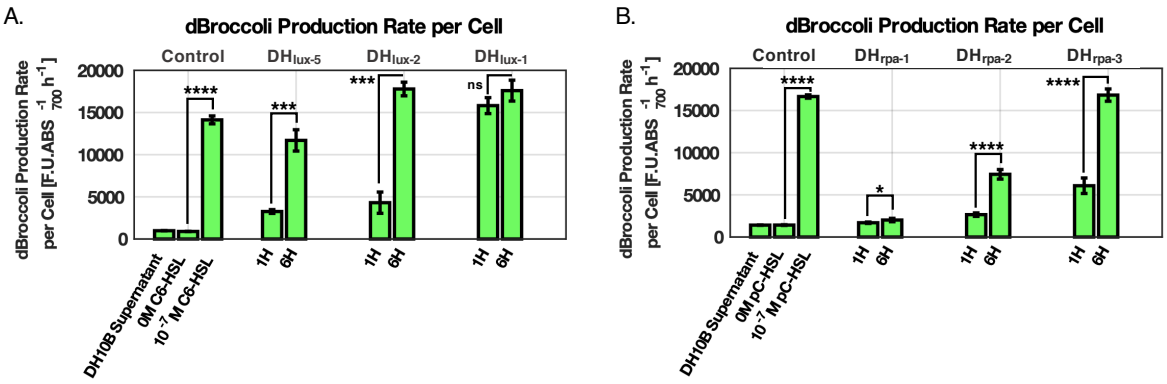


Figure 42: Characterising C6-HSL and pC-HSL producing strains. (A) Detection of C6-HSL by the dBroccoli LLL receiver strain. Supernatants containing C6-HSL produced by the C6-HSL sender strains were collected after 1 hour and 6 hours of growth. Controls are the LuxR-receiver strain mixed with the supernatant of the wild-type DH10B and with fresh media supplemented with either 0M or 10^{-7}M of C6-HSL. (B) Detection of pC-HSL by the dBroccoli LRR receiver strain. Supernatants containing pC-HSL produced by the pC-HSL sender strains were collected after 1 hour and 6 hours of growth. Controls are the dBroccoli RpaR-receiver strain mixed with the supernatant of the wild-type DH10B and with fresh media supplemented with either 0M or 10^{-7}M of pC-HSL. Experiment was done in DH10B. Fluorescence was monitored in a timecourse plate-reader assay. Data represent the mean values of n = 3 biological replicates ± s.d. Statistically significant differences were determined using two-tailed Student's t-test (**** represents $p<0.0001$, *** represents $p<0.001$, ** represents $p<0.01$, * represents $p<0.1$, ns represents not significant).

Using the quantification workflow of Figure 41, I measured the difference in dBroccoli expression when the LuxR- and RpaR-Receiver strains were mixed with supernatants from sender strains grown for 1 hour and 6 hours (Figure 42). In Figure 42.A, I present a subset of the LuxR-Receivers response to C6-HSL producing strains. We observe that both DH_{lux-1} and DH_{lux-2} have a good ratio between the C6-HSL production from 1H and 6H. So, at low cell density, not much C6-HSL is produced but the receiver strain is still able to detect it as the dBroccoli production rate is above that of the negative control. At high density, large

amounts of C6-HSL are produced as the dBroccoli expression has reached comparable levels to the positive control which is induced with saturating concentration of C6-HSL. DH_{lux-3} however has very little difference between 1 hour and 6 hours of C6-HSL production. In Figure 42.B, I compared the pC-HSL production of three pC-HSL producing strains. DH_{rpa-1} produces very little pC-HSL as there is little difference in dBroccoli expression between 1 hour and 6 hours. DH_{rpa-2} and DH_{rpa-3} are higher pC-HSL producers.

When collecting the supernatants at each hour of growth of the sender strains, we obtain an increasing gradient of dBroccoli expression shown in Figure 43. The gradient is present both in exponential phase at maximum growth rate (Figure 43.A), and during entry into stationary phase at maximum dBroccoli expression (Figure 43.B).

I used DH_{lux-5} and DH_{rpa-3} sender strains to highlight this increase of dBroccoli expression when the receiver strains are mixed with supernatants taken from the whole growth curve of the sender strains (Figure 43.C). It is interesting to note that at maximum growth rate, dBroccoli expression in the LuxR- and RpaR-receivers are very similar. But at maximum dBroccoli expression, the RpaR-receiver produces a lot more dBroccoli in response to pC-HSL present in the supernatants from the different time points than the LuxR-receiver.

I also verified that the production of quorum sensing molecules by DH_{lux-5} and DH_{rpa-3} did not have a severe impact on host growth (Appendix 90). In fact, I found that C6-HSL and pC-HSL production had a minimal impact on the growth of the DH10B strains.

In this section I built a range of strains that produce different levels of C6-HSL and pC-HSL. Though I have quantified the strength of the quorum sensing signals using dBroccoli, it would have also been possible to more accurately quantify the concentration of produced C6-HSL and pC-HSL by mass spectrometry. MS data would not have allowed us to directly select for the desired phenotypes as I was able to do using the dBroccoli reporter, but it could have provided some insight for building a mathematical model predicting the circuit's behaviour. I found that the amounts of both quorum sensing molecules produced by the sender strains can be detectable by the receiver strains. The receiver strains are also sensitive to the amount of quorum sensing molecules produced over time by the sender strains, demonstrating that different cell density of a population can regulate the expression of an RNA output into

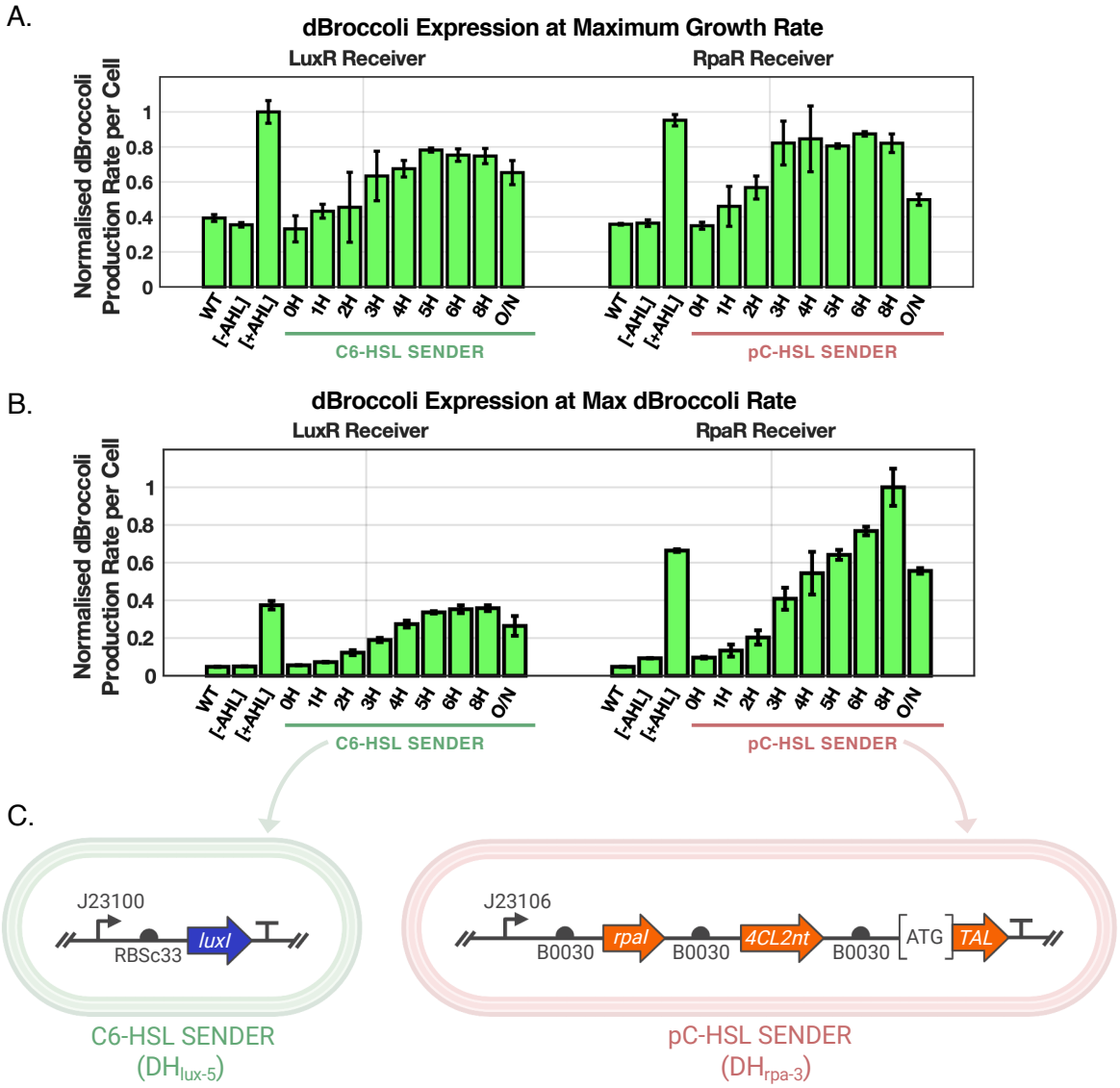


Figure 43: dBroccoli expression increases with sender strain growth. (A) dBroccoli expression at maximum growth rate (in exponential phase) when the LuxR and RpaR receiver strains are mixed with the supernatant of C6-HSL- and pC-HSL-producing strains respectively. Supernatants were collected after 1 hour to 8 hours of growing the sender strains. Controls are the receiver strains mixed with fresh M9 supplemented with either 0M or 10^{-7}M of C6/pC-HSL, [-AHL] and [+AHL] respectively. (B) dBroccoli expression at maximum dBroccoli expression (in stationary phase) when the LuxR and RpaR receiver strains are mixed with the supernatant of C6-HSL- and pC-HSL-producing strains respectively. Supernatants were collected after 1 hour to 8 hours of growing the sender strains. Controls are the receiver strains mixed with fresh M9 supplemented with either 0M or 10^{-7}M of C6/pC-HSL, [-AHL] and [+AHL] respectively. (C) AHL-producing pathways of the C6-HSL and pC-HSL sender strains. Experiment was done in DH10B. Fluorescence was monitored in a timecourse plate-reader assay. Data represent the mean values of n = 3 biological replicates ± s.d.

another cell population. These strains are a good basis to start looking at the behaviour of the STAR-based comparator when sensing the HSL signals from the sender strains.

3.2.5 Linking the comparator and the communication modules

In Chapter 2, I characterised the behaviour of the comparator module in the presence of exogenously added HSL molecules. Having constructed multiple strains producing different amounts of HSL, I can now link the comparator module to the communication module making its own endogenous HSL production.

I link the comparator and the communication modules by following the workflow of Figure 41. In Figure 44, to study the behaviour of the LuxR-comparator in response to the endogenous production of C6-HSL by the C6-HSL sender strains (Figure 44.A). I collected the supernatants of the C6-HSL sender strains after growing them for 1 hour and 6 hours. The original LuxR-comparator and the LuxR-comparator with the RiboJ insulator were then grown in the plate-reader with the supernatant collected from the sender strains. In Figure 44.B, I report the change in mRFP repression of the two comparator designs when mixed with the different supernatants. We observe that the comparators that are mixed with the strongest C6-HSL producing strains have the highest level of mRFP repression, as it is expected. When the sender strains produced little HSL after 1 hour of growth, the comparator is weakly repressed. But when mixed with supernatant from 6 growth hours, mRFP expression is downregulated compared to the 1-hour supernatant. Interestingly, the LuxR-comparator with the RiboJ insulator is less repressed than the original LuxR-comparator. This is surprising as from Figure 36.C, we saw that the input-output response of the RiboJ design was less tight, such that at lower C6-HSL concentrations, it inhibited mRFP production more than the original comparator.

Here I connected the lux communication module with the LuxR-comparator. By tuning endogenous production of C6-HSL and LuxR levels, I can tune the inhibitory response of the LuxR-comparator to be more or less sensitive to low concentrations of C6-HSL present in the supernatant of the sender strains.

Next, after connecting the lux communication module to the LuxR-comparator, I show in

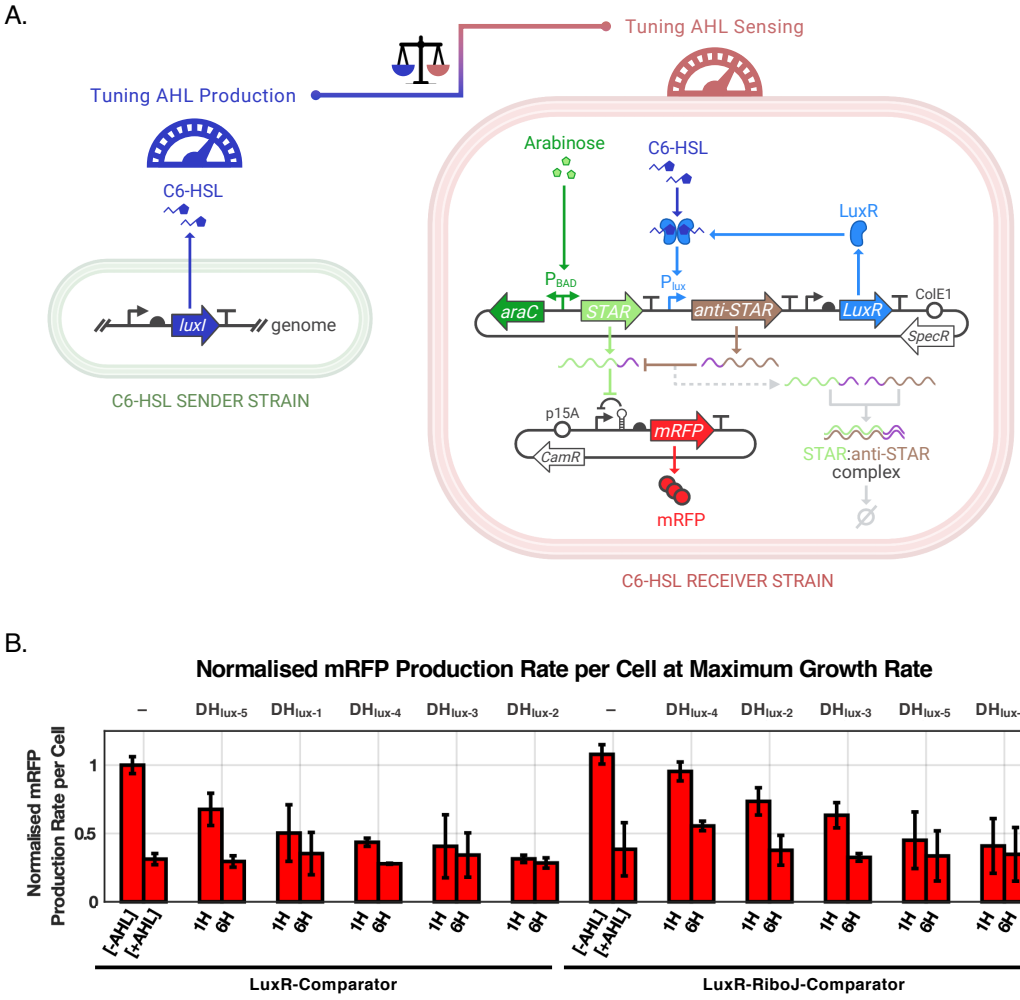
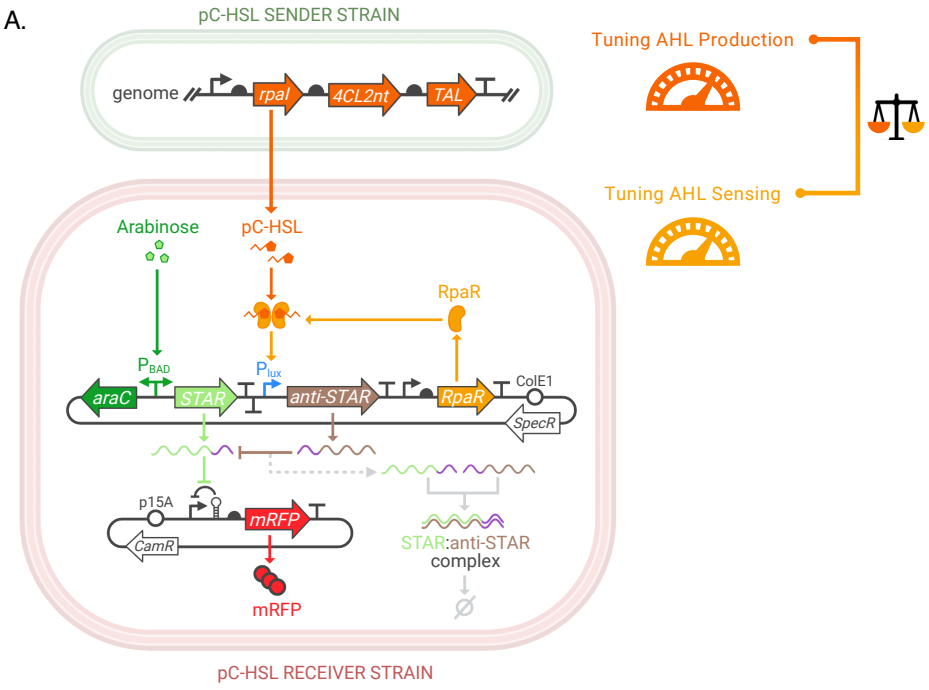


Figure 44: Response of the LuxR-Comparators to C6-HSL produced by the sender strains. (A) The sender strain expresses LuxI to produce C6-HSL. The receiver strain senses C6-HSL to trigger anti-STAR expression. (B) mRFP expression at maximum growth rate when the LuxR-Comparators are mixed with the supernatants of C6-HSL-producing strains. Supernatant were collected after 1 hour and 6 hours of growing the C6-HSL sender strains. Two versions of the LuxR-Comparators were tested: the original design and the one with the RiboJ insulation increasing LuxR cellular levels. Controls are the comparators mixed with fresh M9 supplemented with either 0M or 10^{-7}M of C6-HSL, [-AHL] and [+AHL] respectively. Experiment was done in DH10B. Fluorescence was monitored in a timecourse plate-reader assay. Data represent the mean values of n = 3 biological replicates ± s.d.

Figure 45.A that I can also connect the rpa communication module to the RpaR-comparator. To do so I selected a set of four sender strains producing pC-HSL and collected their supernatant after growing them for 1 hour and 6 hours. I mixed the RpaR-receiver strains with the supernatant and monitored the decrease in mRFP fluorescence in the plate-reader



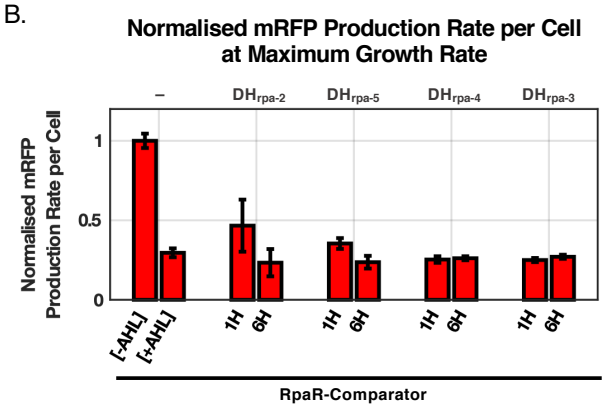


Figure 45: Response of the RpaR-Comparators to pC-HSL produced by the sender strains. (A) The sender strain expresses the rpa pathway to produce pC-HSL. The receiver strain senses pC-HSL to trigger anti-STAR expression. (B) mRFP expression at maximum growth rate when the RpaR-Comparator is mixed with the supernatants of pC-HSL-producing strains. Supernatant were collected after 1 hour and 6 hours of growing the pC-HSL sender strains. Controls are the comparators mixed with fresh M9 supplemented with either 0M or 10^{-7}M of pC-HSL, [-AHL] and [+AHL] respectively. Experiment was done in DH10B. Fluorescence was monitored in a timecourse plate-reader assay. Data represent the mean values of n = 3 biological replicates ± s.d.

(Figure 45.B). I observed that RpaR-comparator was able to detect the presence of pC-HSL in the supernatant collected at both 1 hour and 6 hours of sender strain growth. The selected sender strains produced high amounts of pC-HSL as I observe that comparator strains

mixed with all 1-hour supernatants have their mRFP production rate per cell inhibited by at least 50% compared to the negative control that is grown in M9 with 0M of pC-HSL. DH_{rpa-4} and DH_{rpa-3} have such high pC-HSL production that the comparator operates in the saturation range when it is already mixed with the 1-hour supernatants from these two strains. There is therefore no difference in mRFP expression between the 1-hour and 6-hour supernatants in these two strains.

I have confirmed that the RpaR-comparator can sense the pC-HSL levels produced by the pC-HSL producing strains. Tuning of the pC-HSL production and comparator response will have to be tuned according to the need of the growth regulation module, depending on how strong the regulation is in both C6-HSL and pC-HSL sensing strains. I now have the tools necessary to do this: strains producing different levels of quorum sensing molecules and comparators with different input/output properties.

3.3 Conclusions

In this chapter, I have identified two quorum sensing systems with output promoter properties that are similar and signal orthogonal. The lux promoter driving anti-STAR expression in one strain is driven by the LuxR and C6-HSL complex, while in the second strain it is driven by the RpaR and pC-HSL complex. I confirmed that C6-HSL is not able to form an activating complex with RpaR. Similarly, LuxR cannot bind to the pC-HSL ligand to activate gene expression from the lux promoter. Using CRIM integration and lambda red recombination, I built a set of strains that genomically produce both C6-HSL and pC-HSL at different rates. I characterised the strength of the quorum sensing molecules production using the dBroccoli fluorescent aptamer. Using this information, I selected strains that displayed the largest difference in expression at low and high population density. By increasing the expression of the LuxR regulator protein, I showed that I could play with the sensitivity and tightness of the STAR-based comparator. The set of quorum sensing producing strains and different comparators will be used to modulate the strength of signal to detection ratio in the final coculture. I now have the communication tools to enable propagation of information about population density in our coculture. I also have the necessary tools to tune the response to

population density based on the strength of the growth regulation modules I will develop in the following chapters.

Chapter 4

Controlling Growth Rate Using RNA-based Regulators

Contents

4.1 Introduction 87

4.2 Results and discussion 88

4.2.1 Implementing reversible auxotrophy using CRISPRi 88

4.2.2 Regulating growth rate using sRNA 101

4.2.3 Regulating growth rate through expression burden and STAR 107

4.3 Conclusions 114

4.1 Introduction

In the previous chapters, I have established a 2-way communication channel to allow the two strains in the coculture to exchange information about their respective cellular density. I have also looked at how each strain can process this information about population density to compare it to a reference signal and produce an output signal that will actuate the growth regulation module if needed, that is if the coculture composition set by the reference signal is going out of balance. The next step, which I will explore in this chapter, is to set up a growth regulation mechanism to correct imbalances in coculture composition.

As seen in the introduction, there are already several accounts of regulating growth rates in cocultures. Down-regulation of the growth rate can be implemented via bacteriocins, toxins (e.g. CcdB), lysis proteins [87, 63, 64]. Producing the resistance gene or the anti-toxin (e.g. CcdA) allows to alleviate the effect of killing agents and rescue the growth rate

of the cell. In the case of lysis, the population is controlled through oscillatory lysis cycles. Growth rate can also be upregulated instead of being down-regulated and then rescued. Stephens et al. showed that they could upregulate growth rate by about 40% by expressing a phosphotransferase system (PTS) protein, HPr, which improves glucose transport in *E. coli* [119]. Lillaci et al. also showed that modulating the expression of an essential gene, *metE*, they could improve growth rate of their cells by 50% [184].

Due the the architecture of our circuit, I need a system that can down-regulate growth rate when the coculture composition is unbalanced due to the two strains growing at different growth rates. Toxins and antimicrobial agents are two commonly used systems to down-regulate growth rate. CcdB is a highly potent toxin that acts by inhibiting DNA gyrase GyrA, which causes double stranded DNA breaks inside the cell [19]. Antibiotic-based strategies also involve the production of highly toxic compounds such as bacteriocins (e.g. microcin-V) and antimicrobial peptides that forms pores in bacterial cellular membranes to kill the cells [185, 21]. Those strategies, though very efficient, rely on killing part of the population to regulate its density. In the spirit of designing a genetic design with the least impact on its host, and hence reduce mutation pressure as much as possible, I decided not to rely on the use of toxins and antibiotics. Instead, in this chapter, I investigate new down-regulation mechanisms of growth instead of killing the cell. More specifically, I study how to use RNA-based regulators to control bacterial growth rates.

First I will look at using clustered regularly interspaced short palindromic repeats interference (CRISPRi) and small RNA (sRNA) to implement a reversible auxotrophy strategy to tune growth rate based on the expression level of an RNA regulator. Then I will explore how to directly use STAR to tune the expression level of a large protein or operon of interest in order to control growth rate using the pathway of interest directly. This would allow to minimise the number of genetic elements that have to be expressed in the cell.

4.2 Results and discussion

4.2.1 Implementing reversible auxotrophy using CRISPRi

In this section I will show that CRISPRi can be connected to the output of the quorum-controlled STAR-based comparator module to modulate growth rate based on HSL concen-

tration in the media.

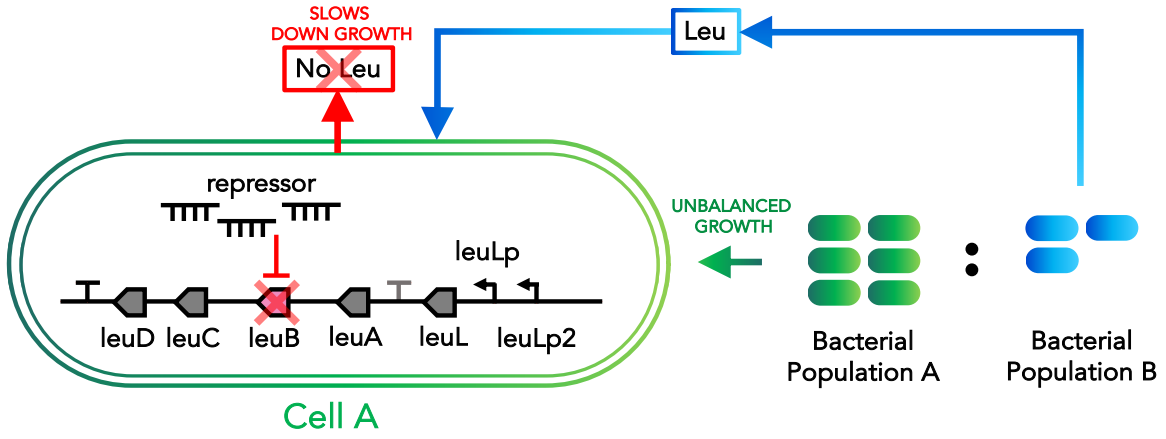


Figure 46: Growth rate modulation via reversible auxotrophy. When the coculture composition is out of balance, an RNA-based repressor is expressed to tune growth rate and as a result correct coculture ratio.

Reversible auxotrophy is the ability to knockdown the expression of an essential gene to decrease growth rate, without removing the gene entirely like it is the case for gene knockouts. The advantage of using essential gene knockdowns is that the knockdown effect is potentially reversible, permitting one to design a dynamic control system. I summarise the reversible auxotrophy approach in Figure 46. If in a coculture composed of two strains, which I call population A and population B, the population composition is driven out of equilibrium, tuning the expression of an essential gene will either slow down or improve growth rate of the strains in the coculture to restore the desired ratio between these two strains. In addition, when an essential gene knockdown is activated in one strain, it creates a dependency of this strain upon the other such that it can only survive by importing the essential molecule it can no longer produce from the other strain, or by mutating the knockdown regulator species. I hypothesise that the syntrophic relationship between the two strains can lessen the mutation pressure on the knockdown species since the metabolite is still present in the growth media. Therefore I decided to prioritise targeting genes producing metabolites that can be exported and imported between the two species.

Previously, some studies have designed genome-wide CRISPRi screens to identify essential genes [146, 186] that can act as switches for growth regulation. One category of essential genes they identified was genes involved in amino acid biosynthesis. I will focus on using leucine

and histidine as examples for growth regulation using CRISPRi.

4.2.1.1 Programming CRISPRi to target the LeuLp promoter

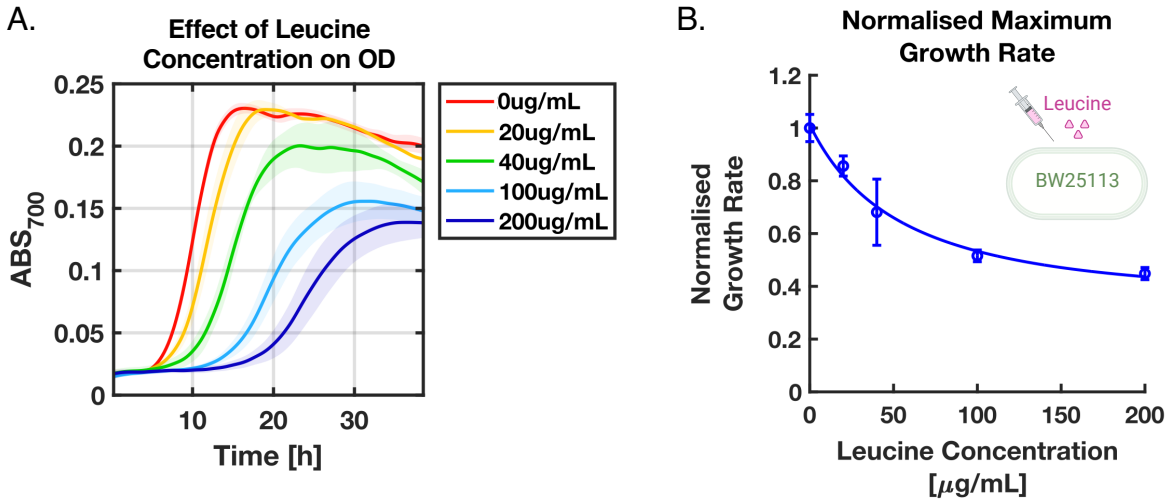
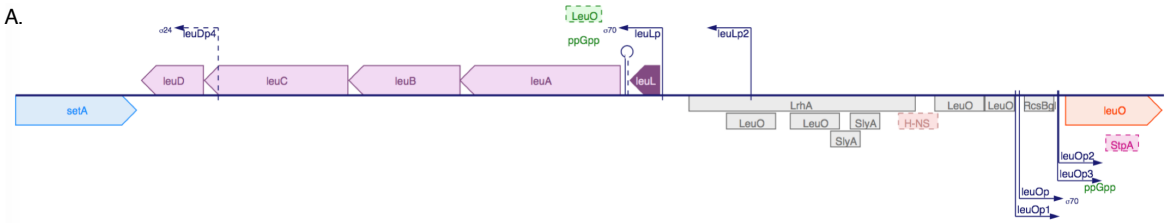


Figure 47: Growth rate modulation via external chemical control. (A) BW25113 cells were grown in amino acid deficient M9 media with different concentrations of L-leucine. L-leucine causes toxicity by inhibiting the expression of the ilvGM and ilvBN operons unless none or all three branched amino acids (leu, val, ile) are present in the media.(B) Maximum growth rate of BW25113 when different concentrations of leucine are exogenously added to the media. Experiment was done in BW25113. Data represent the mean values of n = 3 biological replicates ± s.d.

First I verified that our strain could grow in minimal M9 media that is not supplemented with any amino acid (Figure 47.A). The parent strain of the Keio collection, BW25113, could grow in the absence of leucine. In the presence of leucine, growth rate was inhibited up to 60% as leucine concentration increased. That is because leucine inhibits the expression of two operons, ilvGM and ilvBN, involved in valine and isoleucine synthesis. Repression of ilvGM and ilvBN does not occur if all three branched amino acids or none of them are present in the growth media. I envision that L-leucine could be used to modulate growth rate in cocultures controlled with an *in silico* feedback loop.

CRISPRi requires the expression of both a gRNA composed of a spacer and scaffold sequences, and of the deactivated Cas9 (dCas9) protein. The gRNA spacer is the component of the CRISPRi system that drives the specific targeting to a predefined sequence. To repress leucine production, I decided to design a gRNA that would target the leucine operon (Figure 48.A). It has been shown that targeting an operon promoter or a gene within the operon



Target	gRNA spacer sequence	On-Target Score	Off-Target Score
LeuLp	agagttactggatacaaaaa	41.8	50
LeuLp2	gatttttttgatattgatt	49.1	50
leuB	ccatattgccgtattgccgg	67.4	49.9

Figure 48: Designing a gRNA to target the LeuLp promoter. (A) Structure of the native leucine operon in BW25113 from EcoCyc [187]. (B) The LeuLp promoter annotated with the -35, -10 and +1 sites. The pink "LeuLp sgRNA" annotation identifies the promoter region that will be targeted by the guide RNA (gRNA). (C) The on-target and off-target scores of the LeuLp gRNA.

was effective to turn down expression of all subsequent genes in the operon [188, 147]. Using Benchling's CRISPR Design Tool, I searched for "NGG" PAM sequences in the LeuLp and LeuLp promoter as well as in the beginning of the coding sequence of the essential *leuB* gene [189]. I selected the 20 nt gRNA spacer designs with the best on-target score (the higher the better), and the best off-target score (the higher the less off-target activity). I show the best gRNA spacer in the the LeuLp promoter in Figure 48.B and the target scores of the gRNAs are recorded Figure 48.C.

Once the spacers were designed, I cloned them upstream of a gRNA scaffold from the *Streptococcus pyogenes* CRISPR/Cas9 system [35]. To ensure the proper folding of the transcribed gRNA without suffering from the genetic context in which the gRNA is expressed, I decided to flank both sides of the gRNA with self-cleaving ribozymes [190, 191]. I flanked the 5' side of the gRNA with a hammerhead ribozyme (HH) sequence and the 3' side with the hepatitis delta virus ribozyme (HDV) sequence, such that after cleavage the gRNA would not contain extraneous sequences from either the promoter or the terminator sequences. This ensures that though I characterise the system by expressing the gRNA using the araBAD promoter, a different promoter should be able to be used without impacting gRNA folding.

dCas9 is the last component of the CRISPRi that needs to be expressed to test whether

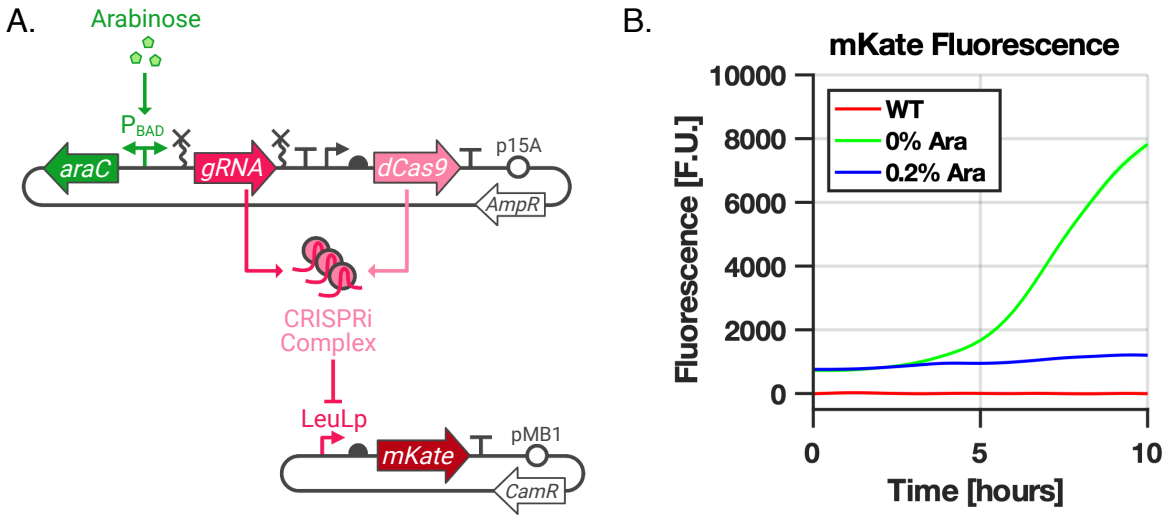


Figure 49: Using CRISPRi to knockdown the LeuLp promoter. (A) gRNA expression is driven by the arBAD promoter. The gRNA sequence is flanked by the Hammerhead ribozyme (HH) on its 5' side and by the hepatitis delta virus ribozyme (HDV) on its 3' side. dCas9 is expressed using a weak constitutive promoter and RBS sequences. gRNA and dCas9 bind to form a CRISPRi complex that targets the LeuLp promoter controlling mKate expression. (B) In the absence of L-arabinose, the LeuLp promoter drives expression of mKate. But in the presence of L-arabinose (0.2%), gRNA is produced and forms a complex with dCas9. The complex binds to the LeuLp promoter and inhibits its activity. Experiment was done in BW25113. Growth and fluorescence were monitored in a timecourse plate-reader assay. Data represent the mean values of n = 3 biological replicates ± s.d.

I can successfully target the LeuLp promoter. Previous works reported that high expression of dCas9 can be toxic for the cell, but that high enough dCas9 expression is required to maintain CRISPRi activity [192]. I expressed the dCas9 protein from a medium copy plasmid with a very weak promoter and RBS according to our previous work published by Ceroni et al. to prevent impacting cell growth rate while still maintaining a good activity level of the dCas9:gRNA complex [35].

In Figure 49, I expressed the gRNA containing the spacer targeting the LeuLp promoter followed by a fluorescence reporter protein (mKate). When no L-arabinose was externally added to the media, the LeuLp promoter was not repressed and drove expression of mKate (Figure 49.B). However, when gRNA production was activated in the presence of L-arabinose, mKate production was completely repressed, confirming that our CRISPRi complex was effective at targeting the LeuLp promoter. I can now investigate how CRISPRi impacts the growth of the cell when the CRISPRi complex targets the LeuLp promoter controlling the

native leucine pathway.

I note that instead of regulating essential gene expression from the genome, I could have opted for a plasmid-based regulation system. I could have used a strain containing the knockout of an essential gene from the leucine pathway such as *leuB* and clone it onto a plasmid. The CRISPRi complex could have then been used to target the promoter driving *leuB* expression to modulate growth rate as similarly done by Lillacci et al. [184]. I explored this growth control option by transforming the growth controller from Lillacci et al. into BW25113 with the *metE* knockout (JW3805-1) [184]. In their system *metE* was controlled by the sigW σ-factor expressed using the LLL quorum sensing system. Unfortunately their system did not function in our strain (data not shown). It may be due to the fact that their circuit is not robust across different *E. coli* strains. Though this is surprising as JW3805-1 and SKA1328 have very similar phenotypes, though the first is derived from the BW25113 parental strain and the second from MG1655. Since this growth regulation method relied on the use of knockouts, I envision that it could lead to a lack of modularity of our system as each new user would be limited to using the original strain used to develop the system, and if they wanted to use their own strain, re-tuning of the genetic circuit would be required to preserve circuit functionality and input-output properties. Therefore to preserve the modularity of the system, I decided not to use knockout strains.

4.2.1.2 Building a leucine operon knockdown using CRISPRi

Now that I have demonstrated that our gRNA design can target the LeuLp promoter based on a plasmid, I investigated whether it can also target the native LeuLp promoter driving expression of the leucine operon in the genome of BW25113.

In Figure 50.A, I use the ΔLeuB Keio strain as a negative control to verify that in the absence of an essential gene required for leucine biosynthesis, the cell is unable to grow in a medium lacking L-leucine (M9 medium not supplemented with any amino acid). When expressing the CRISPRi system targeting the native LeuLp promoter (Figure 50.B), I observe that unlike the ΔLeuB knockout, the leucine knockdown was able to

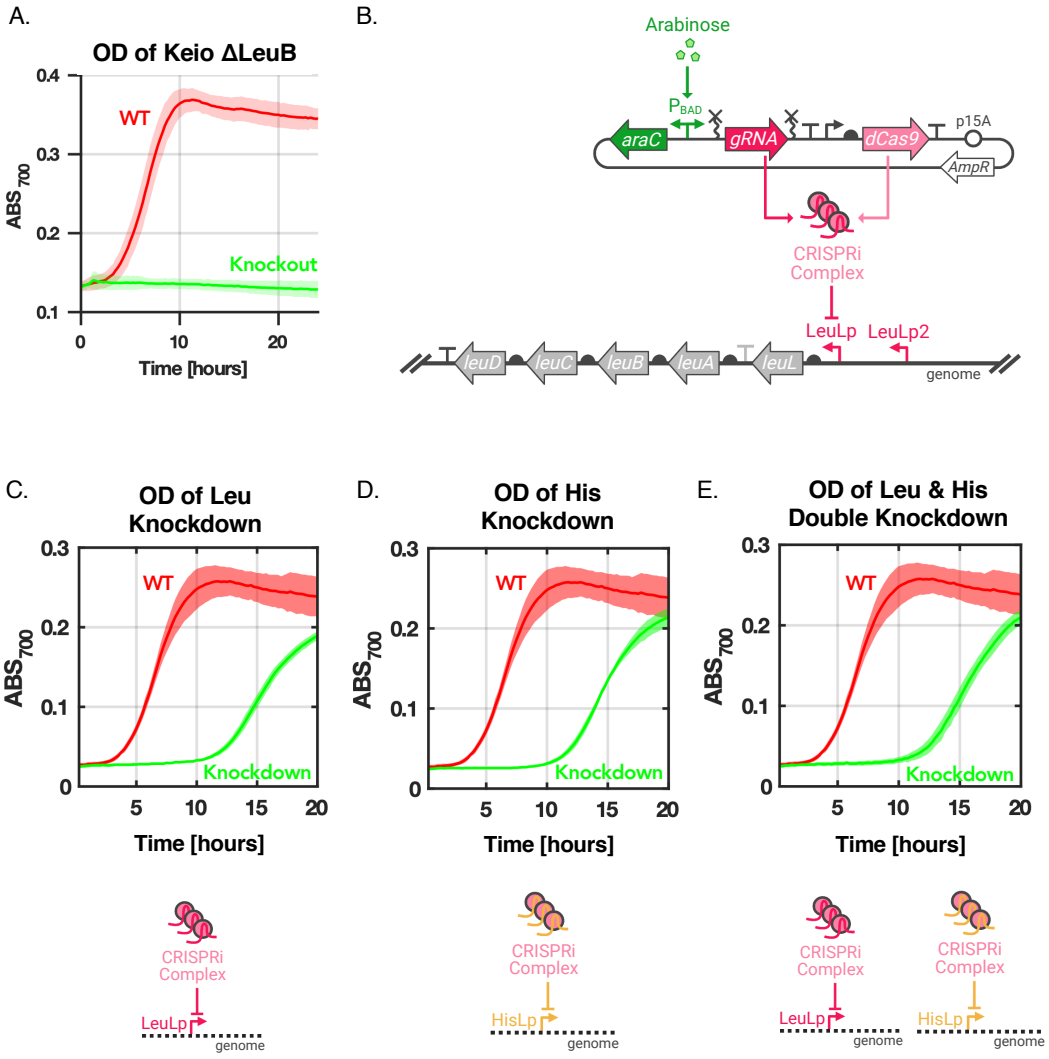


Figure 50: Building gene knockdowns with CRISPRi. (A) Growth of the wild-type BW25113, parent strain of the Keio collection, compared to the growth of the Keio ΔLeuB knockout. (B) The CRISPRi plasmid expresses dCas9 constitutively and a gRNA under the control of the araBAD promoter. The gRNA targets the native LeuLp promoter driving expression of the leucine operon. (C) Growth of wild-type BW25113 and the leucine knockdown when the gRNA:dCas9 complex inhibits transcription of the LeuLp promoter. 0.2% of L-arabinose was externally added to the knockdown strain. (D) Growth of wild-type BW25113 and the histidine knockdown when the gRNA:dCas9 complex inhibits transcription of the HisLp promoter. 0.2% of L-arabinose was externally added to the knockdown strain. (E) Growth of wild-type BW25113 and the double leucine-histidine knockdown when two gRNAs are expressed from the CRISPRi plasmid to target the LeuLp and HisLp promoters. The two gRNAs bind competitively to dCas9. 0.2% of L-arabinose was externally added to the knockdown strain. Experiments were done in BW25113. Strains were grown in M9 medium not supplemented with casaminoacids. Growth was monitored in a timecourse plate-reader assay. Data represent the mean values of n = 3 biological replicates ± s.d.

grow after a lag-phase of about 10 hours (Figure 50.C). A genome-wide CRISPRi screen study performed in *B. subtilis* revealed similar lag-phases in 95% of the knockdowns [193]. This revealed that for limiting concentrations of an essential product due to gene knockdown, the cell population becomes heterogeneous. One portion of the cells were either dead or non-growing, while the other fraction exhibited similar growth to the WT. Similarly for our knockdowns, it seemed that when targeting different essential amino acid biosynthesis pathways (e.g. the histidine pathway in Figure 50.D), a fraction of the cells were non-viable resulting in extended lag times. To verify that the effect on growth was due to our gRNAs targeting either the leucine or histidine operon, I expressed a control gRNA, designed specifically to prevent interaction with the cell (Appendix 8.11) [156]. I confirmed the expression of the control gRNA did not impact growth compared to gRNA targeting the LeuLp and HisLp promoters. When expressing two gRNA simultaneously from the same CRISPRi plasmid, to target two different amino acid pathways (e.g. the leucine and histidine pathways in Figure 50.E), the lag time was not lengthened but instead matched the lag phase duration of both single knockdowns. This result was surprising as I hypothesised that inhibiting the production of two amino acids from different groups such as leucine and histidine would increase the lag-time as the cell would need to acquire multiple mutations to escape CRISPRi inhibition in the leucine and histidine biosynthetic pathways. The fact that the lag-time is similar for both individual knockdowns but also for the double knockdown, suggests that the evolutionary mechanism by which the cell is able to escape CRISPRi inhibition may be common to both amino acid knockdowns. So I suggest that the escape could either be caused by a mutation in the dCas9 CDS or that the strains undergo an evolutionary adaptation that is common to both the leucine and histidine knockdowns. I also hypothesised that the escape from lag-phase could be the result of a heterogeneous population sensitive to low levels of L-leucine and L-histidine in the media.

To be certain that growth after the lag-phase was not due to mutations, I sequenced the different components of the CRISPRi system to identify potential mutations. For three biological replicates, I sequenced the LeuLp promoter, the gRNA and dCas9 by Sanger sequencing. I found that none of the replicates grown from the saturated cultures of Figure 50.C carried mutations in either the target promoter, gRNA or dCas9 protein sequences.

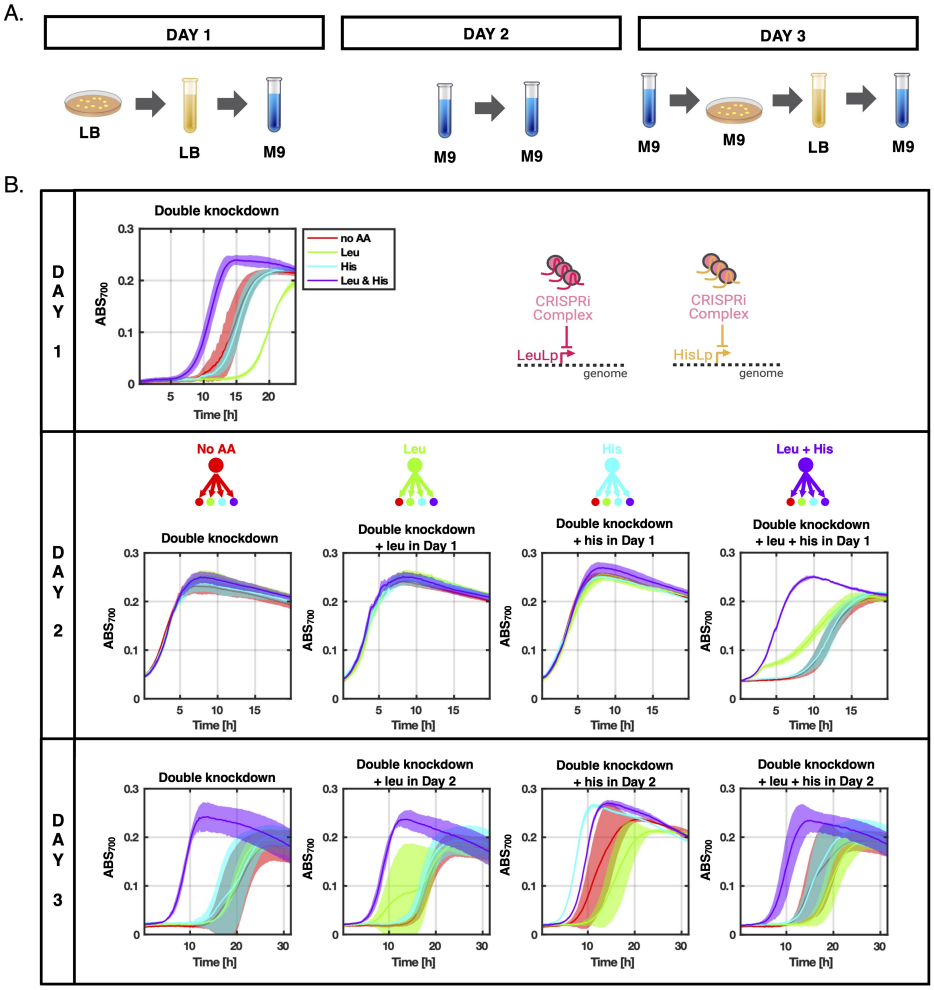


Figure 51: CRISPRi knockdown creates population heterogeneity. (A) Assay to assess the heterogeneity of the CRISPRi knockdown populations. On the first day, double leucine-histidine knockdown colonies were picked from an LB agar plate and grown in LB. Once they reached 0.2 OD_{700}, they were diluted in poor M9 medium either supplemented with no amino acids, with L-leucine only, with L-histidine only, or with both L-leucine and L-histidine. Cell growth was monitored in the plate-reader. On the second day, cells grown in each of the four conditions were diluted back in M9 with the four amino acid conditions and growth was monitored in the plate-reader. Once the cells reached saturation, they were plated on M9 plates with no amino acid. Cells were then grown in LB to 0.2 OD_{700} and diluted back into M9 medium in all four amino acid conditions. (B) Growth observed during each day of the experiment. On Day 1, cells transitioned from rich to poor medium growth. On Day 2, cells had adapted to growing in poor medium. On day 3, cells that had adapted to growing in poor medium before being grown in poor medium again. Growth was monitored in a timecourse plate-reader assay. Experiments were done in BW25113. Data represent the mean values of n = 3 biological replicates ± s.d.

I further investigated whether I could confirm the presence of a heterogeneous population in our knockdown strains. To do so, I created an assay (Figure 51), to study the growth

profile of a double knockdown when passaged from growing in rich medium where there is no limitation on access to essential products to growing in poor medium where few essential products are available for growth. I used the double leucine-histidine knockdown from Figure 50.E to show the effect of amino acid presence on knockdown growth profile. I observed that when cells are grown in poor medium after initially cultured in rich medium (LB), all knockdowns grown in the absence of both L-leucine and L-histidine have a lag-phase of at least 10 hours (Day 1 in Figure 51.B). Interestingly on Day 2 (Figure 51.B), the cells that grew in the absence of both amino acids or at least one amino acid were able to grow without exhibiting any long lag-phase. However the cells that were grown with both L-leucine and L-histidine all exhibited a long lag-phase unless grown in the presence of both amino acids. This suggests that the cells with minimum lag-phase exhibited WT-like growth and were selected as they overtook the saturated culture in Day 1. However when both L-leucine and L-histidine were supplemented, there was no selection of the cells exhibiting WT-like growth as there was no advantage to carrying the WT-like phenotype when amino acid concentration was not limiting. After Day 2, I selected the WT-like phenotype by growing the saturated culture on poor M9 agar plates. I then reset the condition by growing them in rich media before monitoring their growth in poor M9 medium again (Day 3 in 51.B). All strains exhibited extended lag-phases compared to Day 2, suggesting that the adaptation of WT-like knockdowns was lost during growth in non-amino-acid-limiting growth medium. I hypothesised that the adaptation of WT-like knockdowns is the result of pressure due to limited access to essential metabolic products. Further investigation using RNA-seq genome-wide screening would be interesting to uncover the adaptation mechanism that is allowing WT-like knockdowns to grow without extended lag-phases.

Having explored the effects of strong LeuLp repression on our leucine knockdown, I investigate how to tune LeuLp repression to be able to affect knockdown growth rate instead of lag-phase duration. In Figure 52, I placed the expression of gRNA under the control of STAR inducible by C6-HSL (Figure 52.A). dCas9 is constitutively expressed and upon binding with the gRNA, the LeuLp promoter is repressed. In Figure 52.B, I removed the STAR plasmid to check whether gRNA leaky expression from the STAR target had an impact on growth rate. I observed that the leaky expression of gRNA is enough to initiate a long lag-phase of around

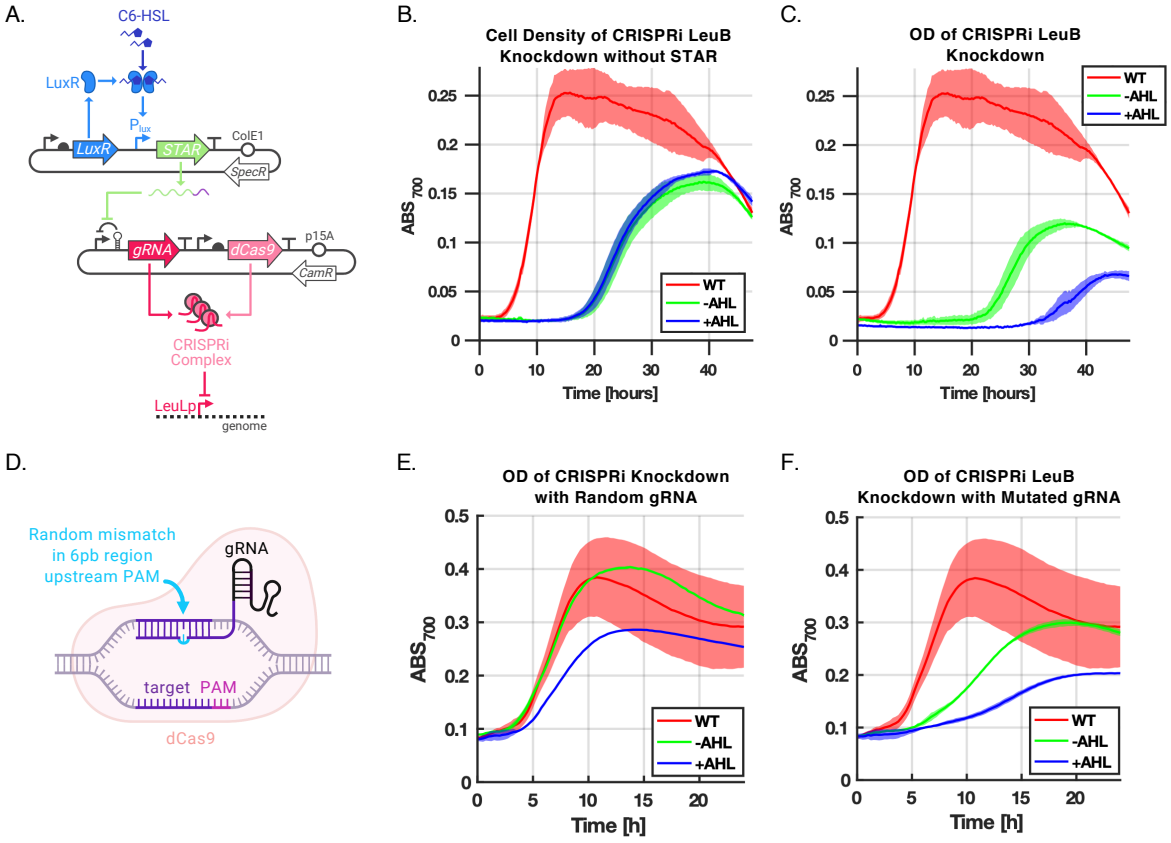


Figure 52: Using CRISPRi to knockdown the leucine operon. (A) The LLL quorum sensing system controls STAR (with Toehold 2) production. In the presence of STAR, gRNA is transcribed and forms an inhibiting complex with dCas9 that targets to LeuLp promoter to repress expression of the leucine operon. "WT" shows OD of the wild-type BW25113 strain. "-AHL" and "+AHL" show growth of the cell containing the CRISPRi plasmid when 0M and 10^{-7}M of C6-HSL is added externally. (B) In the absence the plasmid expressing STAR, OD of the cells is inhibited by leaky transcription of gRNA. (C) In the presence of both plasmids, 10^{-7}M C6-HSL ("+AHL") activates STAR expression, in turn increasing gRNA production, which consequently inhibits cellular growth and extends lag-phase. (D) Building a random library of gRNA containing 1 bp mutation in the 6 bp region preceding the PAM sequence flanking the targeting region in the LeuLp promoter. (E) OD of the cells with the double plasmid system expressing a random gRNA designed with R2oDNA Designer [194]. (F) OD of the cells with the double plasmid system expressing a mutated gRNA (A→C in the bp preceeding the PAM sequence). Experiments were done in BW25113. Growth was monitored in a timecourse plate-reader assay. Data represent the mean values of n = 3 biological replicates ± s.d.

20 hours and that C6-HSL has no impact on growth rate. As the LeuLp promoter is now in the genome, instead of the p15A plasmid from Figure 50, there are significantly less copies of LeuLp, which also exacerbates gRNA leakiness effects since dCas9 binding to the promoter will saturate more quickly. When the STAR plasmid is present (Figure 52.C), I observe that in the absence of STAR production, i.e. when no external C6-HSL is added ("-AHL"), the

lag-phase of the cells is maintained at 20 hours. While when 10^{-7}M of C6-HSL is added ("+AHL"), the lag-phase is increased by 1/3.

To reduce the strength of the impact on growth, I decided to reduce the binding affinity of the CRISPRi complex to the LeuLp promoter. I introduced 1 bp random mutation within the 6 bp preceding the PAM sequence as previously done by Ceroni et al. to modulate the repression strength of the gene of interest (52.D) [35]. As a control for our library, I also designed a random gRNA spacer using R2oDNA Designer [194]. The random spacer was predicted to have minimal interaction with the host DNA, hence expressing the random gRNA should have minimal impact on host growth as shown in 52.E. While testing our library of mutated gRNA, I observed that mutations not occurring in the base pair preceding the PAM sequence did not significantly reduce lag-phase and improve growth (Appendix 8.10). Only mutations occurring in the base pair directly preceding the PAM sequence improved the growth profile of our cells (52.F). Expression of the gRNA in the "+AHL" condition reduced the maximum growth rate of the strain by 31% compared to the "-AHL" condition, for with growth rate inhibition was only due to leaky expression of the gRNA.

In this section, I have identified gRNA sequences that can successfully target native promoters driving expression of essential amino acid operons in the BW25113 strain. I have also highlighted the importance of tuning CRISPRi repression to modify growth rates instead of inducing prolonged lag phases. In the future, I envision using multiple mutations with the gRNA to further reduce the impact of gRNA on growth rate that is due to leaky expression of gRNA.

4.2.1.3 Connecting the comparator to the CRISPRi growth regulation module

After having shown that I could repress maximum growth rate by about 30% by expressing a mutated gRNA, I link the production of gRNA to the STAR-based comparator from Chapter 2. I use the version of the comparator based on the LLL quorum sensing system such that rescue of the growth inhibition mechanism is enabled via the sensing of C6-HSL.

I used the gRNA mutated sequence from Figure 52.F as a target for STAR activation (53.A). In the presence of L-arabinose, STAR is produced and inhibits the formation of the

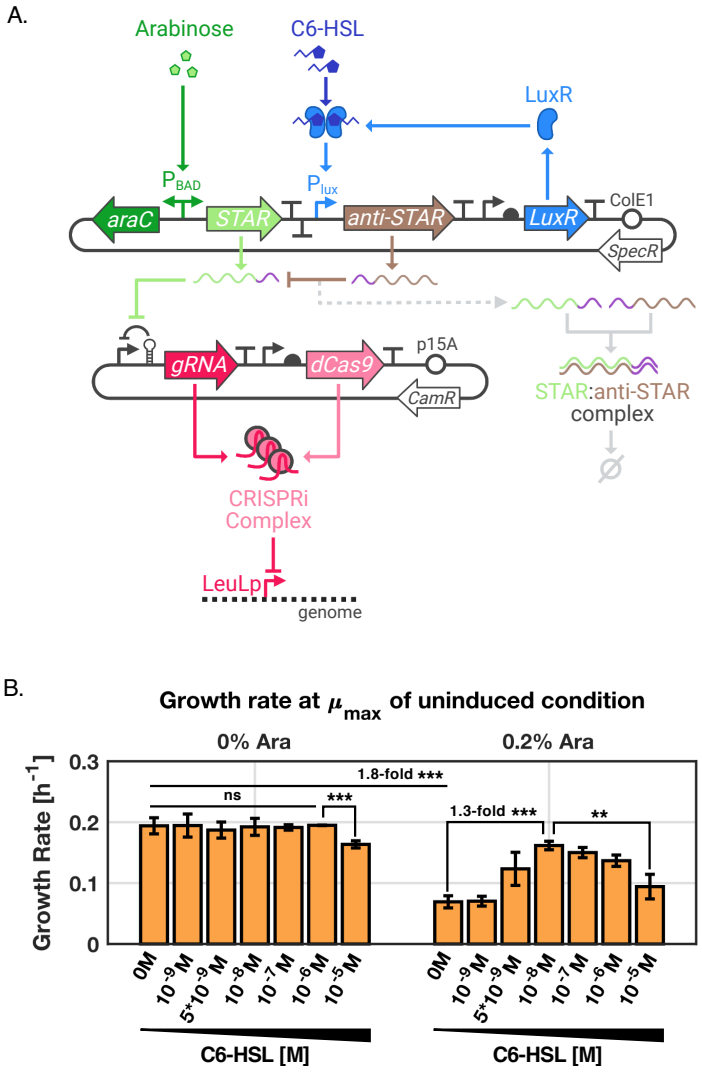


Figure 53: Connecting the comparator to the CRISPRi module. (A) The STAR-based comparator with Toehold 2 controls the expression of mutated gRNA targeting the LeuLp promoter. Anti-STAR expression is driven by the LLL quorum sensing system. (B) Growth rate of the comparator linked to the CRISPRi module targeting leucine expression at the time of maximum growth rate of the uninduced condition (0% L-arabinose, 0M C6-HSL). Growth rate is shown for two induction levels of STAR by L-arabinose (0% and 0.2%) and seven induction levels of C6-HSL (from 0M to 10^{-5}M). Experiments were done in BW25113. Growth was monitored in a timecourse plate-reader assay. Data represent the mean values of n = 3 biological replicates ± s.d. Statistically significant differences were determined using two-tailed Student's t-test (**** represents p<0.0001, *** represents p<0.001, ** represents p<0.01, * represents p<0.1, ns represents not significant).

termination hairpin of the RNA STAR target. This leads to increasing the intracellular levels of gRNA, which once bound in a complex with the constitutively expressed dCas9, will inhibit transcriptional initiation of the LeuLp promoter, causing growth rate repression as a result.

However in the presence of C6-HSL quorum sensing molecule, STAR's complementary RNA species, anti-STAR, will be produced and sequester available STAR RNA strands in the cell, effectively rescuing cell growth. In Figure 53.B, I observe that first, expressing the rescue mechanism alone reduces growth rate by up to 15.6%, that is when the system is only externally induced with C6-HSL to produce anti-STAR. When no rescue mechanism is in place, that is for 0M of C6-HSL when no anti-STAR is expressed, growth rate was reduced by 1.8-fold when the gRNA targeting the LeuLp promoter is produced using maximal levels of L-arabinose (0.2%) compared to when no arabinose is externally added to induced the CRISPRi growth module. Further, in the presence of 0.2% L-arabinose, the anti-STAR rescue mechanism is able to rescue growth rate by 1.3-fold.

I have shown that the STAR-based comparator can successfully decrease and rescue growth rate based on the sensing of the C6-HSL quorum sensing molecule. Though current results demonstrate that the comparator can work in concert with the CRISPRi module to control cell growth, improvements are needed to improve the tunability of the CRISPRi module. With further modifications to the gRNA, I hope that in the future I can reduce the leaky effect of gRNA on growth rate, and improve the fold recovery of cellular growth rate.

4.2.2 Regulating growth rate using sRNA

As seen in the introduction, small RNAs (sRNA) have been a useful tool for synthetic biology to study essential gene silencing and regulate gene circuits in *E. coli* [165, 131, 161, 162, 195]. sRNA have the advantage to bind to mRNA to regulate gene expression, instead of regulating expression by binding to DNA directly as CRISPRi. Though CRISPRi is very efficient at targeting DNA, it also has very slow unbinding kinetics [196, 197]. As the rate of dCas9 unbinding is slower than replication, it is likely that once the CRISPRi regulation system is in place, it is nearly impossible to turn it off. This significantly reduces the dynamic potential of the circuit, especially when it comes to growth regulation through amino acid knockdowns. Using sRNA should solve this dynamics problem as the turnover of sRNA is much higher than the unbinding kinetics of dCas9. Indeed, sRNA promotes the fast degradation of the sRNA:mRNA complex by RNAse E [198, 159]. In this section, I explore whether I can build a dynamic growth regulation module based on the use of sRNAs.

4.2.2.1 Using RNA silencing to build essential gene knockdowns

Our first approach to regulating growth rate with sRNAs consisted of designing sRNAs targeting the mRNAs of essential genes involved in amino acid production (Figure 54). I designed the sRNA using the MicC scaffold from Na et al. to enable binding of the native Hfq chaperone protein [131]. I selected 24-bp target-binding sequences targeting the Shine-Dalgarno region of the leuB, metA, thrC, hisD, glyA, tyrA and ilvA mRNAs.

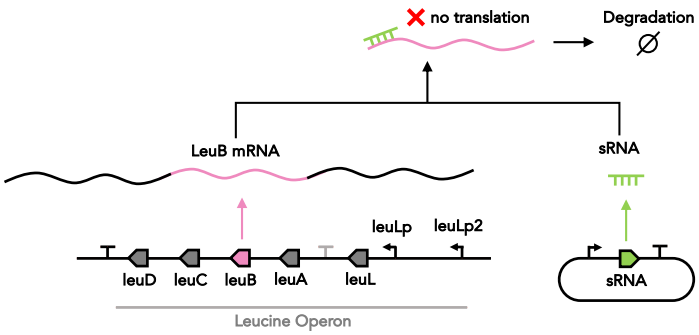


Figure 54: Concept of a sRNA-based essential gene knockdown. LeuB expression can be inhibited by expressing a sRNA that targets the Shine-Dalgarno region of LeuB mRNA and promotes degradation of the sRNA:target mRNA complex by RNAse E.

Using the design principles in outlined by Na et al. and Kelly et al., I investigated whether I could silence essential gene mRNA to control growth rates [131, 162]. In Figure 55, I used STAR expression driven by the C6-HSL quorum sensing molecule to regulate sRNA production (Figure 55.A). When expressing a sRNA designed to target and bind to the leuB mRNA, sRNA production seemed to decrease both growth rate and the maximum carrying capacity of the culture compared to the non-induced system (-AHL) (Figure 55.B). By removing the STAR plasmid from the system, to test whether leaky expression of leuB sRNA caused any decrease in growth rate, I observed that cells lacking STAR had the same growth profile as the BW25113 wild-type strain (Figure 55.C). Therefore either leuB leaky expression was not high enough to decrease growth rate, or the decrease in growth rate was due to STAR expression rather than sRNA expression.

To investigate whether the decrease in growth rate was due to STAR expression or sRNA expression, I designed a sRNA targeting sfGFP mRNA. As no sfGFP was present in the cell,

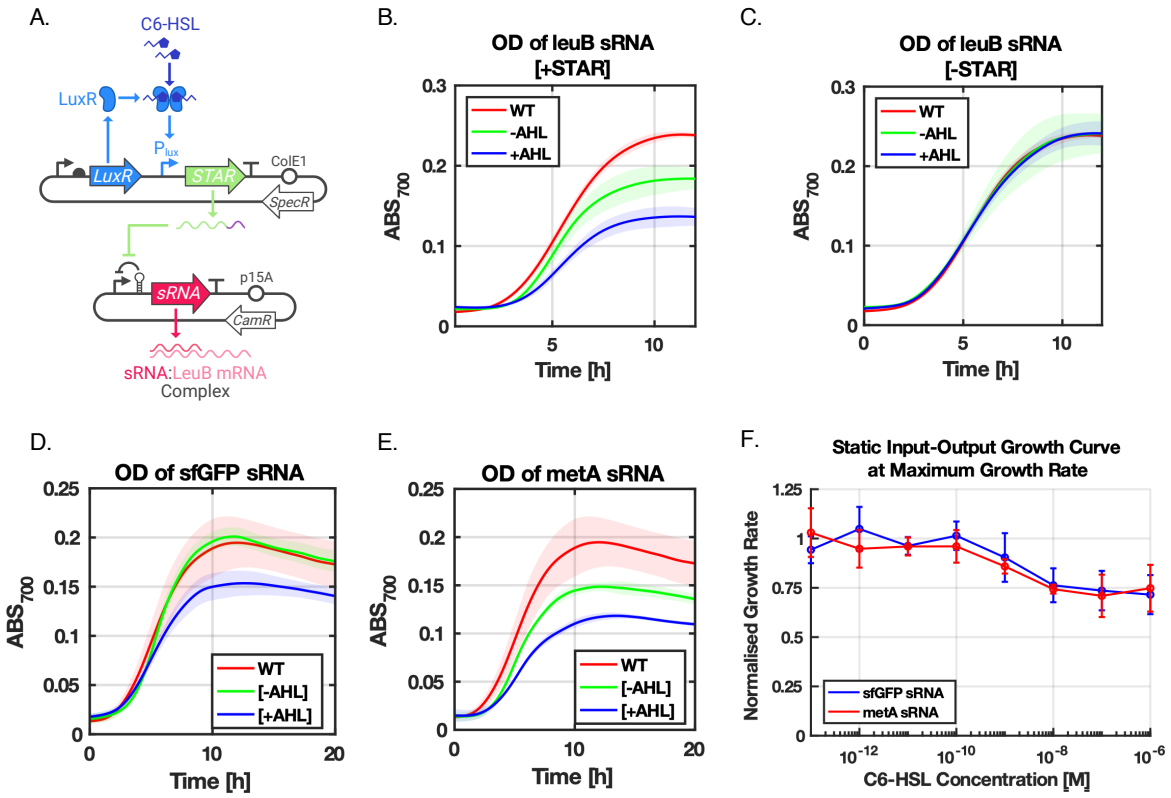


Figure 55: Using sRNA to reduce maximum carrying capacity. (A) sRNA targeting the mRNA of an essential gene involved in amino acid production (e.g. leuB for leucine production), is controlled by STAR induction. STAR is expressed in the presence of C6-HSL quorum sensing molecule. (B) OD of cells carrying the STAR plasmid and the plasmid carrying the sRNA targeting leuB mRNA. WT refers to the wild-type BW25113 strain, while "-AHL" and "+AHL" refer to the double plasmid system being induced with either 0M or 10^{-7}M of C6-HSL respectively. (C) OD of cells carrying only the plasmid carrying the sRNA targeting leuB mRNA. WT refers to the wild-type BW25113 strain, while "-AHL" and "+AHL" refer to the single plasmid system being induced with either 0M or 10^{-7}M of C6-HSL respectively. (D) OD of cells carrying the STAR plasmid and the plasmid carrying the sRNA targeting sfGFP mRNA. WT refers to the wild-type BW25113 strain, while "-AHL" and "+AHL" refer to the double plasmid system being induced with either 0M or 10^{-7}M of C6-HSL respectively. (E) OD of cells carrying the STAR plasmid and the plasmid carrying the sRNA targeting metA mRNA. WT refers to the wild-type BW25113 strain, while "-AHL" and "+AHL" refer to the double plasmid system being induced with either 0M or 10^{-7}M of C6-HSL respectively. (F) Effect of varying C6-HSL concentration on growth rate of the double plasmid system from D and E. Experiments were done in BW25113. Growth was monitored in a timecourse plate-reader assay. Data represent the mean values of n = 3 biological replicates ± s.d.

I predicted that the sfGFP sRNA should have minimal interaction with other mRNA species in the cell. Expressing the sfGFP sRNA had a small impact on growth rate and final OD (Figure 55.D). When targeting metA mRNA, I also observed a more pronounced effect on the final optical density of the culture as when I targeted the leuB mRNA (Figure 55.E and B).

However when plotting the relationship between growth rate and C6-HSL concentration in Figure 55.F, I observe that in both the case of the sfGFP sRNA and metA sRNA expression, decrease in growth rate correlated with increasing C6-HSL concentration and that growth rate was indeed the same during mid-exponential phase. This highlights that during the first half of the exponential phase, RNA turnover might be too high to regulate essential mRNA translation rate. In addition, it also highlights that growth rate regulation is solely due to STAR expression levels in the cell (Section 2.2.4.2). Chen et al. revealed that mRNA cleavage by RNAse E is reduced in exponential phase, compared to the transition between exponential to stationary phase [199]. Perhaps, reduced cleavage activity of the bound sRNA:mRNA complex during exponential phase explains why more leuB mRNA is able to be translated. While in stationary phase, the RNA complex can be more easily degraded, thus decreasing available L-leucine and L-methionine intracellular levels. However it has also been demonstrated that Hfq levels are higher in exponential phase than in stationary phase [200, 201]. As Hfq inhibits the formation of the translational initiation complex, it would mean that sRNA translational inhibition should be strongest during exponential phase. More research would need to be conducted to determine whether essential gene knockdown using sRNA relies primarily on RNA degradation by the degradosome or on translation inhibition by Hfq binding.

I attempted to improve the effect of sRNA growth inhibition by increasing the strength of the promoter upstream of the STAR target regulating sRNA transcription. I imagined that increasing sRNA levels in the cell would improve the hybridization kinetics of the sRNA to the target mRNA, thus compensating for lower RNAse E cleavage rate in exponential phase. I attempted to drive sRNA expression with the J23100, J23119 Anderson promoters, the strong Pr phage promoter and the Tac promoter, without more success (data not shown). Another way to increase cellular sRNA levels would be to express the sRNA targeting essential gene mRNA from a high copy plasmid. However, the STAR system requires the STAR target to be expressed from a lower copy plasmid than STAR. Thus, growth regulation using sRNA may be more viable in a system operating on a high copy plasmid without plasmid titration constraints.

In this section, I have shown that sRNA can be used to target essential gene expression to downregulate the final biomass of the system. However more work is needed to understand how essential mRNA levels vary as sRNA is expressed during the different phases of growth, and how this knowledge can be used to build more effective knockdowns of essential mRNAs involved in the production of amino acids.

4.2.2.2 Using N1 sRNA to regulate growth rate

Small RNAs are versatile and can be programmed to target and bind to a variety of mRNA targets. Noro et al. and Kawano et al. built a random library of sRNAs by introducing random mutations within the sequence encoding the targeting of the sRNA [166, 167]. Using their pool of sRNA, they searched for reduced growth phenotypes. I envisioned that I could use sRNA causing growth reduction in *E. coli* to control the growth rate of our coculture strains.

After testing a couple of sRNA target sequences identified by Noro et al. and Kawano et al., I realised that sRNA folding was important to preserve sRNA function [166, 167]. Indeed I introduced the sRNA target sequence within our own sRNA design and scaffold from Figure 55, and I was unable to obtain the same growth reduction phenotype as described in their studies. Therefore I realised that preserving the sRNA genetic context was essential to maintain sRNA function. The Kawano lab kindly sent us the plasmid expressing the N1 sRNA and it was able to successfully repress growth in our BW25113 strain (Figure 56.B). I also showed that I could tune the growth rate of our strain by titrating L-arabinose levels driving expression of the N1 sRNA. Thus, the N1 sRNA constitutes a good candidate to build a tunable growth regulation module.

Linking the STAR-based comparator to the expression of N1 sRNA, was unsuccessful at rescuing cell growth. From the work of Kawano et al., it is unclear what the target of the N1 sRNA is, and it might target multiple mRNA species [167]. However it is clear that very low expression levels of N1 sRNA are enough to trigger strong growth reduction in *E. coli*. The fold-repression of the STAR-based comparator may not have been strong enough to sufficiently reduce N1 sRNA expression to rescue cell growth.

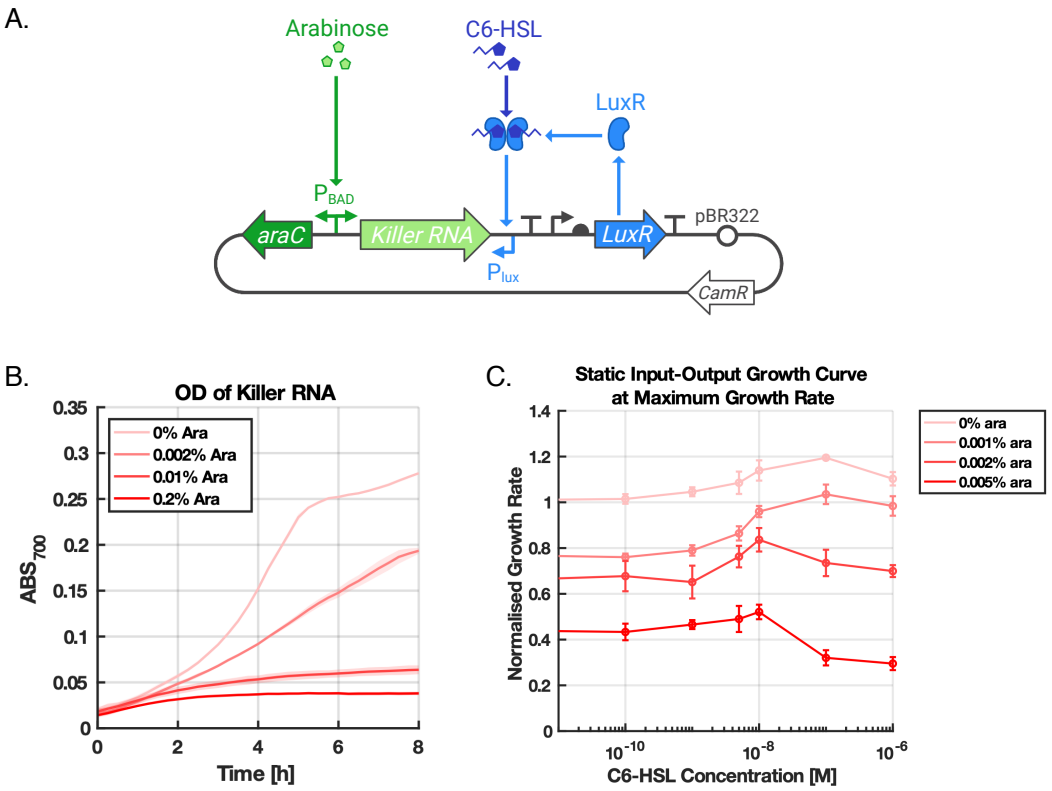


Figure 56: Using interfering sRNA to down-regulate and rescue growth. (A) The N1 sRNA from Kawano et al. is expressed using the araBAD promoter [167]. In the presence of C6-HSL, RNAP initiates anti-sense transcription of N1 sRNA to decrease N1 sRNA expression, rescuing cell growth. (B) Effect of increasing L-arabinose concentration on cell growth. Induction is done with either 0%, 0.002%, 0.01% or 0.2% of L-arabinose and 0M of C6-HSL. (C) Effect of increasing C6-HSL concentration on growth rate. Induction is with either 0%, 0.002%, 0.01% or 0.2% of L-arabinose and a range of C6-HSL concentrations ranging from 0M to 10^{-6}M. Experiments were done in BW25113. Growth was monitored in a timecourse plate-reader assay. Data represent the mean values of n = 3 biological replicates ± s.d.

To tackle this problem, I decided to use antisense transcription to suppress N1 sRNA expression in the presence of a quorum sensing signal. Anti-sense transcription was shown to repress expression of a gene of interest by over 30-fold depending on the strength of the promoter driving antisense transcritpion [202]. The circuit used to enable growth rescue through quorum-sensing driven antisense transcription is depicted in Figure 56.A. Despite not using the STAR-based comparator system, the circuit can still act as a comparator, effectively comparing the strength of transcriptional activation driven by the reference promoter, here the araBAD promoter, and the quorum sensing promoter, pLux, sensing coculture strain density. Increasing the induction of the pLux promoter by increasing C6-HSL concentration,

enabled us to recover up to 25% of the maximum growth rate of the cell compared to when the rescue mechanism is not activated 56.B. I observed that growth rate recovery can only be enabled when L-arabinose induction is low, otherwise the strength of the araBAD promoter wins over that of the maximally induced pLux promoter. I also observed that for 0% L-arabinose, induction with C6-HSL is able to rescue cell growth by 20%, showing that even in the absence of L-arabinose, leaky expression of the N1 sRNA down-regulates growth rate, thus further demonstrating the strong potent nature of the N1 sRNA.

Kawano et al., also described less potent sRNA designs [167]. Perhaps using less potent N1 sRNAs, would enable antisense transcription to have a fairer tug of war with the promoter driving N1 sRNA transcription, and would also potentially allow to improve the achievable fold change in growth rate.

Overall in this section, I highlighted the potential of sRNA to control growth rate. I showed that antisense transcription can be used as a rescue mechanism to build a new kind of minimal RNA-based comparator.

4.2.3 Regulating growth rate through expression burden and STAR

Finally I propose to regulate growth rate directly through modulating expression of VioB, a large burdensome protein [8]. Heterologous gene expression has been shown to divert essential resources (e.g. RNAP, ribosomes, tRNA) from the cell to provide for its own expression needs [8, 35]. I propose to use the output of the STAR-based comparator to directly modulate the expression of VioB, thus controlling the portion of free resources available for the accumulation of biomass. As a result, when coculture ratio diverts from its set equilibrium, the comparator will act to modulate expression of a gene of interest to restore the preset ratio (Figure 57).

First, I constructed a circuit to demonstrate that I could use STAR to sequester cellular resources by activating gene expression of a large heterologous protein (Figure 58.A). VioB-mCherry, is a large fusion protein of 3.7 kb which was shown to cause burden and activate the stress response of the cell when expressed at high levels [8, 35]. STAR expression was regulated by the araBAD promoter. In the presence of L-arabinose, STAR activates the

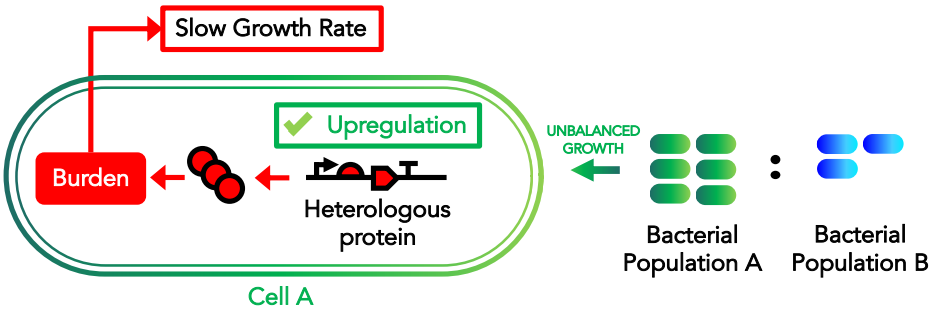


Figure 57: Growth regulation module using expression burden. When the coculture ratio is driven out of balance, growth rate of each strain can be adjusted by tuning the level of heterologous gene expression in the cell. Increasing heterologous gene expression sequesters more cellular resources, thus decreasing overall growth rate. Similarly, decreasing gene expression will free up cellular resources, improving overall growth rate.

transcription of VioB-mCherry, thus sequestering vital cellular resources otherwise used for biomass accumulation (Figure 58.B). As L-arabinose concentration increases in the cell, I observed that VioB-mCherry production rate in the cell increases, causing a dramatic drop in GFP capacity which reflects the portion of free resources in the cell. As a result of the drop in cellular resources, growth rate decreases by about 55% for the maximal induction level of L-arabinose.

Next, I link the STAR-based comparator (with Toehold 2) to the burden-based growth regulation plasmid expressing VioB-mCherry (Figure 59.A). I varied STAR expression levels, to study the behaviour of the comparator when controlling growth rate through burden regulation (Figure 59.B). At low STAR expression levels, no VioB-mCherry is produced, however anti-STAR expression alone contributes to decreasing GFP capacity by 40%, significantly pulling away cellular resources. This drop of GFP capacity explains why growth rate also drops by 20% when anti-STAR is expressed. At medium STAR expression levels, VioB-mCherry is expressed at 60% of its maximum production rate and is successfully inhibited by anti-STAR at increasing C6-HSL concentrations. GFP capacity improves slightly by 15% and growth rate is stable across concentrations of C6-HSL. So at medium STAR expression level, the cost of expressing the controller is compensated by the rescue of cellular resources sequestered by VioB-mCherry expression. Finally, at high STAR expression levels, VioB-mCherry is maximally induced and repressed at low and high C6-HSL concentrations.

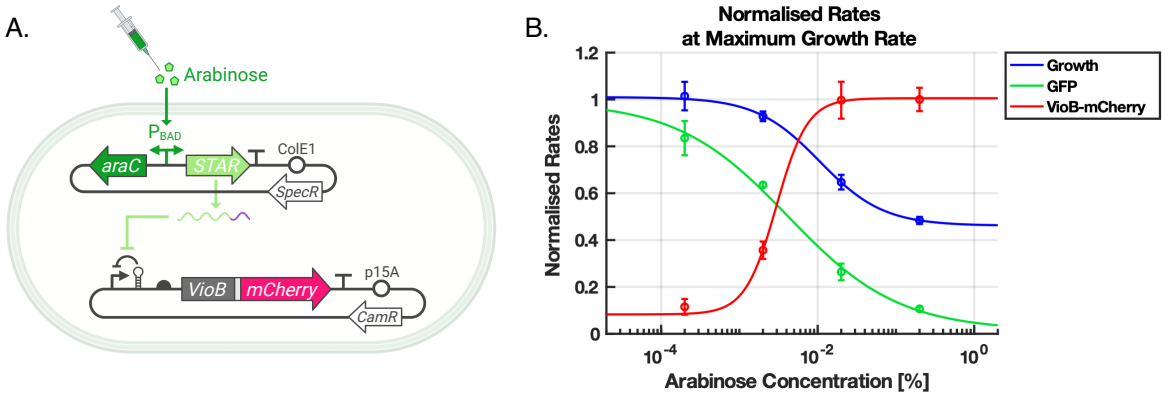


Figure 58: Controlling growth rate using VioB-mCherry expression. (A) VioB-mCherry, a 3.7kb fusion protein, is expressed under STAR control. In the presence of L-arabinose, STAR is expressed and upregulates production of VioB-mCherry. (B) Effect of increasing L-arabinose concentration on cellular growth rate, GFP capacity (GFP production rate per cell) and VioB-mCherry expression (VioB-mCherry production rate per cell). As L-arabinose concentration increases, VioB-mCherry expression is upregulated, causing a decrease in available cellular resources reflected in the decrease of GFP expression. As a consequence of scarce cellular resources, growth rate also decreases with increasing L-arabinose concentration. Experiments were done in DH10B-GFP. Growth was monitored in a timecourse plate-reader assay. Data represent the mean values of n = 3 biological replicates ± s.d.

GFP capacity increases by 56% with anti-STAR rescue, and similarly growth rate improves by 46% with anti-STAR rescue. The comparator is therefore able to tune growth rate and rescue cellular resources when expression of a burdensome protein causes a significant diversion in free cellular resources. I note that for high concentration of both L-arabinose and C6-HSL, the cost of expressing the comparator RNA species increases, leading to a slight decrease in both GFP capacity and growth rate.

Modulation of heterologous protein expression thus appears to be a convenient way to modulate the growth profile of a strain. It does not result in extended lag phases, but instead it can be tuned to obtain a range of different growth rates.

I also decided to study the behaviour of the two versions of the comparators: with or without Toehold 2 from Chapter 2. From Figure 25 of Chapter 2, I showed that the comparator without toehold yielded higher production rates of the gene of interest, mRFP, than the version of the comparator that was expressing STAR and anti-STAR with Toehold 2. I wanted to test whether using the comparator without toehold would also yield a higher

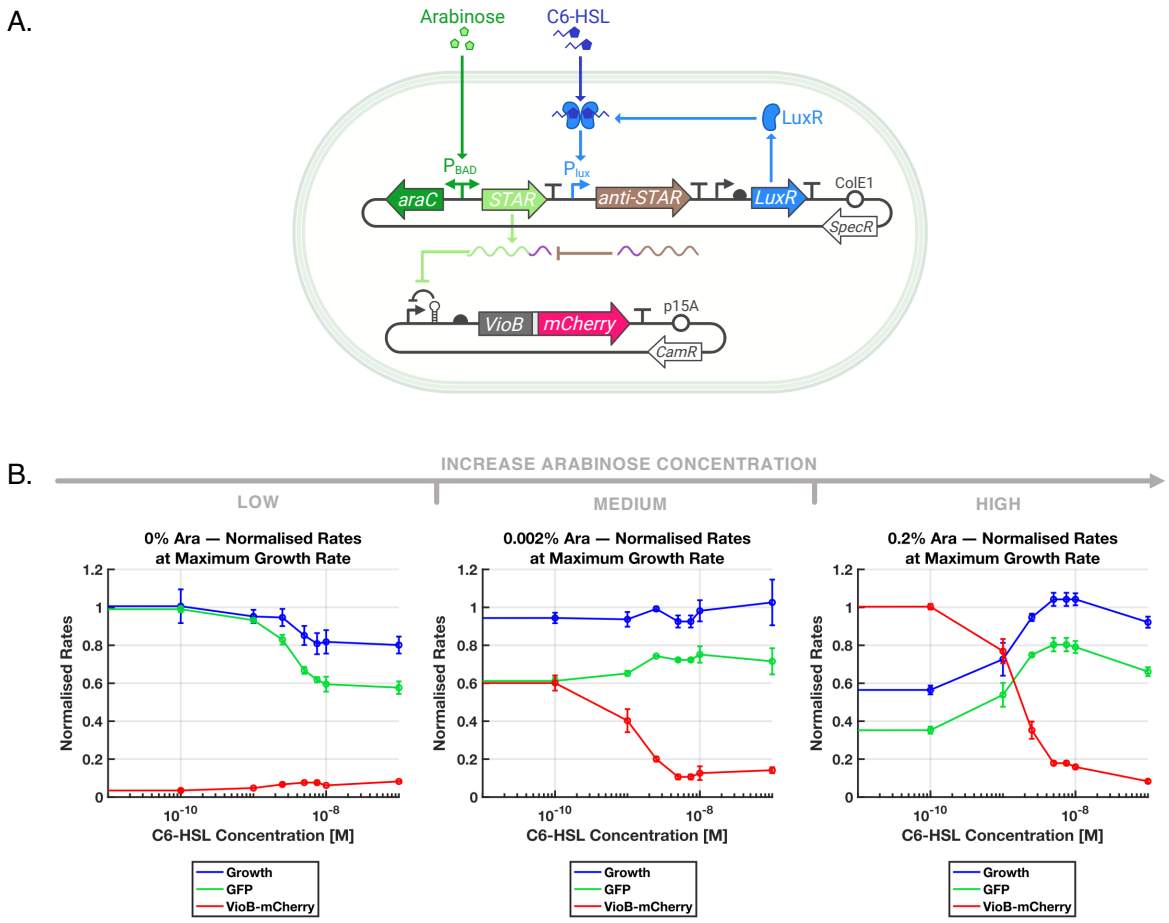


Figure 59: A burden approach to the STAR-based comparator controlling growth rate. (A) The STAR-based comparator with Toehold 2 based on the LLL quorum sensing system is linked to VioB-mCherry production to control growth rate. (B) Effect of increasing C6-HSL concentration on growth rate, GFP capacity (GFP production rate per cell) and VioB-mCherry expression (VioB-mCherry production rate per Cell) for three different concentrations of L-arabinose. For the low arabinose induction, the system was induced with 0% L-arabinose, for medium induction : 0.002% L-arabinose and for high induction: 0.2% L-arabinose. System was induced with a range of C6-HSL concentration from 0M to 10^{-7}M. Growth rates and GFP capacities were normalised with the growth rate at the system induced with 0% L-arabinose and 0M C6-HSL. VioB-mCherry expressions were normalised with the VioB-mCherry production rate per cell of the system induced with 0.2% L-arabinose and 0M C6-HSL. Experiments were done in DH10B-GFP. Growth was monitored in a timecourse plate-reader assay. Data represent the mean values of n = 3 biological replicates ± s.d.

VioB-mCherry production rate in the context of our burden-driven growth regulation module. If VioB-mCherry production rate was higher, it would then mean that there would be more burden imposed on the host and the range over which growth rate could be regulated would increase. To test this hypothesis, I transformed our DH10B-GFP capacity monitor strain with the VioB-mCherry plasmid controlled with the STAR-based comparators with or

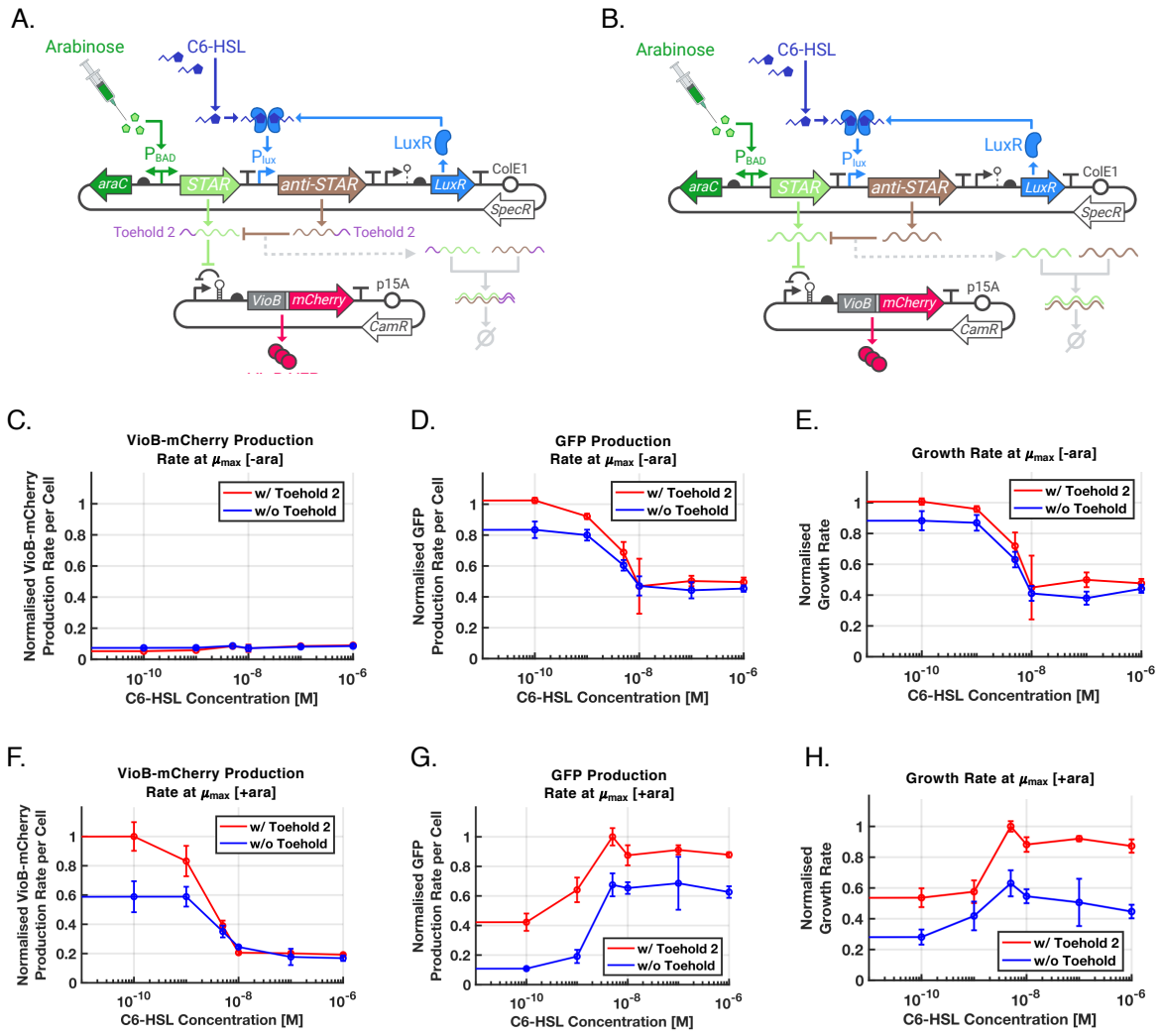


Figure 60: Controlling VioB-mCherry expressing with a comparator with or without toehold. (A) The STAR-based comparator with Toehold 2 based on the LLL quorum sensing system is linked to VioB-mCherry production to control growth rate. (B) The STAR-based comparator without Toehold based on the LLL quorum sensing system is linked to VioB-mCherry production to control growth rate. (C-E) Comparison of VioB-mCherry production rate per cell, GFP capacity and growth rate of the comparators with and without toehold 2 when the circuits are externally induced with 0% L-arabinose and a range of C6-HSL concentration from 0M to 10^{-6}M. (F-H) Comparison of VioB-mCherry production rate per cell, GFP capacity and growth rate of the comparators with and without toehold 2 when the circuits are externally induced with 0.2% L-arabinose and a range of C6-HSL concentration from 0M to 10^{-6}M. Experiments were carried in DH10B-GFP. Growth was monitored in a timecourse plate-reader assay. Data represent the mean values of n = 3 biological replicates ± s.d.

without Toehold 2 (Figure 60.A-B). The DH10B-GFP strain would allow us, once again, to monitor the availability of free cellular resources in the host. First I did not externally induce

the strains with arabinose, but instead I observed the behaviour of the circuits for increasing concentrations of C6-HSL (Figures 60.C-E). Increasing the concentration of C6-HSL causes an upregulation of anti-STAR production. As I first observed in Figure 26 of Chapter 2, anti-STAR expression causes a reduction in both GFP capacity and growth rate (Figures 60.D-E). Both GFP capacity and growth rate recorded a decrease as high as 60%. Then I externally added 0.2% of L-arabinose to the system to trigger the production of STAR, with or without Toehold 2, that will lead the promote the transcription of VioB-mCherry (Figures 60.F-H). In opposition with the results found in Figure 25 of Chapter 2, I found that VioB-mCherry production rate per cell was higher when STAR had a toehold domain than when it didn't as there was a 40% difference in the maximum production rate per cell between the two designs (Figure 60.F). This result could be explained with the higher GFP capacity exhibited by the circuit with toehold (Figure 60.G). If the system with toehold is less impacted by burden and has more available resources, it could result in a higher production rate of the product of interest. The greater loss of available resources of the system without toehold is also cause for a greater impact on the growth rate of the cell (Figure 60.H). Though both comparators are able to rescue cell growth through the expression of anti-STAR at increasing concentrations of C6-HSL, the comparator with toehold offers a better recovery performance than its counterpart with no toehold.

So both comparator designs are able to tune the level of burden caused by the production of VioB-mCherry, and as a result are able to modify the growth rate of their host. However both designs impose a different burden cost on their own through the expression of STAR and anti-STAR which further decrease host fitness, and this effect is more pronounced when they do not carry a toehold domain. Naturally I favour the comparator design that exhibits the least impact on its host, that is when STAR and anti-STAR have a toehold domain. However, in a consortium that have very different growth rates, I can imagine equipping the fastest growing strain with the comparator without toehold to further decrease its growth rate if expression of the burdensome protein is not enough to compensate for the difference in growth rate between the two strains.

Finally, I show that the burden regulation strategy can be applied to regulate pathways of interest. So far I have shown that the comparator can regulate growth rate by modulating

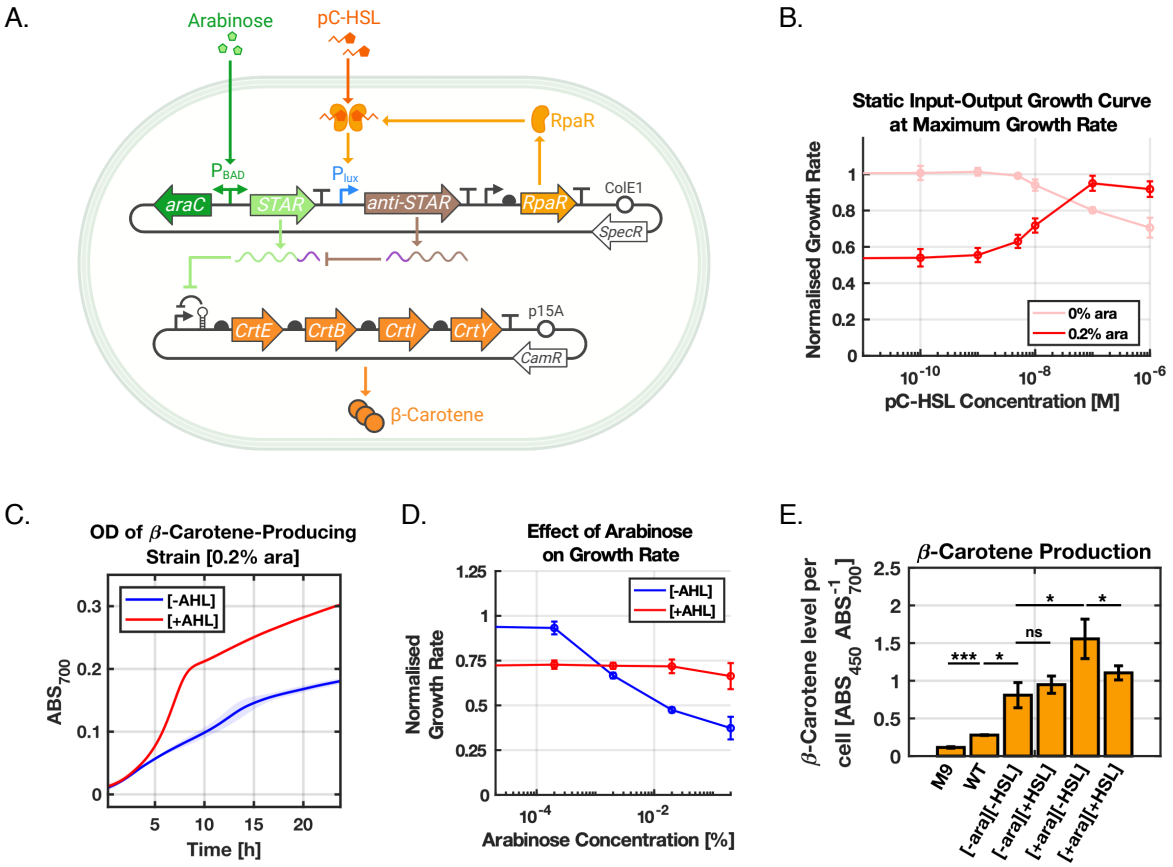


Figure 61: A burden approach to the STAR-based comparator controlling growth rate through β-carotene production. (A) The STAR-based comparator (with Toehold 2) based on the LRR quorum sensing system is linked to β-carotene production to control growth rate. β-carotene is produced through the expression of four enzymes: *CrtE*, *CrtB*, *CrtI* and *CrtY* organised in an operon as described by Borkowski et al. [27]. (B) Effect of increasing pC-HSL concentration on growth rate when the cells are induced with either 0% L-arabinose or 0.2% L-arabinose. Cells were induced with a range of pC-HSL from 0M to 10^{-6}M. Growth rate was normalised with the growth rate of the system induced with 0% L-arabinose and 0M of pC-HSL. (C) Effect of adding pC-HSL on the growth profile of the cells expressing maximal levels of STAR. Cells were induced with 0.2% L-arabinose. In the "-AHL" conditions, 0M of pC-HSL was externally added to the media, while in the "+AHL" condition, 10^{-7}M of pC-HSL was added. (D) Effect of increasing L-arabinose concentration on normalised growth rate with 0M or 10^{-7}M of pC-HSL was added to the media ("-AHL" and "+AHL" respectively). Growth rate was normalised with the growth rate of the system induced with 0% L-arabinose and 0M of pC-HSL. (E) β-carotene production per cell measured as the absorbance read at 450 nm divided by absorbance read at 700 nm. The conditions refer to the concentration of inducer externally added to the media. "-ara": 0% of L-arabinose, "+ara": 0.2% of L-arabinose, "-AHL": 0M of pC-HSL, "+AHL": 10^{-7}M of pC-HSL. Experiments were done in DH10B. Growth was monitored in a timecourse plate-reader assay. Data represent the mean values of n = 3 biological replicates ± s.d. Statistically significant differences were determined using two-tailed Student's t-test (**** represents p<0.0001, *** represents p<0.001, ** represents p<0.01, * represents p<0.1, ns represents not significant).

expression of one gene. Here I show that the comparator can also regulate operons to achieve growth modulation.

I adapted the β-carotene pathway from Borkowski et al. by putting it under the regulation of the STAR target (Figure 61.A) [27]. When STAR is expressed in the presence of L-arabinose, the four-gene β-carotene operon is activated, causing a 47% drop in growth rate (Figure 61.B). However, in the presence of pC-HSL, anti-STAR sequesters STAR, thus inhibiting transcription of the β-carotene operon and improving growth rate by 44%. The anti-STAR rescue mechanism is able to almost completely restore growth rate of the cell. In Figure 61.C, I show the growth profile of the system when STAR is maximally expressed and when the quorum-sensing-driven rescue is activated or not. At all levels of L-arabinose induction, the rescue mechanism of the growth controller is able to keep growth rate constant, while growth rate is inhibited up to 63% in the absence of pC-HSL (Figure 61.D). Additionally, I measured β-carotene level produced by the system for the different inducers combinations (Figure 61.E). I confirmed that STAR could up-regulate β-carotene production levels, while anti-STAR expression could inhibit them by 25%.

Thus I confirmed that the burden based strategy is a generalisable approach to control growth rate based on the comparison of two input signals. I showed that both versions of the STAR-based controller based on either the LLL or the LRR quorum sensing systems had the potential to regulate growth rate through the modulation of transcription of a gene of interest.

4.3 Conclusions

In this chapter, I investigated three main avenues for coculture growth regulation based on non-toxic strategies: CRISPRi knockdowns, sRNA knockdowns, and burden. I envision that these growth regulation strategies are viable avenues to control population composition in synthetic microbial consortia.

CRISPRi was a very effective strategy to knockdown essential genes involved in amino acid production. Linking it to the STAR-based comparator allowed us modulate growth

rates within a range of 1.3-fold. The main challenge of the CRISPRi growth control strategy is to control the dynamics of dCas9 unbinding to guarantee that the population composition control strategy will be dynamic to adapt to fluctuating ratios in time. More work studying the dynamics of the CRISPRi will be needed to determine whether introducing more mutations in the gRNA will increase the unbinding kinetics of the gRNA:dCas9 complex with the target DNA sequence. Additionally, adding mutations in the gRNA should reduce the impact on growth of gRNA leaky expression. As result, this should improve both the fold rescue and dynamics of the CRISPRi-based coculture ratio controller.

Growth regulation mediated by sRNA production did not prove as trivial. Proper sRNA folding was critical to ensure proper mRNA targeting. Though knocking down essential gene expression through mRNA sequestration could only decrease the total final biomass, I found that expressing non-target-specific sRNA could regulate growth rate. Creation of randomised RNA pools, seems the best approach so far to building functional RNA with desired phenotypes *in vivo*. Linking the N1 sRNA to the STAR-based comparator module, I could modulate growth rate by 25%. Further work in exploring the use of less potent sRNA may help improve the leaky effect of sRNA expression on growth, and thus the fold change in growth modulation achievable by the comparator. I designed a new comparator based on antisense transcription to counteract the leaky expression of N1 sRNA from the reference promoter. I could also explore using the STAR-based comparator implemented with the double STAR target, which I showed had lower basal expression in Chapter 2.

Finally, I showed that a simple way to modulate growth rate is through the control of heterologous gene expression. I connected the STAR-based comparator to the expression of both a single gene and a four-gene operon and demonstrated that growth rate could be modulated up to 45%. The advantage of using the burden-based growth regulation approach is that it can be adapted to the gene or pathway of interest of the user. If a gene is known to cause burden to its host, coculture ratio could be regulated directly by modulating the genes of interest in both strains making up the coculture. However, if the coculture strains express genes that generate little or no burden, VioB-mCherry (or another burdensome protein) can be expressed to adjust population ratio if both strains have different intrinsic growth rates.

Additionally, if the user does not want to tamper with the expression of the genes of interest, VioB-mCherry (or another burdensome protein) can be expressed in parallel to the GOIs to provide a mean to regulate coculture composition without tampering with the production process of interest.

For the next chapter implementing growth regulation at the multi-cellular level in order to control coculture ratio, I decided to use the burden-based growth regulation approach as it has so far the best growth rate modulation range of the approaches I have tested. I have shown that it is modular, it can be used while expressing different genes and number of genes. It is also dynamic as the regulation mechanism does not rely on strong protein binding interactions.

Chapter 5

Bottom-Up Engineering of an *E.coli-E.coli* Coculture

Contents

5.1 Introduction 117

5.2 Results and discussion 119

5.2.1 Building the open-loop co-culture 119

5.2.2 Validation of the pC-HSL communication channel for coculture regulation 122

5.2.3 Validation of the C6-HSL communication channel for coculture regulation 126

5.2.4 Ratio stabilisation in a 2-way-communicating co-culture 130

5.2.5 The co-culture under turbidostat conditions 139

5.3 Conclusions 143

5.1 Introduction

In the previous chapters, I have investigated how to construct the modules necessary for building a coculture maintaining its population composition over time. In this chapter, I investigate how to link all three modules (comparator, communication and growth regulation) together to build a stable coculture.

To explore the properties of our modules to maintain population ratio, I build a circuit that will allow us to easily monitor population ratio and VioB expression over time (Figure 62). VioB expression will be regulated by the comparator module in response to the quorum sensing signals produced in the coculture. I tagged one of the two strains with a

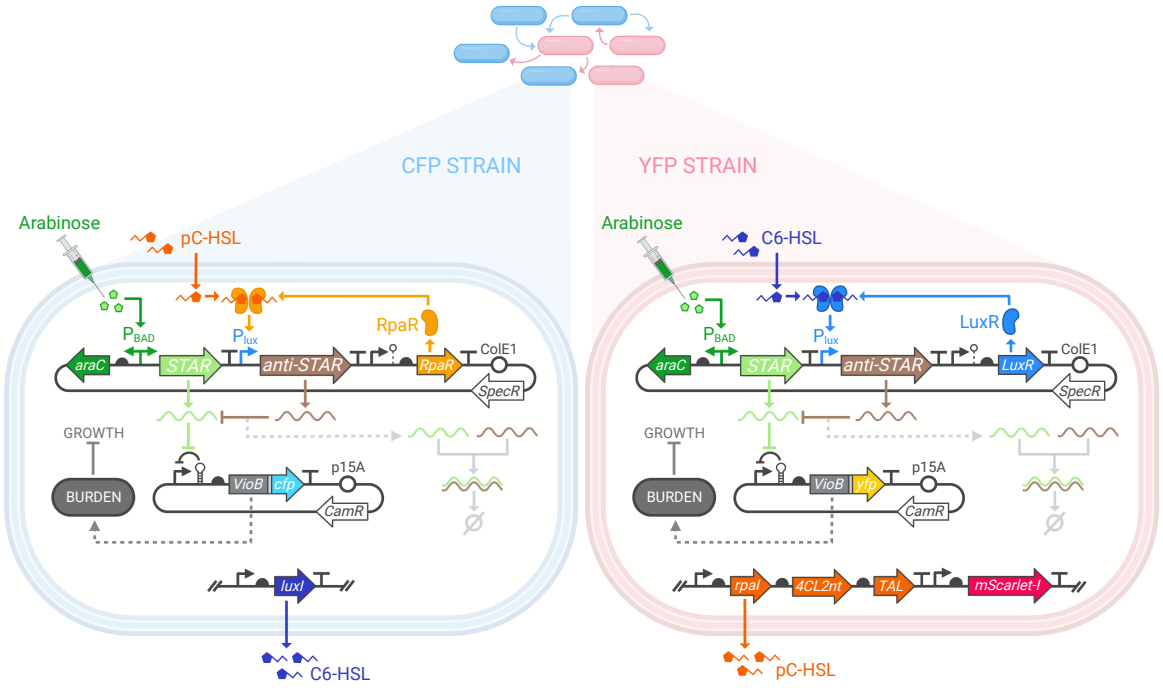


Figure 62: A burden-based circuit for coculture composition regulation. The CFP strain is equipped with the LRR STAR-based comparator regulating the expression of VioB-CFP. The CFP strain synthesises C6-HSL to regulate the density of the YFP strain. The YFP strain is equipped with the LLL STAR-based comparator regulating the expression of VioB-YFP. It produces pC-HSL to regulate the density of the CFP strain when the coculture composition is out of balance.

mScarlet-I marker that is constitutively expressed in order to track the proportion of red to non-red cells in the coculture over time. I also tagged the VioB burdensome protein with two different fluorescent reporters: sfCFP and sfYFP in order to continuously monitor expression levels of the growth control module. This will allow us to track the response of both strain to the quorum sensing signals they produce, scaling with their population density.

I will first build two strains with different maximal growth rates, such that when they are grown together in a coculture, the faster dividing strain will overtake the coculture instead of keeping the coculture composition to a 1:1 ratio. I will then investigate the critical impact of quorum sensing signal strength on the behaviour of the coculture to mitigate population ratio imbalances. Then, I will see how the two-way communicating coculture is able to stabilise population ratio in batch culture, and how the target coculture composition can be tuned based on different properties of the modules. Finally, I study the stability of the coculture

when grown in continuous cultures using the Chi.bio turbidostat from Steel et al. [177].

5.2 Results and discussion

5.2.1 Building the open-loop co-culture

First, I need to build two strains that will allow us to monitor the output of the growth control module. As a result, I will be able to study the impact of quorum sensing produced by the two different strains on growth regulation. To be able to clearly measure the effect of the coculture composition controller (closed-loop), I will need a negative control coculture (open-loop) to show that without communication between the two strains, the composition controller cannot function. There are two ways to achieve this goal. One is to break the communication by not producing the quorum sensing signals, so by removing the C6-HSL and pC-HSL biosynthesis pathway from the strains. The second, is to remove the C6-HSL and pC-HSL sensing mechanism by removing either the transcription factors LuxR and RpaR, or by removing the *pLux* promoter driving anti-STAR expression. I chose to remove the quorum sensing biosynthesis pathways as it will allow us to study the behaviour of the open-loop coculture in the presence of externally-added C6-HSL and pC-HSL.

Another criterion to build these two strains is that they should not have the same maximum growth rate such that in the open-loop coculture, population composition is not stable over time as one strain will out-compete the other. I chose to fuse the sfYFP and sfCFP fluorescent reporters from Alnahhas et al. to VioB, our burdensome protein of interest [116]. I then characterised the strain behaviours when the LLL and LRR STAR-based comparator controlls VioB-YFP and VioB-CFP expression respectively (Figure 63.A,D). I observed that in both strains, VioB-YFP and VioB-CFP levels decrease for increasing levels of C6-HSL and pC-HSL respectively (Figure 63.B,E). As VioB-YFP and VioB-CFP expression decreases, growth rate of the YFP and CFP strains improves. However the VioB-YFP appears to cause more burden to the YFP strain than VioB-CFP causes to the CFP strain. Regulation of VioB-YFP expression allows to modulate the growth rate of the YFP strain by 40% (Figure 63.C), while regulating VioB-CFP expression allows to regulate the growth rate of the CFP strain by only 20% (Figure 63.F). This result is surprising as

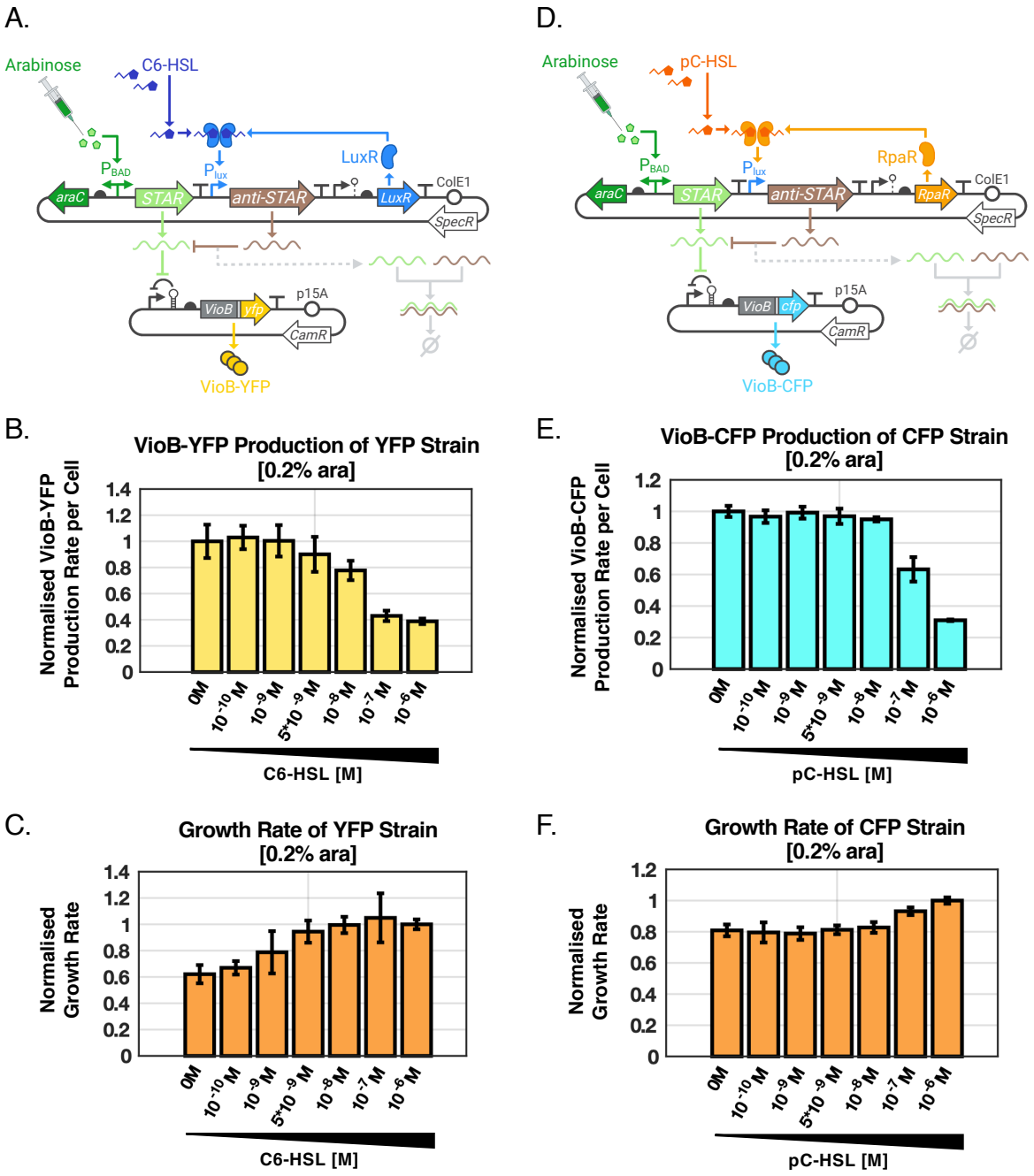


Figure 63: Building coculture strains with different burden. (A) The YFP strain regulates VioB-sfYFP production under the control of the LLL STAR-based comparator with Toehold 2. VioB-sfYFP is activated by L-arabinose and inhibited with increasing concentration of C6-HSL. (B-C) The YFP strain is induced with 0.2% of L-arabinose to activate VioB-sfYFP expression. Increasing C6-HSL levels gradually turns down VioB-sfYFP and improve growth rate. (D) The CFP strain regulates VioB-sfCFP expression using the LRR STAR-based comparator with Toehold 2. (E-F) The CFP strain is induced with 0.2% L-arabinose to activate VioB-sfCFP expression. Increasing pC-HSL concentration gradually turns down VioB-sfYFP expression and recovers growth rate. Experiments were done in DH10B. Fluorescence and OD measurements were collected in the plate-reader. Data represent the mean values of n = 3 biological replicates ± s.d.

sfCFP and sfYFP have been previously used as reporters in coculture circuits, where they were reported to have similar impacts on cell growth [203, 73, 116]. Since sfCFP and sfYFP have exactly the same coding sequence, except for 9 nucleotides substitutions, I imagine that those substitutions may interfere with the folding of VioB, causing the formation of more misfolded VioB-YFP proteins than VioB-CFP proteins. Protein misfolding has been shown to trigger the cell's stress response which could explain why VioB-YFP impacts growth rate more than VioB-CFP [204, 205, 206, 207]. As a result, the sfYFP and sfCFP fluorescent tags do not only allow us to track VioB expression levels in the cell, but they also allow us to use VioB-CFP and VioB-YFP as examples of two protein expression systems that impact the growth rate of their host differently.

Next, I verify that the CFP strain expressing VioB-CFP under the control of the LRR STAR-based comparator, and the YFP strain expressing VioB-YFP under the control of the LLL STAR-based comparator make an unstable coculture when growth together (Figure 64.A). Both strains are grown together without producing quorum sensing molecules, thus no ratio control is in place. In Figure 64.B when the coculture is not induced with L-arabinose, both VioB-YFP and VioB-CFP are not expressed. Both strains grow at a similar growth rate, thus keeping the population ratio stable around 1:1. However, when L-arabinose is externally added, VioB-YFP and VioB-CFP expression levels increase and the ratio of the coculture is no longer stable around a 1:1 ratio (Figure 64.C). I also externally added saturating concentrations of both C6-HSL and pC-HSL to the coculture induced with L-arabinose (Figure 64.D). This revealed that quorum sensing could inhibit VioB-CFP and VioB-YFP expression to maintain coculture composition to a 1:1 ratio.

In this section, I confirmed that I could use both the YFP and CFP strains to build an unstable open-loop coculture. By externally adding C6-HSL and pC-HSL I demonstrated that our circuit can stabilise coculture composition. I will now investigate how production of quorum sensing signals will contribute to autonomously regulate the coculture ratio of an unbalanced coculture.

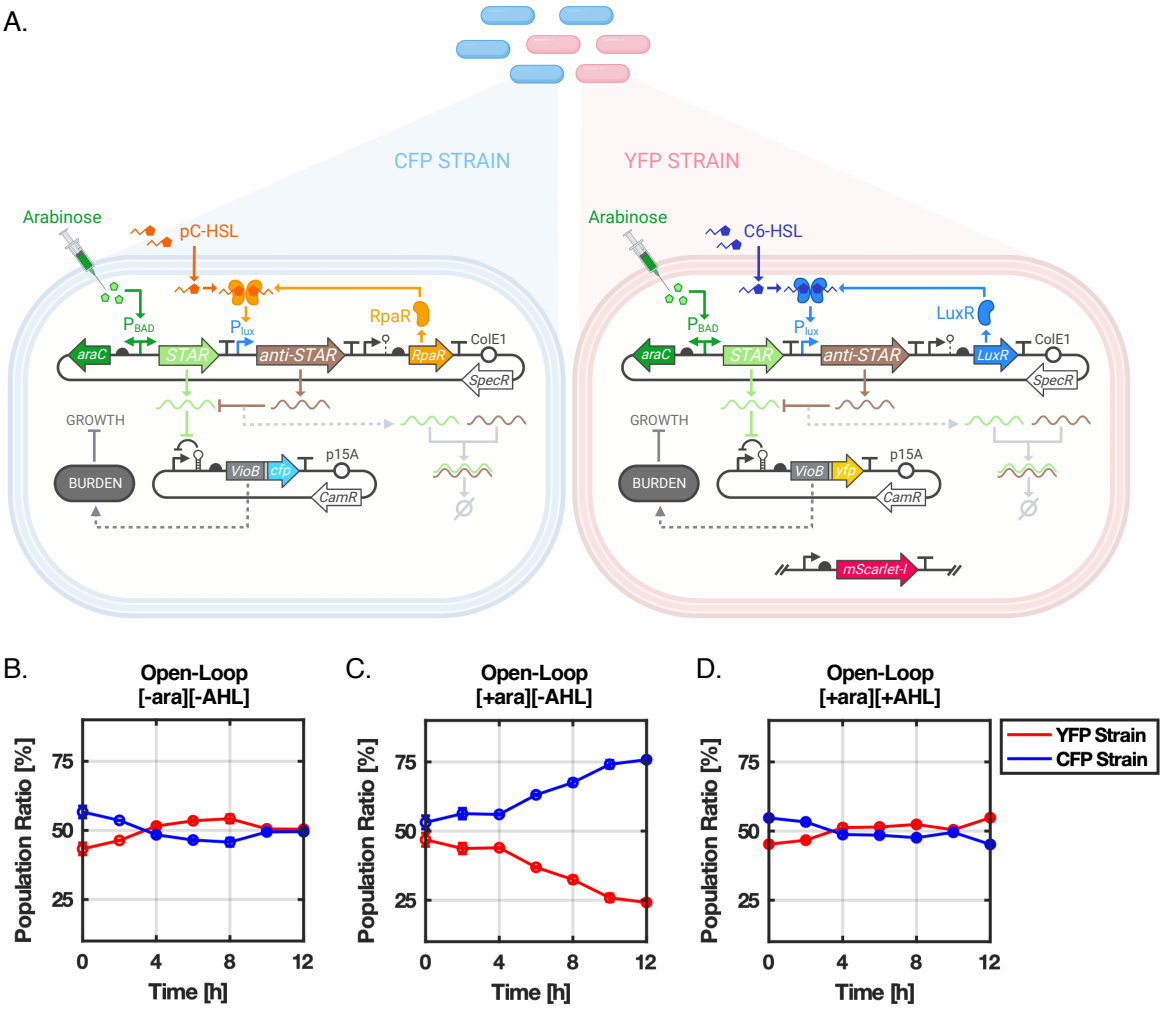


Figure 64: Open-Loop coculture expressing VioB-YFP and VioB-CFP. (A) Open-loop circuit of the coculture composed of the CFP and YFP strain. Both strains do not produce either C6-HSL or pC-HSL so no rescue mechanism is in place to maintain coculture composition at a 1:1 ratio. The YFP strain constitutively expresses mScarlet-I to facilitate measuring coculture ratio using flow-cytometry. (B) Population ratio of the open-loop coculture when it is not induced with either L-arabinose, C6-HSL or pC-HSL. (C) Population ratio of the open-loop coculture when it is induced with 0.2% L-arabinose only. (D) Population ratio of the open-loop coculture when it is induced with 0.2% L-arabinose, 10^{-7}M of C6-HSL and 10^{-7}M of pC-HSL. Experiments were done in DH10B. Population ratio was measured through flow-cytometry. Data represent the mean values of n = 3 biological replicates ± s.d.

5.2.2 Validation of the pC-HSL communication channel for coculture regulation

Next, I checked that the production of pC-HSL by the pC-HSL sender strain can trigger a response in the pC-HSL receiver strain. This way, I verify that pC-HSL communication

channel is operational to control the growth of the CFP strain based on the population density of the YFP strain.

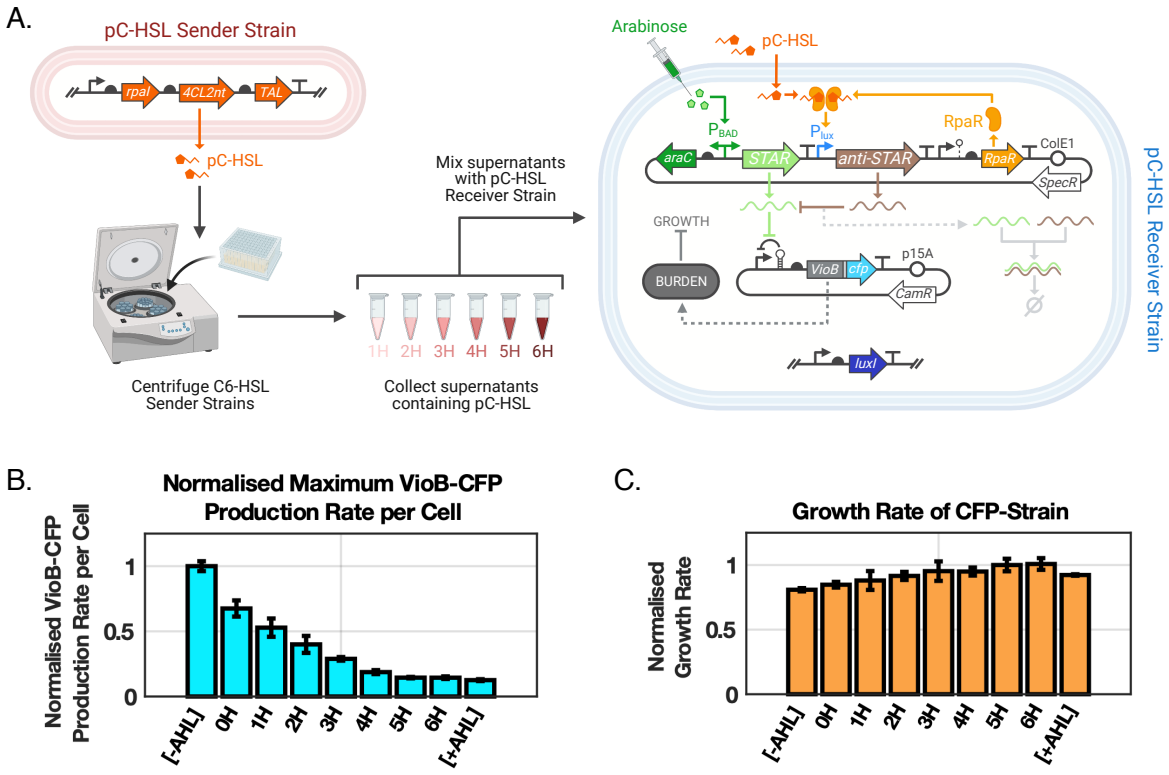


Figure 65: Detection of pC-HSL by the VioB-CFP producing strain. (A) The pC-HSL sender strain is cultivated for 1 to 6 hours. Sender strains are spun down to collect their supernatants containing pC-HSL. The supernatants are then used to grow the CFP strain equipped with the LRR STAR-based comparator sensing pC-HSL concentration. (B-C) The CFP strain is induced with 0.2% L-arabinose and grown in the different supernatants collected at different times of growth of the pC-HSL sender strain. The controls "-AHL" and "+AHL" are grown in fresh M9 medium and supplemented with 0M of pC-HSL and 10^{-7}M of pC-HSL respectively. Increasing pC-HSL concentration turns down VioB-CFP production (B) and improves growth rate (C). Experiments were done in DH10B. CFP and OD measurements were collected in the plate-reader. Data represent the mean values of n = 3 biological replicates ± s.d.

To study the effect of pC-HSL sender strain growth on the growth regulation mechanism taking place in the pC-HSL receiver strain I applied the workflow from Figure 41 from Chapter 3. I grew the pC-HSL sender strain from 1h to 6h and collected the supernatants by centrifugation (Figure 65.A). I then mixed the supernatants corresponding to the different times of growth with the pC-HSL receiver strain expressing VioB-CFP under the control of the LRR STAR-based comparator. I observed that the VioB-CFP production rate decreases

as the CFP strain is mixed with supernatants corresponding to longer incubation periods of the pC-HSL sender strain (Figure 65.B). So as pC-HSL concentration increases as a function of pC-HSL density, VioB-CFP expression is inhibited in the pC-HSL receiver strain, which contributed to recover 20% of the growth rate of the CFP strain (Figure 65.C). I note that there is already a 30% decrease in VioB-CFP production rate when the pC-HSL receiver strain is mixed with freshly diluted pC-HSL sender cells: 0H in Figure 65.B. So the CFP strain is very sensitive to pC-HSL expressed at low densities of pC-HSL sender cells.

To inspect the impact of pC-HSL production by the pC-HSL sender strain, I selected a high (DH_{rpa-3}), medium (DH_{rpa-4}) and low (DH_{rpa-2}) pC-HSL producing strains from Chapter 3. The pC-HSL receiver strain, sensing the different levels of pC-HSL produced by the three selected strains, drives the expression of VioB-YFP from the araBAD version of the LRR STAR-based comparator. I transformed the C6-HSL receiver strains with VioB-CFP controlled by the LLL STAR-based comparator in which STAR is driven by the rhaBAD promoter instead of the araBAD promoter. I compared the strength of the araBAD and rhaBAD promoters in Appendix 8.9.2 and show the the rhaBAD promoter is much weaker than the araBAD promoter. This way, I can unbalance the coculture to its limit when the system is induced with L-arabinose only and not with L-rhamnose (Figure 66.A). I specifically chose to carry out this experiment using VioB-YFP in combination with the LRR STAR-based comparator as VioB-YFP imposes more burden on its host than VioB-CFP, hence I can unbalance the coculture system further when inducing VioB-YFP expression rather than VioB-CFP expression. In the final system, the LRR STAR-based comparator will however be regulating VioB-CFP expression.

When the pC-HSL sender strain produces small pC-HSL levels, the open-loop and the closed-loop coculture behave very similarly (Figure 66.B). The pC-HSL signal strength is too weak to compensate the difference in growth rate between the two strains to maintain a stable coculture composition over time. However, in Figures 66.C and D, when the pC-HSL sender strain produces more pC-HSL as its population density increases, the population ratio of the closed-loop coculture is stabilised compared to the open-loop coculture. In Figure 66.E, I confirm that the overall VioB-YFP production rate per cell does not decrease when the pC-HSL sender strain produces low levels of pC-HSL. However, when the pC-HSL signal

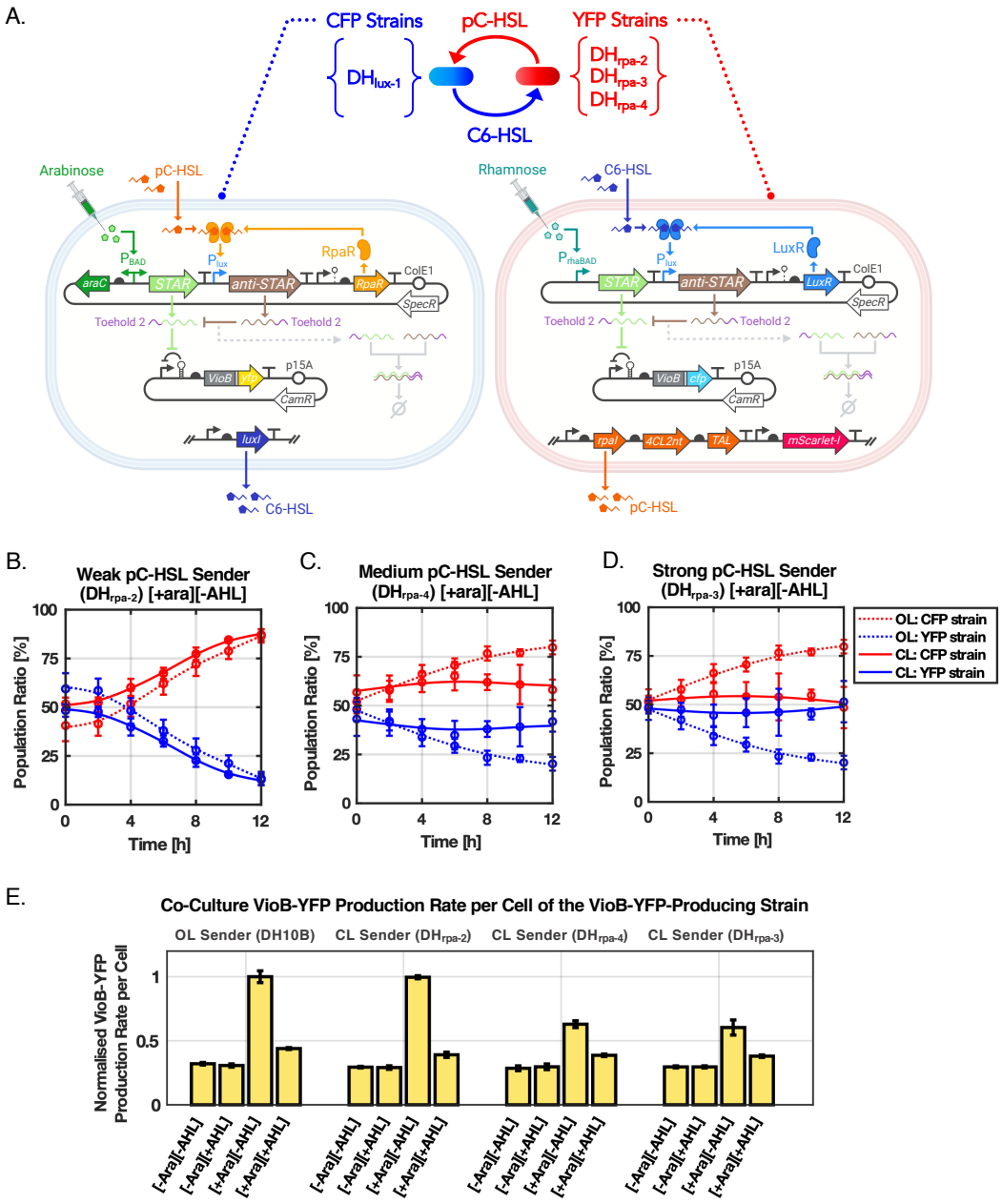


Figure 66: Effect of pC-HSL production on coculture composition. (A) $DH_{rpa-2,3,4}$ pC-HSL sender strains, or CFP strains, are tested to study the effect of pC-HSL signal strength on coculture composition of the closed-loop circuit. The YFP strain produces VioB-YFP in the presence of L-arabinose and VioB-YFP production is down-regulated by pC-HSL. The CFP strain produces VioB-CFP in the presence of L-rhamnose and VioB-CFP production is down-regulated by C6-HSL. In the open-loop circuit, both strains do not produce either quorum sensing molecule to break communication between the strains. (B) Change in population ratio when the coculture is made up of the weak pC-HSL DH_{rpa-2} sender CFP strain and the DH_{lux-1} YFP strain. Coculture is induced with 0.2% of L-arabinose and 0% of L-rhamnose. (C) Change in population ratio when the coculture is made up of the medium-strength pC-HSL DH_{rpa-4} sender CFP strain and the DH_{lux-1} YFP strain. Coculture is induced with 0.2% of L-arabinose and 0% of L-rhamnose. (D) Change in population ratio when the coculture is made up of the strong pC-HSL DH_{rpa-3} sender CFP strain and the DH_{lux-1} YFP strain. Coculture is induced with 0.2% of L-arabinose and 0% of L-rhamnose. (Caption continued on the following page.)

Figure 66: (E) Normalised VioB-sfYFP production rate per cell of the open-loop coculture, and closed-loop coculture with the $DH_{rpa-2,3,4}$ pC-HSL sender strains. Four inducer conditions were tested by externally adding different combinations of the four inducers. (1) "[-Ara][-AHL]": 0% of L-arabinose, 0% of L-rhamnose, 0M of pC-HSL, 0M of C6-HSL. (2) "[-Ara][+AHL]": 0% of L-arabinose, 0% of L-rhamnose, 10^{-7}M of pC-HSL, 0M of C6-HSL. (3) "[+Ara][-AHL]": 0.2% of L-arabinose, 0% of L-rhamnose, 0M of pC-HSL, 0M of C6-HSL. (4) "[+Ara][+AHL]": 0.2% of L-arabinose, 0% of L-rhamnose, 10^{-7}M of pC-HSL, 0M of C6-HSL. Experiments were done in DH10B. Population ratio was measured through flow-cytometry. VioB-sfYFP fluorescence was measured in a timecourse plate-reader assay. Data represent the mean values of n = 3 biological replicates ± s.d.

strength increases with DH_{rpa-4} and DH_{rpa-3}, VioB-YFP expression is reduced, though it is not maximally inhibited as demonstrated by the control in which the coculture was induced with both L-arabinose and pC-HSL ("[+Aara][+AHL]" in Figure 66.E). So varying the level of pC-HSL production by the pC-HSL sender strain contributes to the stabilisation of coculture composition without completely turning off the expression of the protein of interest.

In this section, I highlighted the importance of tuning pC-HSL production by the pC-HSL sender strain for stabilisation of the coculture ratio. Tuning pC-HSL expression also provides a way to tune the desired ratio of the coculture in batch culture. Stabilisation of the coculture composition was possible through reducing burden due to VioB expression in the pC-HSL receiver strain, and thus I have validated that the composition controller responds to pC-HSL signal as expected.

5.2.3 Validation of the C6-HSL communication channel for coculture regulation

Having established the pC-HSL communication channel between pC-HSL sender and receiver strains, I now look at doing the same with the C6-HSL communication channel. In this section, I will validate the growth regulation response of the C6-HSL receiver strain to the quorum sensing signal produced by the C6-HSL sender strain.

First, I verify that the C6-HSL receiver strain can sense the C6-HSL quorum sensing signal produced by the C6-HSL receiver strain and adapt its level of expression of protein of interest to modulate its growth rate.

I proceeded similarly to test the impact of pC-HSL production by the pC-HSL sender

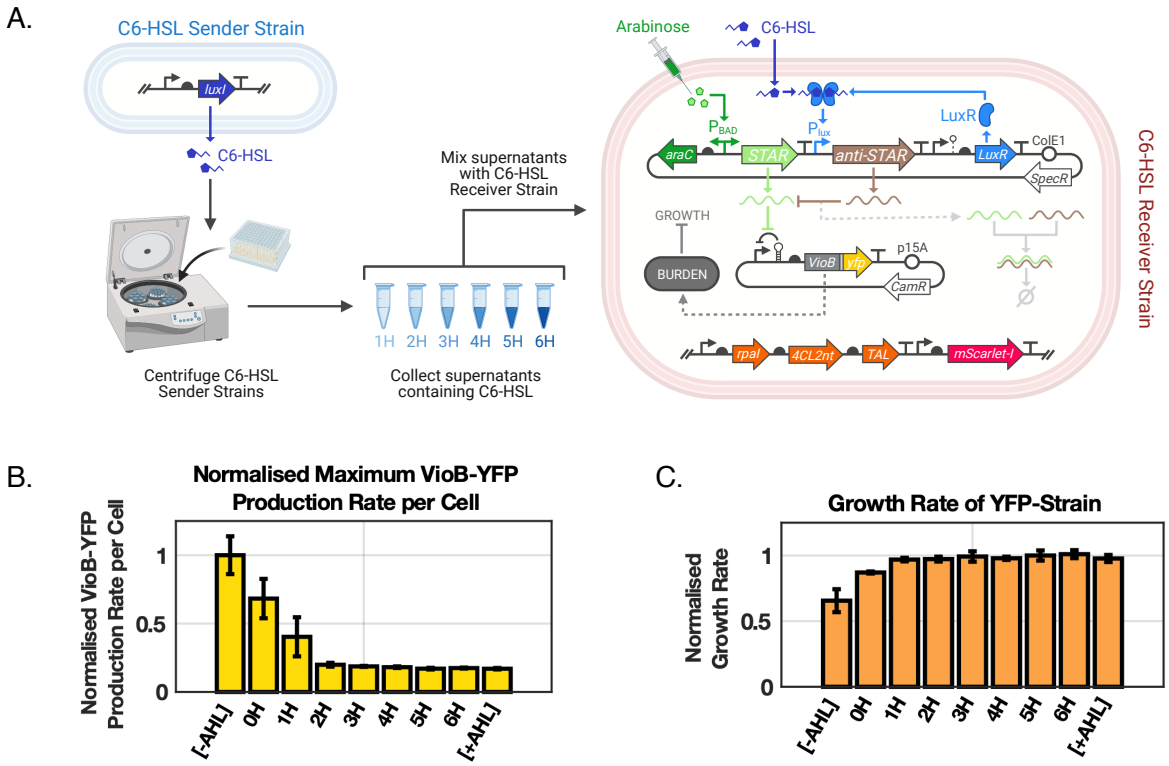


Figure 67: Detection of C6-HSL by the VioB-YFP producing strain. (A) The C6-HSL sender strain is cultivated for 1 to 6 hours. Sender strains are spun down to collect their supernatants containing C6-HSL. The supernatants are then used to grow the YFP strain equipped with the LLL STAR-based comparator sensing C6-HSL concentration. (B-C) The YFP strain is induced with 0.2% L-arabinose and grown in the different supernatants collected at different times of growth of the C6-HSL sender strain. The controls "-AHL" and "+AHL" are grown in fresh M9 medium and supplemented with 0M of C6-HSL and 10^{-7}M of C6-HSL respectively. Increasing C6-HSL concentration turns down VioB-YFP production (B) and improves growth rate (C). Experiments were done in DH10B. YFP and OD measurements were collected in the plate-reader. Data represent the mean values of n = 3 biological replicates ± s.d.

strain on the pC-HSL receiver strain in the previous section. More specifically, I cultivated a C6-HSL sender strain from 1 hour to 6 hours (Figure 67.A). I collected the supernatants of the C6-HSL sender strains corresponding to the different growth periods and mixed the supernatants with the C6-HSL receiver strain. In this context, the C6-HSL receiver strain expresses VioB-YFP under the control of the LLL STAR-based comparator. When the C6-HSL receiver strain is induced with L-arabinose, VioB-YFP expression is expressed ("[-AHL]") in Figure 67.B. As the concentration of C6-HSL increases when the C6-HSL receiver strain is mixed with supernatants issued from longer incubation periods of C6-HSL sender cells, the production rate per cell of VioB-YFP decreases. As

a result, the growth rate of the C6-HSL receiver strain, or YFP strain, increases (Figure 67.C). As in the case of the pC-HSL communication channel, I observe that the C6-HSL receiver strain is sensitive to low densities of C6-HSL sender cells since the VioB-YFP production rate is already impacted by a 30% decrease when the sender cells were freshly diluted: "0H" in Figure 67.B. So the C6-HSL receiver strain is able to sense the different concentrations of C6-HSL produced by the C6-HSL sender strain at different stages of growth.

Next, I look at the impact of the strength of C6-HSL production on the stability of our coculture (Figure 68.A). To push the coculture to its limit, I transformed the C6-HSL sender strain, or CFP strain, with VioB-CFP controlled by the rhaBAD STAR-based comparator. As I will not induce the coculture with L-rhamnose, the CFP strain will not be subjected to burden and its only role in the coculture will be to produce C6-HSL quorum sensing signal to help balance coculture composition. I will test two versions of the C6-HSL sender strain, one producing high levels of C6-HSL (DH_{lux-1}), and one producing weaker levels of C6-HSL (DH_{lux-2}) according to our results found in Chapter 3. The C6-HSL receiver strain, or YFP strain, is transformed with VioB-YFP regulated by the araBAD LLL STAR-based comparator such that when the coculture is induced with L-arabinose, VioB-YFP production is upregulated in the YFP strain.

First I tested the coculture made up of the weak C6-HSL sender strain DH_{lux-2} (Figure 68.B). I observed that when the coculture is induced with L-arabinose only, both the open-loop and closed-loop coculture could not balance coculture composition and that the CFP strain out-competed the YFP strain after 12 hours of growth. However, when I added both L-arabinose and C6-HSL to the system, coculture composition stabilised around a 3:2 ratio (Figure 68.C). So the weak C6-HSL sender strain DH_{lux-2} does not synthesise enough C6-HSL to rescue the YFP strain for the given difference in growth rate between the YFP and CFP strain. However, when I used a stronger C6-HSL sender strain, DH_{lux-1}, to build our coculture, I observed that the closed-loop coculture was able to stabilise its population composition to a 1:1 ratio (Figure 68.D).

In Figures 68.E and F, I confirm that the stabilisation of the coculture composition is

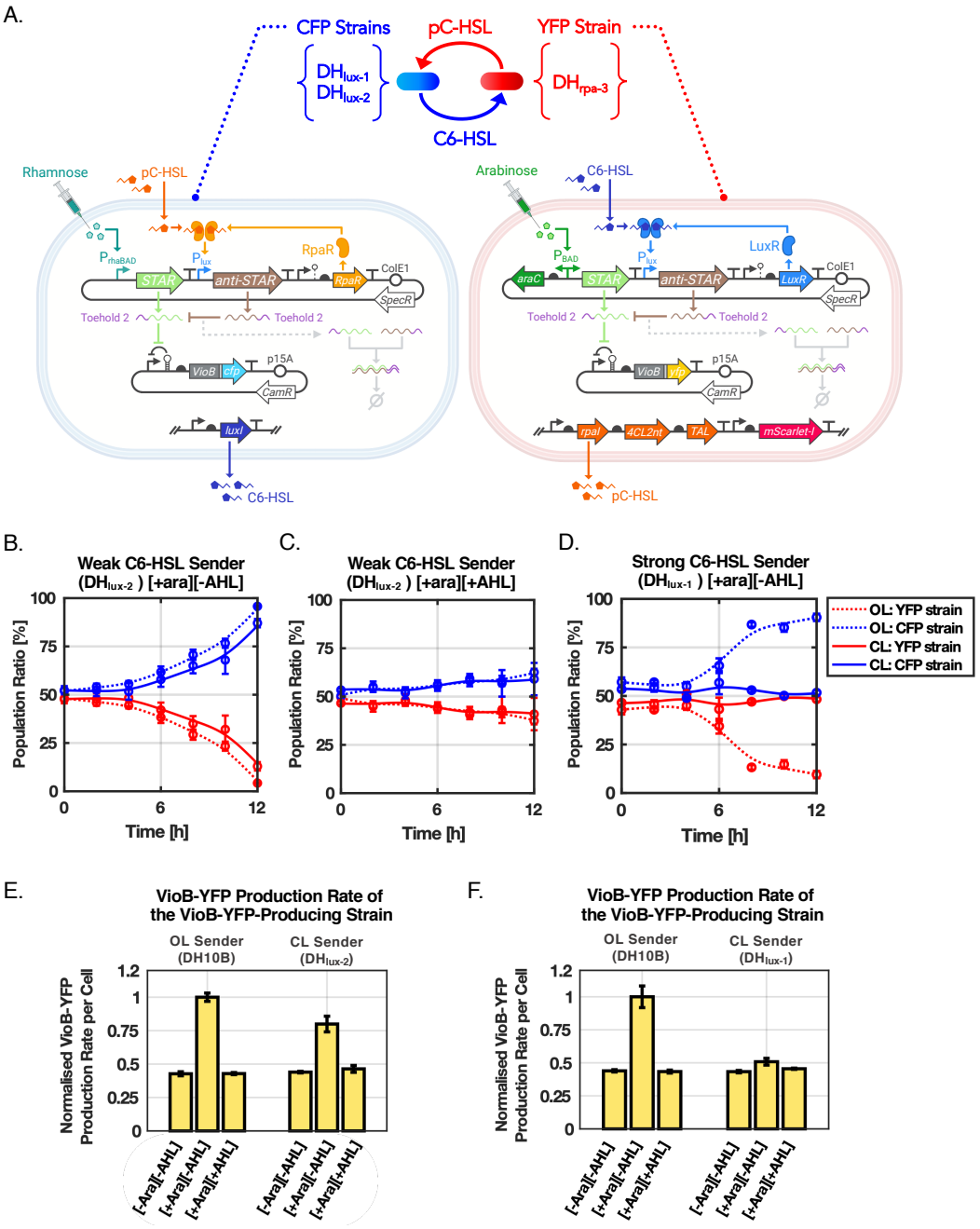


Figure 68: Effect of C6-HSL production of coculture composition. (A) $DH_{lux-1,2}$ C6-HSL sender strains, or CFP strains, are tested to study the effect of C6-HSL signal strength on coculture composition of the closed-loop circuit. The YFP strain produces VioB-YFP in the presence of L-arabinose and VioB-YFP production is down-regulated by C6-HSL. The CFP strain produces VioB-CFP in the presence of L-rhamnose and VioB-CFP production is down-regulated by pC-HSL. In the open-loop circuit, both strains do not produce either quorum sensing molecule to break communication between the strains. (B) Change in population ratio when the coculture is made up of the weak C6-HSL DH_{lux-2} sender CFP strain and the DH_{rpa-3} YFP strain. Coculture is induced with 0.2% of L-arabinose, 0% of L-rhamnose, and 0M of both C6-HSL and pC-HSL. (C) Change in population ratio when the coculture is made up of the weak C6-HSL DH_{lux-2} sender CFP strain and the DH_{rpa-3} YFP strain, when the coculture is induced with 0.2% of L-arabinose, 0% of L-arabinose, 10^{-7}M of both C6-HSL and pC-HSL. (Caption continued on the following page.)

Figure 68: (D) Change in population ratio when the coculture is made up of the strong C6-HSL DH_{lux-1} sender CFP strain and the DH_{rpa-3} YFP strain. Coculture is induced with 0.2% of L-arabinose, 0% L-rhamnose and 0M of both C6-HSL and pC-HSL. (E-F) Normalised VioB-sfYFP production rate per cell of the open-loop coculture, and closed-loop coculture with the $DH_{lux-1,2}$ C6-HSL sender strains. Three inducer conditions were tested by externally adding different combinations of the four inducers. (1) "[-Ara][-AHL]": 0% of L-arabinose, 0% of L-rhamnose, 0M of pC-HSL, 0M of C6-HSL. (2) "[+Ara][-AHL]": 0.2% of L-arabinose, 0% of L-rhamnose, 0M of pC-HSL, 0M of C6-HSL. (3) "[+Ara][+AHL]": 0.2% of L-arabinose, 0% of L-rhamnose, 10^{-7}M of pC-HSL, 0M of C6-HSL. Experiments were done in DH10B. Population ratio was measured through flow-cytometry. VioB-sfYFP fluorescence was measured in a timecourse plate-reader assay. Data represent the mean values of n = 3 biological replicates ± s.d.

done through the down-regulation of VioB-YFP expression. The coculture composed of the weak C6-HSL sender strain DH_{lux-2} could only downregulate VioB-YFP production rate by 20% compared to the open-loop ("[+Ara][-AHL]"), which was not enough to significantly improve the YFP strain growth rate to stabilise the coculture composition (Figure 68.E). In the case of the strong C6-HSL sender strain however, VioB-YFP production rate was inhibited up to 50% by the quorum sensing signal produced by the CFP strain DH_{lux-1} compared to the open-loop ("[+Ara][-AHL]") (Figure 68.F). This down-regulation in VioB-YFP expression was enough to compensate for the difference in growth rate between the CFP and YFP strains to stabilise their ratio when grown in a batch setting.

In this section, I have shown the importance of the C6-HSL signal strength to regulate coculture composition. Our C6-HSL receiver strain is able to detect increasing C6-HSL levels and adjust its growth rate accordingly in order to compensate for the difference in growth rate between two strains in a coculture.

5.2.4 Ratio stabilisation in a 2-way-communicating co-culture

So far, I have only been looking at stabilising the ratio of a coculture in which only one of the two strains was producing a burdensome product. In this section I will be looking at stabilising the ratio of a coculture in which both strains are producers, one producing VioB-YFP and the other producing VioB-CFP.

In previous the subsections (5.2.2 - 5.2.3), I have seen the importance of producing enough pC-HSL and C6-HSL to downregulate VioB expression in the pC-HSL and C6-HSL receiver strains respectively. In Figures 66 and 67, I pushed the coculture to its limit by only inducing burden through the expression of VioB in only one of the two *E. coli* strains. In

Figure 66, I showed that the DH_{rpa-3} produced enough pC-HSL to maintain the coculture composition around a 1:1 ratio. Similarly, in Figure 67, it was the DH_{lux-1} strain that was producing enough C6-HSL to maintain the coculture composition around a 1:1 ratio. Now that I am aiming to express a burdensome protein in both strains, I expect the difference in burden to be less than between the cocultures of Figures 66 and 67, as now both strains will be experiencing some burden. As I previously showed that the DH_{rpa-3} and DH_{lux-1} strains could maintain the coculture composition to a 1:1 ratio for larger differences in burden that I am now expecting, I decided that those two strains would be good candidates to guarantee a strong communication link between the strains to stabilise coculture composition around a 1:1 ratio.

Using these two strains, I built the coculture from Figure 62 to verify whether two producing strains would be able to autonomously stabilise the population composition of their coculture (Figure 69.A). First I monitored the coculture when no L-arabinose or quorum sensing was externally added to the culture (Figure 69.B). I observed that the open-loop coculture kept a constant coculture composition, while the closed-loop ratio increased slightly after 6 hours from a 1:1 ratio towards a 3:1 ratio. That is likely due to the cost of producing anti-STAR without a toehold in the YFP strain while the CFP strains produces anti-STAR with Toehold 2, which I showed to be less costly on the host than its no toehold counterpart in Figure 25 of Chapter 2. I confirm this hypothesis by externally adding both C6-HSL and pC-HSL to the open-loop and closed-loop cocultures in Figure 69.C. Now that the open-loop is producing anti-STAR without and with toehold in the YFP and CFP strains respectively as in the closed-loop circuit, both OL and CL coculture see their ratio increase after 6 hours from 1:1 towards 3:1. The fact that population ratio is not destabilised before 6 hours suggests that C6-HSL levels are not high enough before 6 hours to produce enough anti-STAR without toehold in the YFP strain to destabilise coculture composition.

Next, I induced the open-loop and closed-loop cocultures with L-arabinose (Figure 69.D). There I show that even though the expression of STAR and anti-STAR imposes a different cost of the YFP and CFP strains, regulation of VioB-YFP and VioB-CFP expression enables the stabilisation of the coculture composition in the closed-loop circuit. After 12 hours of growth, the open-loop coculture as reaches a 9:1 ratio between the CFP strain and the YFP

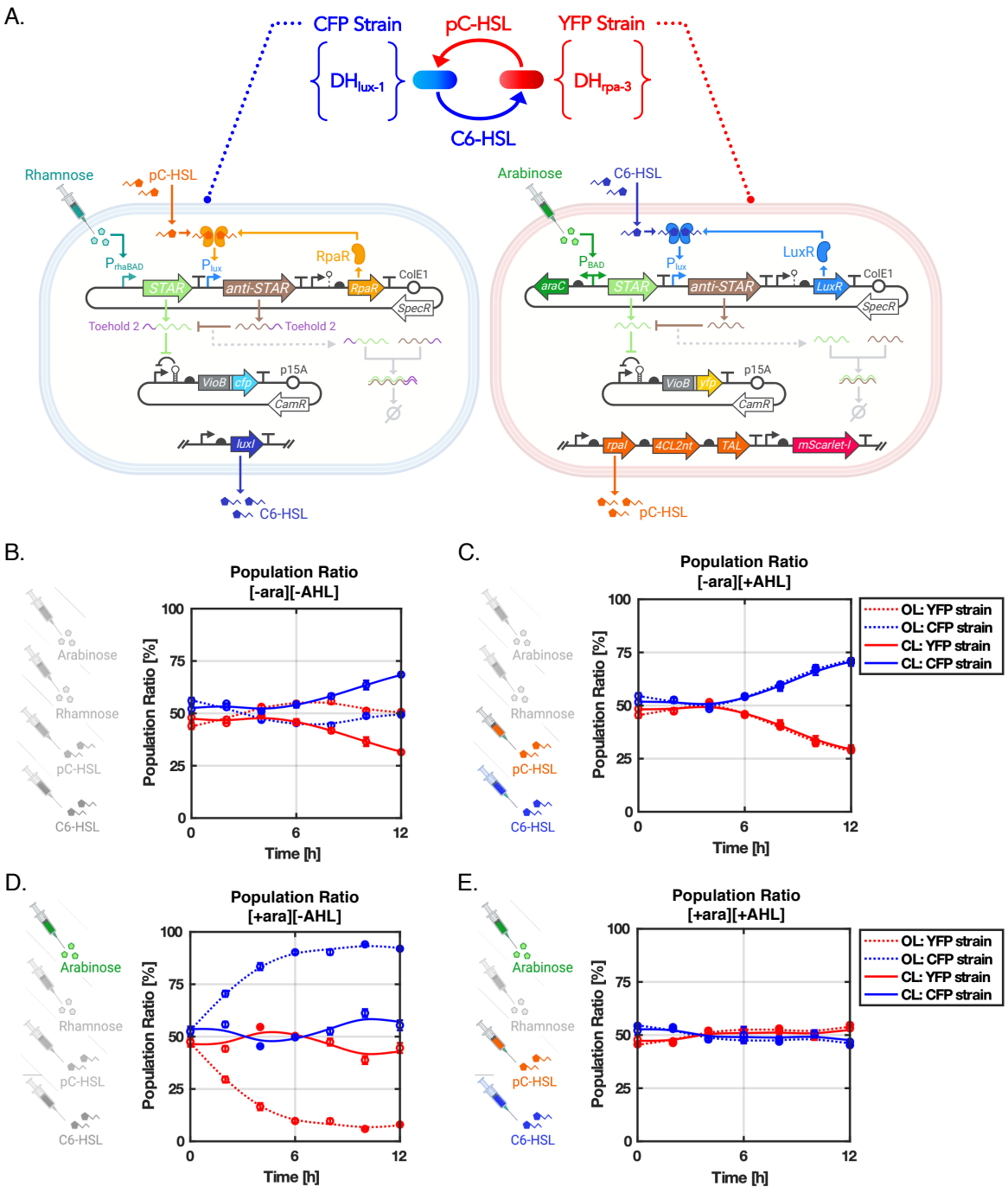


Figure 69: Two-way communication coculture stabilises coculture composition. (A) In the closed-loop (CL) coculture, the YFP strain, DH_{rpa-3}, synthesises pC-HSL. It controls VioB-sfYFP expression by comparing L-arabinose and C6-HSL signals strength. The CFP strain, DH_{lux-1}, synthesises C6-HSL. It controls VioB-sfCFP expression by comparing L-arabinose and pC-HSL signals strength. In the open-loop (OL) coculture the YFP and CFP strains do not produced quorum sensing signals. The YFP strain expresses a comparator with Toehold 2, while the CFP strain expresses a comparator without toehold. (Caption continues on the next page.)

Figure 69: (B) Population ratio of the open-loop and closed-loop cocultures when externally induced with 0% of L-arabinose, and 0M of both C6-HSL and pC-HSL. (C) Population ratio of the open-loop and closed-loop cocultures when induced with 0% L-arabinose, 10^{-7}M of C6-HSL and 0M of pC-HSL. (D) Population ratio of the open-loop and closed-loop cocultures when induced with 0.2% L-arabinose, 0M of both C6-HSL and pC-HSL. (E) Population ratio of the open-loop and closed-loop cocultures when induced with 0.2% L-arabinose, 10^{-7}M of both C6-HSL and pC-HSL. Experiments were done in DH10B. Population ratio was measured through flow-cytometry. Data represent the mean values of n = 3 biological replicates ± s.d.

strain. In contrast, the closed-loop circuit successfully stabilised the population composition by fluctuating around a 1:1 ratio.

Finally, I added L-arabinose, C6-HSL and pC-HSL to the cocultures (Figure 69.E). I confirmed that the open-loop circuit could maintain the coculture ratio at 1:1 when both pC-HSL and C6-HSL were present to inhibit VioB-CFP and VioB-YFP production. Interestingly, I noticed that the amplitude of the population ratio oscillations exhibited by the closed-loop coculture in the absence of externally added quorum sensing molecules were higher than when HSL molecules were added. This suggests that the closed-loop in Figure 69.D is not operating in a saturating regime in which HSL concentrations would be so high that they would turn off the production of the protein of interest immediately.

I decided to test the performance of our coculture design when it is pushed to its limit, that is when there is the greatest difference in growth rate between the two strains. This would allow us to test whether the system is able to correct for coculture composition instability when only one of the strains has the ability to modulate its growth rate.

To do so I constructed a new version of the STAR comparator. So far STAR expression has been driven by the araBAD strong promoter inducible with L-arabinose. I built a version in which STAR expression was now driven by the rhaBAD promoter inducible with L-rhamnose. By transforming the comparator inducible by L-arabinose in the YFP strain and the L-rhamnose-inducible comparator in the CFP strain, this would allow us to set the reference signal independently in both strains (Figure 70.A). Because I am looking into pushing the coculture design to its limit, I would only externally add L-arabinose, and no L-rhamnose, to the system such that the YFP strain would be the only strain producing a compound of interest causing burden in the strain and thus destabilising the coculture composition. First

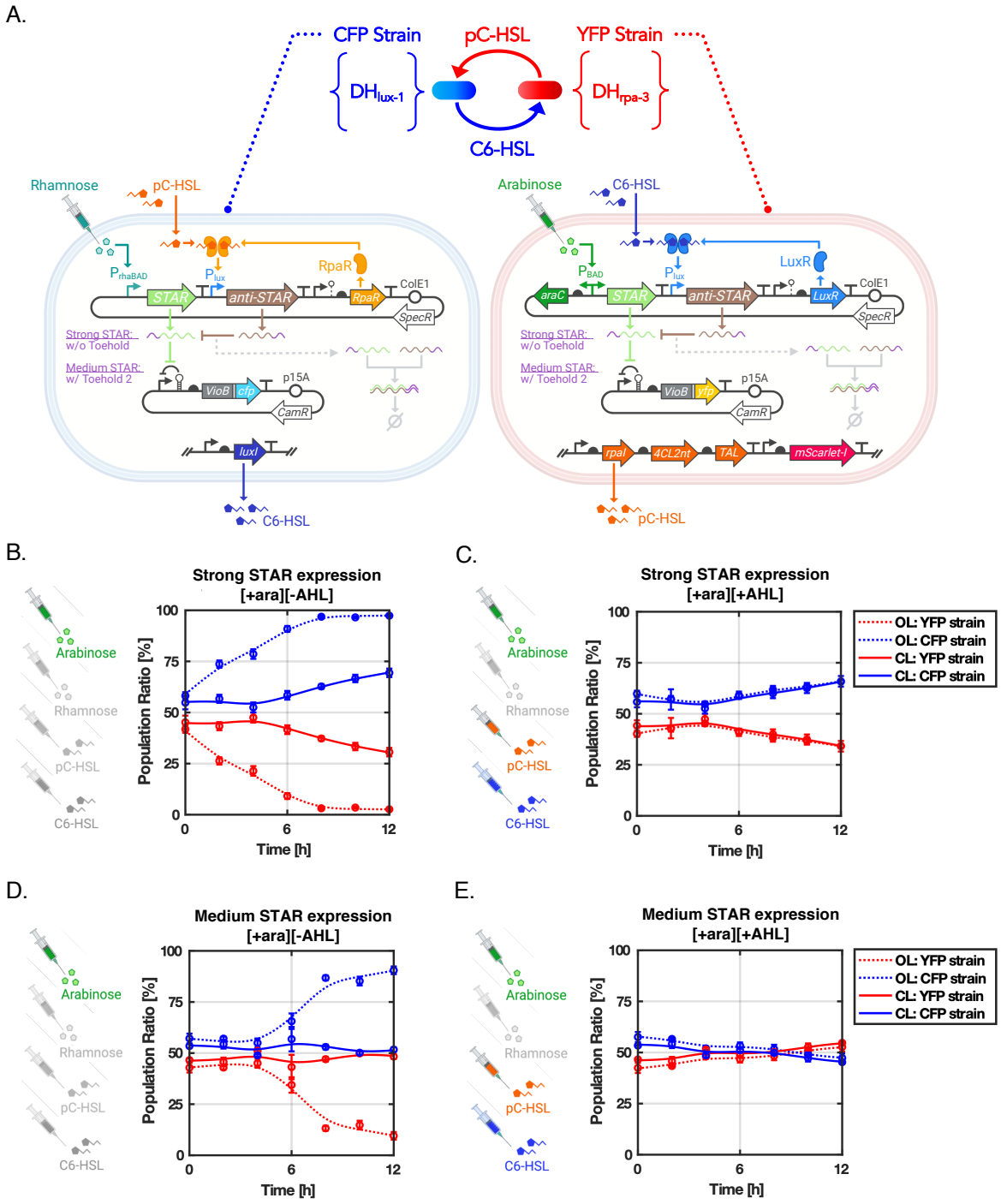


Figure 70: C6-HSL and STAR expression tunes coculture composition. (A) In the closed-loop two-strain coculture, the CFP strain produced C6-HSL and control the expression of VioB-CFP under the control of the rhaBAD LRR STAR-based comparator with or without Toehold 2. The YFP strain produces pC-HSL and controls the expression of VioB-YFP under the control of the araBAD LLL STAR-based comparator with or without Toehold 2. In the open-loop coculture the CFP and YFP strains do not produce C6-HSL and pC-HSL respectively. (Caption continues on the next page.)

Figure 70: (B-C) The CFP and YFP strains carry the STAR-based comparator without toehold ("Strong STAR"). The ratio between the two strains is monitored over time when the coculture is externally induced with 0.2% L-arabinose only or when it is induced with 0.2% L-arabinose, 10^{-7}M of C6-HSL and 10^{-7}M of pC-HSL. (D-E) The CFP and YFP strains carry the STAR-based comparator with Toehold 2 ("Medium STAR"). The ratio between the two strains is monitored over time when the coculture is externally induced with 0.2% L-arabinose only or when it is induced with 0.2% L-arabinose, 10^{-7}M of C6-HSL and 10^{-7}M of pC-HSL. Experiments were done in DH10B. Population ratio was measured through flow-cytometry. Data represent the mean values of n = 3 biological replicates ± s.d.

I examined the behaviour of the coculture when both strains carried the comparators with STAR and anti-STAR having no toehold domain. I compared the behaviour of the coculture composition as I externally add the quorum sensing molecules (Figure 70.B) or if neither C6-HSL nor pC-HSL are supplemented into the coculture media. I observed that the closed-loop coculture autonomously mitigated the difference in growth rate between the CFP and YFP strains through the mediation of quorum sensing signal. Indeed in the open-loop coculture the CFP strains completely overtake the YFP strain after 8 hours of growth (Figure 70.B), while upon external addition of quorum sensing molecule, the divergence was mitigated to achieve a 1:2 ratio after 12 hours (Figure 70.C), a comparable final ratio to the closed-loop coculture.

In comparison, when the YFP and CFP strains were transformed with the comparator with Toehold 2, that is a system that does not achieve as high levels of gene of interest production as its no toehold counterpart (Figure 25 Chapter 2) and induces less burden on the cell (Figure 26 Chapter 2), the final ratio is of the closed-loop coculture was closer to 1:1 (Figures 70.D-E). Because the comparator imposes less burden on its host, the difference in growth rate between the YFP and CFP strains is smaller than in the previous case, when the comparators did not have toehold domain. This is reflected in the time that the CFP strain takes to out-compete the YFP strain in the open-loop coculture. When the comparator has toehold domains, the CFP strain did not completely overtake the coculture, instead finishing at a 1:9 ratio at 12 hours, and the coculture ratio did not start diverging until 4 hours (Figure 70.D). So when the toehold is present, and the closed-loop circuit is pushed to its limit, it is able to down-regulate VioB-YFP production to the point that the growth rate in the CFP and YFP strain is similar. However, when no toehold is present, and the system is tested to its limit, the YFP strain is able to improve its growth rate and stabilise

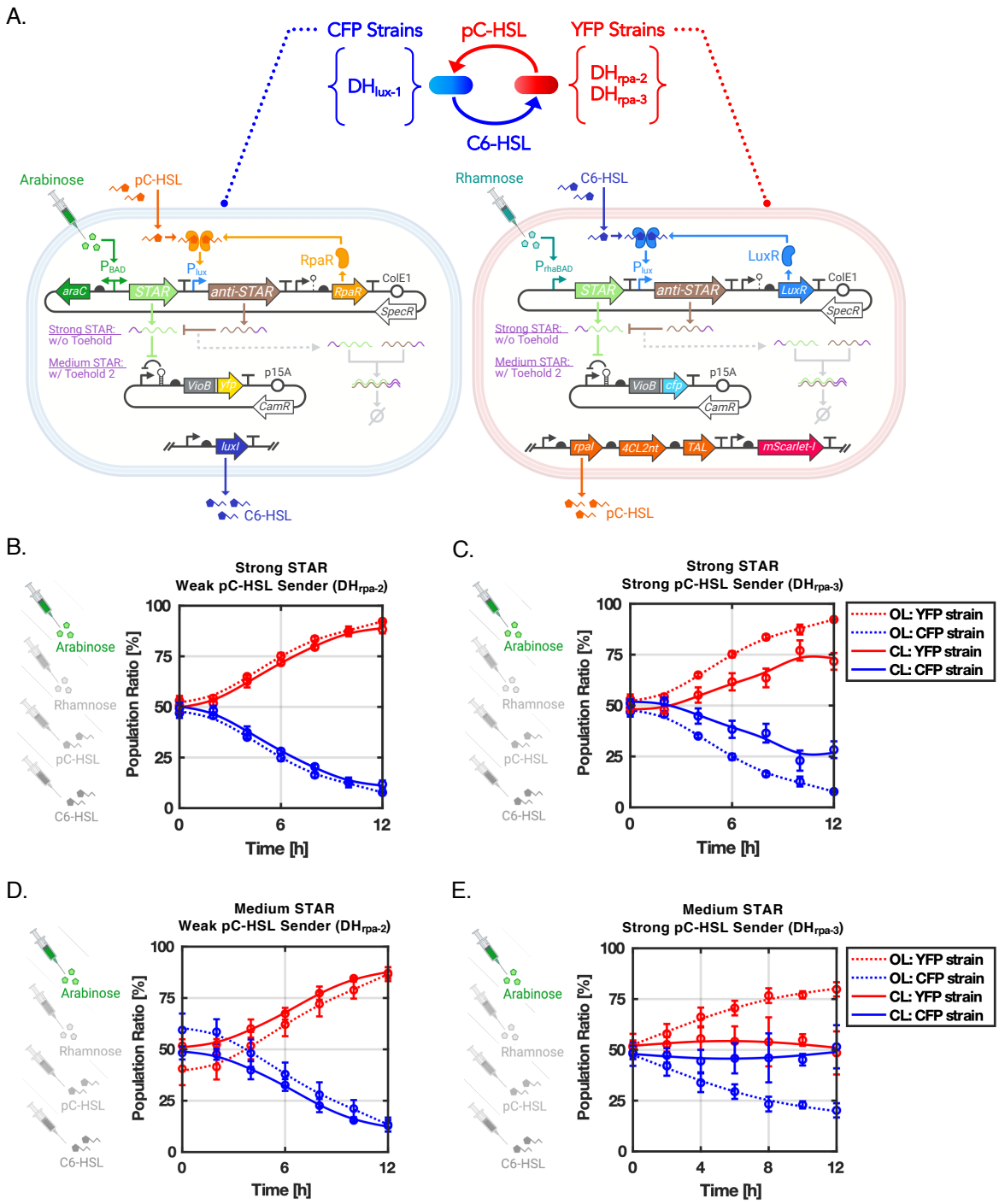


Figure 71: pC-HSL and STAR expression tunes coculture composition. (A) In the closed-loop coculture, the CFP strain, DH_{rpa-2} or DH_{rpa-3}, synthesises pC-HSL. It controls VioB-sfCFP expression by comparing L-rhamnose and C6-HSL signals strength. The YFP strain, DH_{lux-1}, synthesises C6-HSL. It controls VioB-sfYFP expression by comparing L-arabinose and pC-HSL signals strength. In the open-loop coculture the YFP and CFP strains do not produce quorum sensing signals. (Caption continues on the next page.)

Figure 71: (B-C) Population ratio of the cocultures when the CFP strain, DH_{rpa-2} or DH_{rpa-3}, produces small or high amounts of pC-HSL respectively. Cocultures are induced with 0.2% L-arabinose, 0M of pC-HSL and 0M of C6-HSL. Both the YFP and CFP strains carry the strong STAR-based comparator without Toehold. (D-E) Population ratio of the cocultures when the CFP strain, DH_{rpa-2} or DH_{rpa-3}, produces small or high amounts of pC-HSL respectively. Cocultures are induced with 0.2% L-arabinose, 0M of pC-HSL and 0M of C6-HSL. Both the YFP and CFP strains carry the medium-strength STAR-based comparator with Toehold 2. Experiments were done in DH10B. Population ratio was measured through flow-cytometry. Data represent the mean values of n = 3 biological replicates ± s.d.

the coculture ratio, though without fully compensating for the difference in growth rate between the two strains. This shows that using the different STAR designs with different downstream gene activation can be a way to tune the desired ratio of the coculture.

To further explore the different tuning knobs that can be used to modulate the desired population ratio of the coculture, I pushed the coculture to the limit of the pC-HSL sender strain's ability to rescue growth of the pC-HSL receiver stain. To do so, I used different coculture circuit configurations in which the CFP strain is controlled by the rhaBAD STAR-based comparator, and the YFP strain is controlled by the araBAD STAR-based comparator (Figure 71.A). In Figures 71.B-E, I show that by increasing the strength of quorum sensing production, here pC-HSL, by using either DH_rpa-2 or DH_rpa-3 in combination with DH_lux-1, the coculture ratio stabilises closer to a 1:1 ratio. Indeed, when DH_lux-1 is grown together with the weak pC-HSL sender DH_rpa-2, the OL and CL coculture behave similarly (Figures 71.B and D). However, when DH_lux-1 is growth with the strong pC-HSL sender DH_rpa-3, the CL coculture maintains a composition closed to a 1:1 ratio than the OL coculture (Figures 71.C and E). I also show that the coculture stabilises closer to a 1:1 ratio when the STAR signal is weaker. To play with the strength of VioB-YFP activation I used the STAR designs from Figure 25 of Chapter 2 with and without Toehold 2. The comparator design with Toehold 2 was shown to have a 55% reduction in mRFP expression compared to the design without Toehold 2. I will refer to the comparator without Toehold 2 as the "Strong STAR" system and the comparator with Toehold 2 as the "Medium STAR" system. Increasing the strength of the STAR activation signifies that more anti-STAR has to be produced to down-regulate expression of VioB. So a stronger quorum sensing signal will be needed in order to achieve the same desired ratio

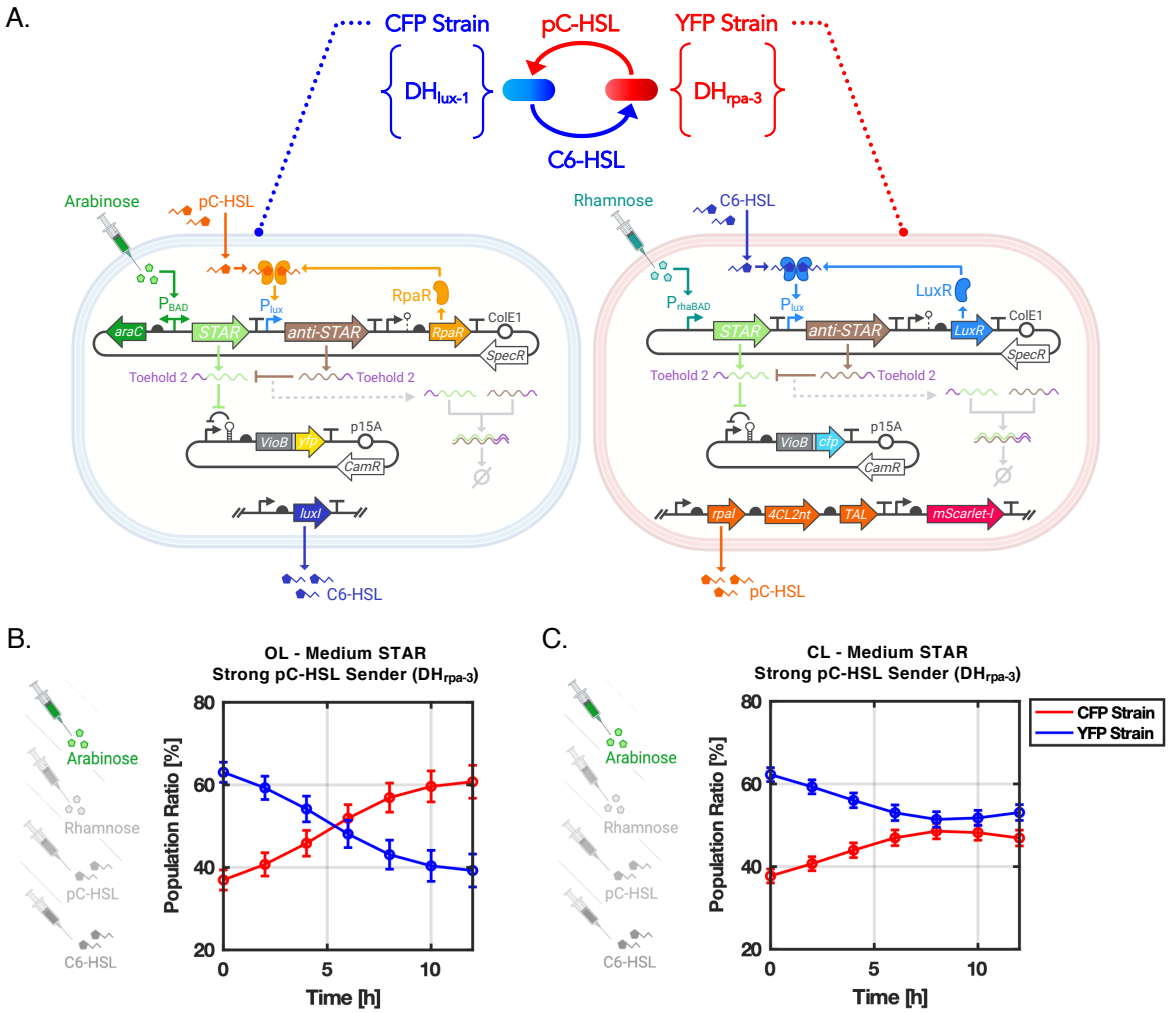


Figure 72: Stabilisation of coculture composition for 2:3 inoculation ratio. (A) In the closed-loop coculture, the CFP strain, DH_{rpa-3}, synthesises pC-HSL. It controls VioB-sfCFP expression by comparing L-rhamnose and C6-HSL signals strength. The YFP strain, DH_{lux-1}, synthesises C6-HSL. It controls VioB-sfYFP expression by comparing L-arabinose and pC-HSL signals strength. Both strains express versions of the STAR-based comparator with Toehold 2. In the open-loop coculture the YFP and CFP strains do not produce quorum sensing signals. (B) Open-loop coculture ratio over time when induced with 0.2% of L-arabinose, 0% of L-rhamnose and 0M of both C6-HSL and pC-HSL. The inoculation ratio was set to 3:2. (C) Closed-loop coculture ratio over time when induced with 0.2% of L-arabinose, 0% of L-rhamnose and 0M of both C6-HSL and pC-HSL. The initial inoculation ratio was set to 3:2. Experiments were done in DH10B. Population ratio was measured through flow-cytometry. Data represent the mean values of n = 3 biological replicates ± s.d.

as if using the "Medium STAR" design. This is what I observe in Figures 71.C and E: the "Strong STAR" CL achieves a final ratio of 3:1 after 12 hours of growth, while the "Medium STAR" CL achieves a final ratio of 1:1. Therefore both quorum sensing production strength

and STAR activation strength are means of tuning the coculture desired ratio.

Finally, I started exploring the impact of inoculation ratio on the behaviour of the closed-loop coculture. Until now, I always started the coculture assays by inoculating the CFP and YFP strains at a 1:1 ratio. In Figure 72 I investigate what would happen if I started from a different inoculation ratio such as a 3:2 ratio. For this assay, I decided to push the system to its limit by transforming the CFP strain with the rhaBAD STAR-based comparator with Toehold 2, such that in the absence of L-rhamnose in the growth media, the CFP strain would not express VioB-CFP. The imbalance of the coculture will be caused by the production of VioB-YFP controlled by the araBAD STAR-based comparator in the YFP strain (Figure 72.A). In the case of the open-loop coculture, the CFP strain gradually takes over the YFP strain fraction (Figure 72.B). However, in the case of the closed-loop coculture, the coculture composition stabilises from 6 hours onward around a 1:1 ratio (Figure 72.C). This suggests that the closed-loop coculture has the potential to stabilise the ratio of coculture starting from different inoculation ratios. If inoculation ratio fluctuations can be treated as a perturbation, then the system may be able to compensate for this perturbation by bringing the coculture back to the desired ratio.

In this section I have shown that our closed-loop coculture circuit is able to stabilise coculture ratio when both strains are expressing different levels of VioB-sfYFP and VioB-sfCFP. I showed that the coculture ratio can be tuned by modulating the production of the quorum sensing communication signals or by modulating the strength of STAR activation. Finally I showed that the circuit has the potential to provide robustness to inoculation ratio perturbations.

5.2.5 The co-culture under turbidostat conditions

In this last section, I wanted to explore the behaviour of our closed-loop coculture circuit in a continuous culture environment. Continuous cultures have gained popularity over the years, especially to study the behaviour of microbial consortia [208, 209, 42, 73, 65, 87]. Whether the dilutions are carried out manually or automatically using a chemostat, turbidostat or microfluidic chamber, continuous culture provide a means to study the genetic stability of

synthetic microbial consortia over time. It can also help understand the robustness of the system to external and internal perturbations, such as pH or temperature, or how it responds to the accumulation of specific metabolites over time. Here I would like to know if our circuit can maintain population composition over extended periods of time in a continuous culture.

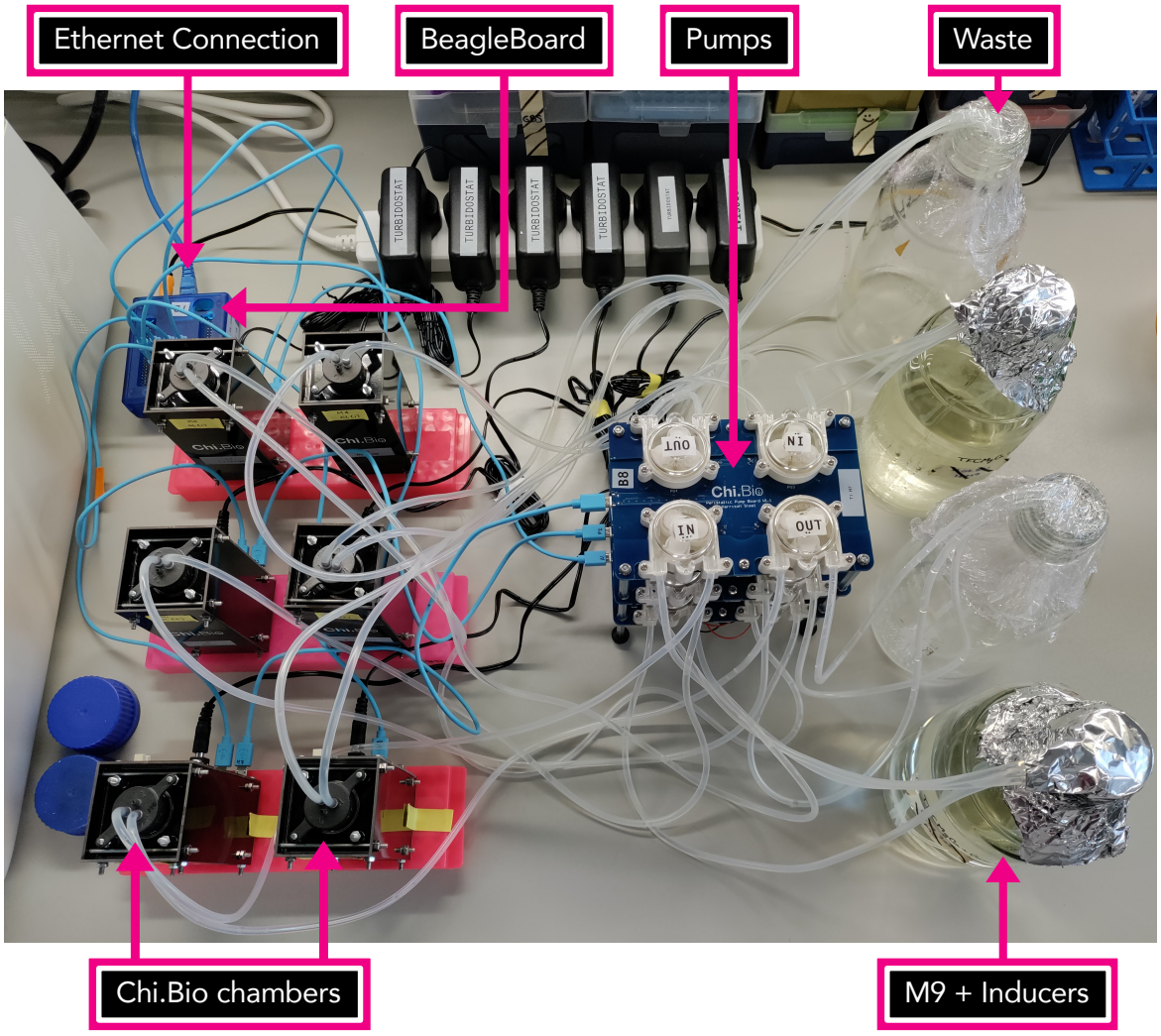


Figure 73: Chi.bio turbidostat setup. Experimental setup of the Chi.bio to run the coculture continuously. The coculture are set up in the Chi.bio chambers. Peristaltic pump deliver fresh media and pump waste out when the OD of the cultures reach a defined OD threshold. The pumps and Chi.bio chambers are controlled by a BeagleBoard microcomputer connected to the University network by an Ethernet cable.

To explore the behaviour of our circuit, we set up the Chi.bio turbidostat platform from

Steel et al. in the lab [177]. The platform is composed of a BeagleBoard microcomputer that controls the Chi.bio chambers and the pump board the deliver fresh media to the chambers and retrieve culture overflow from the chamber into waster containers (Figure 73). The BeagleBoard is connected to the university network by an Ethernet connection such that any computer on campus can control the Chi.bio platform.

I inoculated the Chi.bio chambers with the same open-loop and closed-loop cocultures described in Figure 69. In this system, both the CFP and YFP strains control VioB-CFP and VioB-YFP expression with the araBAD STAR-based comparator (Figure 74.A). In Figure 74.B, I show that the population ratio of the open-loop circuit diverges from the initial 1:1 ratio less quickly than the closed-loop. Repression of VioB-YFP in the YFP strain is very weak (Figure 74.C). This suggests that the production of quorum sensing molecule, especially pC-HSL is not high enough to reduce the expression of the burdensome protein in a continuous coculture. So the batch coculture circuit cannot be directly used in a continuous coculture conetxt and requires further tuning to adapt to the rate of quorum sensing dilution.

Interestingly, I observed that the growth rate of the open-loop cocultures increased by more than 5-fold between 15 hours and 20 hours of continuous growth. I believe that this may be caused by the appearance of deleterious mutations caused by the burden of VioB expression. However, this hypothesis needs to be verified through sequencing of the open-loop coculture strain. Before this increase in growth rate at ∼15 hours, the open-loop coculture was growing slowly as indicated by the slow period of the triangular wave OD signal. Since the turbidostat aims to keep OD at a constant value, we can look at the time taken to complete a dilution period, that is the time taken to reach the maximum OD threshold again after a dilution event. In the very beginning of the experiment, the growth rate of the open-loop coculture slows down as L-arabinose was added at 0 hours, and the strains start producing VioB-CFP and VioB-YFP. The period of the triangular waves for the open-loop is longer than that of the closed-loop system. The closed-loop system also maintained a relatively stable growth rate (0.25 h^{-1}) over the course of the 24 hours of the experiment. So, despite not being able to stabilise the coculture composition, the closed-loop coculture grew better than the open-loop. If the closed-loop coculture strains were growing faster, due

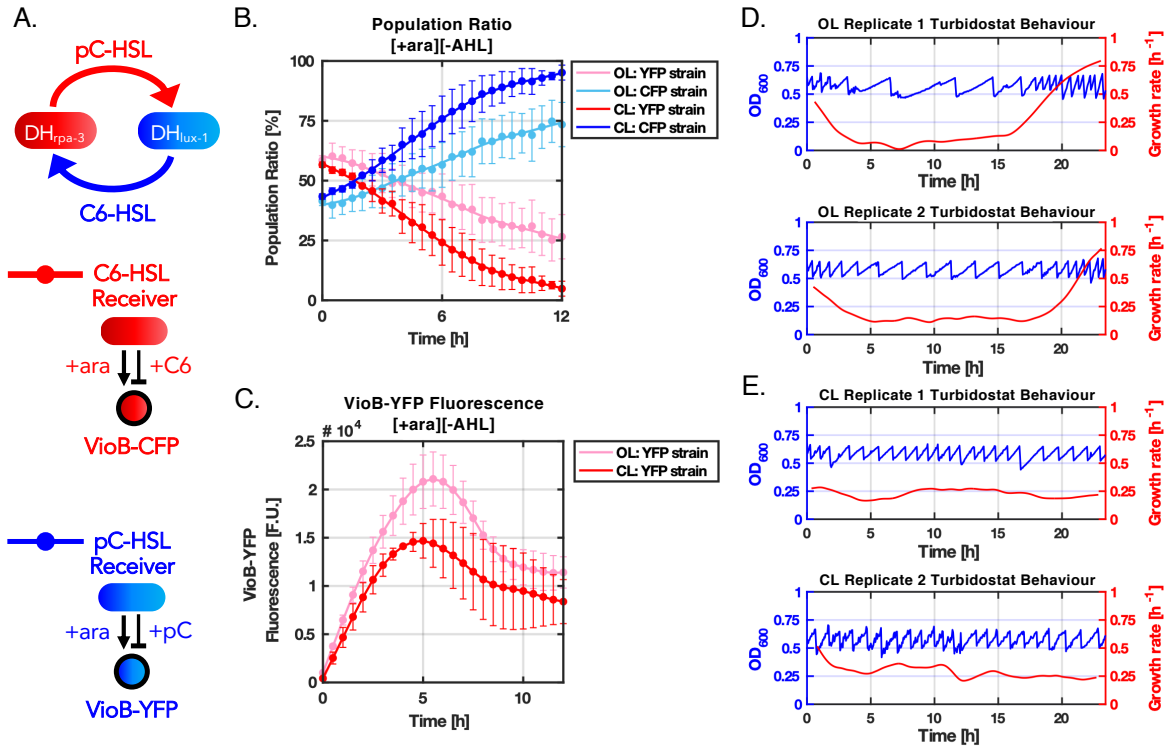


Figure 74: Coculture behaviour in continuous culture. (A) In the closed-loop (CL) coculture, the YFP strain, DH$_{rpa-3}$, synthesises pC-HSL. It controls VioB-sfYFP expression by comparing L-arabinose and C6-HSL signals strength. The CFP strain, DH$_{lux-1}$, synthesises C6-HSL. It controls VioB-sfCFP expression by comparing L-arabinose and pC-HSL signals strength. In the open-loop (OL) coculture the YFP and CFP strains do not produce quorum sensing signals. (B) Population ratio when the closed-loop and open-loop cocultures are induced with 0.2% L-arabinose and 0M of both C6-HSL and pC-HSL. (C) VioB-YFP fluorescence of the YFP strain from the closed-loop and open-loop cocultures. (D) OD_{600} and growth rate of two replicates of the closed-loop and open-loop cocultures. The third biological replicate is shown in Supplementary Figure (92). Experiments were done in DH10B. Cultures were grown in Chi.bio chambers [177]. Fluorescence and population ratio were measured through flow-cytometry. Data represent the mean values of n = 3 biological replicates ± s.d.

to light down-regulation of VioB-CFP and VioB-YFP, this may explain why the CFP strain was able to overtake the YFP population faster in the closed-loop than in the slow dividing open-loop (Figure 74.B). So it suggests that in the closed-loop, the composition controller was strong enough improve the growth rate of the coculture, but not strong enough to correct the imbalance between both strains due to VioB expression. This is an optimistic sign that further increasing the strength of C6-HSL and pC-HSL production may be able to stabilise coculture composition in continuous cultures.

5.3 Conclusions

In this section, I have connected all the modules developed in the previous results chapters to build a self-stabilising coculture. I demonstrated that our two consortium members are able to produce detectable levels of both C6-HSL and pC-HSL. These signals are sensed and activate the expression of anti-STAR that rescues cell growth by turning down expression of either VioB-YFP or VioB-CFP. I used two strains expressing VioB-YFP and VioB-CFP to build an unstable open-loop coculture that can only be rescued in the presence of detectable quorum sensing molecules. It is the first time that quorum sensing is used as an input to control growth rate via the modulation of protein expression in a two-member bacterial consortia.

Next I showed that the closed-loop coculture circuit successfully stabilised coculture composition in batch culture. Coculture composition could be tuned using different properties of the circuit. First, it was tuned by playing with the strength of the quorum sensing production. Increasing quorum sensing production, brought the coculture composition closer to a 1:1 ratio. Secondly, increasing the strength of STAR activation contributed to increase the strength of the reference signal of the comparator. This means that higher quorum sensing input strength was required to achieve the same level of down-regulation on the gene of interest than when the reference signal is lower. Those two knobs have the potential to tune the microbial consortium composition within the limit of growth rate modulation achievable in both strains. I showed that for the first time RNA logic could be used at the multi-cellular level to control coculture composition.

Finally, I showed that further optimisation is needed to stabilise population ratios in a continuous growth environment. I characterised our closed-loop circuit in the Chi.bio turbidostat platform and showed that though the strength of quorum sensing production was not high enough to stabilise the population ratio, it was enough to induce a small reduction of VioB-YFP per cell in the YFP strain. This caused an overall increase in growth rate of the closed-loop coculture compared to the open-loop coculture. I hope that increasing expression of the quorum sensing signals will further improve the growth rate of the coculture strains to enter a regime in which they can self-regulate the coculture composition based on their

respective densities.

Chapter 6

Discussion

Contents

6.1 Summary 145

6.2 A tool-set for building burden-driven cocultures 146

6.2.1 A new platform to study the benefit of division of labor 146

6.2.2 Optimisation of the coculture platform 148

6.2.3 Further applications of the coculture platform 155

6.3 Conclusions 161

6.1 Summary

In this thesis, I have used a set of synthetic biology tools to build a communication module, a comparator module and a growth regulation module that can be used for stabilising coculture composition in a two-*E. coli* strain consortium. I uncovered how to tune the ON/OFF properties of a RNA-based sequestration system *in vivo* using toehold domains. I refined this mechanism into a module that could detect the strength of a quorum sensing signal and compare it to a reference signal to modulate the growth rate of the strains composing a bacterial coculture, thus stabilising the coculture composition around a defined ratio. I then explored the properties of the circuit that allowed us to tune the coculture ratio in batch cultures. In this chapter, I will discuss this new circuit for coculture engineering and in particular how it compares to previous circuits, its limitations, and further applications for the production of high-value compounds. I also discuss the concept of using RNA species *in vivo* to build regulatory cascades while minimising impact on host fitness. Furthermore, I will

discuss what I have learned from designing these RNA-based circuits, and our expectations of this technology for the future of synthetic biology.

6.2 A tool-set for building burden-driven cocultures

6.2.1 A new platform to study the benefit of division of labor

Since their discoveries in the early 1980s, quorum sensing molecules have been providing a tool to sense population densities [92, 91, 93]. This property attracted a lot of attention for the bottom-up construction of microbial consortia since the early 2000s [**?**, 63]. From these landmark studies, Balagaddé et al. developed a predator-prey two-strain consortium in which coexistence between two strains was sustained by the exchange of quorum sensing molecules that would either kill or rescue the strains based on their population densities. Since then, circuits harnessing the properties of quorum sensing have focused on multi-cellular strain behaviour and exploring the different relationships that can lead to the stable existence of strains grown together in a coculture. However, for applications in metabolic engineering, there is still a lack of tools to control coculture behaviour through time.

Coculture behaviour is usually adjusted by changing the initial inoculation ratio of the strain and monitoring the yield of the final product and intermediate metabolites over time. Syntrophy is currently the most widely used tool to construct synthetic consortia made up of different bacterial or yeast species [209, 57, 58]. Though syntrophy can sustain the coexistence of different microbial species for long periods of time, they do not provide a way to dynamically adjust the population composition of the consortium.

There have been several attempts in controlling coculture composition over time and through the addition of external inducers [60, 119, 210]. However all these studies highlighted that the burden caused by the genetic circuit tasked with controlling coculture composition largely hindered the performance and benefit of implementing division of labour. Indeed, dividing large metabolic pathways should have the benefit of decreasing the total load of heterologous expression on the host. However, if the cost of the genetic circuit sustaining a stable coculture is too high, the different strains could end up with similar or more load than they would have experienced if they were tasked with expressing the entire metabolic pathway in a monoculture, thus taking away the benefit of implementing division of labour.

Though previous computational works have highlighted the benefits and trade-offs of implementing division of labour strategies and have particularly focused on the burden cost of genetic circuitry, no tool has been yet developed to assess this cost *in vivo* [74, 211]. As a result, it is unclear what the current cost of the previously developed circuits for population composition control is and how such circuits compare to each other and impact the coculture design landscape. Also, if the circuits had been implemented in different strains, their burden effects would not have been comparable. This is currently limiting our ability to build robust and predictable cocultures with embedded control of population composition. By extension, it is preventing further investigations of the importance of temporal, spatial and composition control of microbial consortia for different applications such as producing high value compounds, energy generation or wastewater treatment [53].

In this work, I set out to assess *in vivo* the cost of putting in place genetic circuits set to control coculture composition. By using the DH10B-GFP capacity monitor strain developed by Ceroni et al., I put in place a method to assess the consumption of free cellular resources by the different modules of the genetic circuit controlling coculture composition [8]. Though numerous quorum sensing modules and growth regulation mechanisms have been developed before, I now propose a way to evaluate the impact on their host to estimate the cost of the circuit on the coculture design landscape. As a result, I can evaluate its potential benefit in the development of division of labour solutions based on the specific metabolic pathways that need to be expressed by the microbial coculture.

To mitigate burden from our genetic circuit, I decided to rely on the use of regulatory RNAs as much as possible, making the assumption that sequestration of cellular resources for heterologous transcription is less burdensome for the cell than for heterologous translational processes [8]. I developed an RNA-based comparator using Small Transcriptional Activating RNA (STAR) that can compare the strength of two different input signals [130]. Through studying the transcriptional profile of quorum sensing signals using the dBroccoli aptamer and using toehold domains, I provided a way to tune sensitivity and ON/OFF properties of the comparator. This allowed us to create comparators with comparable input-output properties such that both *E. coli* composing the coculture would carry input-output compatible genetic circuits to tune coculture composition.

I harnessed the burden caused by heterologous expression to control coculture composition. As a result, I was able to stabilise coculture ratio in a consortium composed of two *E. coli* strains with a difference of up to 40% in their maximum growth rate. The ratio at which the coculture would stabilise was defined by the strength of the quorum sensing signal inputs or by the downstream activation strength of the STAR-based comparator. Though the coculture circuit was tested in batch culture, I envision its expansion to continuous culture modes. Continuous cultures are not yet commonly used in biotechnology processes [212, 213, 214]. But building a controller that functions in different culturing conditions may improve its adoption by a wider number of potential users.

Our coculture platform is modular and can be adapted to different communication and growth regulation modules. It can (i) process different quorum sensing inputs, (ii) control growth rate through different growth regulation mechanisms, (iii) be tuned to adjust coculture composition ratio

6.2.2 Optimisation of the coculture platform

6.2.2.1 Faster screening of the STAR-based comparator

To design the STAR-based comparator, I largely relied on a rational design approach to tune its ON/OFF properties. I could have also relied on a selection pipeline that would have allowed us to screen for a large set of toehold sequences to quickly find the comparator with the best dynamic range. I describe this pipeline in Figure 75. Predicting RNA behaviour *in vivo* is a time consuming task and relying on efficient design and selection pipelines would likely reduce the time-frame for the design of efficient and tailored functional RNAs.

The pipeline relies on an iterative cycle of design and selection of the best performing STAR-based comparator. A minimal STAR-based comparator can be built by using antisense transcription as shown in Figure 75 [202]. As STAR and anti-STAR are complementary to each other, they could be causing recombination or mutational events which would disrupt the stability of the coculture composition control circuit over time. However, in the minimal STAR-based comparator, STAR and anti-STAR are expressed from the same DNA sequence

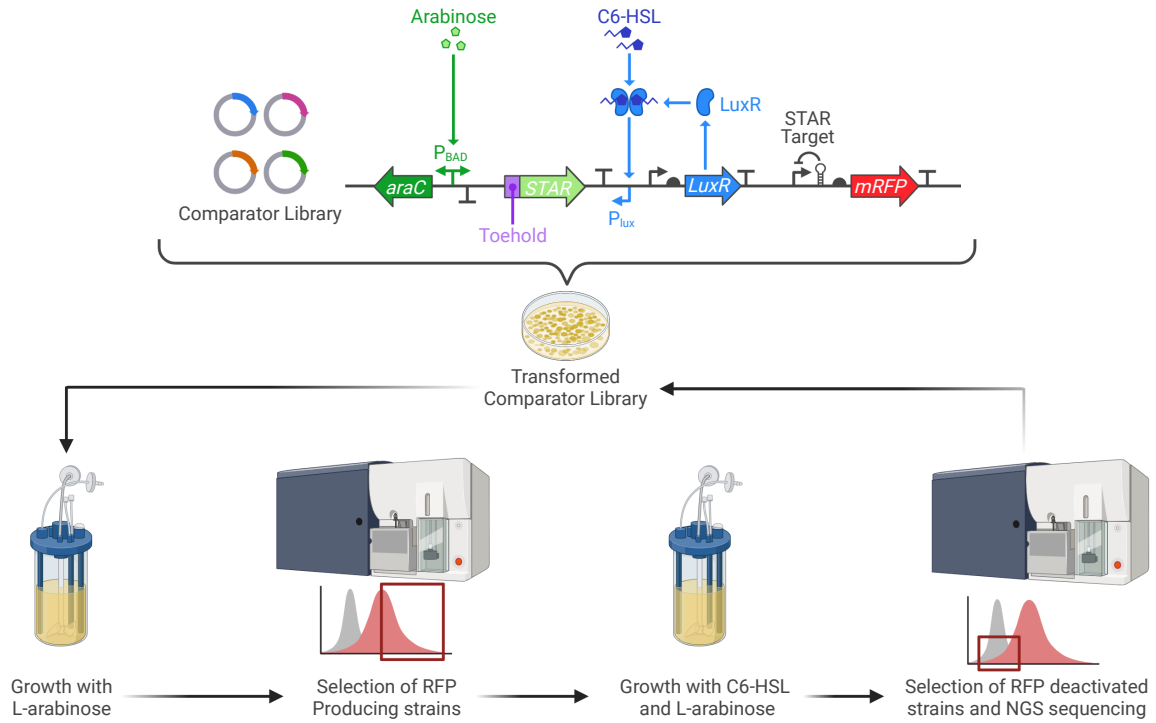


Figure 75: *In vitro* evolution of RNA for *in vivo* regulation and selection pipeline to design a RNA-based comparator with optimal ON/OFF properties. The STAR-based comparator could also be created through the design of random library of comparator. STAR and anti-STAR expression would be driven by two inducible systems. First the library would be grown in media containing L-arabinose driving STAR expression. Selection of the highest mRFP producing strains would be selected via FACS. The highest producers would then be cultured in presence of both L-arabinose and C6-HSL. Selection of the lowest mRFP producing strains, exhibiting the best fold deactivation, via FACS and NGS sequencing would get the comparator design with the best ON and OFF state. Based on the NGS results, multiple rounds of library designs could be tested until a comparator with the best dynamic range is obtained.

in either the sense or anti-sense strand, thus proofing the system against potential mutations due to the STAR/anti-STAR inverted motif [215]. In Chapter 2, I saw that toeholds could not only tune the input-output properties of the STAR-based comparator, but that they could also reduce the burden caused by the expression of STAR and anti-STAR alone. So to build the comparator library, the STAR sequence is designed to be followed by a randomised toehold library. The transformed library is then grown in the presence of L-arabinose to activate the production of STAR, thus activating the downstream expression of the gene of interest, here mRFP. Using Fluorescence-Activated Cell Sorting (FACS), the cells induced with L-arabinose are sorted into bins to select the ones with the best fold activation. The

selected strains are then grown in the presence of both L-arabinose and C6-HSL such that the STAR sequence would be maximally transcribed in both the sense and anti-sense directions. Again using FACS, cells with the lowest fluorescence are now selected in order to select the comparator designs with best OFF states. Selected strains are sequenced through Next-Generation Sequencing (NGS). Analysis of the sequencing data can reveal patterns to design a new tailored library of STAR sequences, or the design with the best ON/OFF property can be selected as the final minimal STAR-based comparator design.

I envision that in the future, this pipeline can be used to further optimise the STAR-based comparator design from Chapter 2. Particularly, this could allow to identify a design in which the expression of STAR and anti-STAR is less resource burdensome to the cell, thus contributing to decreasing their impact on cellular growth rate.

After experimentally validating the pipeline, I also imagine that it could be used for accelerating the design of comparators tailored to new input signals, not only limited to detecting L-arabinose or C6-HSL. Also, if the current ON/OFF properties of the module do not meet the criteria for the design of a new coculture implementation, the module can quickly be optimised for the specific needs of the user.

6.2.2.2 Extending the coculture platform to strains with minimal metabolic burden

In our current coculture composition controller implementation, I demonstrated that I could stabilise the coculture composition by modulating the expression of the burdensome gene causing a fluctuation in growth rate. This mechanism compensates for the difference in growth rate between the two strains. However if the cells do not experience much burden and the cost of the controller exceeds the cost of expressing the heterologous genes of interest, the composition control circuit will fail to successfully stabilise coculture ratio as there will not be much burden to modulate the strains' growth rates. In such a system, our coculture platform will need to be equipped with a different growth regulation module. This module could be based on the expression of a toxin to downregulate growth rate [216, 87] or based of the amino acid knockdown mechanism developed in Chapter 3 [184].

As I obtained encouraging results from the N1 sRNA growth regulation module from Chapter 3, I imagined a minimal coculture composition control circuit that could be applied to a wide range of bacterial strains. Indeed, in their study, Kawano et al. showed that sRNA had the potential to inhibit growth in both *E. coli* and *Salmonella enterica*, so using sRNA has the potential to be applied to a wide range of genetic backgrounds [167].

This new circuit would also allow us to tackle another limitation of our coculture. I saw in Chapter 3 that I had to select the LLL and LRR quorum sensing systems as they were the only two systems available with comparable maximum output, dynamic range and operational range. Other quorum sensing systems and combinations of the different promoter, transcription factor and inducer molecule did not have similar input-output properties. So they would have required some level of tuning before being usable in the circuit. However, using the LLL and LRR quorum sensing that are not completely orthogonal, but only signal orthogonal, meant that I had to use the same *lux* promoter to compare the densities of both strains. To accommodate for this, I used a reference signal as a second input signal instead of using two different quorum sensing inputs, each one sensing the population density of one of the strains in the coculture. The limitation of this architecture lies in the fact that the input signal driving STAR expression, and subsequently expression of the gene of interest is not driven only by population density but also by either a constitutive promoter or an inducible promoter. When using a constitutive promoter, expression of the gene of interest would always be turned ON. This may impair the ability of the strain to grow in a monoculture before its inoculation in a coculture. If both strains are under a high level of burden, they may never reach a high enough cell density to rescue each other's growth. Thus, the use of a constitutive promoter in this circuit topology may not be the best suited for metabolic engineering applications that impose high metabolic burden on the hosts. Inducible promoters are more suited to this particular circuit topology as production of the gene of interest can be activated once the cells are grown in a coculture and in the best metabolic state suited to the production of the compound of interest. For small-scale experiments, using inducible promoters does not constitute a severe limitation to the system. However, for industrial scales externally adding inducers can be costly, depending on the nature of the chemical inducer. For example, 10 mg of C6-HSL costs £54 while 500g of sodium salicylate costs £54. If maximally inducing the circuit following

the maximum induction concentrations provided by Meyer et al., this would mean that for the same price you could prepare 4.7 L of C6-HSL-maximally-induced media and 31230 L of sodium salicylate-maximally-induced media [182]. Electrogenetics [217, 218, 219] and optogenetics could constitute a viable alternative to the use of chemical inducers. For example, the CCaS/CCaR optogenetic system, or the light-inducible AraC could be used to drive expression of VioB [220, 221, 222]. Though scaling up photo-bioreactors has been difficult due to culture turbidity, new types of bioreactors have been developed to achieve different culture optical densities and to produce different compounds [223, 224, 225, 226]. Light- and electricity-based inducible systems thus present an interesting solution to scaling up our coculture circuit to large-scale bioreactors without relying on the external addition of chemical inducers [227].

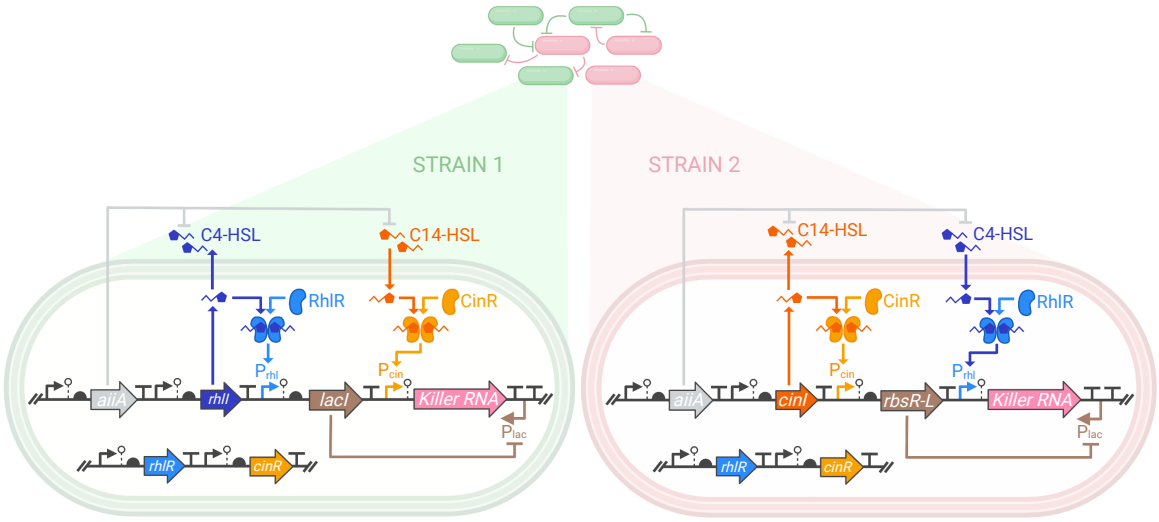


Figure 76: A minimal circuit for stabilising coculture composition. Each strain produces a quorum sensing molecule that is completely orthogonal to the other (i.e. C4-HSL and C14-HSL). Each strain has the ability to sense their own quorum sensing signal, as well as the one produced by the other strain. The quorum sensing signal received from the other strain activates the expression of a growth-impairing N1 sRNA from Chapter 4. N1 sRNA transcription is inhibited by anti-sense transcription from the *lac* promoter. The self-produced quorum sensing signal activates the expression of a repressor (i.e. LacI or RbsR-L) that will inhibit anti-sense transcription from the *lac* promoter. As a result, a balance given by the difference in cell density between the two strains will tune the N1 sRNA transcription rate to autonomously adjust the ratio of the strains in the coculture. The *AiiA* gene codes for a quorum-quenching lactonase that will actively degrade both C4-HSL and C14-HSL to prevent the system from being saturated with quorum sensing molecules [228, 229].

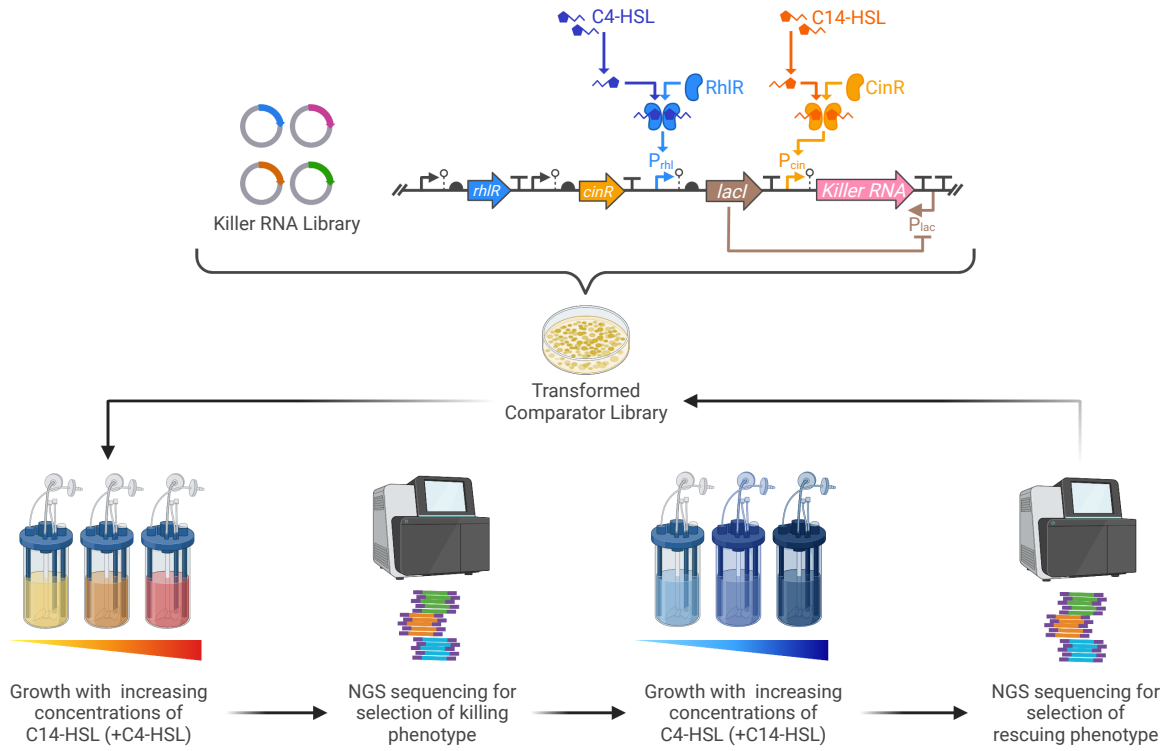


Figure 77: *In vitro* evolution of N1 sRNA for growth regulation. A library of N1 sRNA is controlled by the *cin* promoter induced by the C14-HSL:CinR dimerised complex. Growth rate is rescued by anti-sense transcription of N1 sRNA from the *lac* promoter. Upon induction with C4-HSL, C4-HSL and RhlR transcription factor form a complex to activate the *rhl* promoter driving expression of *lacI*. As LacI concentration increases in the cell, *lac* promoter activity is inhibited, thus lowering the level of anti-sense transcription of the N1 sRNA and, as a result, weakening growth rate rescue. The library is transformed/integrated into *E. coli*. Colonies are picked and grown in chemostat environments supplied with at least three different C14-HSL concentrations and with maximum induction of C4-HSL. NGS sequencing will allow to determine which N1 sRNA sequences decreased growth rate of the cell with increasing C14-HSL concentration. The N1 sRNA sequences that negatively regulated cell growth are then grown in chemostat environments supplied with at least three C4-HSL concentrations and with maximum C14-HSL induction. NGS sequencing will now allow to determine which N1 sRNA sequences allow for efficient anti-sense transcription to rescue cell growth. The N1 sRNA sequences of the strains that displayed growth rescue by C4-HSL addition are selected and used either directly in the final circuit or to design a new library of N1 sRNAs.

Instead of further increasing the burden caused by our circuit by adding new genetic components to build a light-activated STAR-based comparator, I placed our N1 sRNA from Chapter 4 under the control of two orthogonal quorum sensing systems in both the sense and anti-sense direction (Figure 76). In this configuration, the N1 sRNA is not expressed until both strains have reached a high enough cell density. If one is cultured without the other, the growth down-regulation module will not be activated which would allow for the

easy cultivation of the strains before they are mixed in a coculture. At low strain density of the coculture, anti-sense transcription of the N1 sRNA is dominant in both strains. As population densities increase, level of the N1 sRNA in the cell is driven by the difference in population density between the two strains. The strength of the killing and rescue response through the sense or anti-sense transcription of the N1 sRNA respectively, can be modulated by tuning the strength of the quorum sensing production and/or by tuning the levels of quorum regulator protein expression. As I showed in Chapter 4 that small levels of N1 sRNA were enough to effectively down-regulate growth rate, I envision the possibility to integrate the circuit into the genome to decrease the leakiness and improve the titrability of the N1 sRNA. Moving from a plasmid-based controller to a genome-based controller would also contribute to further decreasing the overall burden caused by the expression of the controller circuit, thus improving the genetic stability of the strain [38, 39, 36]. This circuit would be fully autonomous and would not require external addition of chemical inducers. Creating different strains producing a range C4-HSL and C14-HSL concentrations would allow users to build cocultures with different pre-defined stabilisation ratios. I note that the ratio could still be externally modulated during coculture growth through the external addition of IPTG [116]. The end product would then be a library of strains which would be ready to be transformed with the metabolic pathways of interest.

To improve the growth rescue from anti-sense transcription of the N1 sRNA, I propose a pipeline to select a N1 sRNA cassette with the best killing and rescue properties. Based on the current N1 sRNA, I can create a library of randomised sRNA sequences (Figure 77). The library is transformed in *E. coli* and the transformants are grown in chemostats supplied with maximum concentration of C4-HSL to inhibit fully anti-sense transcription, and with different concentrations of C14-HSL to down-regulate cell growth through increasing expression of the sRNA library. Cells are then sequenced through NGS sequencing to select which sRNA sequences down-regulated cell growth most upon increasing concentrations of C14-HSL: abundance of the sequences would reflect the property of the sRNA designs to reduce growth of their host over time. The sRNA sequences that successfully down-regulated growth rate most with increasing C14-HSL over time are selected and then grown in chemostats with maximum concentration of C14-HSL to activate maximum sense transcription of the sRNAs,

and with a range of C4-HSL to tune the growth rescuing response through the anti-sense transcription of the sRNA. Again, analysing the NGS data and specifically looking at the abundance of the difference sRNA sequences over time and for the different C4-HSL concentrations, I can select the sRNA sequences that promote more growth rate rescue with decreasing concentrations of C4-HSL.

I expect that this minimised circuit will further contribute to building stable coculture for strains that may not be subjected to a lot of burden from expression of the metabolic pathways of interest. The goal is to provide a circuit that is as minimal as possible to reduce the burden caused the coculture composition controller, to enhance the stability and scalability of the coculture, and to really start exploring the coculture design space for the sustainable bio-production of high-value compounds.

6.2.3 Further applications of the coculture platform

6.2.3.1 Production of high-value products

While in this thesis I have focused on the development of a platform to stabilise coculture composition, I envision its use to study the benefits of division of labour for the production of high-value compounds. As I discussed in the Introduction Chapter, currently coculture tuning relies on testing a range of inoculation ratio to determine which one leads to the highest final yield of the product of interest. Our platform would allow to study the benefits of stabilising coculture composition around a set target ratio. This way, synthetic biologists have a new tuning knob to not only modulate intracellular expression of the divided pathway, but also modulate the proportion of the divided parts of the pathway at the multi-cellular level.

In their work, Lin et al. produced muconic acid, a precursor for making PET, in a single *E. coli* strain [24]. Muconic acid was produced through the expression of three genetic modules. The APTA module improved intracellular levels of the muconic acid precursor: chorismate [230]. The EP module converted chorismate to isochorismate and then to salicylic acid through the expression of isochorismate synthase (ICS) and an isochorismate

pyruvate lyase (IPL) enzymes. The NC module then expressed salicylate 1-monoxygenase (SMO) to convert salicylic acid to catechol, and catechol 1,2-dioxygenase (CDO) to convert catechol to muconic acid. Lin et al. highlighted that they optimised muconic acid yields by testing the expression of the different modules from low-, medium- and high-copy plasmids [24]. They were surprised that expressing the NC module from medium- and high-copy plasmids led to lower yields than when it was expressed from a low-copy plasmid. They hypothesised that high expression of the NC module may interfere with the other modules, impacting cell viability and decreaseing the overall yield of muconic acid (Supplementary Figure 96). The EP and APTA modules produce salicylic acid which can diffuse out of the cell [183], so it should be possible to divide the APTA-EP and NC modules into two different strains to see if division of labour could further improve the yield of muconic acid (Figure 78).

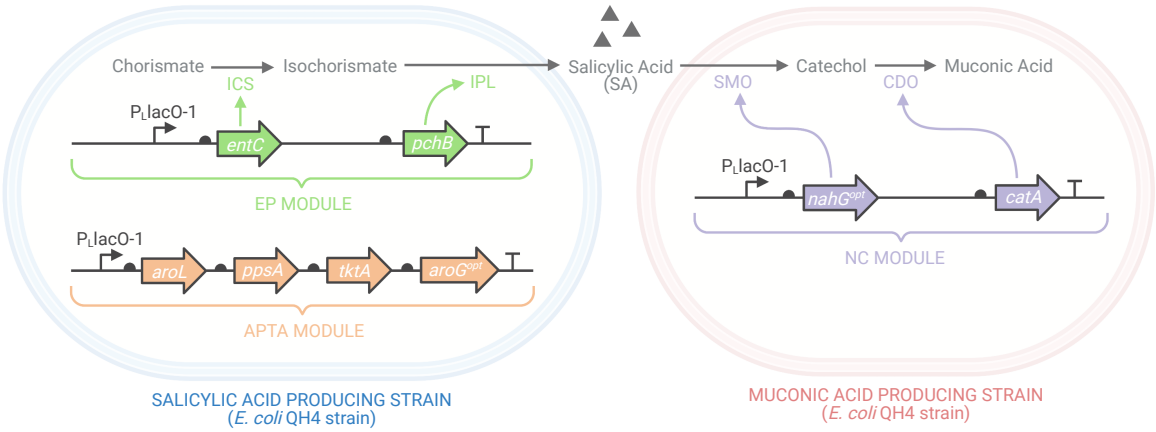


Figure 78: Coculture for the production of muconic acid. Proposed split of the muconic acid metabolic pathway implemented in a single *E. coli* by Lin et al. [24]. The first strain would produce salicylic acid from chorismate by expressing an isochorismate synthase (ICS) and an isochorismate pyruvate lyase (IPL). Salicylic acid can diffuse out of the cell membrane to be used as a substrate in the muconic acid producing strain [182, 183]. The producing strain catalyses the production of catechol from salicylic acid by expressing salicylate 1-monoxygenase (SMO). Catechol is then converted into muconic acid by catechol 1,2-dioxygenase (CDO). Equipping both strains with our coculture composition circuit would allow to study the impact of coculture ratio on muconic acid yield by division of labour.

While searching for examples of metabolic pathways to express in our bacterial coculture, I realised that many compounds produced using cocultures until now were phenylpropanoids [231, 232]. Production of those phenylpropanoids requires a secure pool of both Mal-CoA and p-coumaric acid. As I saw in Chapter 3, production of p-coumaric acid is needed for

producing pC-HSL, one of the quorum sensing molecule used to enable communication between the two strains. Competition for p-coumaric acid could impact the strength of pC-HSL production, hence tuning the ratio of the coculture in an undesirable way. Thus, to avoid direct interference when using p-coumaric acid as a precursor, production of flavonoids should be engineered in the C6-HSL producing strain as C6-HSL is derived from fatty acids instead.

Interesting compounds that could be produced using our coculture platform include flavonoids such as anthocyanidin or naringenin, which have already been produced using bacterial cocultures and have a wide range applications ranging from natural food colorant, hair dyes, anti-cancer drugs or treatment for Alzheimer's disease [233, 234, 118, 235]. Polyphenols such as caffeic acid and ferulic acid are also potential candidates for division of labour in *E. coli*. They are known for their antioxidant, anti-inflammatory, anti-cancer, antiviral, anti-diabetic, and anti-depressive properties in the pharmaceutical industry, but they can also form liquid crystals for applications in the electronic industry [236, 237]. Resveratrol reduces the risk of coronary heart disease and was also shown to have improved yields when produced using cocultures [238]. As another example, I can also consider the production of 4-hydroxybenzoic acid (4HB) which is a widely used compound as it forms the basis for the production of parabens used in toiletries, eye drops and the cosmetic industry [239]. In all these examples, production yield of the compound of interest was improved by using division of labour. Being able to tune coculture composition may provide a new way to tune the properties of the coculture to further improve product yields.

6.2.3.2 Towards more complex feedback mechanisms

So far efforts have been focusing on building relationships between strains, whether it be competitive or cooperative, to ensure the survival of all strains and to stabilise the ratio of the cocultured strains. This is only a first step towards building more complex microbial consortia as three levels of regulations are available when building microbial consortia: time, space and coculture composition [53].

Work by Briat et al. showed that molecular sequestration motifs can be used to build

antithetic integral feedback circuits that are robust to perturbations [240, 184, 241, 242]. Since our comparator mechanism relies on the sequestration of two RNA species and the half-life of mRNA in *E. coli* is around 3-30 minutes, it suffers from a high degradation rate which would not make it a good candidate to build such an integral feedback [243, 244]. Indeed the sequestrating species need to have a slow turnover rate to sustain the integral property of the feedback motif. RNA-based sequestration mechanisms may however be able to meet the criteria for building antithetic feedback networks in mammalian cells, where the mRNA half-life is around 600 minutes, at least 20 times higher than in *E. coli* [245]. Exploring the possibility to build an integral feedback motif in a coculture circuit is an interesting perspective to ensure that the ratio between the two strains is robust to external perturbations.

I can imagine building upon coculture stabilisation circuits such as the one built in this thesis, to add more feedback layers so as to further expand the optimisation strategies that I can use to balance production with host cell growth. Microbial consortia can improve bioproduction compared to monocultures by reducing the metabolic and expression burden via splitting of the pathway across cells and using cellular membrane separation to reduce byproduct formation and prevent enzymes from reacting with non-desirable substrates [246]. These strategies can be coupled with feedback strategies already developed in monocultures to further improve product yields in each strain of the consortia. Previously developed control methods in monocultures include temporal control of gene expression [113, 247], metabolic stress mitigation circuits [25, 34] or burden mitigation circuits [156, 18]. Such methods applied to the different strains in the consortia would allow users to further optimise the production of the intermediate and final products. To push this idea further, I imagine that the feedback mechanisms should not be limited to self-regulation but that all species in the coculture could act in unison to build multicellular-level feedback. For example, a multicellular feedback mechanism could up- or down-regulate intermediate product production or it could sense the level of product from each strain and adjust the population ratio between the two strains to optimise the ratio between intermediate-producing strain and final product-producing strain. If an intermediate product was toxic to another strain, either production of the compound or fraction of its producer cells could be reduced when

stress is detected in the other strain(s). Multicellular feedback could be used to further expand the level of control achieved by cocultures to build optimised division-of-labour cocultures that are genetically stable and robust to perturbations.

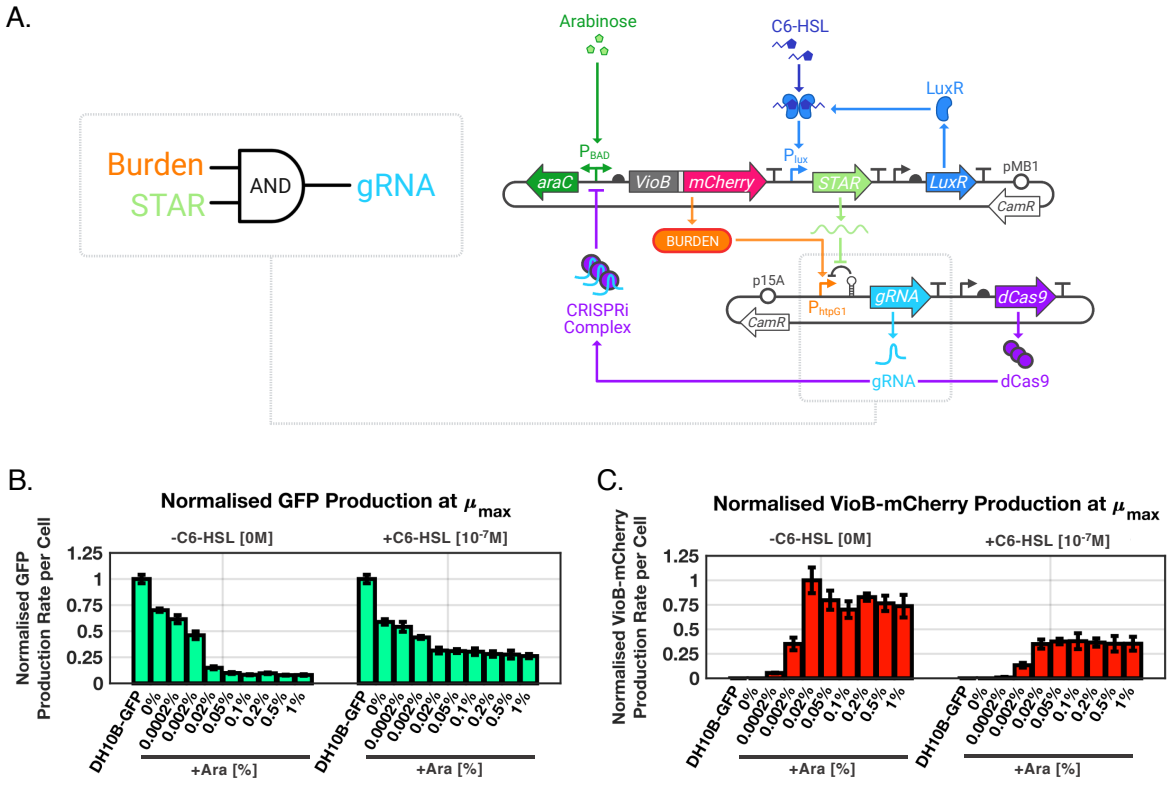


Figure 79: Design of an *in vivo* burden and STAR AND gate. (A) Schematic and genetic circuit of the burden and STAR AND gate. Induction of VioB-mCherry by L-arabinose increases burden in the cell. Burden activates the burden-responsive *htpG1* promoter which drives expression of a gRNA targeting the araBAD promoter [156]. dCas9 is constitutively expressed at low levels in the cell such that in the presence of gRNA, it forms a CRISPRi complex with the gRNA and inhibits transcription activation of the araBAD promoter. STAR expression is driven by the C6-HSL:LuxR dimerised complex. gRNA can only be produced when both STAR is present and the *htpG1* promoter is activated by burden. STAR can modulate the transcriptional activation of gRNA when *htpG1* promoter is activated. (B) GFP Capacity and (C) VioB-mCherry production rate per cell measured in the DH10B-GFP capacity monitor strain. The strain was transformed with the circuit in (A) and induced with either 0M or 10^{-7}M of C6-HSL and a range of L-arabinose concentrations from 0% to 1%. GFP capacity was compared to the WT DH10B-GFP strain. Experiments were done in DH10B-GFP. OD, GFP and RFP were measured in a timecourse plate-reader assay. Data represent the mean values of n = 3 biological replicates ± s.d.

As an example to demonstrate that the coculture composition controller has the potential to be linked to existing intracellular mechanisms, I decided to explore how it could

be connected to the burden-driven feedback from Ceroni et al. (Figure 79) [156]. The burden-driven feedback is a negative feedback motif designed to mitigate burden caused by heterologous gene expression. It works in the following way: a heterologous fusion protein, VioB-mCherry, is expressed in the presence of L-arabinose, which sequesters cellular resources, causing burden in the cell. In the presence of burden, the burden-responsive *htpG1* promoter activates the production of a gRNA, which binds to a constitutively expressed dCas9 to form a CRISPRi complex that inhibits the *araBAD* promoter, thus downregulating the expression of VioB-mCherry. To show how the two circuits can be connected, I linked quorum-driven STAR expression to the burden-driven feedback circuit I developed by Ceroni et al. (Figure 79.A) [156]. STAR provides a new layer of regulation to modulate the transcription rate of the *htpG1* promoter [172]. The gRNA can only be expressed in the presence of both burden and STAR, effectively creating an AND gate, whose expression can be modulated by the cellular concentration of STAR. Indeed, in the presence of STAR, VioB-mCherry production rate is downregulated and GFP capacity is maintained around 25% of the WT GFP capacity for L-arabinose concentrations higher than 0.02% (Figures 79.B-C). This demonstrates that I can link STAR to an already existing burden-mitigating strategy. So in the coculture, the STAR-based comparator could be used to not only directly regulate heterologous expression or the growth control mechanism, but also to modulate internal feedback motifs based on ratio composition.

I thus showed that our STAR-based circuit has the potential to be linked to existing host-aware feedback strategies. As a result, information collected at the multicellular level, here coculture composition, could have the potential to act on internal feedback loops of the different strains making up the coculture. I hope that further works will explore that possibility to link multicellular level information with intracellular circuits and unlock the full potential of using division of labour for bioproduction, especially across different microbial species [50, 58, 248, 249].

6.3 Conclusions

In Chapter 1, I outlined our proposed circuit to stabilise coculture composition of two *E. coli* strains with significantly different growth rates. Using quorum sensing, burden and RNA-based synthetic biology tools such as STAR, RNA aptamer, sRNA and gRNA, I built three genetic modules that can be connected in a plug-and-play fashion to implement a coculture composition controller. Although the controller has only been demonstrated to work in batch culture so far, and limitations remain with the burden caused by the expression of the controller, I believe that the circuit I have developed in this thesis, constitutes a step forward to tuning coculture properties for the production of high-value products. Being able to stabilise coculture composition and tune the ratio between the strains will allow researchers to further explore the coculture design landscape for efficient engineering of division of labour, bringing us one step closer to further improving the productivity and efficiency of bioproduction processes for metabolic engineering.

In addition to developing the coculture composition controller circuit, I have also achieved a significant milestone on the road to understanding the role and impact of burden in the design of division of labour. So far, by using the capacity monitor strain, I established a novel way to evaluate the impact of the controller circuit expression on the benefits of division of labour *in vivo*, which will be a critical measure for the design of future microbial consortia. As whole-cell computational models continue to develop, I expect to see more work predicting, *in silico*, the impact and benefits of using coculture composition controllers. Combined with *in vivo* quantification methods as the ones used in this work opens research avenues for further exploring how to design multicellular controllers with minimal impact on their host, which is crucial for the effective splitting of metabolic pathway across strains and species.

As cocultures grow in complexity, regulation of the population composition will be used in concert with intracellular and multicellular feedback loops to optimise the division of metabolic pathways across strains while reducing burden and metabolic stress as much as possible. I believe that the modular strategy presented in this work is expandable to be

used in combination with more complex production and stress control strategies. With the accelerating interest over engineering microbiomes and small ecological niches for metabolic engineering, it is likely that via stable cocultures, new control strategies will emerge to improve coculture designs strategies. I am excited to see how cells will continue to work together to shape the future performance and affordability of engineering biology.

Chapter 7

Materials and Methods

Contents

7.1 Materials 164

7.1.1 *E. coli* strains 164

7.1.2 Antibiotics 166

7.1.3 Inducers and dyes 166

7.1.4 Media and Buffers 167

7.1.5 Amino Acids 168

7.2 Molecular Biology Methods 169

7.2.1 Culturing 169

7.2.2 Competent cells preparation and transformation 169

7.3 General DNA Manipulation 172

7.3.1 Around-the-world PCR 172

7.3.2 START/STOP Assembly 173

7.3.3 Gibson Assembly 173

7.4 Genomic integration 173

7.4.1 CRIM integration 173

7.4.2 λ-Red integration 176

7.5 Data collection and analysis 178

7.5.1 Plate-reader timecourse assays 178

7.5.2 Flow cytometry measurements 181

7.5.3 Quorum sensing sender-receiver assay 182

7.5.4 Coculture assay 183

7.5.5 β-Carotene assay 183

7.5.6 Chi.bio turbidostat assay 184
7.6 DNA parts and Plasmids 186
7.6.1 DNA Parts 186
7.6.2 Plasmids 200

7.1 Materials

7.1.1 *E. coli* strains

Invitrogen DH10B competent *E. coli* (F– mcrA Δ(mrr-hsdRMS-mcrBC) ϕ80lacZΔM15 ΔlacX74 recA1 endA1 araD139 Δ(ara,leu)7697 galU galK λ– rpsL(StrR) nupG) was used for cloning purposes. Electrocompetent and chemical competent cells were prepared following the protocols below.

E. coli parental strains used in this study and their genotype and are recorded in the Table 7.1 below:

Table 7.1: *E. coli* strains used in this study

Name	Genotype	Antibiotic	Source/Parent
DH10B	K-12 strain, F– mcrA Δ(mrr-hsdRMS-mcrBC) ϕ80lacZΔM15 ΔlacX74 recA1 endA1 araD139 Δ(ara,leu)7697 galU galK λ– rpsL(StrR) nupG	Streptomycin	Invitrogen
BW25113	K-12 strain, acI+rrnBT14 ΔlacZWJ16 hsdR514 ΔaraBADAH33 ΔrhaBADLD78 rph-1 Δ(araB–D)567 Δ(rhaD–B)568 ΔlacZ4787(::rrnB-3) hsdR514 rph-1	None	Keio Collection
BW25113(*rpsL150*)	*rpsL150*(strR)	Streptomycin	BW25113
PIR2 One Shot	F- Δlac169 rpoS(Am) robA1 creC510 hsdR514 endA recA1 uidA(ΔMluI)::pir	None	Invitrogen
TransforMax EC100D pir+	F- mcrA Δ(mrr-hsdRMS-mcrBC) ϕ80dlacZΔM15 ΔlacX74 recA1 endA1 araD139 Δ(ara, leu)7697 galU galK λ- rpsL nupG pir+(DHRF)	None	Lucigen
JW5807	ΔleuB	None	BW25113
JW2002	ΔhisD	None	BW25113
JW3973	ΔmetA	None	BW25113

Table 7.1: *E. coli* strains used in this study

Name	Genotype	Antibiotic	Source/Parent
JW0003	ΔthrC	None	BW25113
JW3745	ΔilvA	None	BW25113
JW2580	ΔpheA	None	BW25113
JW3582	ΔcysE	None	BW25113
JW2786	ΔargA	None	BW25113
JW1254	ΔtrpC	None	BW25113
JW2535	ΔglyA	None	BW25113
DH10B-GFP	J23100–sfGFP–BBa_1002 at att_λ	KanR	DH10B
DH10B-mScarlet	J23100–mScarlet-I–BBa_1002 at att_λ	KanR	DH10B
BW25113-GFP	J23100–sfGFP–BBa_1002 at att_λ	KanR	BW25113
BW25113-mScarlet	J23100–mScarlet-I–BBa_1002 at att_λ	KanR	BW25113
DH_{lux-1}	J23100–B0030–luxI–L3S2P55 at att_λ (CRIM plasmid pAB553)	KanR	DH10B
DH_{lux-2}	J23106–B0030–luxI–L3S2P55 at att_λ (CRIM plasmid pAB554)	KanR	DH10B
DH_{lux-3}	J23105–B0030–luxI–L3S2P55 at att_λ (CRIM plasmid pAB564)	KanR	DH10B
DH_{lux-4}	J23115–B0030–luxI–L3S2P55 at att_λ (CRIM plasmid pAB566)	KanR	DH10B
DH_{lux-5}	J23100–RBSc33–luxI–L3S2P55 at att_λ (CRIM plasmid pAB386)	KanR	DH10B
DH_{lux-6}	J23100–RBSc33–luxI–L3S2P55 at att_λ (CRIM plasmid pAB384)	KanR	DH10B-GFP
DH_{rpa-1}	J23109–B0030–rpaI–B0030–4CL2nt–B0032–TAL–L3S2P55 at att_λ (CRIM plasmid pAB572)	KanR	DH10B-mScarlet
DH_{rpa-2}	J23109–B0030–rpaI–B0030–4CL2nt–B0030–TAL–L3S2P55 at att_λ (CRIM plasmid pAB496)	KanR	DH10B-mScarlet
DH_{rpa-3}	J23106–B0030–rpaI–B0030–4CL2nt–B0030–TAL-–L3S2P55 at att_λ (CRIM plasmid pAB493)	KanR	DH10B-mScarlet
DH_{rpa-4}	J23105–B0030–rpaI–B0030–4CL2nt–B0030–TAL–L3S2P55 at att_λ (CRIM plasmid pAB494)	KanR	DH10B-mScarlet
DH_{rpa-5}	J23114–B0030–rpaI–B0030–4CL2nt–B0030–TAL–L3S2P55 at att_λ (CRIM plasmid pAB495)	KanR	DH10B-mScarlet
DH_{rpa-6}	J23100–B0030–rpaI–B0030–4CL2nt–B0032–TAL–L3S2P55 at att_λ (CRIM plasmid pAB482)	KanR	DH10B-mScarlet

7.1.2 Antibiotics

Antibiotics were dissolved in the appropriate solvent as described in Table 7.2 to prepare antibiotic stocks. Antibiotic stocks were filter sterilised using 0.22 μm filters. Tetracycline was stored in black Eppendorf tubes to prevent light degradation. All stocks were stored in the -20°C freezer.

Table 7.2: Antibiotics used in this study

Antibiotic	Solvent	Stock Concentration	Working Concentration
Ampicillin	ddH_2O	100 mg/mL	100 μg/mL
Kanamycin	ddH_2O	50 mg/mL	50 μg/mL
Spectinomycin	ddH_2O	60 mg/mL	60 μg/mL
Streptomycin	ddH_2O	100 mg/mL	100 μg/mL
Chloramphenicol	100% EtOH	34 mg/mL	34 μg/mL
Tetracycline	70% EtOH	10 mg/mL	10 μg/mL

7.1.3 Inducers and dyes

Inducers were prepared by dissolving in the appropriate solvent as described in the Table 7.3 below. Inducers were filter sterilised with a 0.22 μm filter and stored in the -20°C freezer.

Table 7.3: Inducers used in this study

Promoter	Inducer	Solvent	Stock concentration
$P_{ara_{BAD}}$	L-arabinose	ddH_2O	20%
$P_{rha_{BAD}}$	L-rhamnose	ddH_2O	20%
P_{lux}	3OC6-HSL	DMSO	100 mM
P_{rpa}	pC-HSL	DMSO	100 mM
P_{LacIq}	IPTG	ddH_2O	1 M
P_{tet}	aTc	50% EtOH	200 μM
P_{van}	Vanillic acid	100% EtOH	100 mM
P_{sal}	Sodium salicylate	ddH_2O	1 M
P_{CymRC}	Cuminic acid	100% EtOH	100 mM
P_{PhlF}	DAPG	DMSO	25 mM

Table 7.4: Dye used in this study

Aptamer	Dye	Solvent	Stock concentration
dBroccoli	DFHBI-1T dye	DMSO	100 mM

7.1.4 Media and Buffers

7.1.4.1 SOB Medium

SOB medium used for the preparation of competent cells was made by mixing a SOB (Mg-) solution and a Magnesium Mix solution to avoid precipitate formation. The SOB (Mg-) solution (20g/L tryptone from casein, 5g/L yeast extract, 0.6g/L NaCl, 0.2g/L KCl) was mixed by vortexing and autoclaved for sterilisation. The Magnesium mix solution (0.5M $MgCl_2$, 0.5M $MgSO_4$) was mixed by vortexing and autoclaved. When SOB is needed for competent cell preparation, mix 1 L of SOB (Mg-) for 20 mL of Magnesium Mix under sterile condition to obtain SOB.

7.1.4.2 SOC Medium

SOC medium used for recovery of transformed *E. coli* cells, is made by mixing 1 L of sterile SOB (recipe in the section above) with 20 mL of 20% filter sterilised glucose solution.

7.1.4.3 M9 Medium

Rich M9 media used in our experiments (Table 7.5) consisted of M9 minimal salts (5X) supplemented with 0.2% casaminoacids (MP Biomedicals), 0.25 mg/mL thiamine hydrochloride, 2 mM $MgSO_4$, 0.1 mM $CaCl_2$, 0.8% fructose, and the appropriate antibiotic(s).

Table 7.5: Protocol to make 400 mL of rich M9 0.8% fructose supplemented with Casaminoacids

Solution	Volume
Autoclaved Distilled Water	278 mL
Autoclaved M9 Minimum Salts (5X)	80 mL
Filter sterilised thiamine hydrochloride (10mg/mL)	10 mL
Filter sterilised fructose (20%)	16 mL
Autoclaved casaminoacids (10%)	8 mL
Autoclaved $MgSO_4$ (0.1M)	8 mL
Autoclaved $CaCl_2$ (0.1M)	400 μL

Poor M9 media used in our experiments (Table 7.6) consisted of M9 minimal salts (5X) supplemented with 0.25 mg/mL thiamine hydrochloride, 2 mM $MgSO_4$, 0.1 mM $CaCl_2$, 0.8% fructose, and the appropriate antibiotic.

Table 7.6: Protocol to make 400 mL of poor M9 0.8% fructose

Solution	Volume
Autoclaved Distilled Water	286 mL
Autoclaved M9 Minimum Salts (5X)	80 mL
Filter sterilised thiamine hydrochloride (10mg/mL)	10 mL
Filter sterilised fructose (20%)	16 mL
Autoclaved $MgSO_4$ (0.1M)	8 mL
Autoclaved $CaCl_2$ (0.1M)	400 μL

M9 Salts (5X) stock solution sterilised by autoclaving and stored at room temperature. Thiamine hydrochloride was filter sterilised and stored at room temperature in a sterile container surrounded by aluminum foil to protect it from the light. Fructose solution was filter sterilised on stored at 4°C. We used fructose as the main carbon source to avoid the strong catabolite repression of the *araBAD* and *rhaBAD* promoters in the presence of glucose. Casaminoacids, magnesium sulfate and calcium chloride were sterilised by autoclaving and stored at room temperature.

7.1.4.4 TSS buffer

To prepare 50 mL of TSS buffer we mixed 5 g of PEG 3350, 1.5 mL of 1 M $MgCl_2$ (or 0.30 g of $MgCl_2$*6H20) and add LB media to up to 47.5 mL. We filter sterilised the buffer with a 0.22 μm filter. We then added 2.5 mL of DMSO (added last to avoid dissolving the cellulose-based membrane. The buffer was stored in the fridge at 4°C.

7.1.4.5 PBS buffer

To prepared 1 L of 10X PBS buffer by dissolving PBS tablets (Sigma) according to the manufacturor's instructions. The buffer was autoclaved and stored at room temperature.

7.1.5 Amino Acids

Stocks of 10 mg/mL of amino acids (Phe, Gly, His, Leu, Cys, Phe, Met, Arg, Ile, Thr) were prepared by dissolving in ddH_2O and were stored in the -80°C freezer. Amino acids were

used to supplement poor M9 medium at the working concentration of 40 μg/mL.

7.2 Molecular Biology Methods

7.2.1 Culturing

For cloning purposes, *E. coli* strains were grown and selected in Lysogeny Broth (LB) medium at 37°C. The LB medium was supplemented with the appropriate antibiotics at the following concentrations when cells where transformed with high copy plasmids: ampicillin 100 μg/mL, kanamycin 50 μg/mL, chloramphenicol 34 μg/mL, spectinomycin 60 μg/mL, tetracycline 10 μg/mL and streptomycin 100 μg/mL. When cells where co-transformed with two plasmids, half the concentration of antibiotics was used: ampicillin 50 μg/mL, kanamycin 25 μg/mL, chloramphenicol 17 μg/mL, spectinomycin 30 μg/mL, tetracycline 5 μg/mL and streptomycin 50 μg/mL.

7.2.2 Competent cells preparation and transformation

7.2.2.1 Preparation of chemical competent cells and transformation

DH10B strains were prepared using the TSS competent cells methods. A single colony was inoculated into 5 mL of LB in a 15 mL culture tube and grown to saturation over night in a shaking incubator at 37°C. In the morning, 1 mL of saturated culture was used to inoculate 100 mL of LB in a 500 mL baffled conical flask. Cells were grown at 30°C until OD_600 was $\sim$ 0.6 and then immediately transferred in an ice cold bath for 10 minutes. All subsequent steps are carried at 4°C. Culture was transferred to two 50 mL Falcon tube and spun down for 10 minutes at 4000 rpm at 4°C. Supernatant was discarded and remaining supernatant was removed via pipeting. Cells in each Falcon tube were resuspended in 2.5 mL of TSS buffer before being aliquoted by batches of 100 μL in 0.2 mL PCR tubes sitting on dry ice. Aliquots were stored at -80°C. To transform DNA, the aliquot was thawed for 10 minutes on ice. DNA was added to the tube, which was then loaded to the thermocycler with the following protocol: 30 minutes at 4°C, 1 hour at 37°C.

BW25113 strains were prepared using the $CaCl_2$ method. Before preparing the competent cells, a solution of 0.1 M $CaCl_2$ was autoclaved and kept at 4°C in the fridge. Another solution of 0.1 M $CaCl_2$ mixed with 15% glycerol was autoclaved and stored at 4°C. A single *E. coli* colony was inoculated in 5 mL of SOB in a 15 mL culture tube in the evening and was grown to saturation overnight at 37°C shaking incubator. The following morning, we used 500 μL of the saturated culture to inoculate 100 mL of SOB medium in a 500 mL sterile baffled conical flask. The culture was grown in the shaking incubator at 30°C for about 3 hours until OD_600 was $\sim$ 0.6. Cells were then immediately transferred to an ice bath and gently swirled for efficient cooling and then left in the ice bath for 10 minutes. All subsequent steps are carried at 4°C. The cooled culture to pre-chilled 50 mL Falcon tubes, and centrifuged (Centrifuge Eppendorf 5810R) at 4°C and at 4000 rpm for 5 minutes. The supernatant was discarded by gentle inversion of the tubes into the waste bucket and remaining supernatant was removed by pipetting. Cells were then gently resuspended by pipetting with 10 mL of cold 0.1 M $CaCl_2$ before being incubated on ice for 20 minutes. Cells were then collected by another centrifugation step of 5 minutes at 4000 rpm and 4°C. After discarding the supernatant, cells were resuspended in 5 mL of 0.1 M $CaCl_2$ + 15% glycerol. 100 μL of resuspended cells were then aliquoted on dry ice in pre-chilled 0.2 mL PCR tubes, and stored at -80°C. To transform the DNA, an aliquot was thawed on ice for 10 minutes. The DNA was added to tube, which was then loaded into the thermocycler with the following protocol: 20 minutes at 4°C, 1 minute at 42°C, and then 1 minute at 4°C. The cells were then transferred to a 1.5 mL Eppendorf tube containing 900 μL of SOC medium (pre-warmed to 37°C) and incubated for 1 hour at 37°C in the shaking incubator. 100 μL of the culture was plated on a selective LB agar plate. The rest of the culture was spun down and 800 μL of the supernatant was discarded. The remaining 100 μL were resuspended and plated on a selective LB agar plate.

Before using the cells for transformation experiments, transformation efficiency (TE) of the aliquoted cells was measured by transforming 100 pg of pUC19 in 50 μL of cells. Cells were outgrown in 250 μL of SOC, 10 μL was diluted to 1 mL of fresh SOC and 30 μL plated on ampicillin selective LB agar plate. TE was calculated as follows: TE = colonies/μg/Dilution = colonies/0.001/((10/300)*(30/1000)).

7.2.2.2 Preparation of electrocompetent cells

Electrocompetent cells were prepared for genomic integration into *E. coli*. Before preparing competent cells, autoclave a solution of 10% glycerol and store it in the fridge. A single colony of the cells to make competent was inoculated in 5 mL of SOB in a 15 mL culture tube and grown overnight at 37°C in a shaking incubator. In the morning, 200 μL of culture was used to inoculate 50 mL of SOB in a 500 mL sterile baffled conical flask. Cells were grown to OD600 0.5-0.6 before being put in an ice bath for 10 minutes. All subsequent tasks were carried on ice. The culture was split into two 50 mL Falcon tubes and spun down in a pre-cooled centrifuged at 4°C for 10 minutes at 3000 rpm. Supernatant was discarded and tubes were centrifuged for another 1 minute at 4000 rpm. Supernatant was discarded by pipetting out the remaining medium. 1 mL of ice-cold 10% glycerol was used to resuspend the pellet by pipetting. 30 mL of 10% glycerol was added and mixed by inverting the tube several times before centrifugation (Centrifuge Eppendorf 5810R) for 10 minutes at 4000 rpm. The supernatant was discarded and cells were resuspended in 1 mL of ice-cold 10% glycerol and the mix was transferred into a 1.5 mL pre-chilled Eppendorf tube. The tube was centrifuged in a pre-cooled centrifuge (Thermo Scientific Heraeus Fresco 17) at 4°C for 30 seconds at 9000 rpm. Supernatant was removed by pipetting and 10% glycerol was added up to 500 μL. The final volume should be 1% of the original culture volume in SOB. Aliquot by 25 μL of competent culture in pre-chilled 0.2 mL PCR tubes placed on ice. Aliquots were stored at -80°C until use for electroporation. Cells can be defrosted on ice and frozen again for one time without significant loss of efficiency.

To transform DNA, thaw the aliquot of ice for 10 minutes as well as 1 mm electroporation cuvettes. If more than 2 μL of DNA should be used, it was dialised by placing it on a 0.025 μm membrane (MF-Millipore) floating on the surface of sterile ddH_2O in a petri dish, left for 15 minutes and collected back by pipetting. DNA was added to the cells, gently mixed by pipetting and added to the electroporation cuvette in between the electrodes. Sides of the cuvette were wiped with blue roll to avoid arcing. Electroporate with the Bacteria setting (the time should be around 2.5-5.5 ms). 1 mL of SOC was

directly added to the cuvette, mixed and transferred to a 1.5 mL Eppendorf tube. The tube was incubated with shaking for 1 hour at 37°C. Dilutions were plated on selective agar plates.

7.3 General DNA Manipulation

All the genetic parts built during this study were constructed using the cloning techniques described in the section below. They were either generated using one or a combination of the described techniques. Oligonucleotides were designed using Benchling and ordered from Integrated DNA Technologies (IDT). When larger parts were not readily available in the lab, they were ordered as gBlocks from IDT and codon optimised using the codon optimisation tool from IDT. All enzymes were obtained for NEB unless otherwise stated. Q5 High-Fidelity Mastermix from NEB was used for DNA amplification under the advised protocol and conditions from the manufacturer. Colony PCR was done using the GoTaq Green Mastermix Mix from Promega using the standard protocol from the manufacturer. Qiagen kits were used for the following techniques: gel extraction, PCR cleanup and plasmid miniprep. DNA concentrations were measured using the NanoDrop 1000 Spectrophotometer from NBS Biologicals.

7.3.1 Around-the-world PCR

Around-the-world PCR was used for site directed mutagenesis or for introducing small modification to existing plasmids (for example for building the STAR and anti-STAR toehold library or modifying the spacer sequence of the gRNA). For randomised libraries, one primer would be ordered with 5' phosphorylation from IDT. The Q5 High-Fidelity 2X (NEB) was used to amplify template plasmid. If one of the primer was 5' phosphorylated, 1 μL of DpnI (NEB) was directly added to the 25 μL PCR reaction for a 1-hour digestion at 37°C. The reaction was then purified by gel electrophoresis (in 0.8-1% TAE, with NEB 1kb Plus DNA Ladder and NEB Quick-Load Purple loading dye). At this stage, if one primer was phosphorylated, the purified linear DNA was ligated using T4 ligase from NEB following the manufacturer's standard protocol. If none of the primers were phosphorylated, the purified

linear DNA was treated with DpnI, phosphorylated and ligated using the KLD Enzyme Mix (NEB).

7.3.2 START/STOP Assembly

START/STOP assembly was used to build the STAR-based comparator plasmids, STAR target plasmids and quorum sensing plasmids [250]. We used the protocol developed by [250] and we thank the first author George Taylor for kindly sharing his collection of backbones, promoters, RBSs and terminators with us. New parts and backbones were designed using the original START/STOP recognition sites. New DNA parts ordered as gBlocks from IDT were designed with START/STOP level 0 appropriate recognition sites flanking the part of interest and were cloned into the level 0 backbone via BsaI-HF v2 (NEB) digestion. New promoters, RBSs and terminator parts were cloned into the level 0 backbone using around-the-world PCR described above. And CDSs available in the lab were cloned into the level 0 backbone using Gibson assembly described in the section below.

7.3.3 Gibson Assembly

Gibson assembly was used to modify existing plasmids that were not previously constructed with the START/STOP format [250]. The NEBuilder Hifi Assembly Mix (NEB) was used for Gibson assembly reactions and was used following the standard protocol from the manufacturer.

7.4 Genomic integration

7.4.1 CRIM integration

We used the plasmids and protocol described by [251] for genomically integrating constructs at the λ phage attachment site in *E. coli*. We summarise the steps needed for CRIM integration in Figure 80. Two plasmids are required for CRIM Integration:

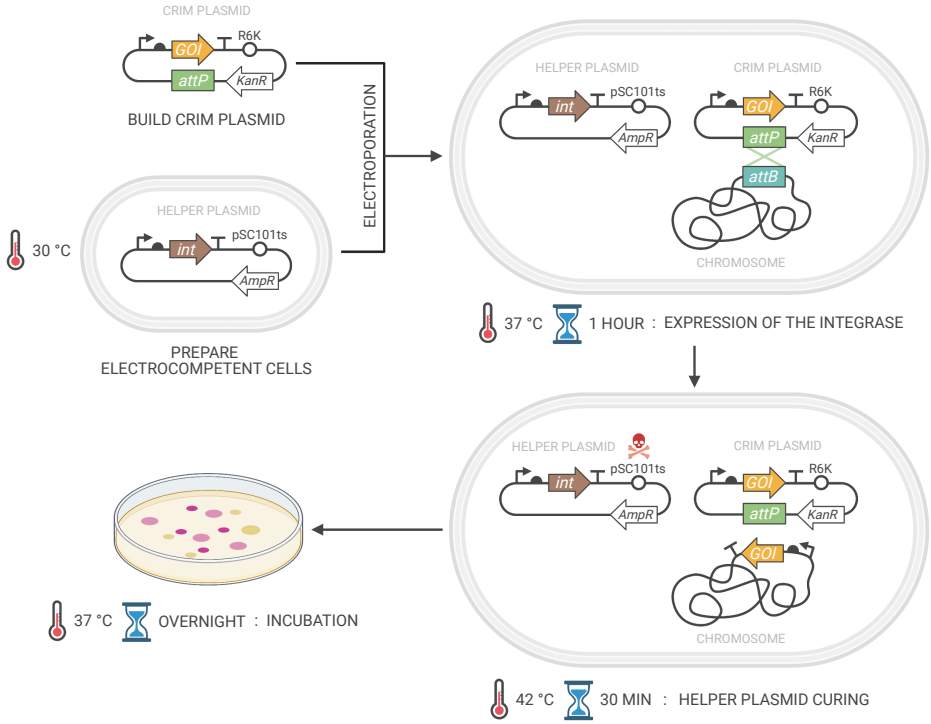


Figure 80: Graphical representation of the CRIM integration protocol.

1. The helper plasmid pINT-ts (available on Addgene https://www.addgene.org/66076/)

2. The CRIM plasmid based on the pAH63 plasmid for integration at the λ phage attachment site. We used the burden monitor cloned inside plasmid pAH63 from [8] (available on Addgene: https://www.addgene.org/66073/) as a template for building our CRIM plasmids.

The CRIM system works by placing the genetic circuit of interest into the CRIM plasmid corresponding to the phage integration site of interest. The CRIM plasmid has the γ replication origin of R6K, which requires the trans-acting Π protein (encoded by *pir*) for replication. This means that these plasmids can only be maintained in cells which have a pir+ genotype. There are two types of pir+ strains: strains with the wild-type pir gene will maintain the vector at 15 copies per cell, while strains with the mutant allele pir116 will maintain the vector at 250 copies per cell. We used PIR2 One Shot Chemically Competent E. coli (Invitrogen) or TransforMax EC100D pir+ (Lucigen) for cloning CRIM plasmids as

they contain the wild-type pir gene so maintain the plasmid at 15 copies per cell, such that overexpression of the cassettes would not be toxic for the cell.

For integration at the λ phage attachment site, we transformed the pINT-ts helper plasmid (Ampicillin resistant) into the *E. coli* strain of interest (DH10B or BW25113). Cells carrying the pINT-ts plasmid should always be grown at 30°C (solid and liquid culture). In parallel, we constructed the CRIM integration plasmid (Kanamycin resistance) by inserting the construct of interest into the pAH63 plasmid using Gibson assembly. Transform the reaction into pir+ *E. coli* chemical competent cells. After verification by sequencing, 200 ng of the CRIM plasmid was electroporated into the electrocompetent cells carrying the pINT-ts helper plasmid. Following electroporation, we suspended the cells in SOC media, incubated them at 37°C for 1 h, then 42°C for 30 min, and finally spread onto kanamycin LB agar plates. (The phage integrase (Int) enzyme is synthesised at elevated temperatures from the CRIM helper plasmid pINT-ts. The helper plasmid has a temperature sensitive origin of replication such that resulting colonies are nearly always cured of the helper plasmid, which is why you had to grow the pINT-ts cells at 30°C). To test for stable integration at the λ site, we picked a couple of colonies and grew them overnight at 37°C and then streaked them onto ampicillin and kanamycin plates and incubate overnight at 37°C. In the morning, if colonies were obtained on the ampicillin plate, we repeated the overnight growth in liquid culture until we only obtain colonies on the kanamycin plate and none of the ampicillin plate. This was to make sure that the helper plasmid has been cured from the cells. Finally, we verified that the insert had been correctly integrated by amplifying the insert with colony PCR with the appropriate primers and send to sequencing. Primers from [251] (Table 7.7) were used for verification of the integration at both extremities of the inserted plasmid: P1/P2 pair for one side and P3/P4 for the other side (Table 7.8).

Table 7.7: Primers used in this study to verify correct integration of the CRIM plasmid at the λ attP phage attachment site.

Primer	Sequence
P1	GGCATCACGGCAATATAC
P2	ACTTAACGGCTGACATGG
P3	ACGAGTATCGAGATGGCA
P4	TCTGGTCTGGTAGCAATG

Table 7.8: Primers pairs used in this study to verify correct integration of the CRIM plasmid at the λ attP phage attachment site.

Primer Pair	Test	Size	$T^{\circ}_{annealing}$
P1/P4	No integrant	741 bp	63°C
P1/P2	Single integrant	577 bp	63°C
P3/P4	Single integrant	666 bp	63°C

7.4.2 λ-Red integration

λ-Red integration was used to build strains that could quickly be edited by swapping the promoter of the C6-HSL and pC-HSL biosynthetic pathway. Plasmids pPRK and pDL17 from [252] were a gift from Sergey Sineoky and Tigran Yuzbashev (Addgene plasmid 106483; http://n2t.net/addgene:106483; RRID:Addgene_106483)). The counter-selection mechanism was based on the introduction of the RpsL150 mutation conferring streptomycin resistance to the *E. coli* strain of interest which contains the *recA* gene (e.g. BW25113). For introducing the RpsL150 mutation, we first transformed the BW25113 strain with the pDL17 plasmid and selected on ampicillin LB agar plates. We then picked a colony and prepared electrocompetent cells carrying the pDL17 (AmpR) plasmid according to the electrocompetent cell preparation protocol from Section 7.2.2.2 except that when cells reach OD_{600} 0.35, we added 1 mL of 20% L-rhamnose to the 50 mL culture (0.4% final L-rhamnose concentration) and culture at the flask at 37°C until OD_{600} 0.6. Then 100 ng per kb of the linear DNA (rpsL150-R oligonucleotide) was electroporated and cells were recovered for 1 hour at 37°C. Cells were plated on streptomycin selective LB agar plates to confirm the streptomycin resistant phenotype conferred by the RpsL150 mutation. We picked single colonies and streaked them onto streptomycin selective LB agar plates supplemented with IPTG (1 mM) to eliminate the pDL17 helper plasmid. The following day, we checked that the pDL17 plasmid was lost by plating cells on LB agar plates supplemented with ampicillin.

Table 7.9: Primer for introducing RpsL150 mutation in BW25113 to confer streptomycin resistance

Primer	Usage	Sequence
rpsL150-R	Introduce RpsL150 mutation	GAACACGGCATACTTTACGCAGCGCGGAGTTC GGTTTTCTAGGAGTGGTAGTATATACACGAGT ACATAC

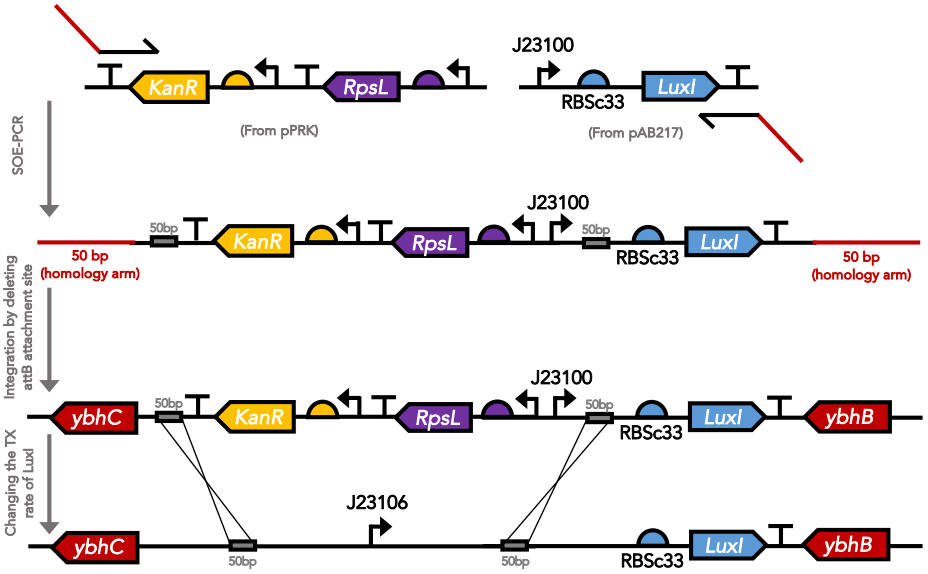


Figure 81: λ-Red integration strategy for building C6-HSL producing BW25113.

New electrocompetent cells were prepared with the cells carrying the *rpsL150* mutation and the pDL17 plasmid according to the electrocompetent cell preparation protocol from Section 7.2.2.2 except that when cells reach OD_{600} 0.35, we added 1 mL of 20% L-rhamnose to the 50 mL culture (0.4% final L-rhamnose concentration) and culture at the flask at 37°C until OD_{600} 0.6. DNA used for electroporation was assembled by SOE-PCR to fuse the *kanR* and *rpsL* genes from the pPRK plasmid to the construct of interest (*luxI* cassette) (Figure 81). Primers used for SOE-PCR are recorded in Table **??**. The pPRK and pAB383 were first amplified and purified separately with the appropriate primer pair (50 μL reaction for 20 cycles) and then attB-M13R-F and attB-luxI-R primers were used to amplify the two previous products (in 200 μL reaction for 30 cycles). The PCR product was for treated with DpnI for 1 hour before purification by gel extraction. 1 mg of the purified PCR product was used for electroporation in BW23115(*rpsL150*) with pDL17 and cells were recovered for 1 hour at 37°C. Cells were plated on kanamycin selective LB agar plates. We picked single colonies and streaked them onto kanamycin selective LB agar plates supplemented with IPTG (1 mM) to eliminate the pDL17 helper plasmid. The following day, we checked that the pDL17 plasmid was lost by plating cells on LB agar plates supplemented with ampicillin. We checked correct integration by colony PCR using the primers in Table **??** and Sanger

sequencing.

Table 7.10: Primers for integrating *luxI* with λ-Red. Sequences in orange represent the 50 bp homology sequences

Primer	Usage	Sequence
attB-M13R-F	Amplify pPRK with luxI-M13F-R for SOE-PCR (1753 bp)	TCACAGGTTGCTCCGGGCTATGAAATAG AAAAATGAATCCGTTGAAGCCT ATGTTG TGTGGAATTGTGAGC
luxI-M13F-R	Amplify pPRK with attB-M13R-F for SOE-PCR (1753 bp)	GCTAGCCGTCAACAGGGTTTTCCCAGTC ACGA
M13F-luxI-F	Amplify pAB383 with attB-luxI-R for SOE-PCR (773 bp)	GGAAAACCCTGTTGACGGCTAGCTCAGT CCT
attB-luxI-R	Amplify pAB383 with M13F-luxI-F for SOE-PCR (773 bp)	AAGGTATTAAAAACAACTTTTTGTCTTTT TACCTTCCCGTTTCGCTCAAG GGACCAA AACGAAAAAAGACG
Chr-attB-F	Amplify with pMH10seqF12 for checking integration (919bp)	GCGCCAGACGGGAAACTG
pMH10seqF12	Amplify with Chr-attB-F for checking integration (919bp)	AGCGGGAAGGGACTGGCT
luxI-seq-F	Amplify with AB538 for checking integration (519bp)	GGCGTTTATTACCTACAACAG
AB538	Amplify with luxI-seq-F for checking integration (519bp)	TCACTCTGCCAGATGGCGCA

Table 7.11: Universal primers for deletion of λ-Red markers *RpsL* and *KanR*

Primer	Sequence
M13-F	CAGGGTTTTCCCAGTCACGA
M13-R	ATGTTGTGTGGAATTGTGAGC

7.5 Data collection and analysis

7.5.1 Plate-reader timecourse assays

Time-course experiments were performed in clear flat-bottom 96-well plates (Costar) with three biological replicates in the Spark (Tecan) microplate reader or the Synergy HT (Biotek). Cells transformed with the constructs of interest and control plasmids were inoculated with 5 mL of M9 (with casaminoacids otherwise states) supplemented with the appropriate antibiotics, and grown overnight at 37°C with aeration in a shaking incubator. In the morning, we diluted cultures by 1:4 with fresh M9 in 1 cm cuvettes to measure the

OD_{700} of each sample in the spectrophometer (WPA Biowave II). Each sample was diluted to OD_{700} 0.01 in 2 mL of fresh M9 supplemented with the appropriate antibiotics (volume was adjusted depending on the experiment). For dBroccoli measurements, DFHBI-1T dye (Bio-Techne) was added to a final concentration of 100 μM unless otherwise stated. 200 μL of each sample was then transferred into a sterile 96-well plate and covered with a Breath-Easy membrane (Sigma). The plate was placed into a microplate reader and incubated at 37°C for 1 h (Tecan Spark: Double orbital shaking, 1.5 mm amplitude; Biotek Synergy HT: Medium shaking). Take measurements of OD_{700} and fluorescence (Table 7.12) were taken every 15 minutes. 1 hour into the incubation, we briefly removed the microplate from the plate-reader, carefully remove the Breath-Easy membrane and added the appropriate inducers (Table 7.3) to the each wells with the appropriate concentrations. We then covered the microplate with a new Breath-Easy Membrane and introduced it back into the plate-reader and set this time point as "time 0" by creating a “new plate” in the experiment. OD_{700} and fluorescence (Table 7.12) were taken every 15 minutes. Cells were grown for 6 to 24 hours depending on the experiment. Data were exported into an Excel Spreadsheet and analyzed using a MATLAB script.

For variants of the timecourse plate-reader assay when cells were diluted every 2 hours: after inducing the 96-well plate, cover the plate with its transparent plastic lid and cultivate in the Tecan Spark at 37°C. Every 2 hours, pause the Magellan program, retrieve the 96-well plate and dilute with fresh rich M9 medium. Dilutions were performed by removing a volume by pipetting corresponding to the rate of dilution needed for the experiment. The remove volume of culture was then replaced with the same volume of fresh rich M9 medium supplemented with the appropriate antibiotics and inducers. The volume to replace was calculated using the following formula from [87]:

$$V_{remove} = V_{total} - \frac{V_{total}}{\exp\left(D \times \delta t\right)}$$

Where V_{remove} is the volume of culture to pipette out and to replace with fresh medium, V_{total} is the total volume of culture in the well (200μL), D is the desired dilution rate (h^{-1}) and δt is the time between each dilutions (2 hours).

Table 7.12: Emission and excitation wavelength used for each fluorescent protein on the Tecan Spark and Synergy HT plate-readers. All fluorescence measurements was read from the bottom of the plate.

Fluorescent Protein/Aptamer	Tecan Spark	Synergy HT
sfCFP	430(20) nm ex./465(35) nm em.	—
sfYFP	485(20) nm ex./535(25) nm em.	485(20) nm ex./528(20) nm em.
GFP	485(20) nm ex./535(25) nm em.	485(20) nm ex./528(20) nm em.
dBroccoli	485(20) nm ex./535(25) nm em.	485(20) nm ex./528(20) nm em.
mScarlet-I (alone)	530(25) nm ex./595(35) nm em.	530(20) nm ex./590(35) nm em.
mScarlet-I (with GFP or sfYFP)	560(20) nm ex./620(20) nm em.	590(20) nm ex./645(40) nm em.
mCherry	560(20) nm ex./620(20) nm em.	590(20) nm ex./645(40) nm em.

Analysis was done using MATLAB. OD and fluorescence raw data were first subtracted with the mean of M9 media well replicates over time. Data were then smoothed using MATLAB smoothingspline function (smoothing parameter: 0.8648426188005848). Growth rate and fluorescence production rate per cell was calculated as described in [8]:

$$\text{Growth rate}|_{t_2} = \frac{\ln(\text{OD}|_{t_3}) - \ln(\text{OD}|_{t_1})}{t_3 - t_1}$$

$$\text{Fluorescence expression }|_{t_2} = \left(\frac{\text{FU}|_{t_3} - \text{FU}|_{t_1}}{t_3 - t_1}\right) \Big/ \text{OD}|_{t_2}$$

And for red fluorescence production rate per cell (e.g. mCherry):

$$\text{Red fluorescence expression }|_{t_2} = \left[\left(\frac{\text{FU}|_{t_3} - \text{FU}|_{t_1}}{t_3 - t_1}\right) \Big/ \text{OD}|_{t_2}\right] + 400$$

Where t_1 corresponds to 0 min after induction, t_2 to 15 min after induction and $t_3 = 30$ min after induction. We added 400 was added to all red fluorescence production rates per cell to account for the background red fluorescence of M9 media that is consumed by the cells over the time-course [8]. Mean values and standard deviations were calculated from the three biological replicates of each sample.

For figures representing input-output response curves, we used the nlinfit and fitnlm MATLAB functions to fit a four-parameter logistic regression model (4PL model) to the data

and determine the R-squared and p-value of the model:

$$\text{4PL model: } F(1) + \frac{F(2) - F(1)}{1 + \left(\frac{x}{F(3)}\right)^{F(4)}}$$

7.5.2 Flow cytometry measurements

Flow cytometry was used to measure coculture composition by counting the number of red fluorescent cells and non fluorescent cells. Cell fluorescence was measured in the Attune NxT (Thermo Scientific) flow cytometer using the following parameters: FSC 660 V, SSC 500 V, violet laser VL1 (405 nm ex./440(50) nm em.) 420 V, blue laser BL1 (488 nm ex./530(30) nm em.) 450 V, yellow laser YL2 (561 nm ex./620(15) nm em.) 560 V. The following threshold were used: AND FSC 0.5x1000, AND SSC 4x1000. 5 mixing cycles were used between each sample. 10,000 cells were collected for each sample and data were analysed using FlowJo and plotted with MATLAB. In FlowJo, we first gated *E. coli* cells from dust and cell debris by plotting SSC-A vs FSC-A. Then we gated the *E. coli* population to find the singlets population by plotting FSC-H vs FSC-A. Finally, the red and non-red singlets populations were determined by plotting BL1-H vs YL2-H.

For graphs representing fluorescence intensity, points represent the mean of the median fluorescence of three biological samples.

Deactivation percentage of the STAR-based comparator was calculated using the following formula:

$$\text{Deactivation percentage} = \left(\frac{F_{STAR} - F_{STAR,\ antiSTAR}}{F_{STAR} - F_{neg.}}\right) \times 100\%$$

Where F represents the mean of the median fluorescence of three biological samples. F_{STAR} is the fluorescence of the comparator when STAR is expressed, $F_{STAR,\ antiSTAR}$ is

the fluorescence of the comparator when both STAR and anti-STAR are expressed, and $F_{neg.}$ is the fluorescence of the comparator when neither STAR or anti-STAR are expressed.

7.5.3 Quorum sensing sender-receiver assay

A workflow of this protocol is represented in Figure 40 of Section 3.2.4. Sender strains and receiver strains were inoculated in 1 mL of rich M9 medium supplemented with the appropriate antibiotics in a 2 mL deep-well 96-well plate (VWR), covered with a "Breathe Easier" membrane (Sigma), and incubated overnight at 30°C in a plate shaker incubator (Infors HT Multitron) shaking at 700 rpm overnight. In the morning, sender strains were diluted to 1:4 in fresh M9 medium in a 1 cm cuvette and OD_{700} was measured in the spectrophotometer. Cells were diluted to OD_{700} 0.05 in 1 mL of fresh M9 medium with antibiotics in a new 2 mL deep-well 96-well plate, covered with a "Breathe Easier" membrane, and incubated at 700 rpm, 30°C in the plate-shaker incubator. Every hour for 6 hours, the deep-well plate was taken out of the incubator and new wells were inoculated with 1 mL of OD_{700} 0.05 of each culture. Receiver strains were diluted 1:200 in fresh M9 with antibiotics in a new deep-well plate and incubated at 700 rpm, 30°C in the plate-shaker incubator. At 6 hours, 250 μL of each sample from the sender strains deep-well plate was transferred to 1 cm cuvette to measure OD_{700} of each sender strain culture. The sender strains deep-well plate was then centrifuged at 4000 rpm for 5 minutes (Centrifuge Eppendorf 5810R) and the supernatants were transferred by pipetting in a new 2 mL deep-well plate, diluted 1:1 with fresh M9 with antibiotics and the pellets were discarded. The OD_{700} of the receiver strains were measured in the spectrophotometer by diluting 1:2 with fresh M9 in 1 cm cuvettes. Receiver strains were then diluted to OD_{700} 0.01 in 1 mL of the diluted sender strains' supernatants. 200 μL of each sample was transferred to a clear flat-bottom 96-well plate and inducers (and dye if dBroccoli was expressed) were immediately added to the appropriate wells. The microplate was covered with a Breathe-Easy membrane and incubated in the Tecan Spark for 12 hours, OD and fluorescence was measured every 15 minutes (Section 7.5.1).

7.5.4 Coculture assay

Cells carrying the open-loop and closed-loop versions of the composition controller circuits were grown as monocultures in 1 mL of rich M9 medium supplemented with the appropriate antibiotics in 2 mL 96-well deep-well plates (VWR) at 30°C in a plate shaker incubator (Infors HT Multitron) shaking at 700 rpm overnight. In the morning, cells were diluted 1:4 with fresh rich M9 medium and transferred to 1 cm cuvettes to measure OD_{700} in the spectrophotometer. Subsequently, each sample was diluted to OD_{700} 0.01 in a volume of 2 mL (adjusted according the experiment's needs). In a transparent flat-bottom 96-well plate (Costar), 100 μL of each monoculture that will compose the two-strain coculture are mixed in the appropriate wells (total volume of 200 μL in each well). Cocultures and monoculture controls were immediately induced with the appropriate inducers. The 96-well plate was covered its plastic lid, inserted into a Tecan Spark plate-reader and incubated at 37°C with shaking. OD_{700} and fluorescence was measured every 15 minutes. Every 2 hours for 12 hours, we paused the Magellan program running the plate-reader experiment and under sterile condition, we transferred 1-6 μL of cells (0-2 hours: 6 μL; 4-6 hours: 3 μL; 8-10 hours: 1 μL, 12-24 hours: 0.5 μL) into a clear round-bottom 96-well plate (Costar) pre-filled with 200 μL of 1X PBS (Sigma) supplemented with tetracycline (10 μg/mL), we call this plate the "flow plate" as it will be used to measure cell fluorescence in the flow cytometer to determine coculture composition. The "experiment 96-well plate" is covered back with its lid and placed back into the plate-reader where the Magellan program was resumed. The "flow plate" is immediately stored on ice in the fridge at 4°C. When the "flow plate" was entirely filled with coculture samples diluted in PBS, it was run in the flow cytometer according to the protocol in Section 7.5.2.

7.5.5 β-Carotene assay

The protocol was adapted from [27]. For quantification of β-Carotene production, cells carrying the β-Carotene producing plasmids and controls were grown in 5 mL of rich M9 media in 15 mL culture tube overnight at 37°C in shaking conditions. In the morning, cells were diluted 1:4 in fresh M9 media and 1 mL of diluted cultures were transferred to

1 cm cuvettes to measure OD_{700} in the spectrophotometer. Each sample was diluted to OD_{700} 0.01 in a volume of 5 mL in a sterile 15 mL culture tube and induced with the appropriate inducers. After 6 hours of growth 37°C in the shaking incubator, 0.5 mL of each culture was diluted 1:1 with fresh rich M9 media and its OD_{700} was measured in the spectrophotometer. The remaining 4.5 mL of each culture were spun down at 4000 rpm for 10 minutes (Centrifuge Eppendorf 5810R), and remaining supernatant was discarded by pipetting. Pellets were resuspended in 300 μL of acetone in 1.5 mL Eppendorf tubes, homogenised by vortexing for 10 minutes and incubated at 55°C (Eppendorf ThermoMixer C) for 15 minutes. Tubes were centrifuged for 1 minute at 10,000 rpm (Thermo Scientific Heraeus Fresco 17 Centrifuge). 100 μL of the supernatants were collected by pipetting and transferred to a new 1.5 mL Eppendorf tube. A volume of 100 μL of water was added to the 100 μL of supernatants in each tube and mixed by pipetting. The total 200 μL were then transferred to a clear flat-bottom 96-well plate (Costar) and OD_{450} of the microplate was measured in the plate-reader (Tecan Spark). To compare production of β-Carotene between the different samples, OD_{450} of each sample was divided by its corresponding OD_{700}. We note that β-Carotene does not absorb at OD_{700}.

7.5.6 Chi.bio turbidostat assay

Chi.bios were set up according to the Chi.bio manual and connected to the College network via Ethernet cables [177]. Calibrations using monodisperse silica beads (Cospheric) were realised for accurate prediction of optical density. Previous to starting the experiment, Chi.bio chambers, magnets (Fisher Scientific, No:11818862) and caps (3dPrintDirect, PA12 Nylon) were autoclaved in plastic boxes. Cells carrying the open-loop and closed-loop circuits of the composition controller circuits were grown as monocultures in 10 mL of rich M9 media supplemented with the appropriate antibiotics in 50 mL culture tubes at 37°C in shaking conditions overnight. In the morning, silicon tubings from the Chi.bio were filled with 75 % ethanol for 5 minutes, then rinse thoroughly with autoclaved ddH_2O. Tubings were connected to the Chi.bio caps which were previously screwed onto the chambers containing the magnetic stirrer under sterile conditions, and 2 L bottles used as liquid waste were filled with a small volume of Distel. Then, we measured the OD_{600} of the cells

in the spectrophotometer by diluting 1:4 the overnight culture in a 1 cm cuvette. Each monoculture was diluted to OD_{600} 0.6 in 10 mL of fresh rich M9 medium supplemented with the appropriate antibiotics directly in the Chi.bio chambers to obtain a final 20 mL coculture of OD_{600} 0.6. The different Chi.bio units were calibrated with the same Chi.bio chamber and the calibration values were carefully recorded. All chambers were placed inside their respective Chi.bio, the temperature module was set to 37°C and the stirring rate was set on 1 (maximum value). Every 2 minutes, the Chi.bio took 10 successive OD_{600} measurements and the average value was recorded for this timepoint in a .txt file. To avoid that the magnet stirrer would get stuck during the OD measurements, we decreased the stirring speed to 0.5 instead of stopping it completely such that the stirrer would still rotate in the chamber but there would also be no vortex perturbing OD measurements. Using a 250 μL glass syringe (Hamilton), we sampled 50 μL of culture from each Chi.bio chamber into round-bottom 96-well plate, and sterilising the syringe with acetone between samples. 5 μL of each coculture sample was then diluted into 200 μL of 1X PBS (Sigma) supplemented with tetracycline (10 μg/mL) to fix the cells. Fluorescence of the fixed cells was then measured in the flow cytometer according to Section 7.5.2 to determine the fraction of red cells and non-fluorescent cells. Sampling was carried over the course of 12 hours.

7.6 DNA parts and Plasmids

7.6.1 DNA Parts

7.6.1.1 Promoters used in this study

Table 7.13: Promoter sequences used in this study

Promoter	Regulator	Sequence	Source
J23119	σ_{70}	ttgacagctagctcagtcctaggtataatgctagc	iGEM J23119
J23100	σ_{70}	ttgacggctagctcagtcctaggtacagtgctagc	iGEM J23100
J23106	σ_{70}	tttacggctagctcagtcctaggtatagtgctagc	iGEM J23106
J23105	σ_{70}	tttacggctagctcagtcctaggtactatgctagc	iGEM J23105
J23115	σ_{70}	tttatagctagctcagcccttggtacaatgctagc	iGEM J23115
J23114	σ_{70}	tttatggctagctcagtcctaggtacaatgctagc	iGEM J23114
J23109	σ_{70}	tttacagctagctcagtcctagggactgtgctagc	iGEM J23109
P_{RAND14}	σ_{70}	tttacggctagctcagtcctaggtattgtgctagc	[156]
P_{LacIQ}	σ_{70}	gcggcgcgccatcgaatggtgcaaaacctttcgcggtatggcatgatagcgccc	[182]
P_{htpG1}	σ_{32}	acgagagcaggatcacctgctctcgcttgaaattattctcccttgtcccca tctctccca	[8]
P_{Tet}	TetR	tccctatcagtgatagagattgacatccctatcagtgatagagatactga gcac	[130]
P_{lux}	LuxR	acctgtaggatcgtacaggtttacgcaagaaaatggtttgttatagtcga ataaa	[182]
P_{lux_A}	LuxR	acctgtaggatcgtacaggtttacgcaagaaaatggtttgttattgtcga ataaa	[182]
P_{lux_B}	LuxR	acctgtaggatcgtacaggtttacgcaagaaaatggtttgttacagtcga ataaa	[182]
P_{rpa}	RpaR	gcacctgtccgatcggacagtattacgcaagaaaatggtttgttatagtc gaatat	[111]
P_{CymRC}	CymR	aacaaacagacaatctggtctgtttgtattatggaaaatttttctgtataa tagattcaacaaacagacaatctggtctgtttgtattat	[182]
P_{VanCC}	VanR	attggatccaattgacagctagctcagtcctaggtaccattggatccaa	[182]
P_{PhlF}	PhlF	cgacgtacggtggaatctgattcgttaccaattgacatgatacgaaacgt accgtatcgttaaggt	[182]
P_{SalTCC}	NahR	ggggcctcgcttgggttattgctggtgcccggccgggcgcaatattcatg ttgatgatttattatatatcgagtggtgtatttatttatattgtttgctccg ttaccgttattaac	[182]
P_{rhaBAD}	RhaSR	ccacaattcagcaaattgtgaacatcatcacgttcatctttccctggttgc caatggcccattttcctgtcagtaacgagaaggtcgcgtattcaggcgct ttttagactggtcgtaatgaa	[182]

Table 7.13: Promoter sequences used in this study

Promoter	Regulator	Sequence	Source
AraC-P_{araBAD}	AraCE	ttatgacaacttgacggctacatcattcacttttttcttcacaaccggcacg gaactcgctcgggctggccccggtgcatttttttaaatacccgcgagaaat agagttgatcgtcaaaaccaacattgcgaccgacggtggcgataggcat ccgggtggtgctcaaaagcagcttcgcctggctgatacgttggtcctcgc gccagcttaagacgctaatccctaactgctggcggaaaagatgtgacag acgcgacggcgacaagcaaacatgctgtgcgacgctggcgatatcaaa attgctgtctgccaggtgatcgctgatgtactgacaagcctcgcgtaccc gattatccatcggtggatggagcgactcgttaatcgcttccatgcgccgc agtaacaattgctcaagcagatttatcgccagcagctccgaatagcgccc ttccccttgcccggcgttaatgatttgcccaaacaggtcgctgaaatgcg gctggtgcgcttcatccgggcgaaagaaccccgtattggcaaatattgac ggccagttaagccattcatgccagtaggcgcgcggacgaaagtaaaccc actggtgataccattcgcgagcctccggatgacgaccgtagtgatgaatc tctcctggcgggaacagcaaaatatcacccggtcggcaaacaaattctc gtccctgatttttcaccaccccctgaccgcgaatggtgagattgagaata taacctttcattcccagcggtcggtcgataaaaaaatcgagataaccgtt ggcctcaatcggcgttaaacccgccaccagatgggcattaaacgagtat cccggcagcaggggatcattttgcgcttcagccatacttttcatactcccg ccattcagagaagaaaccaattgtccatattgcatcagacattgccgtca ctgcgtcttttactggctcttctcgctaaccaaaccggtaaccccgcttat taaaagcattctgtaacaaagcgggaccaaagccatgacaaaaacgcg taacaaaagtgtctataatcacggcagaaaagtccacattgattatttgc acggcgtcacactttgctatgccatagcatttttatccataagattagcgg atcctacctgacgctttttatcgcaactctctactgtttctccatacccgtt ttttgggctagc	[156]
P_{LacO-1}	LacI	aattgtgagcggataacaattgacattgtgagcggataacaagatactg agcacatcagcaggacgcactgacc	[24]

7.6.1.2 RBSs used in this study

Table 7.14: RBS sequences used in this study

RBS	Sequence	Source
B0030	tactattaaagaggagaaatactag	iGEM B0030
B0031	tctagagtcacacaggaaacctactag	iGEM B0031
B0032	tctagagtcacacaggaaagtactag	iGEM B0032
B0033	tctagagtcacacaggactactag	iGEM B0033
B0034	tactagagaaagaggagaaatactag	iGEM B0034
RBS8B	aagaattcaaaagctctacagaggagaaaggatat	[156]
RBSc33	ctacgtttttagaaaaaggaggtatgcgag	[250]
RBSc44	atcggattggatccaaaggaggttataccg	[250]
RBS_{Bujard}	GAATTCATTAAAGAGGAGAAAGGTACC	[130]
RBS_{VioB}	aggcatctttcaactaaagtaagaggtaataatt	[156]

Table 7.14: RBS sequences used in this study

RBS	Sequence	Source
$RBS_{mCherry}$	aggctgcagcgaaagcg	[156]
RBS_{RFP}	atggcgagtagcg	[130]
RBS_{ctrE}	taaggaggctccta	[27]
RBS_{ctrB}	agaggatacatata	[27]
RBS_{ctrI}	tcaggatttttgta	[27]
RBS_{ctrY}	cgaggaggtaataa	[27]
nah2	ggaagagagtcaattcatgggggttgaat	[182]
van2	ggaagagagtcaattcaggggggtgaata	[182]
phl2	ggaagagagtcaattcatgggggtgaat	[182]
cym1	ggaagagagtcaattcagggtggtgaat	[182]

7.6.1.3 Ribozymes used in this study

Table 7.15: Ribozyme sequences used in this study

Ribozyme	Sequence	Source
HH	atctggctgatgagtccgtgaggacgaaacgagtaagctcgtccc	[190]
HDV	ggccggcatggtcccagcctcctcgctggcgccggctgggcaacaccttcgggtggcgaatgg gact	[190]
RiboJ	agctgtcaccggatgtgctttccggtctgatgagtccgtgaggacgaaacagcctctacaaat aattttgtttaa	[182]

7.6.1.4 Guide RNAs used in this study

The SpCas9 gRNA scaffold used in this study: gttttagagctagaaatagcaagttaaaataaggctagtccg ttatcaacttgaaaaagtggcaccgagtcggtgctttt [156].

The gRNA was flanked with a self-cleaving hammerhead (HH) ribozyme on the 5' side and with the self-cleaving hepatitis delta virus (HDV) ribozyme on the 3' side. Thus, after self-cleaving, the gRNA transcript does not contain exogeneous sequences from either the promoter or terminator region [190].

Table 7.16: Guide RNA sequences used in this study

Target Promoter	Guide	ON-Target Score	OFF-Target Score
TrpCp	acaaacgtgttaaaatgtca	65.5	50

Table 7.16: Guide RNA sequences used in this study

Target Promoter	Guide	ON-Target Score	OFF-Target Score
TrpCp(1)	aaaatgtcacggttttcttc	34.9	50
TrpCp(2)	attttaacacgtttgttaca	41.8	50
TrpCp(3)	acacgtttgttacaaggtaa	51.7	50
HisLp	actttcacgttagaaagcaa	64.8	50
LeuLp	agagttactggatacaaaaa	41.8	50
$LeuLp_2$	gatttttttgatattgatt	49.1	50
GlyAp	gcgataacaggtcttgacaa	71.7	50
AroFp	tcgttacgtcAtcctcgctg	65.4	50
ProCp	ataaacagaactatgccgga	62.5	50
ArgAp	aaacattctttttatattca	35.7	49.9
CysEp	ttgcggaaaaaacgcgcgcg	62.8	50
PheLp	tgacagcgtgaaaacagtac	65.6	50
MetAp	tctggttatcttcagctAtc	26.4	50
ThrLp	aattaaaattttattgactt	45.9	50
IlvAp	acgctcgaggtgacaaagcc	48.1	50
araBAD	gagttgcgataaaaagcgtc	39.9	49.9
No Target	gcacagatttcaggacttat	—	—

7.6.1.5 Small RNAs used in this study

Hybridisation energy of the sRNA with its target mRNA was calculated using IntaRNA [175]. sRNA Hfq scaffold used for all sRNA designs: tttctgttgggccattgcattgccactgattttccaac atataaaaagacaagcccgaacagtcgtccgggctttttttctcgag [131]. The scaffold was directly followed by the T1/TE terminator.

Table 7.17: Small RNA sequences used in this study

Target mRNA	Targeting Sequence (20bp)	Hybridisation Energy
sfGFP	gaacagttcttcgcctttacgcat	-43.1 kcal/mol
GFPmut3b	gaaaagttcttctcctttacgcat	-38.7 kcal/mol
LeuB	gaaaagttcttctcctttacgcat	-38.7 kcal/mol

Table 7.17: Small RNA sequences used in this study

Target mRNA	Targeting Sequence (20bp)	Hybridisation Energy
MetA	gaaaagttcttctcctttacgcat	-39.2 kcal/mol
ThrC	tttcgctaaaacggtttgcatcat	-37.4 kcal/mol
HisD	gtcaatgattgtgttaaagctcat	-37.5 kcal/mol
GlyA	aatgttcatttcacgctttaacat	-33.6 kcal/mol

7.6.1.6 Transcription Factors used in this study

Table 7.18: TF sequences used in this study

TF	Sequence	Source
LuxR	atgaaaaacataaatgccgacgacacatacagaataattaataaaattaaagcttgtagaagcaataa tgatattaatcaatgcttatctgatatgactaaaatggtacattgtgaatattatttactcgcgatcattta tcctcattctatggttaaatctgatatttcaatcctagataattaccctaaaaaatggaggcaatattatg atgacgctaatttaataaaatatgatcctatagtagattattctaactccaatcattcaccaattaattgg aatatatttgaaaacaatgctgtaaataaaaaatctccaaatgtaattaaagaagcgaaaacatcaggt cttatcactgggtttagtttccctattcatacggctaacaatggcttcggaatgcttagttttgcacattca gaaaaagacaactatatagatagtttatttttacatgcgtgtatgaacataccattaattgttccttctct agttgataattatcgaaaaataaatatagcaaataataaatcaaacaacgatttaaccaaaagagaaa aagaatgtttagcgtgggcatgcgaaggaaaaagctcttgggatatttcaaaaatattaggttgcagtg agcgtactgtcactttccatttaaccaatgcgcaaatgaaactcaatacaacaaaccgctgccaaagtat ttctaaagcaattttaacaggagcaattgattgcccatactttaaaaattaa	[130]
RpaR	atgatcgtcggcgaagatcagctttggggacggcgtgcgctggaattcgtcgattccgtcgaacggctcg aggcgccggcgctgatcagccggttcgaatcgctgatcgcgagctgcggatttaccgcctacatcatggc cggcctgccgtcgcgcaatgccggactaccggagctgacgctggccaatggctggccgcgagactggtt cgatctgtatgtcagcgaaaacttcagcgcggtcgatccggtgccgcgccacggcgctaccacggttcat cctttcgtatggtccgatgcaccctacgaccgcgaccgtgatccggccgcccaccgggtcatgacccggg cggcggaattcggactggtcgagggttactgcattccgctgcactacgacgacggtagcgccgcgatca gcatggccggcaaggatccggacctcagcccggccgcgcgcggcgcgatgcagctggtcagcatctacg cgcatagtcgcctgcgcgcactcagccggccaaagccgatccggcgcaaccggctcacgccgcgcgagt gcgagatcctgcaatgggcagcgcagggcaagaccgcctgggaaatctcggtaatcctctgcatcaccg aacgcacggtgaaattccatctgatcgaagccgcccgcaagctcgacgccgccaaccgcaccgcggcgg ttgccaaggcattgacgctcggattgatccgtttgtaa	[111]

Table 7.18: TF sequences used in this study

TF	Sequence	Source
NahR^{AM}	atggaactgcgtgacctggatttaaacctgctggtggtgttcaaccagttgctggtcgacagacgcgtct ctgtcactgcggagaacctgggcctgacccagcctgccgtgagcaatgcgctgaaacgcctgcgcacct cgctacaggacccactcttcgtgcgcacacatcagggaatggaacccacaccctatgccgcgcatctggc cgagcacgtcacttcggccatgcacgcactgcgcaacgccctacagcaccatgaaagcttcgatccgctg accagcgagcgtaccttcaccctggccatgaccgacattggcgagatctacttcatgccgcggctgatgg atgcgctggctcaccaggcccccaattgcgtgatcagtacggtgcgcgacagttcgatgagcctgatgca ggccttgcagaacggaaccgtggacttggccgtgggcctgcttcccaatctgcaaactggcttctttcag cgccggctgctccagaatcactacgtgtgcctatgtcgcaaggaccatccagtcacccgcgaaccccctga ctctggagcgcttctgttcctacggccacgtgcgtgtcatcgccgctggcaccggccacggcgaggtgga cacgtacatgacacgggtcggcatccggcgcgacatccgtctggaagtgccgcacttcgccgccgttggc cacatcctccagcgcaccgatctgctcgccactgtgccgatatgtttagccgactgctgcgtagagcccctt cggcctaagcgccttgccgcacccagtcgtcttgcctgaaatagccatcaacatgttctggcatgcgaag taccacaaggacctagccaatatttggttgcggcaactgatgtttgacctgtttacggattgataa	[182]
VanR^{AM}	atggacatgcctcgtattaaaccgggtcagcgtgttatgatggcactgcgtaaaatgattgcaagcggtg aaatcaaaagtggtgaacgtattgcagaaattccgaccgcagcagcactgggtgttagccgtatgccgg ttcgtatcgcactgcgttcactggaacaagaaggtctggttgttcgtctgggtgcacgtggttatgcagcc cgtggtgttagcagcgatcagattcgtgatgcaattgaagttcgtggtgttctggaaggttttgcagcac gtcgtctggcagaacgtggtatgaccgcagaaacccatgcacgttttgttgtactgattgcagaaggtga agcactgtttgcagccggtcgcctgaatggtgaagatctggatcgttatgccgcatataatcaggcattt catgataccctggttagcgcagcaggtaatggtgcagttgaaagcgcactggcacgtaatggttttgaa ccgtttgcagcagccggtgcactggccctggatctgatggacctgtctgccgaatatgaacatctgctgg cagcacatcgtcagcatcaggcagttctggatgcagttagctgtggtgatgccgaaggtgcagaacgta ttatgcgtgatcatgcactggcagcaattcgtaatgcaaaagttttgaagcagcagcaagcgcaggcg caccgctgggtgcagcatggtcaattcgtgcagattgataag	[182]
PhlF^{AM}	atggcacgtaccccgagccgtagcagcattggtagcctgcgtagtccgcatacccataaagcaattctga ccagcaccattgaaatcctgaaagaatgtggttatagcggtctgagcattgaaagcgtggcacgtcgcg ccggtgcaggcaaaccgaccatttatcgttggtggaccaacaaagcagcactgattgccgaagtgtatg aaaatgaaatcgaacaggtacgtaaatttccggatttgggtagctttaaagccgatctggattttctgct gcataatctgtggaaagtttggcgtgaaaccatttgtggtgaagcatttcgttgtgttattgcagaagca cagttggaccctgtaaccctgacccaactgaaagatcagtttatggaacgtcgtcgtgagataccgaaa aaactggttgaagatgccattagcaatggtgaactgccgaaagatatcaatcgtgaactgctgctggat atgatttttggttttgttggtatcgcctgctgaccgaacagttgaccgttgaacaggatattgaagaatt taccttcctgctgattaatggtgtttgtccgggtacacagtgttgataa	[182]
Cym^{AM}	atgagcccgaaacgtcgtacccaggcagaacgtgcaatggaaacccagggtaaactgattgcagcagc actgggtgttctgcgtgaaaaaggttatgcaggttttcgtattgcagatgttccgggtgcagccggtgtt agccgtggtgcacagagccatcattttccgaccaaactggaactgctgctggcaacctttgaatggctgt atgagcagattaccgaacgtagccgtgcacgtctggcaaaactgaaaccggaagatgatgttattcagc agatgctggatgatgcagcagaatttttttctggatgatgattttagcatcggcctggatctgattgttgca gcagatcgtgatccggcactgcgtgaaggtattcagcgtaccgttgaacgtaatcgttttgttgttgaag atatgtggctgggtgtgctggtgagccgtggtctgagccgtgatgatgccgaagatattctgtggctgat ttttaacagcgttcgtggtctggtagttcgtagcctgtggcagaaagataaagaacgttttgaacgtgtg cgtaatagcaccctggaaattgcacgtgaacgttatgcaaaattcaaacgttgataa	[182]

7.6.1.7 GOIs used in this study

Table 7.19: GOI sequences used in this study

GOI	Sequence	Source
LuxI	atgactataatgataaaaaaatcggatttttggcaattccatcggaggagtataaaggtattctaagtc ttcgttatcaagtgtttaagcaaagacttgagtgggacttagttgtagaaaataaccttgaatcagatga gtatgataactcaaatgcagaatatatttatgcttgtgatgatactgaaaatgtaagtggatgctggcgt ttattacctacaacaggtgattatatgctgaaaagtgtttttcctgaattgcttggtcaacagagtgctcc caaagatcctaatatagtcgaattaagtcgttttgctgtaggtaaaaatagctcaaagataaataactct gctagtgaaattacaatgaaactatttgaagctatatataaacacgctgttagtcaaggtattacagaat atgtaacagtaacatcaacagcaatagagcgatttttaaagcgtattaaagttccttgtcatcgtattgg agacaaagaaattcatgtattaggtgatactaaatcggttgtattgtctatgcctattaatgaacagttta aaaaagcagtcttaa	iGEM C0061
RpaI	atgcaggttcatgtcatccgtcgagagaaccgcgcgctctatgccggtctgctcgaaaagtacttccgca tccgtcaccagatctacgtcgtcgagcgcggctggaaggagctcgatcggccggatggccgcgagatcg atcagttcgacaccgaagacgccgtgtatctgctcggcgtcgacaatgacgacatcgtcgccggcatgc ggatggtgccgaccacgtcaccgacgctcctcagcgacgtcttcccgcagcttgcgctggcaggcccggt gcggcggccggatgcctacgagctgtcgcggatcttcgtggtaccgcgcaagcgcggcgagcatggcgg cccgcgcgccgaagccgtgatccaggcggccgcgatggagtacggcctgtcgatcggtctgtcggccttc accatcgtgctggagacctggtggctgccgcgactggtggaccagggctggaaggcaaagccgctcggc ctgcctcaggacatcaacggattctcgaccaccgcagtgatcgtcgacgtcgacgacgacgcctgggtc ggcatctgcaatcgccgctcggtgcccggacccacgctggaatggcgcgggctcgaagccatccgccgt cattcgcttccggaattccaggtgatttcataa	CIDAR MoClo Extension[1]
4CL2nt	atggagaaagacacgaagcaagttgacatcatttttcgctcgaaactgccggacatttacattccgaatc atctgccgctgcatagctactgcttcgagaacatttctgaattttctagccgtccgtgtctgattaacggt gccaataaacagatctatacgtacgcggacgtcgagttgaacagccgtaaggtcgcagcgggtctgcac aagcaaggcatccagcctaaagataccatcatgattctgttgccaaattctccggagtttgtgtttgcgtt tatcggcgcaagctacctgggtgcgattagcacgatggcaaatccgctgtttaccccggctgaggttgtt aaacaagcaaaagccagcagcgcgaagatcatcgtgacccaagcatgccacgtcaacaaagttaagga ctatgccttcgaaaatgacgtcaagatcatttgcatcgatagcgcgcctgaaggttgtctgcatttcagc gttctgacgcaggctaacgaacacgatattccggaagttgagattcagccggacgatgtggtggccctg ccgtactccagcggtaccaccggcctgccgaaaggcgttatgctgacccacaagggcctggtgacgagc gtcgcccagcaggtcgatggtgaaaacccgaacctgtacatccacagcgaagatgttatgctgtgtgttc tgccactgttccacatctattccctgaacagcgtcctgctgtgcggcctgcgtgtgggcgctgccatttg attatgcagaagtttgacattgtcagcttcttggaactgatccaacgctacaaggtgacgatcggtccgt tcgtcccgccgattgttttggccattgcaaaaagcccaatggtggatgactatgacctgtcgagcgtgcg taccgtgatgtccggtgcagcgccgctgggcaaagagctggaggataccgttcgtgcgaagtttccgaa tgcgaaactgggtcaaggctacggtatgactgaagcaggtccggtgctggcgatgtgcttggcgttcgc gaaagagccgttcgaaatcaaaagcggtgcgtgcggtaccgtggtgcgtaatgctgaaatgaaaattgt ggatccgaaaaccggcaacagcctgccgcgcaaccagagcggtgagatttgtattcgcggtgaccagat tatgaagggctacctgaatgacccggaggccactgcgcgtacgatcgacaaagagggttggctgtatac cggcgacatcggttatatcgatgacgacgacgagctgttcatcgttgatcgcctgaaagagttgattaag tacaagggtttccaagttgcgcctgcggaactggaggctctgctgttgaatcatccgaacattagcgatg cagcagtcgttccgatgaaggatgagcaggcgggtgaagttccggtcgcgtttgttgtgcgtagcaacg gcagcacgatcaccgaggatgaggtaaaggatttcatttccaaacaagtcatcttctataagcgtatcaa gcgtgtgtgtttttcgtcgatgcaatcccgaaaagcccgtccggtaagatcctgcgcaaagacttgcgtgcg aagctggcggcaggtctgccgaattagtaa	[183]

[1]CIDAR MoClo Extension, Volume I was a gift from Richard Murray (Addgene kit #1000000161).

Table 7.19: GOI sequences used in this study

GOI	Sequence	Source
TAL	atgacccaggtggttgaacgccaggccgatcgcctgagtagtcgtgaatacttagctcgcgtcgttcgta gtgccggctgggatgcgggcctaacctcttgtacagatgaagaaattgttcgcatgggcgcgtcagccc gcaccatcgaggaatatttaaaaagtgataaaccgatttatggtttaacccaaggcttcggcccgctggt actgtttgatgcggatagcgaattagaacagggtggtagcctgattagccatctgggcaccggtcaggg cgcgccgctggcgccggaagtgagtcgtttaattctgtggctgcgtattcaaaacatgcgcaaaggttat agcgccgttagcccggttttctggcaaaaactggcagacctatggaataaaggctttaccccggcaattc cgcgtcatggtaccgtttccgcctcgggtgatctgcaaccgctggcgcatgccgcgctggcattcaccgg cgtgggtgaagcgtggacccgcgatgcagatggccgctggagcaccgttccggctgttgatgccctggc agcgctgggtgccgaaccgtttgattggcctgtccgcgaagcactggcgtttgttaatggcaccggagcc agcctggcggttgctgttttaaatcatcgttctgccctgcgcctggttcgcgcgtgtgcggtactgagcgc acgcctggcgaccctgctgggcgcaaatccggaacattatgacgttggtcatggcgttgcccgcggtcag gttggccagctgaccgcggcggaatggattcgtcagggcctgccacgtggtatggtgcgcgatggaagc cgtccgttgcaggaaccttatagccttcgctgcgctccgcaggttctaggcgctgttctggatcagctgga cggtgcgggtgacgtgctggcccgcgaagttgatggttgccaggataaccctattacctacgaaggtga attgctgcatggcggtaacttccatgccatgccggttggttttgcaagtgatcagattggtctggcgatgc acatggcggcctacctggctgaacgccagctgggcctgctggttagcccggtaaccaatggtgatttacc accgatgctgaccccgcgtgccggccgtggtgcgggtcttgctggcgtccagatttctgccaccagcttc gtttctcgtattcgccaactggttttcccggcgtctctgaccaccctgccgaccaacggttggaatcaaga ccatgtaccgatggcactgaatggcgctaatagcgttttcgaagcactggaactgggttggttaaccgtt ggaagcctggcggtgggcgttgcacagctggcggcgatgaccggtcatgcggctgaaggggtttgggc agaactggcaggcatttgcccgccgttagatgccgaccgtccgctgggtgcggaagttcgcgcagcccg tgatctgctgagcgcgcacgctgatcagctgttggtggacgaagccgatggtaaagactttggctaa	[183]

Table 7.19: GOI sequences used in this study

GOI	Sequence	Source
dCas9	atggataagaaatactcaataggcttagctatcggcacaaatagcgtcggatgggcggtgatcactgat gaatataaggttccgtctaaaaagttcaaggttctgggaaatacagaccgccacagtatcaaaaaaaat cttataggggctcttttatttgacagtggagagacagcggaagcgactcgtctcaaacggacagctcgta gaaggtatacacgtcggaagaatcgtatttgttatctacaggagatttttttcaaatgagatggcgaaagt agatgatagtttctttcatcgacttgaagagtctttttttggtggaagaagacaagaagcatgaacgtcat cctatttttggaaatatagtagatgaagttgcttatcatgagaaatatccaactatctatcatctgcgaaa aaaattggtagattctactgataaagcggatttgcgcttaatctatttggccttagcgcatatgattaagt ttcgtggtcatttttttgattgagggagatttaaatcctgataatagtgatgtggacaaactatttatccag ttggtacaaacctacaatcaattatttgaagaaaaccctattaacgcaagtggagtagatgctaaagcg attctttctgcacgattgagtaaatcaagacgattagaaaatctcattgctcagctccccggtgagaaga aaaatggcttatttgggaatctcattgctttgtcattgggtttgacccctaattttaaatcaaattttgatt tggcagaagatgctaaattacagctttcaaaagatacttacgatgatgatttagataatttattggcgca aattggagatcaatatgctgatttgtttttggcagctaagaatttatcagatgctattttactttcagatat cctaagagtaaatactgaaataactaaggctcccctatcagcttcaatgattaaacgctacgatgaacat catcaagacttgactcttttaaaagctttagttcgacaacaacttccagaaaagtataaagaaatcttttt tgatcaatcaaaaaacggatatgcaggttatattgatgggggagctagccaagaagaattttataaatt tatcaaaccaattttagaaaaaatggatggtactgaggaattattggtgaaactaaatcgtgaagattt gctgcgcaagcaacggacctttgacaacggctctattccccatcaaattcacttgggtgagctgcatgct attttgagaagacaagaagacttttatccatttttaaaagacaatcgtgagaagattgaaaaaatcttga cttttcgaattccttattatgttggtccattggcgcgtggcaatagtcgttttgcatggatgactcggaagt ctgaagaaacaattaccccatggaattttgaagaagttgtcgataaaggtgcttcagctcaatcatttat tgaacgcatgacaaactttgataaaaatcttccaaatgaaaaagtactaccaaaacatagtttgctttat gagtattttacggtttataacgaattgacaaaggtcaaatatgttactgaaggaatgcgaaaaccagca tttctttcaggtgaacagaagaaagccattgttgatttactcttcaaaacaaatcgaaaagtaaccgtta agcaattaaaagaagattatttcaaaaaaatagaatgttttgatagtgttgaaatttcaggagttgaag atagatttaatgcttcattaggtacctaccatgatttgctaaaaattattaaagataaagatttttttggat aatgaagaaaatgaagatatcttagaggatattgttttaacattgaccttatttgaagatagggagatg attgaggaaagacttaaaacatatgctcacctctttgatgataaggtgatgaaacagcttaaacgtcgcc gttatactggttggggacgtttgtctcgaaaattgattaatggtattagggataagcaatctggcaaaac aatattagatttttgaaatcagatggttttgccaatcgcaattttatgcagctgatccatgatgatagttt gacatttaaagaagacattcaaaaagcacaagtgtctggacaaggcgatagtttacatgaacatattgc aaatttagctggtagccctgctattaaaaaaggtattttacagactgtaaaagttgttgatgaattggtc aaagtaatggggcggcataagccagaaaatatcgttattgaaatggcacgtgaaaatcagacaactca aaagggccagaaaaattcgcgagagcgtatgaaacgaatcgaagaaggtatcaaagaattaggaagt cagattcttaaagagcatcctgttgaaaatactcaattgcaaaatgaaaagctctatctctattatctcca aaatggaagagacatgtatgtggaccaagaattagatattaatcgtttaagtgattatgatgtcgatgcc attgttccacaaagtttccttaaagacgattcaatagacaataaggtcttaacgcgttctgataaaaatc gtggtaaatcggataacgttccaagtgaagaagtagtcaaaaagatgaaaaactattggagacaactt ctaaacgccaagttaatcactcaacgtaagtttgataatttaacgaaagctgaacgtggaggtttgagtg aacttgataaagctggttttatcaaacgccaattggttgaaactcgccaaatcactaagcatgtggcaca aattttggatagtcgcatgaatactaaatacgatgaaaatgataaacttattcgagaggttaaagtgatt accttaaaatctaaattagtttctgacttccgaaaagatttccaattctataaagtacgtgagattaacaa ttaccatcatgcccatgatgcgtatctaaatgccgtcgttggaactgctttgattaagaaatatccaaaac ttgaatcggagtttgtctatggtgattataaagtttatgatgttcgtaaaatgattgctaagtctgagcaa gaaataggcaaagcaaccgcaaaatatttcttttactctaatatcatgaacttcttcaaaacagaaatta cacttgcaaatggagagattcgcaaacgccctctaatcgaaactaatggggaaactggagaaattgtct gggataaagggcgagattttgccacagtgcgcaaagtattgtccatgccccaagtcaatattgtcaaga aaacagaagtacagacaggcggattctccaaggagtcaattttaccaaaaagaaattcggacaagctt attgctcgtaaaaaagactgggatccaaaaaaatatggtggttttgatagtccaacggtagcttattcag tcctagtggttgctaaggtggaaaaagggaaatcgaagaagttaaaatccgttaaagagttactaggg atcacaattatggaaagaagttcctttgaaaaaaatccgattgacttttagaagctaaaggatataag gaagttaaaaaagacttaatcattaaactacctaaatatagtctttttgagttagaaaacggtcgtaaac ggatgctggctagtgccggagaattacaaaaaggaaatgagctggctctgccaagcaaatatgtgaatt ttttatatttagctagtcattatgaaaagttgaagggtagtccagaagataacgaacaaaaacaattgtt tgtggagcagcataagcattatttagatgagattattgagcaaatcagtgaattttctaagcgtgttattt tagcagatgccaatttagataaagttcttagtgcatataacaaacatagagacaaaccaatacgtgaac aagcagaaaatattattcatttatttacgttgacgaatcttggagctcccgctgcttttaaatattttgata caacaattgatcgtaaacgatatacgtctacaaaagaagttttagatgccactcttatccatcaatccat cactggtctttatgaaacacgcattgatttgagtcagctaggaggtgactaa	[156]

Table 7.19: GOI sequences used in this study

GOI	Sequence	Source
VioB	atgagcattctggatttcccgcgtatccacttccgtggctgggcccgtgtcaatgcgccgaccgcgaacc gcgatccgcacggccacatcgatatggccagcaataccgtggcgatggcgggtgagccgttcgacctgg cacgccatcctacggagttccaccgtcacctgcgctccctgggtccgcgcttcggcttggatggtcgtgct gacccggaaggcccgttcagcctggccgagggctacaacgctgccggtaacaaccacttttcgtgggag agcgcaaccgttagccacgtgcaatgggatggcggtgaggcggatcgtggtgacggtctggtcggtgct cgtttggcactgtggggtcactacaatgattatctgcgtaccaccttcaatcgtgctcgttgggtcgacag cgacccgacgcgccgtgacgctgcacaaatctatgcgggccaattcaccattagcccggctggtgccggt ccgggtacgccgtggctgtttacggcagacattgatgatagccatggtgcacgttggacgcgtggcggc cacattgcagagcgtggcggccacttcttggatgaagagtttggtctggcacgcctgtttcagttctctgt gccgaaagatcacccacattttctgtttcacccgggtccgtttgattccgaggcctggcgtcgtctgcaat tggctctggaggatgacgacgttctgggtctgaccgtgcaatatgcgttgttcaatatgagcaccccgcc tcagccgaacagcccggtttttcacgatatggtcggtgttgtcggtctgtggcgtcgtggtgaactggcg agctacccggctggtcgtctgctgcgtccgcgtcaaccgggtctgggtgacctgaccctgcgcgtcaacg gtggtcgcgttgcgctgaatttggcgtgtgccattccgttcagcactcgtgccgcgcagccaagcgcacc ggaccgcctgaccccggacctgggtgccaaactgccgctgggcgatctgctgctgcgtgatgaggacgg cgcactgttggcacgtgtgccgcaggctctgtaccaagactattggacgaatcacggtattgtggacctg ccgctgctgcgcgaaccgcgtggtagcttgaccctgagcagcgaactggcggagtggcgtgagcaagac tgggtcacccaaagcgacgcgtctaacctgtacctggaggcaccggatcgccgtcacggtcgctttttcc ctgagagcatcgcgctgcgcagctactttcgcggtgaagcgcgtgcgcgtccggatatcccgcatcgtat cgagggcatgggcctggtcggcgtcgaatctcgtcaggatggcgacgctgcggaatggcgtctgacggg tctgcgtccgggtccggcacgcattgttctggacgatggtgccgaggcgatccctctgcgtgttctgcctg acgattgggcgctggatgacgcgaccgtcgaagaagtggattacgccttttgtaccgccacgttatggc gtattacgagctggtgtatccattcatgagcgacaaggtgttttccctggctgatcgttgcaaatgtgaa acgtacgcacgtctgatgtggcagatgtgtgatccgcagaaccgcaacaagtcctattacatgccgagc acccgcgaactgtcggcaccgaaagctcgtttgttcttgaagtatctggcccacgtggaaggccaggcac gcctgcaagcacctccgccagcgggtccggcacgcattgaatctaaagcccagttggcggcagagctgc gtaaagccgtcgacctggagctgtctgtgatgctgcaatacctgtacgcggcgtatagcattccgaacta tgcacagggccaacaacgtgttcgtgacggtgcgtggaccgccgagcagctgcaactggcgtgcggtag cggtgaccgtcgccgtgatggcggtattcgtgcagcactgctggaaattgctcatgaagaaatgattcat tacctggtcgttaacaacctgctgatggccctgggcgagccgttctacgcgggtgtcccgctgatgggcg aagcggcacgtcaggcgtttggcctggacaccgagttcgctctggaaccgtttagcgaaagcacgctgg cacgttttgttcgtctggaatggccgcactttatcccagcaccgggcaaatccatcgcggactgctatgcc gccattcgtcaggcgttttggatctgccggacttgtttggtggcgaggcaggtaagcgtggcggtgaac accacctgttcctgaatgagctgaccaaccgtgcgcatccgggttatcaactggaagttttcgatcgcga ctcggcgctgtttggtattgcatttgtgaccgatcagggcgaaggtggcgctctggacagcccgcactac gaacatagccattttcaacgtctgcgtgaaatgagcgcgcgtatcatggctcaaagcgcaccgttcgaac cggcgctgccggcgttgcgtaatccggttctggatgagagcccgggttgccaacgtgtcgcagacggtc gtgcgcgtgcgctgatggcattgtaccaaggcgtttatgagctgatgtttgcgatgatggcgcagcactt cgccgtgaaaccgctgggtagcttgcgtcgcagccgcctgatgaacgcagcaatcgatctgatgaccgg tctgttgcgtccgctgagctgcgcgctgatgaacctgccaagcggcatcgccggtcgcacggccggtccg ccgctgccgggtccggttgacacccgtagctatgacgactacgcgctgggctgtcgcatgctggcacgcc gttgcgagcgtctgctggagcaggcgagcatgctggaaccgggttggctgccggatgcgcagatggagc tgctggatttctatcgtcgccaaatgctggacttggcgtgcggcaaactga	[8]

Table 7.19: GOI sequences used in this study

GOI	Sequence	Source
mScarlet-I	atggttagcaaaggcgaggcggttatcaaggagtttatgcgttttaaggttcacatggagggtagcatg aatggtcacgagttcgagatcgagggtgaaggcgagggtcgtccgtacgaaggcacccagaccgcgaa gctgaaagtgaccaagggtggcccgctgccgttcagctgggacatcctgagcccgcagttcatgtatgg cagccgtgcgtttatcaaacacccggcggacattccggattactataagcaaagcttcccggaaggtttt aaatgggagcgtgttatgaacttcgaagatggtggcgcggtgaccgttacccaggacaccagcctggag gatggcaccctgatttacaaggtgaaactgcgtggcaccaactttccgccggatggtccggttatgcaga agaaaacgatgggttgggaagcgagcaccgagcgtctgtatccggaagatggcgtgctgaagggtgat atcaaaatggcgctgcgtctgaaggacggtggccgttacctggcggattttaagaccacctataaagcg aagaaaccggtgcaaatgccgggtgcgtacaacgttgaccgtaaactggatattaccagccacaacga ggattataccgtggttgagcaatatgagcgtagcgagggtcgccacagcaccggcggcatggacgaact gtataagtga	CIDAR MoClo Extension
mCherry	atggtgagcaagggcgaggaggataacatggccatcatcaaggagttcatgcgcttcaaggttcacatg gagggctccgtgaacggccacgagttcgagatcgagggcgagggcgagggccgcccctacgagggcac ccagaccgccaagctgaaggtgaccaagggtggccccctgccttcgcctgggacatcctgtcccctcag ttcatgtacggctccaaggcctacgtgaagcaccccgccgacatccccgactacttgaagctgtccttcc ccgagggcttcaagtgggagcgcgtgatgaacttcgaggacggcggcgtggtgaccgtgacccaggac tcctccctgcaagacggcgagttcatctacaaggtgaagctgcgcggcaccaacttccctccgacggcc ccgtaatgcagaagaagactatgggctgggaggcctcctccgagcggatgtaccccgaggacggcgcg ctgaagggcgagatcaagcagaggctgaagctgaaggacggcggccactacgacgctgaggtcaaga ccacctacaaggccaagaagcccgtgcaactgcccggcgcgtacaacgtcaacatcaagttggacatca cctcccacaacgaggactacaccatcgtggaacagtacgaacgcgccgagggccgccactccaccggcg gcatggacgagctgtataagtaa	[156]
mRFP1	atggtgagcaagggcgaggaggataacatggccatcatcaaggagttcatgcgcttcaaggttcacatg gagggctccgtgaacggccacgagttcgagatcgagggcgagggcgagggccgcccctacgagggcac ccagaccgccaagctgaaggtgaccaagggtggccccctgccttcgcctgggacatcctgtcccctcag ttcatgtacggctccaaggcctacgtgaagcaccccgccgacatccccgactacttgaagctgtccttcc ccgagggcttcaagtgggagcgcgtgatgaacttcgaggacggcggcgtggtgaccgtgacccaggac tcctccctgcaagacggcgagttcatctacaaggtgaagctgcgcggcaccaacttccctccgacggcc ccgtaatgcagaagaagactatgggctgggaggcctcctccgagcggatgtaccccgaggacggcgcg ctgaagggcgagatcaagcagaggctgaagctgaaggacggcggccactacgacgctgaggtcaaga ccacctacaaggccaagaagcccgtgcaactgcccggcgcgtacaacgtcaacatcaagttggacatca cctcccacaacgaggactacaccatcgtggaacagtacgaacgcgccgagggccgccactccaccggcg gcatggacgagctgtataagtaa	[130]
sfGFP	atgcgtaaaggcgaggagctgttcactggtgtcgtccctattctggtggaactggatggtgatgtcaacg gtcataagttttccgtgcgtggcgagggtgaaggtgacgcaactaatggtaaactgacgctgaagttca tctgtactactggtaaactgccggtaccttggccgactctggtaacgacgctgacttatggtgttcagtgc tttgctcgttatccggaccatatgaagcagcatgacttcttcaagtccgccatgccggaaggctatgtgc aggaacgcacgatttcctttaaggatgacggcacgtacaaaacgcgtgcggaagtgaaatttgaaggc gataccctggtaaaccgcattgagctgaaaggcattgactttaaagaagacggcaatatcctgggccat aagctggaatacaattttaacagccacaatgtttacatcaccgccgataaacaaaaaaatggcattaaa gcgaattttaaaattcgccacaacgtggaggatggcagcgtgcagctggctgatcactaccagcaaaac actccaatcggtgatggtcctgttctgctgccagacaatcactatctgagcacgcaaagcgttctgtctaa agatccgaacgagaaacgcgatcatatggttctgctggagttcgtaaccgcagcgggcatcacgcatgg tatggatgaactgtacaaataa	[8]

Table 7.19: GOI sequences used in this study

GOI	Sequence	Source
sfCFP	atgcgtaaaggcgaagagctgttcactggtgtcgtccctattctggtggaactggatggtgatgtcaacg gtcataagttttccgtgcgtggcgagggtgaaggtgacgcaactaatggtaaactgacgctgaagttca tctgtactactggtaaactgccggtaccttggccgactctggtaacgacgctgacttggggtgttcagtgc tttgctcgttatccggaccatatgaagcagcatgacttcttcaagtccgccatgccggaaggctatgtgc aggaacgcacgatttccttaaggatgacggcacgtacaaaacgcgtgcggaagtgaaatttgaaggc gataccctggtaaaccgcattgagctgaaaggcattgactttaaagaagacggcaatatcctgggccat aagctggaatacaattacatcagcgacaatgtttacatcaccgccgataaacaaaaaaatggcattaaa gcgaattttaaaattcgccacaacgtggaggatggcagcgtgcagctggctgatcactaccagcaaaac actccaatcggtgatggtcctgttctgctgccagacaatcactatctgagcacgcaaagcgttctgtctaa agatccgaacgagaaacgcgatcatatggttctgctggagttcgtaaccgcagcgggcatcacgcatgg tatggatgaactgtacaaataa	CIDAR MoClo Extension
sfYFP	atgcgtaaaggcgaagagctgttcactggtgtcgtccctattctggtggaactggatggtgatgtcaacg gtcataagttttccgtgcgtggcgagggtgaaggtgacgcaactaatggtaaactgacgctgaagttca tctgtactactggtaaactgccggtaccttggccgactctggtaacgacgctgacttatggtgttcagtgc tttgctcgttatccggaccatatgaagcagcatgacttcttcaagtccgccatgccggaaggctatgtgc aggaacgcacgatttccttaaggatgacggcacgtacaaaacgcgtgcggaagtgaaatttgaaggc gataccctggtaaaccgcattgagctgaaaggcattgactttaaagaagacggcaatatcctgggccat aagctggaatacaattttaacagccacaatgtttacatcaccgccgataaacaaaaaaatggcattaaa gcgaattttaaaattcgccacaacgtggaggatggcagcgtgcagctggctgatcactaccagcaaaac actccaatcggtgatggtcctgttctgctgccagacaatcactatctgagctaccaaagcgttctgtctaa agatccgaacgagaaacgcgatcatatggttctgctggagttcgtaaccgcagcgggcatcacgcatgg tatggatgaactgtacaaataa	CIDAR MoClo Extension
GFPmut3b	atgcgtaaaggagaagaacttttcactggagttgtcccaattcttgttgaattagatggtgatgttaatg ggcacaaattttctgtcagtggagagggtgaaggtgatgcaacatacggaaaacttacccttaaattta tttgcactactggaaaactacctgttccatggccaacacttgtcactactttcggttatggtgttcaatgct ttgcgagatacccagatcatatgaaacagcatgactttttcaagagtgccatgcccgaaggttatgtaca ggaaagaactatatttttcaaagatgacgggaactacaagacacgtgctgaagtcaagtttgaaggtga taccccttgttaatagaatcgagttaaaaggtattgattttaaagaagatggaaacattcttggacacaaa ttggaatacaactataactcacacaatgtatacatcatggcagacaaacaaaagaatggaatcaaagtt aacttcaaaattagacacaacattgaagatggaagcgttcaactagcagaccattatcaacaaaatact ccaattggcgatggccctgtccttttaccagacaaccattacctgtccacacaatctgccctttcgaaaga tcccaacgaaaagagagaccacatggtccttcttgagtttgtaacagctgctgggattacacatggcatg gatgaactatacaaataataa	[112]
CtrE	atgacggtctgcgcaaaaaaacacgttcatctcactcgcgatgctgcggagcagttactggctgatattg atcgacgccttgatcagttattgcccgtggagggagaacgggatgttgtgggtgccgcgatgcgtgaag gtgcgctggcaccgggaaaacgtattcgccccatgttgctgttgctgaccgcccgcgatctgggttgcgc tgtcagccatgacggattactggatttggcctgtgcggtggaaatggtccacgcggcttcgctgatcctt gacgatatgccctgcatggacgatgcgaagctgcggcgcggacgccctaccattcattctcattacggag agcatgtggcaatactggcggcggttgccttgctgagtaaagcctttggcgtaattgccgatgcagatgg cctcacgccgctggcaaaaaatcgggcggtttctgaactgtcaaacgccatcggcatgcaaggattggtt cagggtcagttcaaggatctgtctgaaggggataagccgcgcagcgctgaagctattttgatgacgaat cactttaaaaccagcacgctgttttgtgcctccatgcagatggcctcgattgttgcgaatgcctccagcga agcgcgtgattgcctgcatcgtttttcacttgatcttggtcaggcatttcaactgctggacgatttgaccg atggcatgaccgacaccggtaaggatagcaatcaggacgccggtaaatcgacgctggtcaatctgttag gcccgagggcggttgaagaacgtctgagacaacatcttcagcttgccagtgagcatctctctgcggcctg ccaacacgggcacgccactcaacattttattcaggcctggtttgacaaaaaactcgctgccgtcagttaa	[27]

Table 7.19: GOI sequences used in this study

GOI	Sequence	Source
CtrB	atgaataatccgtcgttactcaatcatgcggtcgaaacgatggcagttggctcgaaaagttttgcgacag cctcaaagttatttgatgcaaaaacccggcgcagcgtactgatgctctacgcctggtgccgccattgtga cgatgttattgacgatcagacgctgggctttcaggcccggcagcctgccttacaaacgcccgaacaacgt ctgatgcaacttgagatgaaaacgcgccaggcctatgcaggatcgcagatgcacgaaccggcgtttgcg gcttttcaggaagtggctatggctcatgatatcgccccggcttacgcgtttgatcatctggaaggcttcgc catggatgtacgcgaagcgcaatacagccaactggatgatacgctgcgctattgctatcacgttgcagg cgttgtcggcttgatgatggcgcaaatcatgggcgtgcgggataacgccacgctggaccgcgcctgtga ccttgggctggcatttcagttgaccaatattgctcgcgatattgtggacgatgcgcatgcgggccgctgtt atctgccggcaagctggctggagcatgaaggtctgaacaaagagaattatgcggcacctgaaaaccgtc aggcgctgagccgtatcgcccgtcgtttggtgcaggaagcagaaccttactatttgtctgccacagccgg cctggcagggttgcccctgcgttccgcctgggcaatcgctacggcgaagcaggtttaccggaaaatagg tgtcaaagttgaacaggccggtcagcaagcctgggatcagcggcagtcaacgaccacgcccgaaaaat taacgctgctgctggccgcctctggtcaggcccttacttcccggatgcgggctcatcctccccgccctgcg catctctggcagcgcccgctctag	[27]
CtrI	atgaaaccaactacggtaattggtgcaggcttcggtggcctggcactggcaattcgtctacaagctgcgg ggatccccgtcttactgcttgaacaacgtgataaacccggcggtcgggcttatgtctacgaggatcaggg gtttacctttgatgcaggcccgacggttatcaccgatcccagtgccattgaagaactgtttgcactggca ggaaaacagttaaaagagtatgtcgaactgctgccggttacgccgttttaccgcctgtgttgggagtcag ggaaggtctttaattacgataacgatcaaacccggctcgaagcgcagattcagcagtttaatccccgcg atgtcgaaggttatcgtcagtttctggactattcacgcgcggtgtttaaagaaggctatctaaagctcgg tactgtccctttttatcgttcagagacatgcttcgcgccgcacctcaactggcgaaactgcaggcatgga gaagcgtttacagtaaggttgccagttacatcgaagatgaacatctgcgccaggcgttttctttccactc gctgttggtgggcggcaatcccttcgccacctcatccatttatacgttgatacacgcgctggagcgtgagt ggggcgtctggtttccgcgtggcggcaccggcgcattagttcaggggatgataaagctgtttcaggatct gggtggcgaagtcgtgttaaacgccagagtcagccatatggaaacgacaggaaacaagattgaagccg tgcatttagaggacggtcgcaggttcctgacgcaagccgtcgcgtcaaatgcagatgtggttcatacctа tcgcgacctgttaagccagcaccctgccgcggttaagcagtccaacaaactgcagactaagcgcatgag taactctctgtttgtgctctattttggtttgaatcaccatcatgatcagctcgcgcatcacacggtttgtttc ggcccgcgttaccgcgagctgattgacgaaatttttaatcatgatggcctcgcagaggacttctcacttta tctgcacgcgccctgtgtcacggattcgtcactggcgcctgaaggttgcggcagttactatgtgttggcgc cggtgccgcatttaggcaccgcgaacctcgactggacggttgaggggccaaaactacgcgaccgtattt ttgcgtaccttgagcagcattacatgcctggcttacggagtcagctggtcacgcaccggatgtttacgcc gtttgattttcgcgaccagcttaatgcctatcatggctcagccttttctgtggagcccgttcttacccagag cgcctggtttcggccgcataaccgcgataaaaccattactaatctctacctggtcggcgcaggcacgcat cccggcgcaggcattcctggcgtcatcggctcggcaaaagcgacagcaggtttgatgctggaggatctg atatga	[27]

Table 7.19: GOI sequences used in this study

GOI	Sequence	Source
CtrY	atgcaaccgcattatgatctgattctcgtgggggctggactcgcgaatggccttatcgccctgcgacttca gcagcagcaacctgatatgcgtattttgcttatcgacgccgcaccccaggcgggcgggaatcatacgtg gtcatttcaccacgatgatttgactgagagccaacatcgttggatagctccgctggtggttcatcactggc ccgactatcaggtacgctttcccacacgccgtcgtaagctgaacagcggctacttttgtattacttctcag cgtttcgctgaggttttacagcgacagtttggcccgcacttgtggatggataccgcggtcgcagaggtta atgcggaatctgttcggttgaaaaagggtcaggttatcggtgcccgcgcggtgattgacgggcggggtt atgcggcaaattcagcactgagcgtgggcttccaggcgtttattggccaggaatggcgattgagccacc cgcatggtttatcatctcccattatcatggatgccacggtcgatcagcaaaatggttatcgcttcgtgtac agcctgccgctctcgccgaccagattgttaattgaagatacgcactatattgataatgcgacattagatc ctgaatgcgcgcggcaaaatatttgcgactatgccgcgcaacagggttggcagcttcagacactgctgc gagaagaacagggcgccttacccattactctgtcgggcaatgccgacgcattctggcagcagcgccccc tggcctgtagtggattacgtgccggtctgttccatcctaccaccggctattcactgccgctggcggttgcc gtggccgaccgcctgagtgcacttgatgtctttacgtcggcctcaattcaccatgccattacgcattttgc ccgcgagcgctggcagcagcagggctttttccgcatgctgaatcgcatgctgtttttagccggacccgcc gattcacgctggcgggttatgcagcgtttttatggtttacctgaagatttaattgcccgtttttatgcggg aaaactcacgctgaccgatcggctacgtattctgagcggcaagccgcctgttccggtattagcagcattg caagccattatgacgactcatcgttaa	[27]
mKate	atggaactgattaaagaaaacatgcatatgaaactgtatatggaaggcaccgtgaacaaccatcacttt aaatgtaccagcgaaggtgaaggtaaaccgtatgaaggcacccagaccatgcgtattaaagcagttga aggtggtccgctgccgtttgcatttgatattctggcaaccagctttatgtatggcagcaaaacctttatta accatacccagggtatcccggatttttcaaacagagctttccggaaggttttacctgggaacgtgttacc acctatgaagatggtggtgttctgaccgcaacccaggataccagtctgcaggatggttgtctgatttata atgtgaaaattcgcggtgtgaactttccgagcaatggtccggttatgcagaaaaaaaaccctgggttggg aagcaagcaccgaaaccctgtatccggcagatggtggcctggaaggtcgtgcagatatggcactgaaa ctggttggtggtggtcatctgatttgcaatctgaaaaccacctatcgtagcaaaaaaacctgccaaaaacc tgaaaatgcctggcgtttattatgttgatcgtcgtctggaacgtatcaaagaggcagataaagaaaccta tgtggaacagcatgaagttgcagttgcacgttattgtgatctgccgagcaaactgggtcatcgttaataa	[27]

7.6.1.8 Terminators used in this study

Table 7.20: TF sequences used in this study

Terminator	Sequence	Source
L3S3P21	ccaattattgaaggcctccctaacgggggggccttttttttgtttctggt ctccc	[253]
ECK120010793	tacgtaaaaacccgcttcggcgggtttttacttt	[253]
T1 (L3S2P55)	ctcggtaccaaagacgaacaataagacgctgaaaagcgtctttttt cgttttggtcc	[250]
T2 (L3S2P21)	ctcggtaccaaattccagaaaagaggcctcccgaaaggggggcctt ttttcgttttggtcc	[250]
T3 (ECK120033737)	ggaaacacagaaaaaagcccgcacctgacagtgcgggctttttttt tcgaccaaagg	[250]
T4 (ECK120029600)	ttcagccaaaaaacttaagaccgccggtcttgtccactaccttgcag taatgcggtggacaggatcggcggttttctttttctcttctcaa	[250]
t500	caaaGCCCGCCgaaaGGCGGGCttttttttt	[254]

Table 7.20: TF sequences used in this study

Terminator	Sequence	Source
B1001	aaaaaaaaaccccgcttcggcggggttttttttt	iGEM B1001
B1002	cgcaaaaaaccccgcttcggcggggttttttcgc	iGEM B1002
B0015	ccaggcatcaaataaaacgaaaggctcagtcgaaagactgggcctttcgttttatctgttgtttgtcggtgaacgctctctactagagtcacactggctcaccttcgggtgggcctttctgcgtttata	iGEM B0015
tL3	aatggcgatgacgcatcctcacgataatatccgggtaggcgcaatcactttcgtctctactccgttacaaagcgaggctgggtatttcccggcctttctgttatccgaaatccactgaaagcacagcggctggctgaggagataaataataaacgaggggctgtatgcacaaagcatcttctgttgagttaagaacgagtatcgagatggcacatagccttgctcaaattggaatcaggtttgtgccaataccagtagaaacagacgaagaa	[251]
rgnB	gatggtagtgtggggtctccccatgcgagagtagggaactgccaggcatcaaataaaacgaaaggctcagtcgaaagactgggcctttcgttttatctgttgtttgtcggtgaacgctctcctgagtaggacaaatccgccgggagcggatttgaacgttgcgaagcaacggcccggagggtggcgggcaggacgcccgccataaactgccaggcatcaaattaagcagaaggccatcctgacggatggccttttgcgt	[251]
rrnB T1	atttgtcctactcaggagagcgttcaccgacaaacaacagataaaacgaaaggcccagtctttcgactgagcctttcgttttatttg	[250]
Lambda t0	gactcctgttgatagatccagtaatgacctcagaactccatctggatttgttcagaacgctcggttgccgccgggcgtttttttattggtgagaat	[250]
T1/TE	ctcgagccaggcatcaaataaaacgaaaggctcagtcgaaagactgggcctttcgttttatctgtttttgtcggtgaacgctctctactagagtcacactggctcaccttcgggtgggcctttctgcgtttata	[131]
His operon terminator	tccggcaaaaaagggcaaggtgtcaccaccctgccctttttctttaaaaccgaaaaga	[8]

7.6.2 Plasmids

Plasmids used in this study are organised by figures.

Table 7.21: Plasmids used in Figure 4.B

Plasmid	Description	Source
H2	AraC - pBAD - RBS$_V$*ioB* - VioB-mCherry - L3S2P55 - ColE1 - CamR	[8]
B0034_GFP	J23106 - B0034 - GFPmut3b - B0015 - pMB1 - CamR	[255]

Table 7.22: Plasmids used in Figure 13.B

Plasmid	Description	Source
pJBL4826	P_{tet} – B0034 – luxR – B0015 – P_{lux} – STAR 5 – t500 – ColE1 – AmpR	[130]
pJBL4882	J23119 – STAR Target 5 – RBS_{RFP} – mRFP – TrrnB – p15A – CamR	[130]
pJBL5945	P_{tet} – B0034 – luxR – B0015 – P_{lux} – STAR 8 – t500 – ColE1 – AmpR	[130]
pJBL5938	J23119 – STAR Target 8 – RBS_{RFP} – mRFP – TrrnB – p15A – CamR	[130]
pJBL5946	P_{tet} – B0034 – luxR – B0015 – P_{lux} – STAR 5 – t500 – ColE1 – AmpR	[130]
pJBL5939	J23119 – STAR Target 6 – RBS_{RFP} – mRFP – TrrnB – p15A – CamR	[130]

Table 7.23: Plasmids used in Figure 14.A-B

Plasmid	Description	Source
pJBL4826	P_{tet} – B0034 – luxR – B0015 – P_{lux} – STAR 5 – t500 – ColE1 – AmpR	[130]
pJBL4882	J23119 – STAR Target 5 – RBS_{RFP} – mRFP – TrrnB – p15A – CamR	[130]
pJBL5946	P_{tet} – B0034 – luxR – B0015 – P_{lux} – STAR 5 – t500 – ColE1 – AmpR	[130]
pJBL5939	J23119 – STAR Target 6 – RBS_{RFP} – mRFP – TrrnB – p15A – CamR	[130]

Table 7.24: Plasmids used in Figure 15.A

Plasmid	Description	Source
pAB127	P_{tet} – B0034 – luxR – B0015 – P_{lux} – STAR6_toehold0 – t500 – ColE1 – SpecR	This study
pJBL5939	J23119 – STAR Target 6 – RBS_{RFP} – mRFP – TrrnB – p15A – CamR	[130]

Table 7.25: Plasmids used in Figure 15.B

Plasmid	Description	Source
pAB128	P_{tet} – B0034 – luxR – B0015 – P_{lux} – anti-STAR6_toehold0 – t500 – ColE1 – SpecR	This study

Table 7.25: Plasmids used in Figure 15.B

Plasmid	Description	Source
pJBL5939	J23119 – STAR Target 6 – RBS_{RFP} – mRFP – TrrnB – p15A – CamR	[130]

Table 7.26: Plasmids used in Figure 15.C

Plasmid	Description	Source
pAB129	P_{tet} – B0034 – luxR – B0015 – P_{lux} – STAR6_toehold0 – t500 – P_{lux} – anti-STAR6_toehold0 – t500 – ColE1 – SpecR	This study
pJBL5939	J23119 – STAR Target 6 – RBS_{RFP} – mRFP – TrrnB – p15A – CamR	[130]

Table 7.27: Plasmids used in Figure 16.B-C

Plasmid	Description	Source
pAB127	P_{tet} – B0034 – luxR – B0015 – P_{lux} – STAR6_toehold0 – t500 – ColE1 – SpecR	This study
pAB147	J23100 – STAR6_toehold0 – t500 – ColE1 – SpecR	This study
pAB127	P_{tet} – B0034 – luxR – B0015 – P_{lux} – STAR6_toehold0 – t500 – ColE1 – SpecR	This study
pAB161	P_{tet} – B0034 – luxR – B0015 – J23100 – STAR6_toehold0 – t500 – P_{lux} – anti-STAR6_toehold0 – t500 – ColE1 – SpecR	This study
pJBL5939	J23119 – STAR Target 6 – RBS_{RFP} – mRFP – TrrnB – p15A – CamR	[130]

Table 7.28: Plasmids used in Figure 18.B

Plasmid	Description	Source
pAB161	P_{tet} – B0034 – luxR – B0015 – J23100 – STAR6_toehold0 – t500 – P_{lux} – anti-STAR6_toehold0 – t500 – ColE1 – SpecR	This study
pJBL5939	J23119 – STAR Target 6 – RBS_{RFP} – mRFP – TrrnB – p15A – CamR	[130]
pAB179	J23119 – Deoptimised STAR Target 6 v1 – RBS_{RFP} – mRFP – TrrnB – p15A – CamR	This study
pAB180	J23119 – Deoptimised STAR Target 6 v2 – RBS_{RFP} – mRFP – TrrnB – p15A – CamR	This study

Table 7.29: Plasmids used in Figure 19.B

Plasmid	Description	Source
pAB127	P_{tet} – B0034 – luxR – B0015 – P_{lux} – STAR6_toehold0 – t500 – ColE1 – SpecR	This study
pJBL5939	J23119 – STAR Target 6 – RBS_{RFP} – mRFP – TrrnB – p15A – CamR	[130]
pAB262	J23119 – STAR Target 6 – STAR Target 6 – RBS_{RFP} – mRFP – TrrnB – p15A – CamR	[130]

Table 7.30: Plasmids used in Figure 19.C

Plasmid	Description	Source
pAB161	P_{tet} – B0034 – luxR – B0015 – J23100 – STAR6_toehold0 – t500 – P_{lux} – anti-STAR6_toehold0 – t500 – ColE1 – SpecR	This study
pJBL5939	J23119 – STAR Target 6 – RBS_{RFP} – mRFP – TrrnB – p15A – CamR	[130]
pAB262	J23119 – STAR Target 6 – STAR Target 6 – RBS_{RFP} – mRFP – TrrnB – p15A – CamR	[130]

Table 7.31: Plasmids used in Figure 20.B-D

Plasmid	Description	Source
pAB161	P_{tet} – B0034 – luxR – B0015 – J23100 – STAR6_toehold0 – t500 – P_{lux} – anti-STAR6_toehold0 – t500 – ColE1 – SpecR	This study
pAB232	P_{tet} – B0034 – luxR – B0015 – J23100 – STAR6_toehold1 – t500 – P_{lux} – anti-STAR6_toehold0 – t500 – ColE1 – SpecR	This study
pAB233	P_{tet} – B0034 – luxR – B0015 – J23100 – STAR6_toehold2 – t500 – P_{lux} – anti-STAR6_toehold0 – t500 – ColE1 – SpecR	This study
pAB234	P_{tet} – B0034 – luxR – B0015 – J23100 – STAR6_toehold3 – t500 – P_{lux} – anti-STAR6_toehold0 – t500 – ColE1 – SpecR	This study
pAB235	P_{tet} – B0034 – luxR – B0015 – J23100 – STAR6_toehold4 – t500 – P_{lux} – anti-STAR6_toehold0 – t500 – ColE1 – SpecR	This study
pAB236	P_{tet} – B0034 – luxR – B0015 – J23100 – STAR6_toehold5 – t500 – P_{lux} – anti-STAR6_toehold0 – t500 – ColE1 – SpecR	This study
pJBL5939	J23119 – STAR Target 6 – RBS_{RFP} – mRFP – TrrnB – p15A – CamR	[130]

Table 7.32: Plasmids used in Figure 21.B-D

Plasmid	Description	Source
pAB409	AraC - P_{araBAD} - RBSc33 - sfGFP - T2 - ColE1 - SpecR	This study
pAB252	P_{tet} - B0034 - luxR - T1 - P_{lux} - RBSc33 - sfGFP - T2 - ColE1 - SpecR	This study

Table 7.33: Plasmids used in Figure 22.A

Plasmid	Description	Source
pAB271	AraC – P_{araBAD} – STAR6_toehold2 – t500 – ColE1 – SpecR	This study
pAB278	P_{tet} – B0034 – luxR – B0015 – AraC – P_{araBAD} – STAR6_toehold2 – t500 – Buffer 1 – P_{lux} – anti-STAR6_toehold2 – t500 – ColE1 – SpecR	This study
pAB517	J23100 – STAR Target 6 – RBS_{Bujard} – VioB-mCherry – L3S2P55 – p15A – CamR	This study

Table 7.34: Plasmids used in Figure 23.B

Plasmid	Description	Source
pAB278	P_{tet} – B0034 – luxR – B0015 – AraC – P_{araBAD} – STAR6_toehold2 – t500 – Buffer 1 – P_{lux} – anti-STAR6_toehold0 – t500 – ColE1 – SpecR	This study
pAB289	P_{tet} – B0034 – luxR – B0015 – AraC – P_{araBAD} – STAR6_toehold2 – t500 – Buffer 2 – P_{lux} – anti-STAR6_toehold0 – t500 – ColE1 – SpecR	This study
pAB300	P_{tet} – B0034 – luxR – B0015 – AraC – P_{araBAD} – STAR6_toehold2 – t500 – Buffer 3 – P_{lux} – anti-STAR6_toehold2 – t500 – ColE1 – SpecR	This study
pJBL5939	J23119 – STAR Target 6 – RBS_{RFP} – mRFP – TrrnB – p15A – CamR	[130]

Table 7.35: Plasmids used in Figure 24.B

Plasmid	Description	Source
pAB300	P_{tet} – B0034 – luxR – B0015 – AraC – P_{araBAD} – STAR6_toehold2 – t500 – Buffer 3 – P_{lux} – anti-STAR6_toehold2 – t500 – ColE1 – SpecR	This study
pAB517	J23100 – STAR Target 6 – RBS_{Bujard} – VioB-mCherry – L3S2P55 – p15A – CamR	This study

Table 7.36: Plasmids used in Figure 25.B-C

Plasmid	Description	Source
pAB271	AraC – P_{araBAD} – STAR6_toehold2 – t500 – ColE1 – SpecR	This study
pAB298	P_{tet} – B0034 – luxR – B0015 – P_{lux} – anti-STAR6_toehold2 – t500 – ColE1 – SpecR	This study
pAB300	P_{tet} – B0034 – luxR – B0015 – AraC – P_{araBAD} – STAR6_toehold2 – t500 – Buffer 3 – P_{lux} – anti-STAR6_toehold2 – t500 – ColE1 – SpecR	This study
pAB317	P_{tet} – B0034 – luxR – B0015 – AraC – P_{araBAD} – STAR6 – t500 – Buffer 3 – P_{lux} – anti-STAR6 – t500 – ColE1 – SpecR	This study
pAB303	AraC – P_{araBAD} – STAR6 – t500 – ColE1 – SpecR	This study
pAB304	P_{tet} – B0034 – luxR – B0015 – P_{lux} – anti-STAR6 – t500 – ColE1 – SpecR	This study
pAB517	J23100 – STAR Target 6 – RBS_{Bujard} – VioB-mCherry – L3S2P55 – p15A – CamR	This study

Table 7.37: Plasmids used in Figure 26.B

Plasmid	Description	Source
pAB300	P_{tet} – B0034 – luxR – B0015 – AraC – P_{araBAD} – STAR6_toehold2 – t500 – Buffer 3 – P_{lux} – anti-STAR6_toehold2 – t500 – ColE1 – SpecR	This study
pAB317	P_{tet} – B0034 – luxR – B0015 – AraC – P_{araBAD} – STAR6 – t500 – Buffer 3 – P_{lux} – anti-STAR6 – t500 – ColE1 – SpecR	This study

Table 7.38: Plasmids used in Figure 27.B-C

Plasmid	Description	Source
pAB300	P_{tet} – B0034 – luxR – B0015 – AraC – P_{araBAD} – STAR6_toehold2 – t500 – Buffer 3 – P_{lux} – anti-STAR6_toehold2 – t500 – ColE1 – SpecR	This study
pJBL5939	J23119 – STAR Target 6 – RBS_{RFP} – mRFP – TrrnB – p15A – CamR	[130]

Table 7.39: Plasmids used in Figure 30.A

Plasmid	Description	Source
pAB252	P_{tet} – B0034 – luxR – T1 – P_{lux} – RBSc33 – sfGFP – T2 – ColE1 – SpecR	This study
pAB253	P_{tet} – B0034 – rpaR – T1 – P_{lux} – RBSc33 – sfGFP – T2 – ColE1 – SpecR	This study

Table 7.40: Plasmids used in Figure 31.B+D

Plasmid	Description	Source
pAB405	P_{lux} – RBSc33 – sfGFP – T2 – ColE1 – SpecR	This study
pAB252	P_{tet} – B0034 – luxR – T1 – P_{lux} – RBSc33 – sfGFP – T2 – ColE1 – SpecR	This study
pAB253	P_{tet} – B0034 – rpaR – T1 – P_{lux} – RBSc33 – sfGFP – T2 – ColE1 – SpecR	This study
pAB387	CRIM plasmid integrated in BW25113 [J23100 – RBSc33 – LuxI – T1 – P_{tet} – B0034 – RpaR – B0015 – R6K – KanR]	This study
pAB398	CRIM plasmid integrated in BW25113 [J23100 – RBSc33 – RpaI – T1 – P_{tet} – B0034 – LuxR – B0015 – R6K – KanR]	This study

Table 7.41: Plasmids used in Figure 33.B-D

Plasmid	Description	Source
pAB420	P_{tet} – B0034 – luxR – T1 – P_{lux} – dBroccoli – T2 – ColE1 – SpecR	This study

Table 7.42: Plasmids used in Figure 34

Plasmid	Description	Source
pAB405	P_{lux} – dBroccoli – T2 – ColE1 – SpecR	This study
pAB420	P_{tet} – B0034 – luxR – T1 – P_{lux} – dBroccoli – T2 – ColE1 – SpecR	This study
pAB421	P_{tet} – B0034 – rpaR – T1 – P_{lux} – dBroccoli – T2 – ColE1 – SpecR	This study
pAB387	CRIM plasmid integrated in BW25113 [J23100 – RBSc33 – LuxI – T1 – P_{tet} – B0034 – RpaR – B0015 – R6K – KanR]	This study
pAB398	CRIM plasmid integrated in BW25113 [J23100 – RBSc33 – RpaI – T1 – P_{tet} – B0034 – LuxR – B0015 – R6K – KanR]	This study

Table 7.43: Plasmids used in Figure 35.C-D

Plasmid	Description	Source
pAB420	P_{tet} – B0034 – luxR – T1 – P_{lux} – dBroccoli – T2 – ColE1 – SpecR	This study
pAB421	P_{tet} – B0034 – rpaR – T1 – P_{lux} – dBroccoli – T2 – ColE1 – SpecR	This study

Table 7.44: Plasmids used in Figure 36.C

Plasmid	Description	Source
pAB300	P_{tet} – B0034 – luxR – B0015 – AraC – P_{araBAD} – STAR6_toehold2 – t500 – Buffer 3 – P_{lux} – anti-STAR6_toehold2 – t500 – ColE1 – SpecR	This study
pAB401	P_{tet} – B0034 – RpaR – B0015 – AraC – P_{araBAD} – STAR6_toehold2 – t500 – Buffer 3 – P_{lux} – anti-STAR6_toehold2 – t500 – ColE1 – SpecR	This study
pJBL5939	J23119 – STAR Target 6 – RBS_{RFP} – mRFP – TrrnB – p15A – CamR	[130]

Table 7.45: Plasmids used in Figure 37.C

Plasmid	Description	Source
pAB300	P_{tet} – B0034 – luxR – B0015 – AraC – P_{araBAD} – STAR6_toehold2 – t500 – Buffer 3 – P_{lux} – anti-STAR6_toehold2 – t500 – ColE1 – SpecR	This study
pAB557	P_{tet} – B0034 – RiboJ – luxR – B0015 – AraC – P_{araBAD} – STAR6_toehold2 – t500 – Buffer 3 – P_{lux} – anti-STAR6_toehold2 – t500 – ColE1 – SpecR	This study
pAB545	P_{tet} – B0030 – luxR – B0015 – AraC – P_{araBAD} – STAR6_toehold2 – t500 – Buffer 3 – P_{lux} – anti-STAR6_toehold2 – t500 – ColE1 – SpecR	This study
pAB401	P_{tet} – B0034 – RpaR – B0015 – AraC – P_{araBAD} – STAR6_toehold2 – t500 – Buffer 3 – P_{lux} – anti-STAR6_toehold2 – t500 – ColE1 – SpecR	This study
pJBL5939	J23119 – STAR Target 6 – RBS_{RFP} – mRFP – TrrnB – p15A – CamR	[130]

Table 7.46: Plasmids used in Figure 37.D

Plasmid	Description	Source
pAB300	P_{tet} – B0034 – luxR – B0015 – AraC – P_{araBAD} – STAR6_toehold2 – t500 – Buffer 3 – P_{lux} – anti-STAR6_toehold2 – t500 – ColE1 – SpecR	This study
pAB570	P_{tet} – B0034 – luxR – B0015 – AraC – P_{araBAD} – STAR6_toehold2 – t500 – Buffer 3 – P_{luxA} – anti-STAR6_toehold2 – t500 – ColE1 – SpecR	This study
pAB571	P_{tet} – B0034 – luxR – B0015 – AraC – P_{araBAD} – STAR6_toehold2 – t500 – Buffer 3 – P_{luxB} – anti-STAR6_toehold2 – t500 – ColE1 – SpecR	This study
pAB401	P_{tet} – B0034 – RpaR – B0015 – AraC – P_{araBAD} – STAR6_toehold2 – t500 – Buffer 3 – P_{lux} – anti-STAR6_toehold2 – t500 – ColE1 – SpecR	This study

Table 7.46: Plasmids used in Figure 37.D

Plasmid	Description	Source
pJBL5939	J23119 – STAR Target 6 – RBS_{RFP} – mRFP – TrrnB – p15A – CamR	[130]

Table 7.47: Plasmids used in Figure 42.A-B

Plasmid	Description	Source
pAB420	P_{tet} – B0034 – luxR – T1 – P_{lux} – dBroccoli – T2 – ColE1 – SpecR	This study
pAB421	P_{tet} – B0034 – rpaR – T1 – P_{lux} – dBroccoli – T2 – ColE1 – SpecR	This study

Table 7.48: Plasmids used in Figure 43.A-B

Plasmid	Description	Source
pAB420	P_{tet} – B0034 – luxR – T1 – P_{lux} – dBroccoli – T2 – ColE1 – SpecR	This study
pAB421	P_{tet} – B0034 – rpaR – T1 – P_{lux} – dBroccoli – T2 – ColE1 – SpecR	This study

Table 7.49: Plasmids used in Figure 44.B

Plasmid	Description	Source
pAB300	P_{tet} – B0034 – luxR – B0015 – AraC – P_{araBAD} – STAR6_toehold2 – t500 – Buffer 3 – P_{lux} – anti-STAR6_toehold2 – t500 – ColE1 – SpecR	This study
pAB557	P_{tet} – B0034 – RiboJ – luxR – B0015 – AraC – P_{araBAD} – STAR6_toehold2 – t500 – Buffer 3 – P_{lux} – anti-STAR6_toehold2 – t500 – ColE1 – SpecR	This study
pJBL5939	J23119 – STAR Target 6 – RBS_{RFP} – mRFP – TrrnB – p15A – CamR	[130]

Table 7.50: Plasmids used in Figure 45.B

Plasmid	Description	Source
pAB401	P_{tet} – B0034 – RpaR – B0015 – AraC – P_{araBAD} – STAR6_toehold2 – t500 – Buffer 3 – P_{lux} – anti-STAR6_toehold2 – t500 – ColE1 – SpecR	This study

Table 7.50: Plasmids used in Figure 45.B

Plasmid	Description	Source
pJBL5939	J23119 – STAR Target 6 – RBS_{RFP} – mRFP – TrrnB – p15A – CamR	[130]

Table 7.51: Plasmids used in Figure 49.B

Plasmid	Description	Source
B0034_mKate	J23106 - B0034 - mKate - B0015 - pMB1 - CamR	[27]
pAB81	P_{RAND14} - RBS8B - dCas9 - rrnB T1 - P_{araBAD} - HH - gRNA(LeuLp) - HDV - p15A - AmpR	This study

Table 7.52: Plasmids used in Figure 50

Plasmid	Description	Source
pAB81	P_{RAND14} - RBS8B - dCas9 - rrnB T1 - P_{araBAD} - HH - gRNA(LeuLp) - HDV - p15A - AmpR	This study
pAB60	P_{RAND14} - RBS8B - dCas9 - rrnB T1 - P_{araBAD} - HH - gRNA(HisLp) - HDV - p15A - AmpR	This study
pAB117	P_{RAND14} - RBS8B - dCas9 - rrnB T1 - P_{araBAD} - HH - gRNA(LeuLp) - HDV - P_{araBAD} - HH - gRNA(HisLp) - HDV - p15A - AmpR	This study

Table 7.53: Plasmids used in Figure 51

Plasmid	Description	Source
pAB81	P_{RAND14} - RBS8B - dCas9 - rrnB T1 - P_{araBAD} - HH - gRNA(LeuLp) - HDV - p15A - AmpR	This study
pAB60	P_{RAND14} - RBS8B - dCas9 - rrnB T1 - P_{araBAD} - HH - gRNA(HisLp) - HDV - p15A - AmpR	This study
pAB117	P_{RAND14} - RBS8B - dCas9 - rrnB T1 - P_{araBAD} - HH - gRNA(LeuLp) - HDV - P_{araBAD} - HH - gRNA(HisLp) - HDV - p15A - AmpR	This study

Table 7.54: Plasmids used in Figure 52

Plasmid	Description	Source
pAB127	P_{tet} – B0034 – luxR – B0015 – P_{lux} – STAR6_toehold0 – t500 – ColE1 – SpecR	This study

Table 7.54: Plasmids used in Figure 52

Plasmid	Description	Source
pAB96	P_{RAND14} - RBS8B - dCas9 - rrnB T1 - J23119 - STAR Target 6 - HH - gRNA(LeuLp) - HDV - p15A - AmpR	This study
pAB205	P_{RAND14} - RBS8B - dCas9 - rrnB T1 - J23119 - STAR Target 6 - HH - gRNA(LeuLp, End-0: A→C) - HDV - p15A - AmpR	This study
pAB58	P_{RAND14} - RBS8B - dCas9 - rrnB T1 - P_{araBAD} - random gRNA - p15A - AmpR	This study

Table 7.55: Plasmids used in Figure 53.B

Plasmid	Description	Source
pAB300	P_{tet} – B0034 – luxR – B0015 – AraC – P_{araBAD} – STAR6_toehold2 – t500 – Buffer 3 – P_{lux} – anti-STAR6_toehold2 – t500 – ColE1 – SpecR	This study
pAB205	P_{RAND14} - RBS8B - dCas9 - rrnB T1 - J23119 - STAR Target 6 - HH - gRNA(LeuLp, End-0: A→C) - HDV - p15A - AmpR	This study

Table 7.56: Plasmids used in Figure 55.B-F

Plasmid	Description	Source
pAB127	P_{tet} – B0034 – luxR – B0015 – P_{lux} – STAR6_toehold0 – t500 – ColE1 – SpecR	This study
pAB162	P_{RAND14} - RBS8B - dCas9 - rrnB T1 - J23119 - STAR Target 6 - HH - sRNA(sfGFP) - p15A - AmpR	This study
pAB125	P_{RAND14} - RBS8B - dCas9 - rrnB T1 - J23119 - STAR Target 6 - HH - sRNA(leuB) - p15A - AmpR	This study
pAB154	P_{RAND14} - RBS8B - dCas9 - rrnB T1 - J23119 - STAR Target 6 - HH - sRNA(metA) - p15A - AmpR	This study

Table 7.57: Plasmids used in Figure 56.B

Plasmid	Description	Source
pAB559	P_{tet} – B0034 – luxR – B0015 – pBAD – N1 sRNA[2] – ECK120010793 - P_{lux} – B1001 – pBR322 – CamR	This study

[2]N1 sRNA sequence: gtgaattcgcggccgcttctagagtcggcgctgggggagctatatttgtactagtagcggccgctgcaggcatgcgaga gtagggaactg [167]

Table 7.58: Plasmids used in Figure 58.B

Plasmid	Description	Source
pAB271	AraC – P_{araBAD} – STAR6_toehold2 – t500 – ColE1 – SpecR	This study
pAB517	J23100 – STAR Target 6 – RBS_{Bujard} – VioB-mCherry – L3S2P55 – p15A – CamR	This study

Table 7.59: Plasmids used in Figure 59.B

Plasmid	Description	Source
pAB300	P_{tet} – B0034 – luxR – B0015 – AraC – P_{araBAD} – STAR6_toehold2 – t500 – Buffer 3 – P_{lux} – anti-STAR6_toehold2 – t500 – ColE1 – SpecR	This study
pAB517	J23100 – STAR Target 6 – RBS_{Bujard} – VioB-mCherry – L3S2P55 – p15A – CamR	This study

Table 7.60: Plasmids used in Figure 60.C-H

Plasmid	Description	Source
pAB300	P_{tet} – B0034 – luxR – B0015 – AraC – P_{araBAD} – STAR6_toehold2 – t500 – Buffer 3 – P_{lux} – anti-STAR6_toehold0 – t502 – ColE1 – SpecR	This study
pAB317	P_{tet} – B0034 – luxR – B0015 – AraC – P_{araBAD} – STAR6 – t500 – Buffer 3 – P_{lux} – anti-STAR6 – t500 – ColE1 – SpecR	This study
pAB517	J23100 – STAR Target 6 – RBS_{Bujard} – VioB-mCherry – L3S2P55 – p15A – CamR	This study

Table 7.61: Plasmids used in Figure 61.B-E

Plasmid	Description	Source
pAB401	P_{tet} – B0034 – RpaR – B0015 – AraC – P_{araBAD} – STAR6_toehold2 – t500 – Buffer 3 – P_{lux} – anti-STAR6_toehold2 – t500 – ColE1 – SpecR	This study
pAB550	J23114 – STAR Target 6 – RBS_{CtrE} – CtrE – RBS_{CtrB} – CtrB – RBS_{CtrI} – CtrI – RBS_{CtrY} – CtrY – L3S2P55 – p15A – CamR	This study

Table 7.62: Plasmids used in Figure 63

Plasmid	Description	Source
pAB300	P_{tet} – B0034 – luxR – B0015 – AraC – P_{araBAD} – STAR6_toehold2 – t500 – Buffer 3 – P_{lux} – anti-STAR6_toehold2 – t500 – ColE1 – SpecR	This study
pAB401	P_{tet} – B0034 – RpaR – B0015 – AraC – P_{araBAD} – STAR6_toehold2 – t500 – Buffer 3 – P_{lux} – anti-STAR6_toehold2 – t500 – ColE1 – SpecR	This study
pAB518	J23100 – STAR Target 6 – RBS_{Bujard} – VioB-sfYFP – L3S2P55 – p15A – CamR	This study
pAB519	J23100 – STAR Target 6 – RBS_{Bujard} – VioB-sfCFP – L3S2P55 – p15A – CamR	This study

Table 7.63: Plasmids used in Figure 64.B-D

Plasmid	Description	Source
pAB300	P_{tet} – B0034 – luxR – B0015 – AraC – P_{araBAD} – STAR6_toehold2 – t500 – Buffer 3 – P_{lux} – anti-STAR6_toehold2 – t500 – ColE1 – SpecR	This study
pAB401	P_{tet} – B0034 – RpaR – B0015 – AraC – P_{araBAD} – STAR6_toehold2 – t500 – Buffer 3 – P_{lux} – anti-STAR6_toehold2 – t500 – ColE1 – SpecR	This study
pAB518	J23100 – STAR Target 6 – RBS_{Bujard} – VioB-sfYFP – L3S2P55 – p15A – CamR	This study
pAB519	J23100 – STAR Target 6 – RBS_{Bujard} – VioB-sfCFP – L3S2P55 – p15A – CamR	This study

Table 7.64: Plasmids used in Figure 65.B-C

Plasmid	Description	Source
pAB401	P_{tet} – B0034 – RpaR – B0015 – AraC – P_{araBAD} – STAR6_toehold2 – t500 – Buffer 3 – P_{lux} – anti-STAR6_toehold2 – t500 – ColE1 – SpecR	This study
pAB519	J23100 – STAR Target 6 – RBS_{Bujard} – VioB-sfCFP – L3S2P55 – p15A – CamR	This study

Table 7.65: Plasmids used in Figure 66.B-E

Plasmid	Description	Source
pAB300	P_{tet} – B0034 – luxR – B0015 – AraC – P_{araBAD} – STAR6_toehold2 – t500 – Buffer 3 – P_{lux} – anti-STAR6_toehold2 – t500 – ColE1 – SpecR	This study

Table 7.65: Plasmids used in Figure 66.B-E

Plasmid	Description	Source
pAB401	P_{tet} – B0034 – RpaR – B0015 – AraC – P_{araBAD} – STAR6_toehold2 – t500 – Buffer 3 – P_{lux} – anti-STAR6_toehold2 – t500 – ColE1 – SpecR	This study
pAB518	J23100 – STAR Target 6 – RBS_{Bujard} – VioB-sfYFP – L3S2P55 – p15A – CamR	This study
pAB519	J23100 – STAR Target 6 – RBS_{Bujard} – VioB-sfCFP – L3S2P55 – p15A – CamR	This study

Table 7.66: Plasmids used in Figure 67.B-C

Plasmid	Description	Source
pAB300	P_{tet} – B0034 – luxR – B0015 – AraC – P_{araBAD} – STAR6_toehold2 – t500 – Buffer 3 – P_{lux} – anti-STAR6_toehold2 – t500 – ColE1 – SpecR	This study
pAB518	J23100 – STAR Target 6 – RBS_{Bujard} – VioB-sfYFP – L3S2P55 – p15A – CamR	This study

Table 7.67: Plasmids used in Figure 68.B-F

Plasmid	Description	Source
pAB300	P_{tet} – B0034 – luxR – B0015 – AraC – P_{araBAD} – STAR6_toehold2 – t500 – Buffer 3 – P_{lux} – anti-STAR6_toehold2 – t500 – ColE1 – SpecR	This study
pAB537	P_{tet} – B0034 – RpaR – B0015 – AraC – P_{araBAD} – STAR6_toehold2 – t500 – Buffer 3 – P_{lux} – anti-STAR6_toehold2 – t500 – ColE1 – SpecR	This study
pAB518	J23100 – STAR Target 6 – RBS_{Bujard} – VioB-sfYFP – L3S2P55 – p15A – CamR	This study
pAB519	J23100 – STAR Target 6 – RBS_{Bujard} – VioB-sfCFP – L3S2P55 – p15A – CamR	This study

Table 7.68: Plasmids used in Figure 69.B-E

Plasmid	Description	Source
pAB300	P_{tet} – B0034 – luxR – B0015 – AraC – P_{araBAD} – STAR6_toehold2 – t500 – Buffer 3 – P_{lux} – anti-STAR6_toehold0 – t500 – ColE1 – SpecR	This study

Table 7.68: Plasmids used in Figure 69.B-E

Plasmid	Description	Source
pAB537	P_{tet} – B0034 – RpaR – B0015 – AraC – P_{araBAD} – STAR6_toehold2 – t500 – Buffer 3 – P_{lux} – anti-STAR6_toehold2 – t500 – ColE1 – SpecR	This study
pAB518	J23100 – STAR Target 6 – RBS_{Bujard} – VioB-sfYFP – L3S2P55 – p15A – CamR	This study
pAB519	J23100 – STAR Target 6 – RBS_{Bujard} – VioB-sfCFP – L3S2P55 – p15A – CamR	This study

Table 7.69: Plasmids used in Figure 70.B-E

Plasmid	Description	Source
pAB300	P_{tet} – B0034 – luxR – B0015 – AraC – P_{araBAD} – STAR6_toehold2 – t500 – Buffer 3 – P_{lux} – anti-STAR6_toehold2 – t500 – ColE1 – SpecR	This study
pAB317	P_{tet} – B0034 – luxR – B0015 – AraC – P_{araBAD} – STAR6 – t500 – Buffer 3 – P_{lux} – anti-STAR6 – t500 – ColE1 – SpecR	This study
pAB537	P_{tet} – B0034 – RpaR – B0015 – AraC – P_{araBAD} – STAR6_toehold2 – t500 – Buffer 3 – P_{lux} – anti-STAR6_toehold2 – t500 – ColE1 – SpecR	This study
pAB403	AraC – P_{rhaBAD} – STAR6 – t500 – Buffer 3 – P_{lux} – anti-STAR6 – t500 – ColE1 – SpecR	This study
pAB518	J23100 – STAR Target 6 – RBS_{Bujard} – VioB-sfYFP – L3S2P55 – p15A – CamR	This study
pAB519	J23100 – STAR Target 6 – RBS_{Bujard} – VioB-sfCFP – L3S2P55 – p15A – CamR	This study

Table 7.70: Plasmids used in Figure 71.B-E

Plasmid	Description	Source
pAB401	P_{tet} – B0034 – RpaR – B0015 – AraC – P_{araBAD} – STAR6_toehold2 – t500 – Buffer 3 – P_{lux} – anti-STAR6_toehold2 – t500 – ColE1 – SpecR	This study
pAB579	P_{tet} – B0034 – RpaR – B0015 – AraC – P_{araBAD} – STAR6 – t500 – Buffer 3 – P_{lux} – anti-STAR6 – t500 – ColE1 – SpecR	This study
pAB399	P_{tet} – B0034 – luxR – B0015 – AraC – P_{rhaBAD} – STAR6_toehold2 – t500 – Buffer 3 – P_{lux} – anti-STAR6_toehold2 – t500 – ColE1 – SpecR	This study
pAB403	AraC – P_{rhaBAD} – STAR6 – t500 – Buffer 3 – P_{lux} – anti-STAR6 – t500 – ColE1 – SpecR	This study

Table 7.70: Plasmids used in Figure 71.B-E

Plasmid	Description	Source
pAB518	J23100 – STAR Target 6 – RBS$_{Bujard}$ – VioB-sfYFP – L3S2P55 – p15A – CamR	This study
pAB519	J23100 – STAR Target 6 – RBS$_{Bujard}$ – VioB-sfCFP – L3S2P55 – p15A – CamR	This study

Table 7.71: Plasmids used in Figure 74.B-E

Plasmid	Description	Source
pAB300	P$_{tet}$ – B0034 – luxR – B0015 – AraC – P$_{araBAD}$ – STAR6_toehold2 – t500 – Buffer 3 – P$_{lux}$ – anti-STAR6_toehold2 – t500 – ColE1 – SpecR	This study
pAB401	P$_{tet}$ – B0034 – RpaR – B0015 – AraC – P$_{araBAD}$ – STAR6_toehold2 – t500 – Buffer 3 – P$_{lux}$ – anti-STAR6_toehold2 – t500 – ColE1 – SpecR	This study
pAB518	J23100 – STAR Target 6 – RBS$_{Bujard}$ – VioB-sfYFP – L3S2P55 – p15A – CamR	This study
pAB519	J23100 – STAR Target 6 – RBS$_{Bujard}$ – VioB-sfCFP – L3S2P55 – p15A – CamR	This study

Table 7.72: Plasmids used in Figure 79.B-C

Plasmid	Description	Source
pAB120	P$_{Tet}$ – B0034 – luxR – B0015 – P$_{lux}$ – STAR 6 – t500 – P$_{araBAD}$ – RBS$_{VioB}$ – VioB-mCherry – his terminator – ColE1 origin – SpecR	This study
pAB126	P$_{RAND14}$ - RBS8B - dCas9 - rrnB T1 - P$_{HtpG1}$ - gRNA(P$_{araBAD}$) - p15A - AmpR	This study

Table 7.73: Plasmids used in Figure 91

Plasmid	Description	Source
pAB252	P$_{tet}$ - B0034 - luxR - T1 - P$_{lux}$ - RBSc33 - sfGFP - T2 - ColE1 - SpecR	This study
pAB409	AraC - P$_{araBAD}$ - RBSc33 - sfGFP - T2 - ColE1 - SpecR	This study
pAB410	P$_{rhaBAD}$ - RBSc33 - sfGFP - T2 - ColE1 - SpecR	This study

Table 7.74: Plasmids used in Figure 92

Plasmid	Description	Source
pAB409	AraC - P_{araBAD} - RBSc33 - sfGFP - T2 - ColE1 - SpecR	This study
pAB410	P_{rhaBAD} - RBSc33 - sfGFP - T2 - ColE1 - SpecR	This study

Table 7.75: Plasmids used in Figure 93

Plasmid	Description	Source
pAB127	P_{tet} – B0034 – luxR – B0015 – P_{lux} – STAR6_toehold0 – t500 – ColE1 – SpecR	This study
pAB96	P_{RAND14} - RBS8B - dCas9 - rrnB T1 - J23119 - STAR Target 6 - HH - gRNA(LeuLp) - HDV - p15A - AmpR	This study
pAB205	P_{RAND14} - RBS8B - dCas9 - rrnB T1 - J23119 - STAR Target 6 - HH - gRNA(LeuLp, End-0 mutation) - HDV - p15A - AmpR	This study
pAB206	P_{RAND14} - RBS8B - dCas9 - rrnB T1 - J23119 - STAR Target 6 - HH - gRNA(LeuLp, End-1 mutation) - HDV - p15A - AmpR	This study
pAB208	P_{RAND14} - RBS8B - dCas9 - rrnB T1 - J23119 - STAR Target 6 - HH - gRNA(LeuLp, End-3 mutation) - HDV - p15A - AmpR	This study

Table 7.76: Plasmids used in Figure 94

Plasmid	Description	Source
pAB58	P_{RAND14} - RBS8B - dCas9 - rrnB T1 - AraC - P_{araBAD} - No Target gRNA - p15A - AmpR	This study
pAB60	P_{RAND14} - RBS8B - dCas9 - rrnB T1 - AraC - P_{araBAD} - gRNA(HisLp) - p15A - AmpR	This study
pAB61	P_{RAND14} - RBS8B - dCas9 - rrnB T1 - AraC - P_{araBAD} - gRNA(LeuLp) - p15A - AmpR	This study

Table 7.77: Plasmids used in Figure 95

Plasmid	Description	Source
pAB300	P_{tet} – B0034 – luxR – B0015 – AraC – P_{araBAD} – STAR6_toehold2 – t500 – Buffer 3 – P_{lux} – anti-STAR6_toehold2 – t500 – ColE1 – SpecR	This study
pAB401	P_{tet} – B0034 – RpaR – B0015 – AraC – P_{araBAD} – STAR6_toehold2 – t500 – Buffer 3 – P_{lux} – anti-STAR6_toehold2 – t500 – ColE1 – SpecR	This study
pAB518	J23100 – STAR Target 6 – RBS_{Bujard} – VioB-sfYFP – L3S2P55 – p15A – CamR	This study

Table 7.77: Plasmids used in Figure 95

Plasmid	Description	Source
pAB519	J23100 – STAR Target 6 – RBS_{Bujard} – VioB-sfCFP – L3S2P55 – p15A – CamR	This study

Table 7.78: Plasmids used in Figure 96

Plasmid	Description	Source
pZE-EP-APTA	P_{LacO-1} – entC – pchB – P_{LacO-1} – aroL – ppsA – tktA – $aroG^{fbr}$ – ColE1 – ampR	[24]
pZE-EP	P_{LacO-1} – entC – pchB – ColE1 – ampR	[24]
pCS-NC	P_{LacO-1} – nah^{opt} – catA – p15A – kanR	[24]
pCS-APTA	P_{LacO-1} – aroL – ppsA – tktA – $aroG^{fbr}$ – p15A – kanR	[24]
pSA-NC	P_{LacO-1} – nah^{opt} – catA – pSC101 – camR	[24]

Chapter 8

Appendix

8.1 STAR sequences

We compile in this section all the STAR sequences used in this thesis for the design of the STAR-based comparator:

Table 8.1: STAR Sequences used in this study

Design	Sequence (5' to 3')	Source
STAR5	TGAACTGTATACATTCCCCGCAGGATAGGAA TTGAAGATGAAACGATGAGACTTGGGACGA	[130]
STAR6	TGAACTGTATACATTCCCCGCTGAACGACGG AAACTTTGACTGGACTGACTTGATGACTGG	[130]
STAR8	TGAACTGTATACATTCCCCGCAGGATAAGAG TAAGTGAGAGTAGGTAGAGATTGAGGATGG	[130]
STAR6_Toehold0	TGAACTGTATACATTCCCCGCTGAACGACGG AAACTTTGACTGGACTGACTTGATGACTGGT AACTCCATTCCATC	This study
STAR6_Toehold1	TGAACTGTATACATTCCCCGCTGAACGACGG AAACTTTGACTGGACTGACTTGATGACTGGT CTTATCTTATCTA	This study
STAR6_Toehold2	TGAACTGTATACATTCCCCGCTGAACGACGG AAACTTTGACTGGACTGACTTGATGACTGGA GTTTGATTACATT	This study
STAR6_Toehold3	TGAACTGTATACATTCCCCGCTGAACGACGG AAACTTTGACTGGACTGACTTGATGACTGGA TCTATTACTACTT	This study
STAR6_Toehold4	TGAACTGTATACATTCCCCGCTGAACGACGG AAACTTTGACTGGACTGACTTGATGACTGGC GATTATGGATTAG	This study
STAR6_Toehold5	TGAACTGTATACATTCCCCGCTGAACGACGG AAACTTTGACTGGACTGACTTGATGACTGGT ATGTAATTGATTT	This study

8.2 STAR Target sequences

We compile in this section all the STAR Target sequences used in this thesis.

Table 8.2: STAR Target sequences

Design	Sequence (5' to 3')	Source
STAR Target 5	TCGTCCCAAGTCTCATCGTTTCATCTTCAAT TCCTATCCTGCGGGGAATGTATACAGTTCAT GTATATATTCCCCGCTTTTTTTTT	This study
STAR Target 6	CCAGTCATCAAGTCAGTCCAGTCAAAGTTTC CGTCGTTCAGCGGGGAATGTATACAGTTCAT GTATATATTCCCCGCTTTTTTTTT	This study
STAR Target 8	CCATCCTCAATCTCTACCTACTCTCACTTACT CTTATCCTGCGGGGAATGTATACAGTTCATG TATATATTCCCCGCTTTTTTTTT	This study
Deoptimised STAR Target 6	CCAGTCATCAAGTCAGTCCAGTCAAAGTTTC CCTGGTTCAGCGGGGAATGTATACAGTTCAT GTATATATTCCCCGCTTTTTTTTT	This study

8.3 Anti-STAR sequences

We compile in this section all the anti-STAR sequences used in this thesis.

Table 8.3: Anti-STAR sequences

Design	Sequence (5' to 3')	Source
anti-STAR6	CCAGTCATCAAGTCAGTCCAGTCAAAGTTTC CGTCGTTCAGCGGGGAATGTATACAGTTCA	This study
anti-STAR6_ Toehold0	GATGGAATGGAGTTACCAGTCATCAAGTCAG TCCAGTCAAAGTTTCCGTCGTTCAGCGGGGA ATGTATACAGTTCA	This study
anti-STAR6_ Toehold1	TAGATAAGATAAGACCAGTCATCAAGTCAGT CCAGTCAAAGTTTCCGTCGTTCAGCGGGGAA TGTATACAGTTCA	This study
anti-STAR6_ Toehold2	AATGTAATCAAACTCCAGTCATCAAGTCAGT CCAGTCAAAGTTTCCGTCGTTCAGCGGGGAA TGTATACAGTTCA	This study
anti-STAR6_ Toehold3	AAGTAGTAATAGATCCAGTCATCAAGTCAGT CCAGTCAAAGTTTCCGTCGTTCAGCGGGGAA TGTATACAGTTCA	This study
anti-STAR6_ Toehold4	CTAATCCATAATCGCCAGTCATCAAGTCAGT CCAGTCAAAGTTTCCGTCGTTCAGCGGGGAA TGTATACAGTTCA	This study

Table 8.3: Anti-STAR sequences

Design	Sequence (5' to 3')	Source
anti-STAR6_ Toehold5	AAATCAATTACATACCAGTCATCAAGTCAGT CCAGTCAAAGTTTCCGTCGTTCAGCGGGGAA TGTATACAGTTCA	This study

8.4 STAR and anti-STAR RNA structures

NUPACK prediction of STAR and anti-STAR folding without and with the different toeholds explored in Chapter 2.

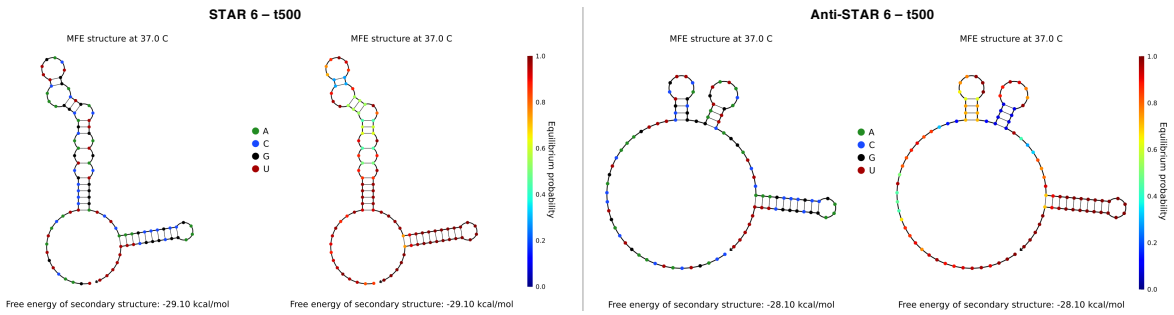


Figure 82: NUPACK secondary structure prediction of STAR and anti-STAR sequences followed by the t500 terminator.

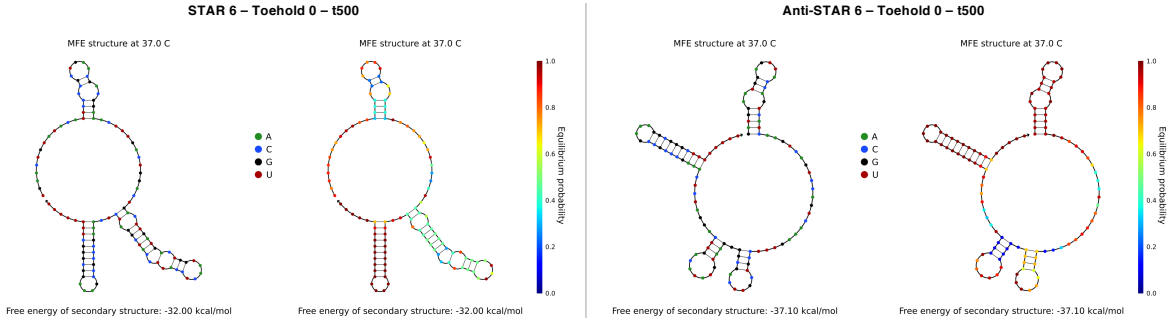


Figure 83: NUPACK secondary structure prediction of STAR and anti-STAR sequences with Toehold 0 followed by the t500 terminator.

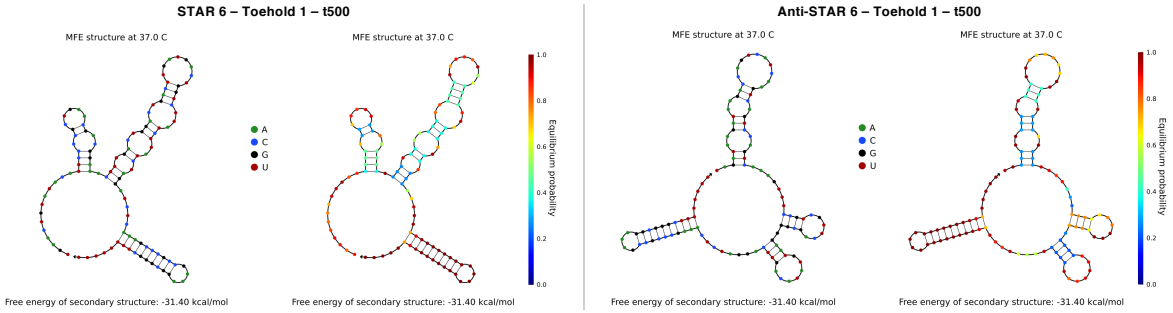


Figure 84: NUPACK secondary structure prediction of STAR and anti-STAR sequences with Toehold 1 followed by the t500 terminator.

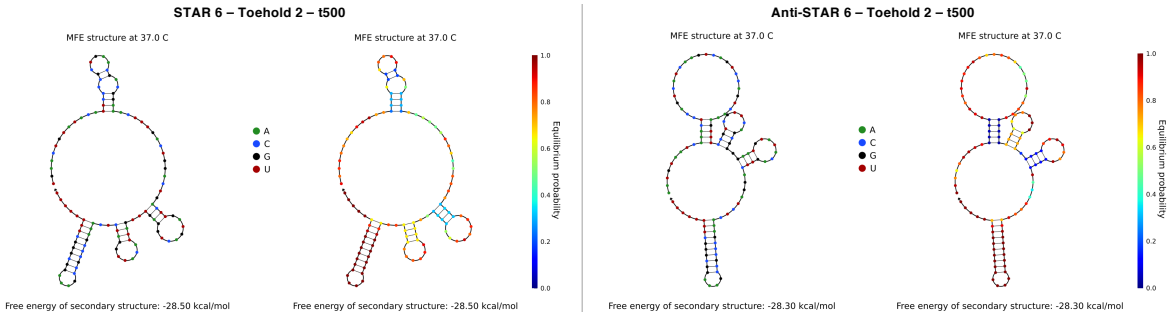


Figure 85: NUPACK secondary structure prediction of STAR and anti-STAR sequences with Toehold 2 followed by the t500 terminator.

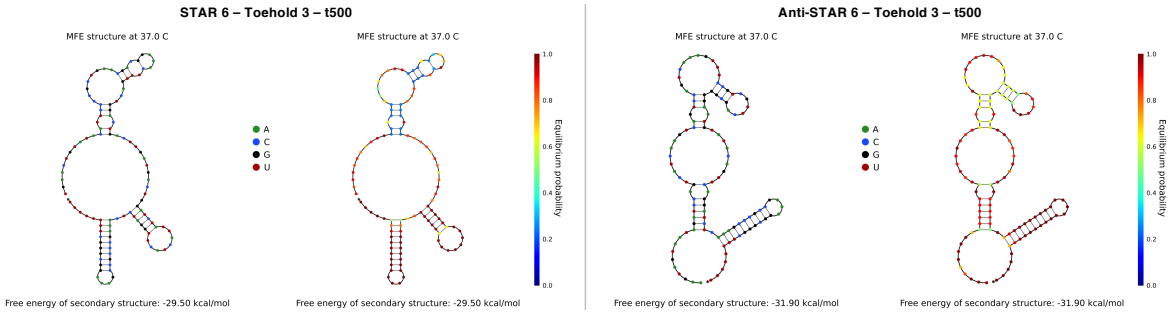


Figure 86: NUPACK secondary structure prediction of STAR and anti-STAR sequences with Toehold 3 followed by the t500 terminator.

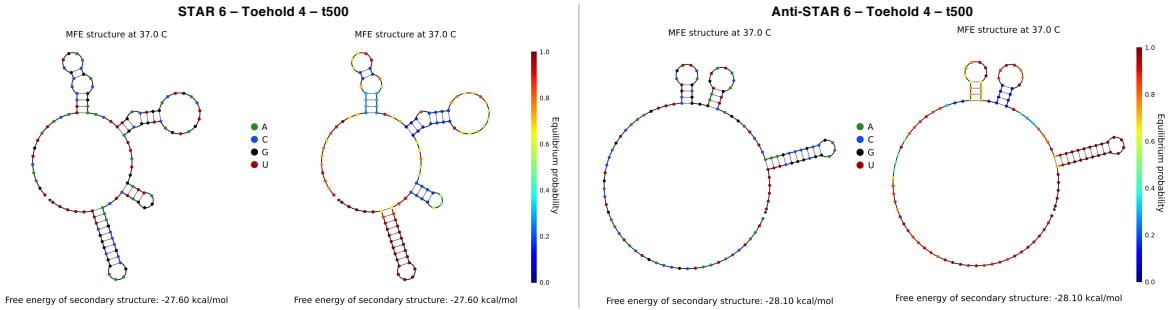


Figure 87: NUPACK secondary structure prediction of STAR and anti-STAR sequences with Toehold 4 followed by the t500 terminator.

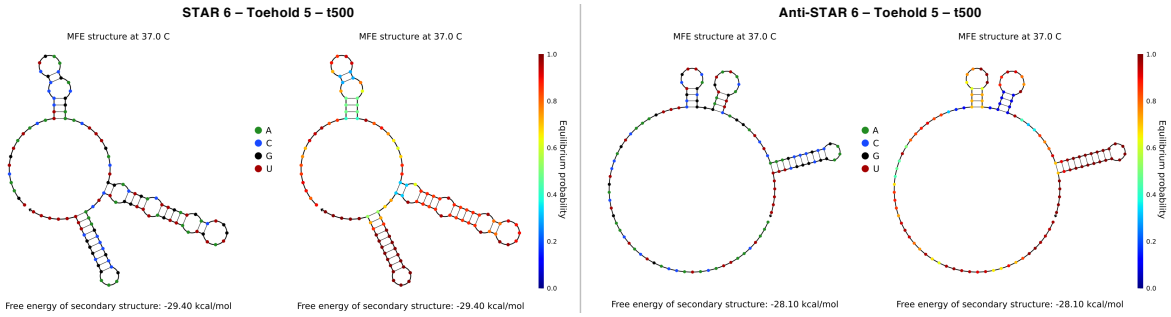


Figure 88: NUPACK secondary structure prediction of STAR and anti-STAR sequences with Toehold 5 followed by the t500 terminator.

8.5 Comparator buffer sequences

We compile in this section 3 buffer sequences used to isolate the STAR and anti-STAR transcriptional units in the STAR-based comparator

Table 8.4: Comparator buffer sequences. Sequence in orange represents iGEM B1001 terminator, purple sequence represents the non-coding region from AND-Gate of [130].

Buffer	**Sequence (5' to 3')**
Buffer 1	ggatccttactcgag
Buffer 2	ggatccttactcgagaaaaaaaaaccccgcttcggcggggttttttttttctggactgcaggcttcctcgctcaccttcctttttcaatattattgaagcatttatcagggttattgtctcatgagcggatacatatttgaatgtatttagaaaaataaacaaatagggttccgcgcacatttccccgaaaagtgccacctgacgtctaagaaaccattattatcatgacattaacctataaaaataggcgtatcacgaggcagaatttcagataaaaaaaatccttagctttcgctaaggatgatttctgg
Buffer 3	ggatccttactcgagaaaaaaaaaccccgcttcggcggggttttttttttctggactgcaggcttcctcgctcac

8.6 Deactivation of the LLL and LRR STAR-based comparators

We measured the deactivation percentage of the STAR-based comparator to compare it to the performance of the combined STAR and antisense RNA system from [173]. In their study, the authors expressed STAR to activate expression of GFP. They also expressed two antisense RNA, one targeting STAR and the other targeting GFP mRNA. They have shown that by expressing the STAR antisense RNA they could achieve 70% repression, 80% repression by expressing the GFP asRNA and 96% repression by expressing both asRNAs.

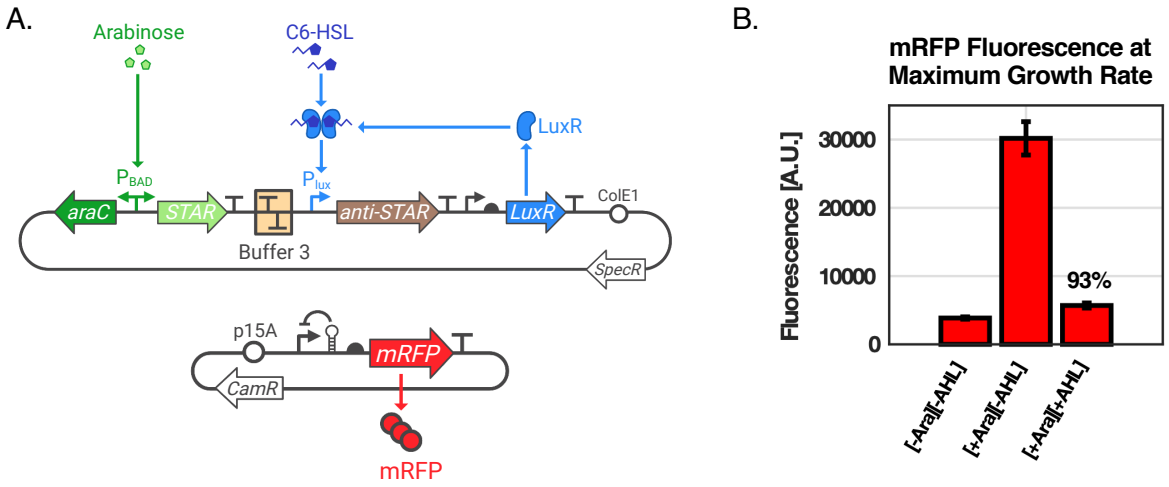


Figure 89: Deactivation of the LLL and LRR STAR-based comparator. (A) The final design of the STAR-based comparator with STAR 6 Toehold 2 and Buffer 3 targets mRFP production. (B) The deactivation percentage is calculated for the LLL and LRR STAR-based comparators. The comparator system is externally induced with three conditions: (1) "[-Ara][-AHL]": is induced with 0% of L-arabinose and 0 M of C6-HSL or pC-HSL for the LLL or LRR comparator respectively; (2) "[+Ara][-AHL]": is induced with 0.2% of L-arabinose and 0 M of C6-HSL or pC-HSL for the LLL or LRR comparator respectively; (3) "[+Ara][+AHL]": is induced with 0.2% of L-arabinose and 10^{-7} M of C6-HSL or pC-HSL for the LLL or LRR comparator respectively. The deactivation percentage is calculated as $((F_{STAR}-F_{STAR,antiSTAR})/(F_{STAR}-F_{neg.}))\times 100\%$, where F_{STAR} corresponds to the fluorescence of the comparator when only STAR is expressed ("[+Ara][-AHL]"), $F_{STAR,\ antiSTAR}$ corresponds to the fluorescence of the comparator when both STAR and anti-STAR are expressed ("[+Ara][-AHL]"), and $F_{neg.}$ corresponds to the fluorescence of the comparator when neither STAR not anti-STAR are expressed ("[-Ara][-AHL]"). Experiment was carried in DH10B. Fluorescence was measured through flow cytometry. Data represent the mean and standard deviation of 3 biological replicates.

Here we show that our design of the STAR-based comparator is able to achieve a similar

deactivation percentage to the multilevel regulation system from [173]. The advantage of our system is that it does not rely on expressing an asRNA targeting GOI mRNA that needs to be redesigned for each different GOI. Our approach thus yields comparable results and has the benefit of being more modular.

8.7 AHL-producing strains

In this appendix, we document all the C6-HSL and pC-HSL producing strains built in this project.

Table 8.5: C6-HSL producing strains and their fluorescent reporter

	Strain	CRIM plasmid	Promoter	RBS	Parent strain	Reporter
1	eAB14	pAB386	J23100	RBSc33	DH10B	-
2	eAB29	pAB553	J23100	B0030	DH10B	-
3	eAB30	pAB554	J23106	B0030	DH10B	-
4	eAB32	pAB564	J23105	B0030	DH10B	-
5	eAB34	pAB566	J23115	B0030	DH10B	-
6	eAB28	pAB384	J23100	RBSc33	DH10B	sfGFP
7	eAB31	pAB556	J23106	B0030	DH10B	sfGFP
8	eAB33	pAB565	J23105	B0030	DH10B	sfGFP
9	eAB35	pAB567	J23115	B0030	DH10B	sfGFP
10	eAB8	pAB386	J23100	RBSc33	BW25113	-
11	eAB7	pAB384	J23100	RBSc33	BW25113	sfGFP

Table 8.6: pC-HSL producing strains and their fluorescent reporter

	Strain Name	CRIM Plasmid	Promoter	RpaI RBS	4CL2nt RBS	TAL RBS	Reporter	Parent Strain
1	eAB13	pAB383	J23100	RBSc33	N/A	N/A	mScarlet-I	DH10B
2	eAB18	pAB482	J23100	B0030	B0030	B0030	mScarlet-I	DH10B
3	eAB19	pAB493	J23106	B0030	B0030	B0030	mScarlet-I	DH10B
4	eAB20	pAB494	J23105	B0030	B0030	B0030	mScarlet-I	DH10B
5	eAB21	pAB495	J23114	B0030	B0030	B0030	mScarlet-I	DH10B
6	eAB22	pAB496	J23109	B0030	B0030	B0030	mScarlet-I	DH10B
7	eAB36	pAB572	J23109	B0030	B0030	B0032	mScarlet-I	DH10B
8	eAB37	pAB573	J23109	B0030	B0030	B0031	mScarlet-I	DH10B
9	eAB38	pAB574	J23109	B0030	B0030	B0033	mScarlet-I	DH10B
10	eAB39	pAB575	J23109	B0030	B0030	B0030-GTG	mScarlet-I	DH10B
11	eAB40	pAB576	J23109	B0030	B0030	B0032-GTG	mScarlet-I	DH10B
12	eAB41	pAB577	J23109	B0030	B0030	B0031-GTG	mScarlet-I	DH10B
13	eAB42	pAB578	J23109	B0030	B0030	B0033-GTG	mScarlet-I	DH10B

Table 8.6: pC-HSL producing strains and their fluorescent reporter

	Strain Name	CRIM Plasmid	Promoter	RpaI RBS	4CL2nt RBS	TAL RBS	Reporter	Parent Strain
14	eAB6	pAB383	J23100	RBSc33	N/A	N/A	mScarlet-I	BW25113
15	eAB10	pAB397	J23100	RBSc33	N/A	N/A	N/A	BW25113
16	eAB16	pAB482	J23100	B0030	B0030	B0030	mScarlet-I	BW25113

Table 8.7: DH10B strains producing C6-HSL and pC-HSL

Strain	Design	CRIM Plasmid
DH_{lux-1}	J23100 – B0030 – luxI – L3S2P55	pAB553
DH_{lux-2}	J23106 – B0030 – luxI – L3S2P55	pAB554
DH_{lux-3}	J23105 – B0030 – luxI – L3S2P55	pAB564
DH_{lux-4}	J23115 – B0030 – luxI – L3S2P55	pAB566
DH_{lux-5}	J23100 – RBSc33 – luxI – L3S2P55	pAB386
DH_{lux-6}	J23100 – RBSc33 – luxI – L3S2P55 – J23100 – sfGFP – BBa_1002	pAB384
DH_{rpa-1}	J23109 – B0030 – rpaI – B0030 – 4CL2nt – B0032 – TAL –L3S2P55	pAB572
DH_{rpa-2}	J23109 – B0030 – rpaI – B0030 – 4CL2nt – B0030 – TAL –L3S2P55	pAB496
DH_{rpa-3}	J23106 – B0030 – rpaI – B0030 – 4CL2nt – B0030 – TAL –L3S2P55	pAB493
DH_{rpa-4}	J23105 – B0030 – rpaI – B0030 – 4CL2nt – B0030 – TAL –L3S2P55	pAB494
DH_{rpa-5}	J23114 – B0030 – rpaI – B0030 – 4CL2nt – B0030 – TAL –L3S2P55	pAB495
DH_{rpa-6}	J23100 – B0030 – rpaI – B0030 – 4CL2nt – B0032 – TAL –L3S2P55	pAB482

8.8 Growth of quorum sender strains

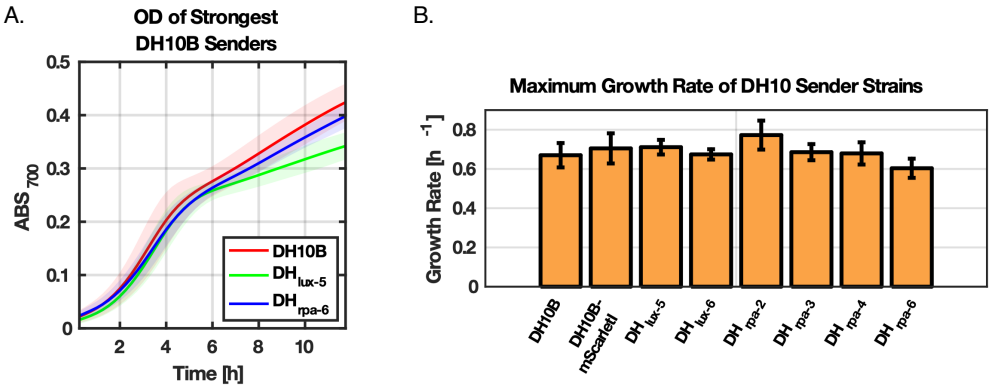


Figure 90: Growth of quorum-sensing-producer strains (A) OD of the strongest C6-HSL-producing DH10B strain (DH_{lux-5}) and the strongest pC-HSL-producing DH10B strain (DH_{rpa-6}) compared to the OD of the wild-type DH10B strain. (B) Growth rate of the different quorum sensing producer strains compared to the growth of DH10B wild-type, the parent strain of DH_lux strains and DH10B-mScarletI, the parent of DH_rpa strains. OD and fluorescence measurements were collected in timecourse plate-reader assay. Data represent the mean values of n = 3 biological replicates ± s.d.

8.9 GFP expression of inducible systems

8.9.1 Comparison of the LLL quorum sensing, araBAD and rhaBAD inducible systems

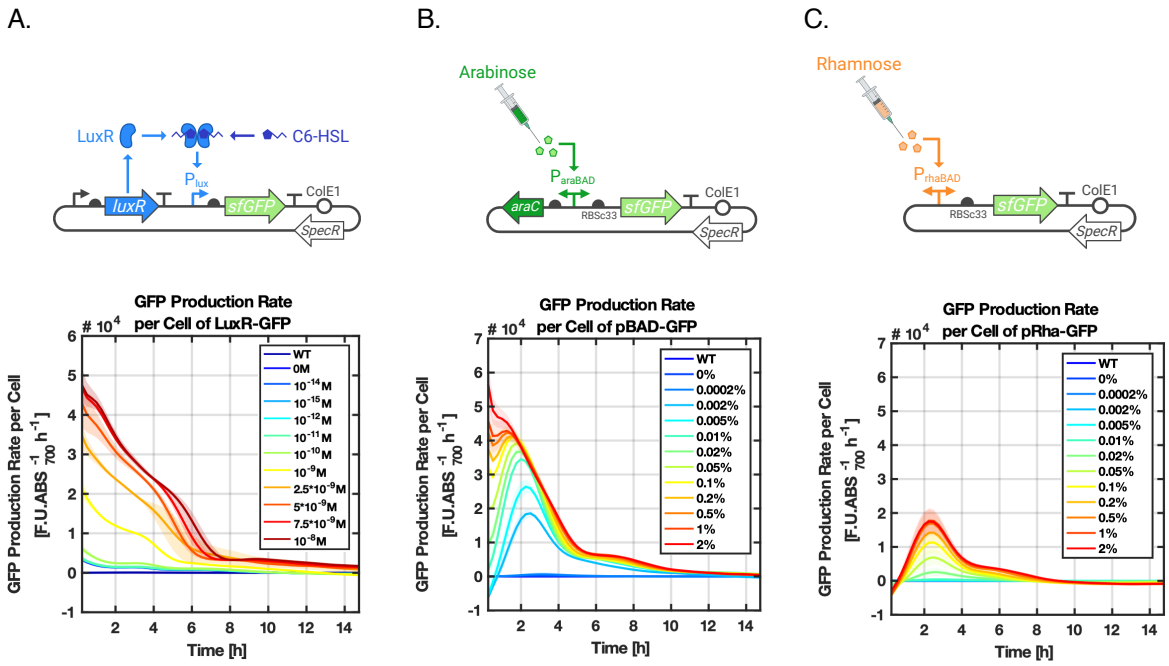


Figure 91: Comparison of the LLL, araBAD and rhaBAD inducible systems. (A) sfGFP is regulated by the LLL quorum sensing system, such that sfGFP production rate per cell increases as C6-HSL concentration increases. (B) sfGFP production rate per cell as a function of increasing L-arabinose concentration. The araBAD promoter driving expression of sfGFP was externally induced with L-arabinose. (C) sfGFP production rate per cell as a function of increasing L-arabinose concentration. The rhaBAD promoter driving expression of sfGFP was externally induced with L-rhamnose. Experiments were done on the same day and in the same plate-reader, in BW25113. Fluorescence measurements were collected in the plate-reader. Data represent the mean values of n = 3 biological replicates ± s.d.

8.9.2 rhaBAD and araBAD promoter characterisation

We characterised and compared the promoter strength of the araBAD and rhaBAD inducible promoters used in this study. The araBAD promoter is inducible with L-arabinose while the rhaBAD promoter is inducible with L-rhamnose.

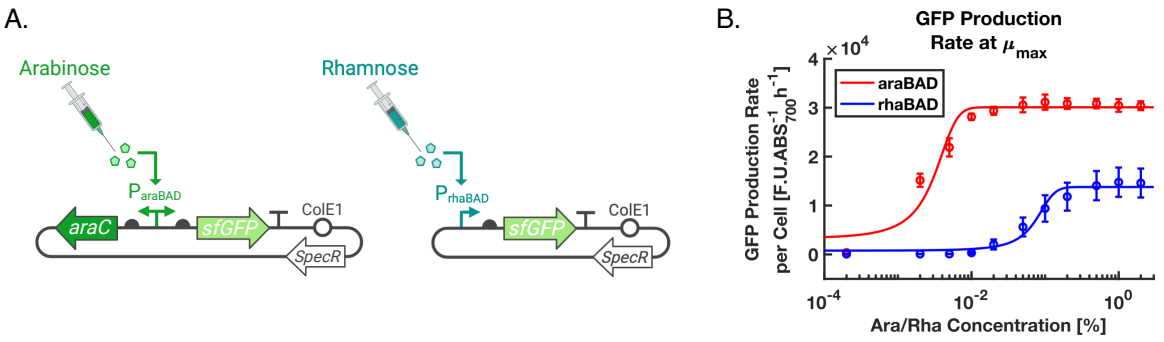


Figure 92: Characterisation of the araBAD and rhaBAD inducible promoters. (A) Genetic circuits used to draw the input-output response curves of the araBAD and rhaBAD promoters. Each promoter is driving expression of sfGFP, used here as a reporter. (B) sfGFP production rate per cell as a function of increasing L-arabinose and L-rhamnose inducers concentrations. The araBAD promoter driving expression of sfGFP was externally induced with L-arabinose, while the rhaBAD promoter driving expression of sfGFP was externally induced with L-rhamnose. Experiments were done in BW25113. Fluorescence and OD were measured with a plate-reader. Data represent the mean values of n = 3 biological replicates ± s.d.

8.10 Mutations in gRNA targeting the native LeuLp promoter

We show in Figure 93, the effect of mutation position in the gRNA spacer targeting the LeuLp promoter. When the mutation occurred further from directly preceding the PAM sequence, it did not significantly reduce lag-phase and improve growth.

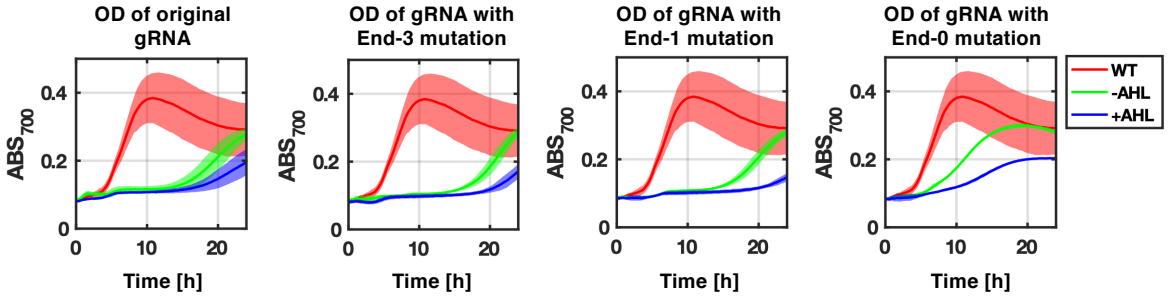


Figure 93: Mutations in gRNA targeting LeuLp promoter. In Figure 50.A, we expressed a gRNA under the control of STAR expressed in the presence of C6-HSL. Here we show the effect of adding 0M or 10^{-7}M of C6-HSL on cell growth for different gRNA containing either no mutation ("Original gRNA"), or mutations at 4 bp, 2 bp or directly before the PAM sequence (denoted "End-3", "End-2" and "End-0" respectively). Experiments were done in BW25113. OD measurements were collected in the plate-reader. Data represent the mean values of n = 3 biological replicates ± s.d.

8.11 Targeting the LeuLp and HisLp promoters with CRISPRi

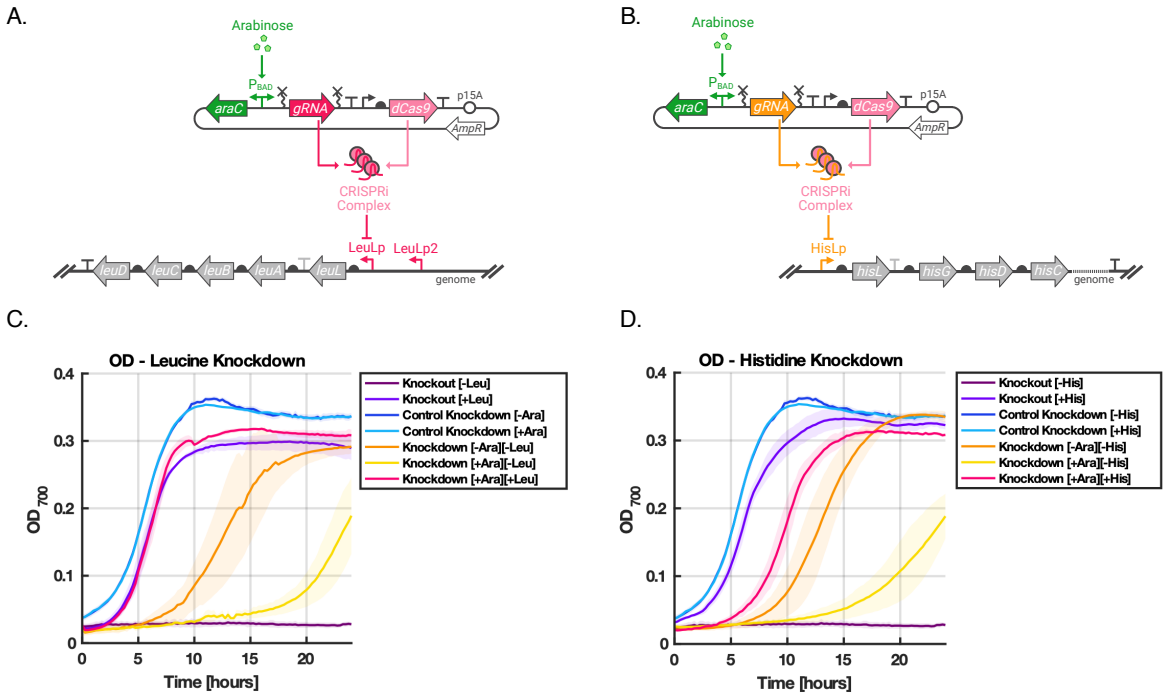


Figure 94: Targeting the LeuLp and HisLp promoters with CRISPRi. (A) The circuit knocking down leucine production consists in a constitutively expressed dCas9, and a L-arabinose inducible gRNA targeting the native LeuLp promoter in the genome. (B) The circuit knocking down histidine production consists in a constitutively expressed dCas9, and a L-arabinose inducible gRNA targeting the native HisLp promoter in the genome. (C) OD of the leucine knockdown, the ΔLeuB knockout from the Keio collection and the control knockdown expressing the "No Target" gRNA from [156]. Conditions are the following "[-Ara]": induction with 0% of L-arabinose, "[+Ara]": induction with 0.2% of L-arabinose, "[-Leu]": poor M9 medium is supplemented with 0 μg/mL of leucine, "[+Leu]": poor M9 medium is supplemented with 40 μg/mL of leucine. (D) OD of the histidine knockdown, the ΔHisD knockout from the Keio collection and the control knockdown expressing the "No Target" gRNA from [156]. Conditions are the following "[-Ara]": induction with 0% of L-arabinose, "[+Ara]": induction with 0.2% of L-arabinose, "[-His]": poor M9 medium is supplemented with 0 μg/mL of L-histidine, "[+His]": poor M9 medium is supplemented with 40 μg/mL of L-histidine. Experiment was done in BW25113. OD measurements were collected in a timecourse plate-reader assay. Data represent the mean values of n = 3 biological replicates ± s.d.

8.12 Continuous coculture

Here we show the third biological replicate of both the open-loop and closed-loop coculture circuits from Figure 74.

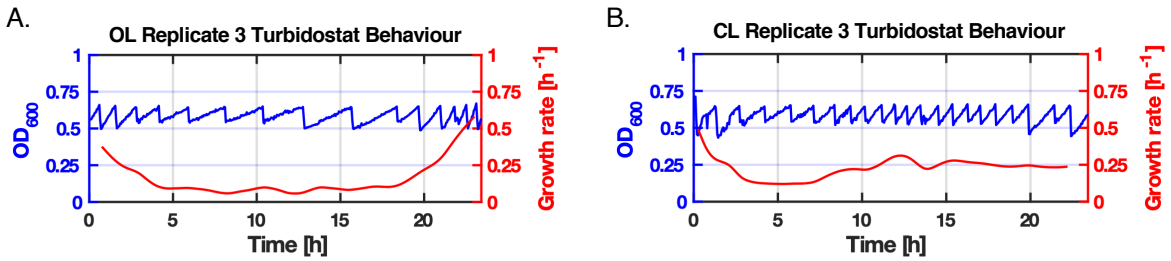


Figure 95: Coculture behaviour in continuous culture. (A) OD_{600} and growth rate of the third replicates of the closed-loop coculture circuit grown in the Chi.bio. (B) OD_{600} and growth rate of the third replicates of the open-loop cocultures circuit grown in the Chi.bio. Experiments were done in DH10B. Fluorescence and population ratio was measured through flow-cytometry. Data represent the mean values of n = 3 biological replicates ± s.d.

8.13 Muconic acid production modules

Here we show the impact of the APTA, EP and NC modules for muconic acid production on the growth rate of the QH4 *E. coli* strain [24].

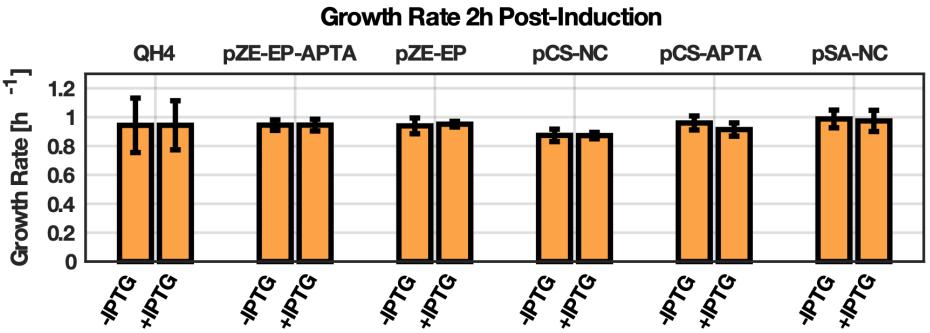


Figure 96: Expression of the muconic acid production modules. The three different modules for muconic acid production from [24] were transformed in the QH4 *E. coli* strain. Growth rate of the strains was monitored over time when induced with either 0 M or 0.25 mM of IPTG. The EP, APTA and NC modules are described in Figure 78 of Chapter 6. The plasmid used for expression of the modules is denoted as follows: "pZE-" for high copy plasmid (ColE1), "pCS-" for medium copy plasmid (p15A), "pSA-" for low copy plasmid (pSC101). Experiments were done in QH4. OD was measured with a plate-reader. Data represent the mean values of n = 3 biological replicates ± s.d.

Bibliography

[1] F. Meng and T. Ellis, "The second decade of synthetic biology: 2010–2020," *Nature Communications*, vol. 11, no. 1, pp. 1–4, 2020. [Online]. Available: http://dx.doi.org/10.1038/s41467-020-19092-2 (Cited on page 2.)

[2] C. A. Voigt, "Synthetic biology 2020–2030: six commercially-available products that are changing our world," *Nature Communications*, vol. 11, no. 1, pp. 10–15, 2020. (Cited on page 2.)

[3] V. de Lorenzo, "15 Years of Microbial Biotechnology: the Time Has Come To Think Big—and Act Soon," *Microbial Biotechnology*, vol. 0, pp. 1–7, 2021. (Cited on page 2.)

[4] Research and Markets, "Global Synthetic Biology Market by Tools (Oligonucleotides, Enzymes, Synthetic Cells), Technology (Gene Synthesis, Genome Engineering), Application (Tissue Regeneration, Biofuel, Consumer Care, Food & Agriculture, Environmental) and Region - Forecast to 2," Tech. Rep., 2021. (Cited on page 2.)

[5] T. S. Moon, S. H. Yoon, A. M. Lanza, J. D. Roy-Mayhew, and K. L. Jones Prather, "Production of glucaric acid from a synthetic pathway in recombinant Escherichia coli," *Applied and Environmental Microbiology*, vol. 75, no. 3, pp. 589–595, 2009. (Cited on page 3.)

[6] O. Borkowski, F. Ceroni, G. B. Stan, and T. Ellis, "Overloaded and stressed: whole-cell considerations for bacterial synthetic biology," *Current Opinion in Microbiology*, vol. 33, pp. 123–130, 2016. [Online]. Available: http://dx.doi.org/10.1016/j.mib.2016.07.009 (Cited on page 3.)

[7] A. Boo, T. Ellis, and G.-b. Stan, "Host-aware synthetic biology," *Current Opinion in Systems Biology*, vol. 14, pp. 66–72, apr 2019. [Online]. Available: https://doi.org/10.1016/j.coisb.2019.03.001https://linkinghub.elsevier.com/retrieve/pii/S245231001930006X (Cited on page 3.)

[8] F. Ceroni, R. Algar, G.-B. Stan, and T. Ellis, "Quantifying cellular capacity identifies gene expression designs with reduced burden," *Nature Methods*, vol. 12, no. 5, pp. 415–418, 2015. [Online]. Available: http://www.nature.com/doifinder/10.1038/nmeth.3339 (Cited on pages 3, 4, 22, 32, 48, 107, 147, 174, 180, 186, 195, 196 and 200.)

[9] M. Scott, E. M. Mateescu, Z. Zhang, and T. Hwa, "Interdependence of Cell Growth Origins and Consequences," *Science*, vol. 330, no. November, pp. 1099–1102, 2010. (Cited on pages 4, 5 and 22.)

[10] T. E. Gorochowski, I. Avcilar-Kucukgoze, R. A. Bovenberg, J. A. Roubos, and Z. Ignatova, "A Minimal Model of Ribosome Allocation Dynamics Captures Trade-offs in Expression between Endogenous and Synthetic Genes," *ACS Synthetic Biology*, vol. 5, no. 7, pp. 710–720, 2016. (Cited on pages 4 and 22.)

[11] S. Cardinale and A. P. Arkin, "Contextualizing context for synthetic biology - identifying causes of failure of synthetic biological systems," *Biotechnology Journal*, vol. 7, no. 7, pp. 856–866, 2012. (Cited on page 4.)

[12] G. W. Li, D. Burkhardt, C. Gross, and J. S. Weissman, "Quantifying absolute protein synthesis rates reveals principles underlying allocation of cellular resources," *Cell*, vol. 157, no. 3, pp. 624–635, 2014. [Online]. Available: http://dx.doi.org/10.1016/j.cell.2014.02.033 (Cited on page 4.)

[13] M. Basan, S. Hui, H. Okano, Z. Zhang, Y. Shen, J. R. Williamson, and T. Hwa, "Overflow metabolism in Escherichia coli results from efficient proteome allocation," *Nature*, vol. 528, no. 7580, pp. 99–104, 2015. (Cited on page 4.)

[14] D. Del Vecchio, A. J. Ninfa, and E. D. Sontag, "Modular cell biology: Retroactivity and insulation," *Molecular Systems Biology*, vol. 4, no. 161, 2008. (Cited on page 4.)

[15] A. Gyorgy, J. I. Jiménez, J. Yazbek, H. H. Huang, H. Chung, R. Weiss, and D. Del Vecchio, "Isocost Lines Describe the Cellular Economy of Genetic Circuits," *Biophysical Journal*, vol. 109, no. 3, pp. 639–646, 2015. (Cited on pages 4 and 22.)

[16] Y. Qian, H. H. Huang, J. I. Jiménez, and D. Del Vecchio, "Resource Competition Shapes the Response of Genetic Circuits," *ACS Synthetic Biology*, vol. 6, no. 7, 2017. (Cited on pages 4 and 22.)

[17] T. Shopera, L. He, T. Oyetunde, Y. J. Tang, and T. S. Moon, "Decoupling Resource-Coupled Gene Expression in Living Cells," *ACS Synthetic Biology*, vol. 6, no. 8, pp. 1596–1604, 2017. (Cited on pages 4 and 6.)

[18] H.-H. Huang, Y. Qian, and D. Del Vecchio, "A quasi-integral controller for adaptation of genetic modules to variable ribosome demand," *Nature Communications*, vol. 9, no. 1, p. 5415, 2018. [Online]. Available: http://dx.doi.org/10.1038/s41467-018-07899-z (Cited on pages 4, 6 and 158.)

[19] E. M. Bahassi, M. H. O'Dea, N. Allali, J. Messens, M. Gellert, and M. Couturier, "Interactions of CcdB with DNA: Gyrase in activation of GyrA, poisoning of the gyrase-DNA complex, and the antidote action of CdcA," *Journal of Biological Chemistry*, vol. 274, no. 16, pp. 10 936–10 944, 1999. [Online]. Available: http://dx.doi.org/10.1074/jbc.274.16.10936 (Cited on pages 4 and 88.)

[20] F. Stirling, L. Bitzan, S. O'Keefe, E. Redfield, J. W. Oliver, J. Way, and P. A. Silver, "Rational Design of Evolutionarily Stable Microbial Kill Switches," *Molecular Cell*, vol. 68, no. 4, pp. 686–697.e3, 2017. [Online]. Available: http://dx.doi.org/10.1016/j.molcel.2017.10.033 (Cited on page 4.)

[21] A. J. Fedorec, T. Ozdemir, A. Doshi, Y. K. Ho, L. Rosa, J. Rutter, O. Velazquez, V. B. Pinheiro, T. Danino, and C. P. Barnes, "Two New Plasmid Post-segregational Killing Mechanisms for the Implementation of Synthetic Gene Networks in Escherichia coli," *iScience*, vol. 14, pp. 323–334, 2019. [Online]. Available: https://doi.org/10.1016/j.isci.2019.03.019 (Cited on pages 4 and 88.)

[22] W. Kong, D. R. Meldgin, J. J. Collins, and T. Lu, "Designing microbial consortia with defined social interactions," *Nature Chemical Biology*, p. 1, 2018. [Online]. Available: http://www.nature.com/articles/s41589-018-0091-7 (Cited on pages 4, 12 and 13.)

[23] E. Imperial College London 2016 iGEM Team, "Ecolibrium project." [Online]. Available: http://2016.igem.org/Team:ImperialCollege (Cited on page 4.)

[24] Y. Lin, X. Sun, Q. Yuan, and Y. Yan, "Extending shikimate pathway for the production of muconic acid and its precursor salicylic acid in Escherichia coli," *Metabolic Engineering*, vol. 23, no. 2014, pp. 62–69, 2014. [Online]. Available: http://dx.doi.org/10.1016/j.ymben.2014.02.009 (Cited on pages 4, 155, 156, 187, 217 and 230.)

[25] R. H. Dahl, F. Zhang, J. Alonso-Gutierrez, E. Baidoo, T. S. Batth, A. M. Redding-Johanson, C. J. Petzold, A. Mukhopadhyay, T. S. Lee, P. D. Adams, and J. D. Keasling, "Engineering dynamic pathway regulation using stress-response promoters," *Nature Biotechnology*, vol. 31, no. 11, pp. 1039–1046, 2013. [Online]. Available: http://dx.doi.org/10.1038/nbt.2689 (Cited on pages 4, 5 and 158.)

[26] T. E. Gorochowski, I. Chelysheva, M. Eriksen, P. Nair, S. Pedersen, and Z. Ignatova, "Absolute quantification of translational regulation and burden using combined sequencing approaches," *Molecular Systems Biology*, vol. 15, no. 5, pp. 1–15, 2019. (Cited on page 5.)

[27] O. Borkowski, C. Bricio, M. Murgiano, B. Rothschild-Mancinelli, G. B. Stan, and T. Ellis, "Cell-free prediction of protein expression costs for growing cells," *Nature Communications*, vol. 9, no. 1, 2018. [Online]. Available: http://dx.doi.org/10.1038/s41467-018-03970-x (Cited on pages 5, 113, 114, 183, 188, 197, 198, 199 and 209.)

[28] A. Y. Weiße, D. A. Oyarzún, V. Danos, and P. S. Swain, "Mechanistic links between cellular trade-offs, gene expression, and growth," *Proceedings of the National Academy of Sciences*, vol. 112, no. 9, 2015. (Cited on page 5.)

[29] C. Liao, A. E. Blanchard, and T. Lu, "An integrative circuit–host modelling framework for predicting synthetic gene network behaviours," *Nature Microbiology*, 2017. [Online]. Available: http://www.nature.com/articles/s41564-017-0022-5 (Cited on page 5.)

[30] E. M. Nikolados, A. Y. Weiße, F. Ceroni, and D. A. Oyarzún, "Growth Defects and Loss-of-Function in Synthetic Gene Circuits," *ACS Synthetic Biology*, vol. 8, no. 6, pp. 1231–1240, 2019. (Cited on page 5.)

[31] A. P. S. Darlington, J. Kim, and D. G. Bates, "Robustness Analysis of a Synthetic Translational Resource Allocation Controller," *IEEE Control Systems Letters*, vol. 1456, no. c, pp. 1–1, 2018. [Online]. Available: https://ieeexplore.ieee.org/document/8449077/ (Cited on page 5.)

[32] A. P. Darlington, J. Kim, J. I. Jiménez, and D. G. Bates, "Dynamic allocation of orthogonal ribosomes facilitates uncoupling of co-expressed genes," *Nature Communications*, vol. 9, no. 1, pp. 1–12, 2018. [Online]. Available: http://dx.doi.org/10.1038/s41467-018-02898-6 (Cited on page 5.)

[33] M. Dragosits, D. Nicklas, and I. Tagkopoulos, "A synthetic biology approach to self-regulatory recombinant protein production in Escherichia coli," *Journal of Biological Engineering*, vol. 6, pp. 1–10, 2012. (Cited on page 5.)

[34] Y. Siu, J. Fenno, J. M. Lindle, and M. J. Dunlop, "Design and Selection of a Synthetic Feedback Loop for Optimizing Biofuel Tolerance," *ACS Synthetic Biology*, vol. 7, no. 1, pp. 16–23, 2018. (Cited on pages 5 and 158.)

[35] F. Ceroni, A. Boo, S. Furini, T. E. Gorochowski, O. Borkowski, Y. Ladak, A. Awan, C. Gilbert, G.-B. Stan, and T. Ellis, "Burden-driven feedback control of gene expression," *Nature Methods*, vol. 15, no. 5, 2018. (Cited on pages 5, 6, 91, 92, 99 and 107.)

[36] T. E. Saleski, M. T. Chung, D. N. Carruthers, A. Khasbaatar, K. Kurabayashi, and X. N. Lin, "Optimized gene expression from bacterial chromosome by high-throughput integration and screening," *Science Advances*, vol. 7, no. 7, p. eabe1767, 2021. (Cited on pages 6 and 154.)

[37] D. J. Rankin, E. P. Rocha, and S. P. Brown, "What traits are carried on mobile genetic elements, and why," *Heredity*, vol. 106, no. 1, pp. 1–10, 2011. (Cited on page 6.)

[38] J. W. Lee, A. Gyorgy, D. E. Cameron, N. Pyenson, K. R. Choi, J. C. Way, P. A. Silver, D. Del Vecchio, and J. J. Collins, "Creating Single-Copy Genetic Circuits," *Molecular Cell*, vol. 63, no. 2, pp. 329–336, 2016. [Online]. Available: http://dx.doi.org/10.1016/j.molcel.2016.06.006 (Cited on pages 6 and 154.)

[39] Y. Park, A. Espah Borujeni, T. E. Gorochowski, J. Shin, and C. A. Voigt, "Precision design of stable genetic circuits carried in highly-insulated E. coli genomic landing pads," *Molecular Systems Biology*, vol. 16, no. 8, pp. 1–19, 2020. (Cited on pages 6 and 154.)

[40] C. Barajas, J. Gibson, L. Sandoval, and D. Del Vecchio, "Ribosome actuator via the SpoT/ppGpp pathway to mitigate gene overexpression burden," *bioRxiv*, 2021. [Online]. Available: http://biorxiv.org/content/early/2021/06/24/2021.02.11.430724.abstract (Cited on page 6.)

[41] B. D. Karkaria, N. J. Treloar, C. P. Barnes, and A. J. Fedorec, "From Microbial Communities to Distributed Computing Systems," *Frontiers in Bioengineering and Biotechnology*, vol. 8, no. July, pp. 1–22, 2020. (Cited on page 6.)

[42] L. Goers, P. Freemont, and K. M. Polizzi, "Co-culture systems and technologies: taking synthetic biology to the next level," *Journal of The Royal Society Interface*, vol. 11, no. 96, pp. 20 140 065–20 140 065, 2014. [Online]. Available: http://rsif.royalsocietypublishing.org/cgi/doi/10.1098/rsif.2014.0065 (Cited on pages 6 and 139.)

[43] J. A. Jones and X. Wang, "Use of bacterial co-cultures for the efficient production of chemicals," *Current Opinion in Biotechnology*, vol. 53, pp. 33–38, 2018. [Online]. Available: https://doi.org/10.1016/j.copbio.2017.11.012 (Cited on page 6.)

[44] X. Cao, J. J. Hamilton, and O. S. Venturelli, "Understanding and Engineering Distributed Biochemical Pathways in Microbial Communities," *Biochemistry*, vol. 58, no. 2, pp. 94–107, 2018. [Online]. Available: http://pubs.acs.org/doi/10.1021/acs.biochem.8b01006 (Cited on page 6.)

[45] H. Lu, J. C. Villada, and P. K. Lee, "Modular Metabolic Engineering for Biobased Chemical Production," *Trends in Biotechnology*, vol. 37, no. 2, pp. 152–166, 2019. [Online]. Available: https://doi.org/10.1016/j.tibtech.2018.07.003 (Cited on page 6.)

[46] C. Ge, H. Sheng, X. Chen, X. Shen, X. Sun, Y. Yan, J. Wang, and Q. Yuan, "Quorum Sensing System Used as a Tool in Metabolic Engineering," *Biotechnology Journal*, vol. 15, no. 6, pp. 1–9, 2020. (Cited on page 6.)

[47] C. J. Hartline, A. C. Schmitz, Y. Han, and F. Zhang, "Dynamic control in metabolic engineering: Theories, tools, and applications," *Metabolic Engineering*, vol. 63, pp. 126–140, 2021. [Online]. Available: https://doi.org/10.1016/j.ymben.2020.08.015 (Cited on pages 6 and 16.)

[48] J. A. Jones, V. R. Vernacchio, A. L. Sinkoe, S. M. Collins, M. H. Ibrahim, D. M. Lachance, J. Hahn, and M. A. Koffas, "Experimental and computational optimization of an Escherichia coli co-culture for the efficient production of flavonoids," *Metabolic Engineering*, vol. 35, pp. 55–63, 2016. (Cited on page 7.)

[49] Z. Chen, X. Sun, Y. Li, Y. Yan, and Q. Yuan, "Metabolic engineering of Escherichia coli for microbial synthesis of monolignols," *Metabolic Engineering*, vol. 39, no. November 2016, pp. 102–109, 2017. (Cited on pages 8 and 9.)

[50] K. Zhou, K. Qiao, S. Edgar, and G. Stephanopoulos, "Distributing a metabolic pathway among a microbial consortium enhances production of natural products," *Nature Biotechnology*, vol. 33, no. 4, pp. 377–383, 2015. [Online]. Available: http://dx.doi.org/10.1038/nbt.3095 (Cited on pages 8, 9 and 160.)

[51] P. K. Ajikumar, W. H. Xiao, K. E. Tyo, Y. Wang, F. Simeon, E. Leonard, O. Mucha, T. H. Phon, B. Pfeifer, and G. Stephanopoulos, "Isoprenoid pathway optimization for Taxol precursor overproduction in Escherichia coli," *Science*, vol. 330, no. 6000, pp. 70–74, 2010. (Cited on pages 8 and 9.)

[52] M. Puiu, I. Babaligea, C. Olmazu, A. Răducan, and D. Oancea, "Peroxidase-mediated oxidation of l-dopa: A kinetic approach," *Biochemical Engineering Journal*, vol. 52, no. 2-3, pp. 248–254, 2010. (Cited on page 9.)

[53] N. E. Grandel, K. Reyes Gamas, and M. R. Bennett, "Control of synthetic microbial consortia in time, space, and composition," *Trends in Microbiology*, vol. 29, no. 12, pp. 1095–1105, 2021. [Online]. Available: https://doi.org/10.1016/j.tim.2021.04.001 (Cited on pages 10, 16, 147 and 157.)

[54] E. H. Wintermute and P. A. Silver, "Emergent cooperation in microbial metabolism," *Molecular Systems Biology*, vol. 6, no. 407, pp. 1–7, 2010. [Online]. Available: http://dx.doi.org/10.1038/msb.2010.66 (Cited on pages 10 and 12.)

[55] A. R. Zomorrodi and D. Segrè, "Genome-driven evolutionary game theory helps understand the rise of metabolic interdependencies in microbial communities," *Nature Communications*, vol. 8, no. 1, p. 1563, 2017. [Online]. Available: http://www.nature.com/articles/s41467-017-01407-5 (Cited on pages 10 and 13.)

[56] E. Libby, L. Hebert-Dufresne, S.-R. Hossein, and A. Wagner, "Syntrophy emerges spontaneously in complex metabolic systems," *PLoS Computational Biology*, vol. 15, no. 7, p. e1007169, 2019. (Cited on page 10.)

[57] M. T. Mee, J. J. Collins, G. M. Church, and H. H. Wang, "Syntrophic exchange in synthetic microbial communities," *Proceedings of the National Academy of Sciences*, vol. 111, no. 20, pp. E2149–E2156, 2014. [Online]. Available: http://www.pnas.org/cgi/doi/10.1073/pnas.1405641111 (Cited on pages 10, 12 and 146.)

[58] O. Ponomarova, D. Sevin, M. Mülleder, K. Zirngibl, and K. Bulya, "Yeast creates a stable niche for symbiotic lactic acid bacteria through nitrogen overflow," *Cell Systems*, pp. 1–13, 2017. (Cited on pages 10, 146 and 160.)

[59] T. E. Saleski, A. R. Kerner, M. T. Chung, C. M. Jackman, A. Khasbaatar, K. Kurabayashi, and X. N. Lin, "Syntrophic co-culture amplification of production phenotype for high-throughput screening of microbial strain libraries," *Metabolic Engineering*, vol. 54, no. April, pp. 232–243, 2019. (Cited on page 10.)

[60] A. Kerner, J. Park, A. Williams, and X. N. Lin, "A programmable escherichia coli consortium via tunable symbiosis," *PLoS ONE*, vol. 7, no. 3, pp. 1–10, 2012. (Cited on pages 11 and 146.)

[61] J. K. Fredrickson, "Ecological communities by design," *Science*, vol. 348, no. 6242, pp. 1425–1427, 2015. (Cited on page 11.)

[62] M. D. Dressler, C. J. Clark, C. A. Thachettu, Y. Zakaria, O. T. Eldakar, and R. P. Smith, "Synthetically engineered microbes reveal interesting principles of cooperation," *Frontiers of Chemical Science and Engineering*, vol. 11, no. 1, pp. 3–14, 2017. (Cited on page 11.)

[63] F. K. Balagaddé, H. Song, J. Ozaki, C. H. Collins, M. Barnet, F. H. Arnold, S. R. Quake, and L. You, "A synthetic Escherichia coli predator-prey ecosystem," *Molecular Systems Biology*, vol. 4, no. 187, pp. 1–8, 2008. (Cited on pages 11, 18, 19, 60, 87 and 146.)

[64] S. R. Scott, M. O. Din, P. Bittihn, L. Xiong, L. S. Tsimring, and J. Hasty, "A stabilized microbial ecosystem of self-limiting bacteria using synthetic quorum-regulated lysis," *Nature Microbiology*, 2017. (Cited on pages 11 and 87.)

[65] M. J. Liao, M. O. Din, L. Tsimring, and J. Hasty, "Rock-paper-scissors: Engineered population dynamics increase genetic stability," *Science*, vol. 365, no. 6457, pp. 1045–1049, 2019. (Cited on pages 11, 20 and 139.)

[66] M. J. Liao, A. Miano, C. B. Nguyen, L. Chao, and J. Hasty, "Survival of the weakest in non-transitive asymmetric interactions among strains of E. coli," *Nature Communications*, vol. 11, no. 1, 2020. [Online]. Available: http://dx.doi.org/10.1038/s41467-020-19963-8 (Cited on pages 11 and 20.)

[67] T. Danino, J. Lo, A. Prindle, J. Hasty, and S. N. Bhatia, " In Vivo Gene Expression Dynamics of Tumor-Targeted Bacteria ," *ACS Synthetic Biology*, vol. 1, no. 10, pp. 465–470, 2012. (Cited on page 11.)

[68] M. O. Din, T. Danino, A. Prindle, M. Skalak, J. Selimkhanov, K. Allen, E. Julio, E. Atolia, L. S. Tsimring, S. N. Bhatia, and J. Hasty, "Synchronized cycles of bacterial lysis for in vivo delivery," *Nature*, vol. 536, no. 7614, pp. 81–85, 2016. [Online]. Available: http://dx.doi.org/10.1038/nature18930 (Cited on page 11.)

[69] A. Miano, M. J. Liao, and J. Hasty, "Inducible cell-to-cell signaling for tunable dynamics in microbial communities," *Nature Communications*, vol. 11, no. 1, pp. 1–8, 2020. [Online]. Available: http://dx.doi.org/10.1038/s41467-020-15056-8 (Cited on pages 11, 19 and 20.)

[70] A. Cubillos-Ruiz, T. Guo, A. Sokolovska, P. F. Miller, J. J. Collins, T. K. Lu, and J. M. Lora, "Engineering living therapeutics with synthetic biology," *Nature Reviews Drug Discovery*, vol. 20, no. 12, pp. 941–960, 2021. (Cited on page 11.)

[71] T. Großkopf and O. S. Soyer, "Synthetic microbial communities," *Current Opinion in Microbiology*, vol. 18, no. 1, pp. 72–77, 2014. [Online]. Available: http://dx.doi.org/10.1016/j.mib.2014.02.002 (Cited on page 12.)

[72] N. S. McCarty and R. Ledesma-Amaro, "Synthetic Biology Tools to Engineer Microbial Communities for Biotechnology," *Trends in Biotechnology*, vol. 37, no. 2, pp. 181–197, 2019. [Online]. Available: https://doi.org/10.1016/j.tibtech.2018.11.002 (Cited on page 12.)

[73] J. K. Kim, Y. Chen, A. J. Hirning, R. N. Alnahhas, K. Josić, and M. R. Bennett, "Long-range temporal coordination of gene expression in synthetic microbial consortia," *Nature Chemical Biology*, vol. 15, no. 11, pp. 1102–1109, 2019. (Cited on pages 13, 16, 121 and 139.)

[74] R. Tsoi, F. Wu, C. Zhang, S. Bewick, D. Karig, and L. You, "Metabolic division of labor in microbial systems," *PNAS*, vol. 115, no. 10, pp. 2–7, 2018. (Cited on pages 13, 21 and 147.)

[75] G. Fiore, A. Matyjaszkiewicz, F. Annunziata, C. Grierson, N. J. Savery, L. Marucci, and M. Di Bernardo, "In-Silico Analysis and Implementation of a Multicellular Feedback Control Strategy in a Synthetic Bacterial Consortium," *ACS Synthetic Biology*, vol. 6, no. 3, pp. 507–517, 2017. (Cited on page 13.)

[76] D. Fiore, D. Salzano, E. Cristòbal-Cóppulo, J. M. Olm, and M. di Bernardo, "Multicellular feedback control of a genetic toggle-switch in microbial consortia," *bioRxiv*, p. 2020.03.05.979138, 2020. (Cited on page 13.)

[77] D. Fiore, D. Salzano, E. Cristòbal-Cóppulo, J. M. Olm, and M. Di Bernardo, "Multicellular feedback control of a genetic toggle-switch in microbial consortia," pp. 151–156, 2021. (Cited on page 13.)

[78] S. S. Jang, K. T. Oishi, R. G. Egbert, and E. Klavins, "Specification and simulation of synthetic multicelled behaviors," *ACS Synthetic Biology*, vol. 1, no. 8, pp. 365–374, 2012. (Cited on page 13.)

[79] M. Gutiérrez, P. Gregorio-Godoy, G. Pérez Del Pulgar, L. E. Munoz, S. Sáez, and A. Rodríguez-Patón, "A New Improved and Extended Version of the Multicell Bacterial Simulator gro," *ACS Synthetic Biology*, vol. 6, no. 8, pp. 1496–1508, 2017. (Cited on page 13.)

[80] K. Oishi and E. Klavins, "Framework for Engineering Finite State Machines in Gene Regulatory Networks," *ACS Synthetic Biology*, vol. 3, no. 9, pp. 652–665, 2014. (Cited on page 13.)

[81] T. E. Gorochowski, A. Matyjaszkiewicz, T. Todd, N. Oak, K. Kowalska, S. Reid, K. T. Tsaneva-Atanasova, N. J. Savery, C. S. Grierson, and M. di Bernardo, "BSim: An agent-based tool for modeling bacterial populations in systems and synthetic biology," *PLoS ONE*, vol. 7, no. 8, 2012. (Cited on page 13.)

[82] A. Matyjaszkiewicz, G. Fiore, F. Annunziata, C. S. Grierson, N. J. Savery, L. Marucci, and M. Di Bernardo, "BSim 2.0: An Advanced Agent-Based Cell Simulator," *ACS Synthetic Biology*, vol. 6, no. 10, pp. 1969–1972, 2017. (Cited on page 13.)

[83] N. J. Treloar, A. J. Fedorec, B. Ingalls, and C. P. Barnes, "Deep reinforcement learning for the control of microbial co-cultures in bioreactors," *PLoS Computational Biology*, vol. 16, no. 4, pp. 1–18, 2020. [Online]. Available: http://dx.doi.org/10.1371/journal.pcbi.1007783 (Cited on page 13.)

[84] B. D. Karkaria, A. J. Fedorec, and C. P. Barnes, "Automated design of synthetic microbial communities," *Nature Communications*, vol. 12, no. 1, pp. 1–12, 2021. [Online]. Available: https://doi.org/10.1038/s41467-020-20756-2 (Cited on page 13.)

[85] C. Ronda and H. H. Wang, "Engineering temporal dynamics in microbial communities," *Current Opinion in Microbiology*, vol. 65, pp. 47–55, 2022. [Online]. Available: https://doi.org/10.1016/j.mib.2021.10.009 (Cited on page 13.)

[86] A. Simons, K. Alhanout, and R. E. Duval, "Bacteriocins, antimicrobial peptides from bacterial origin: Overview of their biology and their impact against multidrug-resistant bacteria," *Microorganisms*, vol. 8, no. 5, 2020. (Cited on page 14.)

[87] A. J. Fedorec, B. D. Karkaria, M. Sulu, and C. P. Barnes, "Single strain control of microbial consortia," *Nature Communications*, vol. 12, no. 1, pp. 1–12, 2021. [Online]. Available: http://dx.doi.org/10.1038/s41467-021-22240-x (Cited on pages 14, 17, 18, 87, 139, 150 and 179.)

[88] C. Chen, X. Yang, and X. Shen, "Confirmed and potential roles of bacterial T6SSs in the intestinal ecosystem," *Frontiers in Microbiology*, vol. 10, no. JUN, pp. 1–11, 2019. (Cited on page 14.)

[89] S. Y. Ting, E. Martínez-García, S. Huang, S. K. Bertolli, K. A. Kelly, K. J. Cutler, E. D. Su, H. Zhi, Q. Tang, M. C. Radey, M. Raffatellu, S. B. Peterson, V. de Lorenzo, and J. D. Mougous, "Targeted Depletion of Bacteria from Mixed Populations by Programmable Adhesion with Antagonistic Competitor Cells," *Cell Host and Microbe*, vol. 28, no. 2, pp. 313–321.e6, 2020. (Cited on page 14.)

[90] A. Boo, R. Ledesma Amaro, and G.-B. Stan, "Quorum sensing in synthetic biology: A review," *Current Opinion in Systems Biology*, vol. 28, p. 100378, 2021. [Online]. Available: https://doi.org/10.1016/j.coisb.2021.100378 (Cited on pages 14, 15, 16, 17, 19 and 60.)

[91] A. Eberhard, A. L. Burlingame, C. Eberhard, G. L. Kenyon, K. H. Nealson, and N. J. Oppenheimer, "Structural Identification of Autoinducer of Photobacterium fischeri Luciferase," *Biochemistry*, vol. 20, no. 9, pp. 2444–2449, 1981. (Cited on pages 14 and 146.)

[92] J. Engebrecht, K. Nealson, and M. Silverman, "Bacterial bioluminescence: Isolation and genetic analysis of functions from Vibrio fischeri," *Cell*, vol. 32, no. 3, pp. 773–781, 1983. (Cited on pages 14 and 146.)

[93] J. A. Engebrecht and M. Silverman, "Identification of genes and gene products necessary for bacterial bioluminescence," *Proceedings of the National Academy of Sciences of the United States of America*, vol. 81, no. 13 I, pp. 4154–4158, 1984. (Cited on pages 14 and 146.)

[94] R. M. Davis, R. Y. Muller, and K. A. Haynes, "Can the natural diversity of quorum-sensing advance synthetic biology?" *Frontiers in Bioengineering and Biotechnology*, vol. 3, p. 30, 2015. [Online]. Available: https://www.frontiersin.org/article/10.3389/fbioe.2015.00030 (Cited on page 14.)

[95] K. Papenfort and B. L. Bassler, "Quorum sensing signal-response systems in Gram-negative bacteria," *Nature Reviews Microbiology*, vol. 14, no. 9, pp. 576–588, 2016. (Cited on page 14.)

[96] Z. Zhang, Y. Zheng, P. Han, H. Dong, X. Liang, G. Yin, D. Wu, Y. Yang, S. Liu, M. Liu, and L. Hou, "N-acyl-homoserine lactones (AHLs) in intertidal marsh: diversity and potential role in nitrogen cycling," *Plant and Soil*, vol. 454, no. 1-2, pp. 103–119, 2020. (Cited on page 14.)

[97] M. B. Miller, K. Skorupski, D. H. Lenz, R. K. Taylor, and B. L. Bassler, "Parallel quorum sensing systems converge to regulate virulence in Vibrio cholerae," *Cell*, vol. 110, no. 3, pp. 303–314, 2002. (Cited on page 15.)

[98] J. C. Van Kessel, S. T. Rutherford, Y. Shao, A. F. Utria, and B. L. Bassler, "Individual and combined roles of the master regulators apha and luxr in control of the Vibrio harveyi quorum-sensing regulon," *Journal of Bacteriology*, vol. 195, no. 3, pp. 436–443, 2013. (Cited on page 15.)

[99] J. G. Cao and E. A. Meighen, "Purification and structural identification of an autoinducer for the luminescence system of Vibrio harveyi," *Journal of Biological Chemistry*, vol. 264, no. 36, pp. 21 670–21 676, 1989. [Online]. Available: http://dx.doi.org/10.1016/S0021-9258(20)88238-6 (Cited on page 15.)

[100] B. L. Bassler, E. P. Greenberg, and A. M. Stevens, "Cross-species induction of luminescence in the quorum-sensing bacterium Vibrio harveyi," *Journal of Bacteriology*, vol. 179, no. 12, pp. 4043–4045, 1997. (Cited on page 15.)

[101] M. G. Surette, M. B. Miller, and B. L. Bassler, "Quorum sensing in Escherichia coli, Salmonella typhimurium, and Vibrio harveyi: A new family of genes responsible for autoinducer production," *Proceedings of the National Academy of Sciences of the United States of America*, vol. 96, no. 4, pp. 1639–1644, 1999. (Cited on page 15.)

[102] S. Schauder, K. Shokat, M. G. Surette, and B. L. Bassler, "The LuxS family of bacterial autoinducers: Biosynthesis of a novel quorum-sensing signal molecule," *Molecular Microbiology*, vol. 41, no. 2, pp. 463–476, 2001. (Cited on page 15.)

[103] D. A. Higgins, M. E. Pomianek, C. M. Kraml, R. K. Taylor, M. F. Semmelhack, and B. L. Bassler, "The major Vibrio cholerae autoinducer and its role in virulence factor production," *Nature*, vol. 450, no. 7171, pp. 883–886, 2007. (Cited on page 15.)

[104] M. Whiteley, S. P. Diggle, and E. P. Greenberg, "Progress in and promise of bacterial quorum sensing research," *Nature*, vol. 551, no. 7680, pp. 313–320, 2017. (Cited on page 15.)

[105] K. Stephens and W. E. Bentley, "Synthetic Biology for Manipulating Quorum Sensing in Microbial Consortia," *Trends in Microbiology*, vol. 28, no. 8, pp. 633–643, 2020. [Online]. Available: https://doi.org/10.1016/j.tim.2020.03.009 (Cited on pages 15 and 16.)

[106] T. Xue, L. Zhao, H. Sun, X. Zhou, and B. Sun, "LsrR-binding site recognition and regulatory characteristics in Escherichia coli AI-2 quorum sensing," *Cell Research*, vol. 19, no. 11, pp. 1258–1268, 2009. (Cited on page 15.)

[107] L. Wang, Y. Hashimoto, C. Y. Tsao, J. J. Valdes, and W. E. Bentley, "Cyclic AMP (cAMP) and cAMP receptor protein influence both synthesis and uptake of extracellular autoinducer 2 in Escherichia coli," *Journal of Bacteriology*, vol. 187, no. 6, pp. 2066–2076, 2005. (Cited on page 15.)

[108] C. Y. Tsao, S. Hooshangi, H. C. Wu, J. J. Valdes, and W. E. Bentley, "Autonomous induction of recombinant proteins by minimally rewiring native quorum sensing regulon of E. coli," *Metabolic Engineering*, vol. 12, no. 3, pp. 291–297, 2010. [Online]. Available: http://dx.doi.org/10.1016/j.ymben.2010.01.002 (Cited on page 15.)

[109] J. H. Ha, P. Hauk, K. Cho, Y. Eo, X. Ma, K. Stephens, S. Cha, M. Jeong, J. Y. Suh, H. O. Sintim, W. E. Bentley, and K. S. Ryu, "Evidence of link between quorum sensing and sugar metabolism in Escherichia coli revealed via cocrystal structures of LsrK and HPr," *Science Advances*, vol. 4, no. 6, p. eaar7063, 2018. (Cited on page 15.)

[110] P. Hauk, K. Stephens, R. McKay, C. R. Virgile, H. Ueda, M. Ostermeier, K. S. Ryu, H. O. Sintim, and W. E. Bentley, "Insightful directed evolution of Escherichia coli quorum sensing promoter region of the lsrACDBFG operon: A tool for synthetic biology systems and protein expression," *Nucleic Acids Research*, vol. 44, no. 21, pp. 10 515–10 525, 2016. (Cited on page 15.)

[111] S. R. Scott and J. Hasty, "Quorum Sensing Communication Modules for Microbial Consortia," *ACS Synthetic Biology*, vol. 5, no. 9, pp. 969–977, 2016. (Cited on pages 15, 19, 60, 61, 62, 63, 64, 186 and 190.)

[112] N. Kylilis, Z. A. Tuza, G. B. Stan, and K. M. Polizzi, "Tools for engineering coordinated system behaviour in synthetic microbial consortia," *Nature Communications*, vol. 9, no. 1, pp. 1–9, 2018. [Online]. Available: http://dx.doi.org/10.1038/s41467-018-05046-2 (Cited on pages 15, 60 and 197.)

[113] A. Gupta, I. M. B. Reizman, C. R. Reisch, and K. L. J. Prather, "Dynamic regulation of metabolic flux in engineered bacteria using a pathway-independent quorum-sensing circuit," *Nature Biotechnology*, vol. 35, no. 3, pp. 273–279, 2017. [Online]. Available: http://www.nature.com/doifinder/10.1038/nbt.3796 (Cited on pages 16, 27, 60 and 158.)

[114] F. Gu, W. Jiang, Y. Mu, H. Huang, T. Su, Y. Luo, Q. Liang, and Q. Qi, "Quorum sensing-based dual-function switch and its application in solving two key metabolic engineering problems," *ACS Synthetic Biology*, vol. 9, no. 2, pp. 209–217, 2020. (Cited on page 16.)

[115] W. Jiang, X. He, Y. Luo, Y. Mu, F. Gu, Q. Liang, and Q. Qi, "Two Completely Orthogonal Quorum Sensing Systems with Self-Produced Autoinducers Enable Automatic Delayed Cascade Control," *ACS Synthetic Biology*, vol. 9, no. 9, pp. 2588–2599, 2020. (Cited on page 16.)

[116] R. N. Alnahhas, M. Sadeghpour, Y. Chen, A. A. Frey, W. Ott, K. Josić, and M. R. Bennett, "Majority sensing in synthetic microbial consortia," *Nature Communications*, vol. 11, no. 1, pp. 1–10, 2020. (Cited on pages 16, 119, 121 and 154.)

[117] P. Bittihn, M. O. Din, L. S. Tsimring, and J. Hasty, "Rational engineering of synthetic microbial systems : from single cells to consortia," *Current Opinion in Microbiology*, vol. 45, pp. 92–99, 2018. [Online]. Available: https://doi.org/10.1016/j.mib.2018.02.009 (Cited on page 16.)

[118] C. V. Dinh, X. Chen, and K. L. Prather, "Development of a Quorum-Sensing Based Circuit for Control of Coculture Population Composition in a Naringenin Production System," *ACS Synthetic Biology*, vol. 9, no. 3, pp. 590–597, 2020. (Cited on pages 16, 17 and 157.)

[119] K. Stephens, M. Pozo, C. Y. Tsao, P. Hauk, and W. E. Bentley, "Bacterial co-culture with cell signaling translator and growth controller modules for autonomously regulated culture composition," *Nature Communications*, vol. 10, no. 1, pp. 1–11, 2019. [Online]. Available: http://dx.doi.org/10.1038/s41467-019-12027-6 (Cited on pages 19, 20, 88 and 146.)

[120] G. Singh, M. Yadav, C. Ghosh, and J. S. Rathore, "Bacterial toxin-antitoxin modules: classification, functions, and association with persistence," *Current Research in Microbial Sciences*, vol. 2, p. 100047, 2021. [Online]. Available: https://doi.org/10.1016/j.crmicr.2021.100047 (Cited on page 18.)

[121] X. Ren, A. A. Baetica, A. Swaminathan, and R. M. Murray, "Population regulation in microbial consortia using dual feedback control," *2017 IEEE 56th Annual Conference on Decision and Control, CDC 2017*, vol. 2018-Janua, no. CDC, pp. 5341–5347, 2018. (Cited on page 20.)

[122] R. D. Mccardell, A. Pandey, and R. M. Murray, "Control of density and composition in an engineered two-member bacterial community," *bioRxiv*, 2019. (Cited on page 20.)

[123] J. Chappell, M. K. Takahashi, S. Meyer, D. Loughrey, K. E. Watters, and J. Lucks, "The centrality of RNA for engineering gene expression," *Biotechnology Journal*, vol. 8, no. 12, pp. 1379–1395, 2013. (Cited on pages 22 and 26.)

[124] J. Chappell, K. E. Watters, M. K. Takahashi, and J. B. Lucks, "A renaissance in RNA synthetic biology: New mechanisms, applications and tools for the future," *Current Opinion in Chemical Biology*, vol. 28, pp. 47–56, 2015. [Online]. Available: http://dx.doi.org/10.1016/j.cbpa.2015.05.018 (Cited on pages 22 and 26.)

[125] M. A. English, R. V. Gayet, and J. J. Collins, "Designing Biological Circuits: Synthetic Biology within the Operon Model and beyond," *Annual Review of Biochemistry*, vol. 90, pp. 221–244, 2021. (Cited on pages 22 and 23.)

[126] M. Verosloff, J. Chappell, K. L. Perry, J. R. Thompson, and J. B. Lucks, "PLANT-Dx: A Molecular Diagnostic for Point of Use Detection of Plant Pathogens," *bioRxiv*, 2018. (Cited on page 22.)

[127] J. S. Gootenberg, O. O. Abudayyeh, M. J. Kellner, J. Joung, J. J. Collins, and F. Zhang, "Multiplexed and portable nucleic acid detection platform with Cas13, Cas12a and Csm6," *Science*, vol. 360, no. 6387, pp. 439–444, 2018. (Cited on page 22.)

[128] J. K. Jung, K. K. Alam, M. S. Verosloff, D. A. Capdevila, M. Desmau, P. R. Clauer, J. W. Lee, P. Q. Nguyen, P. A. Pastén, S. J. Matiasek, J. F. Gaillard, D. P. Giedroc, J. J. Collins, and J. B. Lucks, "Cell-free biosensors for rapid detection of water contaminants," *Nature Biotechnology*, vol. 38, no. 12, pp. 1451–1459, 2020. [Online]. Available: http://dx.doi.org/10.1038/s41587-020-0571-7 (Cited on page 22.)

[129] H. De Puig, I. Bosch, J. J. Collins, and L. Gehrke, "Point-of-Care Devices to Detect Zika and Other Emerging Viruses," *Annual Review of Biomedical Engineering*, vol. 22, pp. 371–386, 2020. (Cited on page 22.)

[130] J. Chappell, A. Westbrook, M. Verosloff, and J. B. Lucks, "Computational design of small transcription activating RNAs for versatile and dynamic gene regulation," *Nature Communications*, vol. 8, no. 1, pp. 1–11, 2017. [Online]. Available: http://dx.doi.org/10.1038/s41467-017-01082-6 (Cited on pages 22, 26, 32, 33, 34, 36, 48, 147, 186, 187, 188, 190, 196, 201, 202, 203, 204, 205, 207, 208, 209, 219 and 223.)

[131] D. Na, S. M. Yoo, H. Chung, H. Park, J. H. Park, and S. Y. Lee, "Metabolic engineering of Escherichia coli using synthetic small regulatory RNAs," *Nature Biotechnology*, vol. 31, no. 2, pp. 170–174, 2013. [Online]. Available: http://dx.doi.org/10.1038/nbt.2461 (Cited on pages 22, 25, 101, 102, 189 and 200.)

[132] I. Farasat, M. Kushwaha, J. Collens, M. Easterbrook, M. Guido, and H. M. Salis, "Efficient search, mapping, and optimization of multi-protein genetic systems in diverse bacteria," *Molecular Systems Biology*, vol. 10, no. 6, p. 731, 2014. (Cited on page 22.)

[133] M. H. Larson, L. A. Gilbert, X. Wang, W. A. Lim, J. S. Weissman, and L. S. Qi, "CRISPR interference (CRISPRi) for sequence-specific control of gene expression," *Nature Protocols*, vol. 8, no. 11, pp. 2180–2196, 2013. (Cited on page 23.)

[134] R. Zhang, W. Xu, S. Shao, and Q. Wang, "Gene Silencing Through CRISPR Interference in Bacteria: Current Advances and Future Prospects," *Frontiers in Microbiology*, vol. 12, no. March, pp. 1–8, 2021. (Cited on page 23.)

[135] J. Santos-Moreno and Y. Schaerli, "CRISPR-based gene expression control for synthetic gene circuits," *Biochemical Society Transactions*, vol. 48, no. 5, pp. 1979–1993, 2020. (Cited on page 23.)

[136] J. Santos-Moreno, E. Tasiudi, J. Stelling, and Y. Schaerli, "Multistable and dynamic CRISPRi-based synthetic circuits," *Nature Communications*, vol. 11, no. 1, pp. 1–8, 2020. [Online]. Available: http://dx.doi.org/10.1038/s41467-020-16574-1 (Cited on page 23.)

[137] Y. J. Lee, A. Hoynes-O'Connor, M. C. Leong, and T. S. Moon, "Programmable control of bacterial gene expression with the combined CRISPR and antisense RNA system," *Nucleic Acids Research*, vol. 44, no. 5, pp. 2462–2473, 2016. (Cited on page 23.)

[138] S. Cho, J. Shin, and B. K. Cho, "Applications of CRISPR/Cas system to bacterial metabolic engineering," *International Journal of Molecular Sciences*, vol. 19, no. 4, 2018. (Cited on page 23.)

[139] Y. Zheng, T. Su, and Q. Qi, "Microbial CRISPRi and CRISPRa Systems for Metabolic Engineering," *Biotechnology and Bioprocess Engineering*, vol. 24, no. 4, pp. 579–591, 2019. (Cited on page 23.)

[140] N. S. McCarty, A. E. Graham, L. Studená, and R. Ledesma-Amaro, "Multiplexed CRISPR technologies for gene editing and transcriptional regulation," *Nature Communications*, vol. 11, no. 1, pp. 1–13, 2020. [Online]. Available: http://dx.doi.org/10.1038/s41467-020-15053-x (Cited on page 23.)

[141] J. Fontana, D. Sparkman-Yager, J. G. Zalatan, and J. M. Carothers, "Challenges and opportunities with CRISPR activation in bacteria for data-driven metabolic engineering," *Current Opinion in Biotechnology*, vol. 64, pp. 190–198, 2020. [Online]. Available: https://doi.org/10.1016/j.copbio.2020.04.005 (Cited on page 23.)

[142] S. K. Kim, G. H. Han, W. Seong, H. Kim, S. W. Kim, D. H. Lee, and S. G. Lee, "CRISPR interference-guided balancing of a biosynthetic mevalonate pathway increases terpenoid production," *Metabolic Engineering*, vol. 38, pp. 228–240, 2016. [Online]. Available: http://dx.doi.org/10.1016/j.ymben.2016.08.006 (Cited on page 23.)

[143] A. Calvo-Villamañán, J. W. Ng, R. Planel, H. Ménager, A. Chen, L. Cui, and D. Bikard, "On-target activity predictions enable improved CRISPR-dCas9 screens in bacteria," *Nucleic Acids Research*, vol. 48, no. 11, 2020. (Cited on page 24.)

[144] J. Dhanjal, D. Vora, N. Radhakrishnan, and D. Sundar, "Computational Approaches for Designing Highly Specific and Efficient sgRNAs," in *Microbial Systems Biology*. Humana, New York, NY, 2022, pp. 147–166. (Cited on page 24.)

[145] H. Todor, M. R. Silvis, H. Osadnik, and C. A. Gross, "Bacterial CRISPR screens for gene function," *Current Opinion in Microbiology*, vol. 59, pp. 102–109, 2021. [Online]. Available: https://doi.org/10.1016/j.mib.2020.11.005 (Cited on page 24.)

[146] F. Rousset, L. Cui, E. Siouve, C. Becavin, F. Depardieu, and D. Bikard, "Genome-wide CRISPR-dCas9 screens in E. coli identify essential genes and phage host factors," *PLoS Genetics*, vol. 14, no. 11, pp. 1–28, 2018. (Cited on pages 24 and 89.)

[147] L. Cui, A. Vigouroux, F. Rousset, H. Varet, V. Khanna, and D. Bikard, "A CRISPRi screen in E. coli reveals sequence-specific toxicity of dCas9," *Nature Communications*, vol. 9, no. 1, pp. 1–10, 2018. [Online]. Available: http://dx.doi.org/10.1038/s41467-018-04209-5 (Cited on pages 24 and 91.)

[148] I. S. Myrbråten, K. Wiull, Z. Salehian, L. S. Håvarstein, D. Straume, G. Mathiesen, and M. Kjos, "CRISPR Interference for Rapid Knockdown of Essential Cell Cycle Genes in Lactobacillus plantarum," *mSphere*, vol. 4, no. 2, pp. e00 007–19, 2019. (Cited on page 24.)

[149] H. H. Lee, N. Ostrov, B. G. Wong, M. A. Gold, A. S. Khalil, and G. M. Church, "Functional genomics of the rapidly replicating bacterium Vibrio natriegens by CRISPRi," *Nature Microbiology*, vol. 4, no. 7, pp. 1105–1113, 2019. [Online]. Available: http://dx.doi.org/10.1038/s41564-019-0423-8 (Cited on page 24.)

[150] J. S. Hawkins, M. R. Silvis, B. M. Koo, J. M. Peters, H. Osadnik, M. Jost, C. C. Hearne, J. S. Weissman, H. Todor, and C. A. Gross, "Mismatch-CRISPRi Reveals the Co-varying Expression-Fitness Relationships of Essential Genes in Escherichia coli and Bacillus subtilis," *Cell Systems*, vol. 11, no. 5, pp. 523–535.e9, 2020. [Online]. Available: https://doi.org/10.1016/j.cels.2020.09.009 (Cited on page 24.)

[151] M. Jost, D. A. Santos, R. A. Saunders, M. A. Horlbeck, J. S. Hawkins, S. M. Scaria, T. M. Norman, J. A. Hussmann, C. R. Liem, C. A. Gross, and J. S. Weissman, "Titrating gene expression using libraries of systematically attenuated CRISPR guide RNAs," *Nature Biotechnology*, vol. 38, no. 3, pp. 355–364, 2020. [Online]. Available: http://dx.doi.org/10.1038/s41587-019-0387-5 (Cited on page 24.)

[152] L. A. Gilbert, M. A. Horlbeck, B. Adamson, J. E. Villalta, Y. Chen, E. H. Whitehead, C. Guimaraes, B. Panning, H. L. Ploegh, M. C. Bassik, L. S. Qi, M. Kampmann, and J. S. Weissman, "Genome-Scale CRISPR-Mediated Control of Gene Repression and Activation," *Cell*, vol. 159, no. 3, pp. 647–661, 2014. [Online]. Available: http://dx.doi.org/10.1016/j.cell.2014.09.029 (Cited on page 24.)

[153] T. Sander, C. Y. Wang, T. Glatter, and H. Link, " CRISPRi-Based Downregulation of Transcriptional Feedback Improves Growth and Metabolism of Arginine Overproducing E. coli ," *ACS Synthetic Biology*, vol. 8, pp. 1983–1990, 2019. (Cited on page 24.)

[154] A. Vigouroux, E. Oldewurtel, L. Cui, D. Bikard, and S. Teeffelen, "Tuning dCas9's ability to block transcription enables robust, noiseless knockdown of bacterial genes," *Molecular Systems Biology*, vol. 14, no. 3, pp. 1–14, 2018. (Cited on page 24.)

[155] A. A. Nielsen and C. A. Voigt, " Multi-input CRISPR / C as genetic circuits that interface host regulatory networks ," *Molecular Systems Biology*, vol. 10, no. 11, p. 763, 2014. (Cited on page 24.)

[156] F. Ceroni, A. Boo, S. Furini, T. E. Gorochowski, O. Borkowski, Y. N. Ladak, A. R. Awan, C. Gilbert, G.-B. Stan, and T. Ellis, "Burden-driven feedback control of gene expression," *Nature Methods*, vol. 15, no. 5, pp. 387–393, 2018. [Online]. Available: http://www.nature.com/doifinder/10.1038/nmeth.4635 (Cited on pages 24, 95, 158, 159, 160, 186, 187, 188, 194, 196 and 229.)

[157] G. Storz, J. Vogel, and K. M. Wassarman, "Regulation by Small RNAs in Bacteria: Expanding Frontiers," *Molecular Cell*, vol. 43, no. 6, pp. 880–891, 2011. (Cited on page 25.)

[158] D. Lalaouna, M. Simoneau-Roy, D. Lafontaine, and E. Massé, "Regulatory RNAs and target mRNA decay in prokaryotes," *Biochimica et Biophysica Acta - Gene Regulatory Mechanisms*, vol. 1829, no. 6-7, pp. 742–747, 2013. [Online]. Available: http://dx.doi.org/10.1016/j.bbagrm.2013.02.013 (Cited on page 25.)

[159] T. Morita and H. Aiba, "RNase E action at a distance: Degradation of target mRNAs mediated by an Hfq-binding small RNA in bacteria," *Genes and Development*, vol. 25, no. 4, pp. 294–298, 2011. (Cited on pages 25 and 101.)

[160] M. R. d. C. R. Lins, L. A. d. S. Amorim, G. G. Corrêa, B. W. Picão, M. Mack, M. O. Cerri, and D. B. Pedrolli, "Targeting riboswitches with synthetic small RNAs for metabolic engineering," *Metabolic Engineering*, vol. 68, no. August, pp. 59–67, 2021. (Cited on page 25.)

[161] A. Ghodasara and C. A. Voigt, "Balancing gene expression without library construction via a reusable sRNA pool," *Nucleic Acids Research*, vol. 45, no. 13, pp. 8116–8127, 2017. (Cited on pages 25 and 101.)

[162] C. L. Kelly, A. W. K. Harris, H. Steel, E. J. Hancock, J. T. Heap, and A. Papachristodoulou, "Synthetic negative feedback circuits using engineered small RNAs," *Nucleic Acids Research*, vol. 46, no. 18, pp. 9875–9889, 2018. [Online]. Available: https://academic.oup.com/nar/advance-article/doi/10.1093/nar/gky828/5096075 (Cited on pages 25, 101 and 102.)

[163] V. Sharma, A. Yamamura, and Y. Yokobayashi, "Engineering artificial small RNAs for Conditional gene silencing in escherichia coli," *ACS Synthetic Biology*, vol. 1, no. 1, pp. 6–13, 2012. (Cited on page 25.)

[164] A. Dwijayanti, M. Storch, G.-b. Stan, G. S. Baldwin, I. Hub, W. C. Campus, B. Building, S. K. Campus, S. Alexander, F. Building, and S. K. Campus, "A modular RNA interference system for multiplexed gene regulation," *bioRxiv*, 2021. (Cited on page 25.)

[165] J. Meng, G. Kanzaki, D. Meas, C. K. Lam, H. Crummer, J. Tain, and H. H. Xu, "A genome-wide inducible phenotypic screen identifies antisense RNA constructs silencing Escherichia coli essential genes," *FEMS Microbiology Letters*, vol. 329, no. 1, pp. 45–53, 2012. (Cited on pages 25 and 101.)

[166] E. Noro, M. Mori, G. Makino, Y. Takai, S. Ohnuma, A. Sato, M. Tomita, K. Nakahigashi, and A. Kanai, "Systematic characterization of artificial small RNA-mediated inhibition of Escherichia coli growth," *RNA Biology*, vol. 14, no. 2, pp. 206–218, 2017. (Cited on pages 25 and 105.)

[167] M. Kawano, S. Morohashi, K. Oda, M. Ishikawa, S. Fujita, and M. Saito, "Artificial small RNA-mediated growth inhibition in Escherichia coli and Salmonella enterica serovar Typhimurium," *Biochemical and Biophysical Research Communications*, vol. 521, no. 3, pp. 577–583, 2020. (Cited on pages 25, 105, 106, 107, 151 and 210.)

[168] J. Chappell, M. K. Takahashi, and J. B. Lucks, "Creating small transcription activating RNAs," *Nature Chemical Biology*, vol. 11, no. 3, pp. 214–220, 2015. (Cited on page 26.)

[169] S. Meyer, J. Chappell, S. Sankar, R. Chew, and J. B. Lucks, "Improving fold activation of small transcription activating RNAs (STARs) with rational RNA engineering strategies," *Biotechnology and Bioengineering*, vol. 113, no. 1, pp. 216–225, 2016. (Cited on page 26.)

[170] A. M. Westbrook and J. B. Lucks, "Achieving large dynamic range control of gene expression with a compact RNA transcription-translation regulator," *Nucleic Acids Research*, vol. 45, no. 9, pp. 5614–5624, 2017. (Cited on page 26.)

[171] S. Hong, D. Jeong, J. Ryan, M. Foo, X. Tang, and J. Kim, "Design and evaluation of synthetic rna-based incoherent feed-forward loop circuits," *Biomolecules*, vol. 11, no. 8, p. 1182, 2021. (Cited on page 26.)

[172] C. J. Glasscock, B. W. Biggs, J. T. Lazar, J. H. Arnold, L. A. Burdette, A. Valdes, M. K. Kang, D. Tullman-Ercek, K. E. Tyo, and J. B. Lucks, "Dynamic Control of Gene Expression with Riboregulated Switchable Feedback Promoters," *ACS Synthetic Biology*, vol. 10, no. 5, pp. 1199–1213, 2021. (Cited on pages 26 and 160.)

[173] Y. J. Lee, S.-j. Kim, and T. S. Moon, "Multilevel Regulation of Bacterial Gene Expression with the Combined STAR and Antisense RNA System," 2018. (Cited on pages 26, 224 and 225.)

[174] A. A. Green, P. A. Silver, J. J. Collins, and P. Yin, "Toehold switches: De-novo-designed regulators of gene expression," *Cell*, vol. 159, no. 4, pp. 925–939, 2014. [Online]. Available: http://dx.doi.org/10.1016/j.cell.2014.10.002 (Cited on pages 36 and 45.)

[175] M. Mann, P. R. Wright, and R. Backofen, "IntaRNA 2.0: Enhanced and customizable prediction of RNA-RNA interactions," *Nucleic Acids Research*, vol. 45, no. W1, pp. W435–W439, 2017. (Cited on pages 36, 40, 41 and 189.)

[176] A.-r. Allouche, "Software News and Updates Gabedit — A Graphical User Interface for Computational Chemistry Softwares," *Journal of computational chemistry*, vol. 32, pp. 174–182, 2012. (Cited on pages 40 and 41.)

[177] H. Steel, R. Habgood, C. Kelly, and A. Papachristodoulou, "In situ characterisation and manipulation of biological systems with Chi.Bio," *PLoS Biology*, vol. 18, no. 7, pp. 1–12, 2020. (Cited on pages 57, 119, 141, 142 and 184.)

[178] A. Halleran and R. M. Murray, "Cell-free and in vivo characterization of Lux, Las, and Rpa quorum activation systems in E. coli," *ACS Synthetic Biology*, p. acssynbio.7b00376, 2017. [Online]. Available: http://pubs.acs.org/doi/abs/10.1021/acssynbio.7b00376 (Cited on page 60.)

[179] G. Pothoulakis, F. Ceroni, B. Reeve, and T. Ellis, "The Spinach RNA aptamer as a characterization tool for synthetic biology," *ACS Synthetic Biology*, vol. 3, no. 3, pp. 182–187, 2014. (Cited on page 66.)

[180] G. S. Filonov and S. R. Jaffrey, "RNA Imaging with Dimeric Broccoli in Live Bacterial and Mammalian Cells," *Current protocols in chemical biology*, vol. 8, no. 1, pp. 1–28, 2016. (Cited on page 66.)

[181] K. P. Clifton, E. M. Jones, S. Paudel, J. P. Marken, C. E. Monette, A. D. Halleran, L. Epp, and M. S. Saha, "The genetic insulator RiboJ increases expression of insulated genes," *Journal of Biological Engineering*, vol. 12, no. 1, pp. 1–6, 2018. (Cited on page 74.)

[182] A. J. Meyer, T. H. Segall-Shapiro, E. Glassey, J. Zhang, and C. A. Voigt, "Escherichia coli "Marionette" strains with 12 highly optimized small-molecule sensors," *Nature Chemical Biology*, vol. 15, no. 2, pp. 196–204, 2019. [Online]. Available: http://dx.doi.org/10.1038/s41589-018-0168-3 (Cited on pages 74, 75, 152, 156, 186, 188 and 191.)

[183] P. Du, H. Zhao, H. Zhang, R. Wang, J. Huang, Y. Tian, X. Luo, X. Luo, M. Wang, Y. Xiang, L. Qian, Y. Chen, Y. Tao, and C. Lou, "De novo design of an intercellular signaling toolbox for multi-channel cell–cell communication and biological computation," *Nature Communications*, vol. 11, no. 1, pp. 1–11, 2020. [Online]. Available: http://dx.doi.org/10.1038/s41467-020-17993-w (Cited on pages 77, 156, 192 and 193.)

[184] G. Lillacci, S. K. Aoki, A. Gupta, A. Baumschlager, and M. Khammash, "A universal rationally-designed biomolecular integral feedback controller for robust perfect adaptation," *Nature*, vol. 570, no. 7762, pp. 533–537, 2019. [Online]. Available: http://dx.doi.org/10.1038/s41586-019-1321-1 (Cited on pages 88, 93, 150 and 158.)

[185] F. Baquero, V. F. Lanza, M. R. Baquero, R. del Campo, and D. A. Bravo-Vázquez, "Microcins in Enterobacteriaceae: Peptide Antimicrobials in the Eco-Active Intestinal Chemosphere," *Frontiers in Microbiology*, vol. 10, no. October, pp. 1–25, 2019. (Cited on page 88.)

[186] S. Li, C. B. Jendresen, J. Landberg, L. E. Pedersen, N. Sonnenschein, S. I. Jensen, and A. T. Nielsen, "Genome-Wide CRISPRi-Based Identification of Targets for Decoupling Growth from Production," *ACS Synthetic Biology*, vol. 9, 2020. (Cited on page 89.)

[187] P. D. Karp, D. Weaver, S. Paley, C. Fulcher, A. Kubo, A. Kothari, M. Krummenacker, P. Subhraveti, D. Weerasinghe, S. Gama-Castro, A. M. Huerta, L. Muñiz-Rascado, C. Bonavides-Martinez, V. Weiss, M. Peralta-Gil, A. Santos-Zavaleta, I. Schröder, A. Mackie, R. Gunsalus, J. Collado-Vides, I. M. Keseler, and I. Paulsen, "The EcoCyc Database Peter," *Physiology & behavior*, vol. 176, no. 12, pp. 139–148, 2017. (Cited on page 91.)

[188] C. Zhao, X. Shu, and B. Sun, "Construction of a gene knockdown system based on catalytically inactive ("dead") Cas9 (dCas9) in Staphylococcus aureus," *Applied and Environmental Microbiology*, vol. 83, no. 12, 2017. (Cited on page 91.)

[189] A. R. Joyce, J. L. Reed, A. White, R. Edwards, A. Osterman, T. Baba, H. Mori, S. A. Lesely, B. Palsson, and S. Agarwalla, "Experimental and computational assessment of conditionally essential genes in Escherichia coli," *Journal of Bacteriology*, vol. 188, no. 23, pp. 8259–8271, 2006. (Cited on page 91.)

[190] Y. Gao and Y. Zhao, "Self-processing of ribozyme-flanked RNAs into guide RNAs in vitro and in vivo for CRISPR-mediated genome editing," *Journal of Integrative Plant Biology*, vol. 56, no. 4, pp. 343–349, 2014. (Cited on pages 91 and 188.)

[191] W. M. Shaw, H. Yamauchi, J. Mead, G. O. F. Gowers, D. J. Bell, D. Öling, N. Larsson, M. Wigglesworth, G. Ladds, and T. Ellis, "Engineering a Model Cell for Rational Tuning of GPCR Signaling," *Cell*, vol. 177, no. 3, pp. 782–796.e27, 2019. (Cited on page 91.)

[192] S. Zhang and C. A. Voigt, "Engineered dCas9 with reduced toxicity in bacteria: Implications for genetic circuit design," *Nucleic Acids Research*, vol. 46, no. 20, pp. 11 115–11 125, 2018. (Cited on page 92.)

[193] J. M. Peters, A. Colavin, H. Shi, T. L. Czarny, M. H. Larson, S. Wong, J. S. Hawkins, C. H. Lu, B. M. Koo, E. Marta, A. L. Shiver, E. H. Whitehead, J. S. Weissman, E. D. Brown, L. S. Qi, K. C. Huang, and C. A. Gross, "A comprehensive, CRISPR-based functional analysis of essential genes in bacteria," *Cell*, vol. 165, no. 6, pp. 1493–1506, 2016. [Online]. Available: http://dx.doi.org/10.1016/j.cell.2016.05.003 (Cited on page 95.)

[194] A. Casini, G. Christodoulou, P. S. Freemont, G. S. Baldwin, T. Ellis, and J. T. Macdonald, "R2oDNA designer: Computational design of biologically neutral synthetic DNA sequences," *ACS Synthetic Biology*, vol. 3, no. 8, pp. 525–528, 2014. (Cited on pages 98 and 99.)

[195] C. Y. Hu, M. K. Takahashi, Y. Zhang, and J. B. Lucks, "Engineering a Functional Small RNA Negative Autoregulation Network with Model-Guided Design," *ACS Synthetic Biology*, 2018. (Cited on page 101.)

[196] E. A. Boyle, J. O. Andreasson, L. M. Chircus, S. H. Sternberg, M. J. Wu, C. K. Guegler, J. A. Doudna, and W. J. Greenleaf, "High-throughput biochemical profiling reveals sequence determinants of dCas9 off-target binding and unbinding," *Proceedings of the National Academy of Sciences of the United States of America*, vol. 114, no. 21, pp. 5461–5466, 2017. (Cited on page 101.)

[197] A. Vigouroux, E. Oldewurtel, L. Cui, D. Bikard, and S. Teeffelen, "Tuning dCas9's ability to block transcription enables robust, noiseless knockdown of bacterial genes," *Molecular Systems Biology*, vol. 14, no. 3, pp. 1–14, 2018. (Cited on page 101.)

[198] K. L. Anderson and P. M. Dunman, "Messenger RNA turnover processes in Escherichia coli, Bacillus subtilis, and emerging studies in Staphylococcus aureus," *International Journal of Microbiology*, vol. 2009, 2009. (Cited on page 101.)

[199] H. Chen, A. Previero, and M. P. Deutscher, "A novel mechanism of ribonuclease regulation: Gcvb and hfq stabilize the mRNA that encodes rnase bn/z during exponential phase," *Journal of Biological Chemistry*, vol. 294, no. 52, pp. 19 997–20 008, 2019. [Online]. Available: http://dx.doi.org/10.1074/jbc.RA119.011367 (Cited on page 104.)

[200] B. Večerek, I. Moll, and U. Bläsi, "Translational autocontrol of the Escherichia coli hfq RNA chaperone gene," *Rna*, vol. 11, no. 6, pp. 976–984, 2005. (Cited on page 104.)

[201] A. Dwijayanti, M. Storch, G. B. Stan, and G. S. Baldwin, "A modular RNA interference system for gene regulation and robust dynamic feedback control," *bioRxiv*, 2019. (Cited on page 104.)

[202] J. A. Brophy and C. A. Voigt, "Antisense transcription as a tool to tune gene expression," *Molecular Systems Biology*, vol. 12, no. 1, 2016. (Cited on pages 106 and 148.)

[203] Y. Chen, J. K. Kim, A. J. Hirning, K. Josić, and M. R. Bennett, "Emergent genetic oscillations in a synthetic microbial consortium," *Science*, vol. 349, no. 6251, pp. 986–989, 2015. (Cited on page 121.)

[204] J. G. Thomas and F. Baneyx, "Protein misfolding and inclusion body formation in recombinant Escherichia coli cells overexpressing heat-shock proteins," *Journal of Biological Chemistry*, vol. 271, no. 19, pp. 11 141–11 147, 1996. (Cited on page 121.)

[205] F. Baneyx and M. Mujacic, "Recombinant protein folding and misfolding in Escherichia coli," *Nature Biotechnology*, vol. 22, no. 11, pp. 1399–1407, 2004. (Cited on page 121.)

[206] Y. Cho, X. Zhang, K. F. R. Pobre, Y. Liu, D. L. Powers, J. W. Kelly, L. M. Gierasch, and E. T. Powers, "Individual and collective contributions of chaperoning and degradation to protein homeostasis in E. coli," *Cell Reports*, vol. 11, no. 2, pp. 321–333, 2015. [Online]. Available: http://dx.doi.org/10.1016/j.celrep.2015.03.018 (Cited on page 121.)

[207] C. R. Evans, Y. Fan, and J. Ling, "Increased mistranslation protects E. coli from protein misfolding stress due to activation of a RpoS-dependent heat shock response," *FEBS Letters*, vol. 593, no. 22, pp. 3220–3227, 2019. (Cited on page 121.)

[208] P. A. Hoskisson and G. Hobbs, "Continuous culture - Making a comeback?" *Microbiology*, vol. 151, no. 10, pp. 3153–3159, 2005. (Cited on page 139.)

[209] W. Shou, S. Ram, and J. M. G. Vilar, "Synthetic cooperation in engineered yeast populations," *Proceedings of the National Academy of Sciences*, vol. 104, no. 6, pp. 1877–1882, 2007. [Online]. Available: http://www.pnas.org/cgi/doi/10.1073/pnas.0610575104 (Cited on pages 139 and 146.)

[210] S. Wu, Y. Xue, S. Yang, C. Xu, C. Liu, X. Liu, J. Liu, H. Zhu, G. R. Zhao, A. Yang, and J. Qiao, "Combinational quorum sensing devices for dynamic control in cross-feeding cocultivation," *Metabolic Engineering*, vol. 67, no. May, pp. 186–197, 2021. [Online]. Available: https://doi.org/10.1016/j.ymben.2021.07.002 (Cited on page 146.)

[211] C. McBride and D. Del Vecchio, "Trade-offs in Robustness to Perturbations of Bacterial Population Controllers," *Proceedings of the American Control Conference*, vol. 2020-July, pp. 4276–4282, 2020. (Cited on page 147.)

[212] T. Li, X. B. Chen, J. C. Chen, Q. Wu, and G. Q. Chen, "Open and continuous fermentation: Products, conditions and bioprocess economy," *Biotechnology Journal*, vol. 9, no. 12, pp. 1503–1511, 2014. (Cited on page 148.)

[213] J. Kopp, A. M. Kolkmann, P. G. Veleenturf, O. Spadiut, C. Herwig, and C. Slouka, "Boosting recombinant inclusion body production—from classical fed-batch approach to continuous cultivation," *Frontiers in Bioengineering and Biotechnology*, vol. 7, p. 297, 2019. (Cited on page 148.)

[214] J. Kopp, C. Slouka, O. Spadiut, and C. Herwig, "The Rocky Road From Fed-Batch to Continuous Processing With E. coli," *Frontiers in Bioengineering and Biotechnology*, vol. 7, p. 328, 2019. (Cited on page 148.)

[215] B. Lavi, E. L. Karin, T. Pupko, and E. Hazkani-Covo, "The prevalence and evolutionary conservation of inverted repeats in proteobacteria," *Genome Biology and Evolution*, vol. 10, no. 3, pp. 918–927, 2018. (Cited on page 149.)

[216] R. McCardell, S. Huang, L. Green, and R. Murray, "Control of bacterial population density with population feedback and molecular sequestration," *bioRxiv*, p. 225045, 2017. (Cited on page 150.)

[217] T. Tschirhart, E. Kim, R. Mckay, H. Ueda, H. C. Wu, A. E. Pottash, A. Zargar, A. Negrete, J. Shiloach, G. F. Payne, and W. E. Bentley, "Electronic control of gene expression and cell behaviour in Escherichia coli through redox signalling," *Nature Communications*, vol. 8, no. 1, pp. 1–11, 2017. (Cited on page 152.)

[218] N. Bhokisham, E. Vanarsdale, K. T. Stephens, P. Hauk, G. F. Payne, and W. E. Bentley, "A redox-based electrogenetic CRISPR system to connect with and control biological information networks," *Nature Communications*, vol. 11, no. 1, pp. 1–12, 2020. [Online]. Available: http://dx.doi.org/10.1038/s41467-020-16249-x (Cited on page 152.)

[219] E. Vanarsdale, D. Hörnström, G. Sjöberg, I. Järbur, J. Pitzer, G. F. Payne, A. J. Van Maris, and W. E. Bentley, "A coculture based tyrosine-tyrosinase electrochemical gene circuit for connecting cellular communication with electronic networks," *ACS Synthetic Biology*, vol. 9, no. 5, pp. 1117–1128, 2020. (Cited on page 152.)

[220] N. T. Ong and J. J. Tabor, "A Miniaturized Escherichia coli Green Light Sensor with High Dynamic Range," *ChemBioChem*, vol. 19, no. 12, pp. 1255–1258, 2018. (Cited on page 152.)

[221] A. Baumschlager, S. K. Aoki, and M. Khammash, "Dynamic Blue Light-Inducible T7 RNA Polymerases (Opto-T7RNAPs) for Precise Spatiotemporal Gene Expression Control," *ACS Synthetic Biology*, vol. 6, no. 11, pp. 2157–2167, 2017. (Cited on page 152.)

[222] E. Romano, A. Baumschlager, E. B. Akmeriç, N. Palanisamy, M. Houmani, G. Schmidt, M. A. Öztürk, L. Ernst, M. Khammash, and B. Di Ventura, "Engineering AraC to make it responsive to light instead of arabinose," *Nature Chemical Biology*, 2021. (Cited on page 152.)

[223] J.-S. Chang, P.-L. Show, T.-C. Ling, C.-Y. Chen, S.-H. Ho, C.-H. Tan, D. Nagarajan, and W.-N. Phong, "Photobioreactors," in *Current Developments in Biotechnology and Bioengineering: Bioprocesses, Bioreactors and Controls*. Elsevier: Amsterdam, The Netherlands, 2017, pp. 313–352. (Cited on page 152.)

[224] E. M. Zhao, Y. Zhang, J. Mehl, H. Park, M. A. Lalwani, J. E. Toettcher, and J. L. Avalos, "Optogenetic regulation of engineered cellular metabolism for microbial chemical production," *Nature*, vol. 555, no. 7698, pp. 683–687, 2018. (Cited on page 152.)

[225] S. Pouzet, A. Banderas, M. L. Bec, T. Lautier, G. Truan, and P. Hersen, "The promise of optogenetics for bioproduction: Dynamic control strategies and scale-up instruments," *Bioengineering*, vol. 7, no. 4, pp. 1–17, 2020. (Cited on page 152.)

[226] T. A. Dixon, T. C. Williams, and I. S. Pretorius, "Sensing the future of bio-informational engineering," *Nature Communications*, vol. 12, no. 1, pp. 1–12, 2021. [Online]. Available: http://dx.doi.org/10.1038/s41467-020-20764-2 (Cited on page 152.)

[227] C. Carrasco-López, S. A. García-Echauri, T. Kichuk, and J. L. Avalos, "Optogenetics and biosensors set the stage for metabolic cybergenetics," *Current Opinion in Biotechnology*, vol. 65, pp. 296–309, 2020. (Cited on page 152.)

[228] Y. H. Dong, J. L. Xu, X. Z. Li, and L. H. Zhang, "AiiA, an enzyme that inactivates the acylhomoserine lactone quorum-sensing signal and attenuates the virulence of Erwinia carotovora," *Proceedings of the National Academy of Sciences of the United States of America*, vol. 97, no. 7, pp. 3526–3531, 2000. (Cited on page 152.)

[229] D. Liu, J. Momb, P. W. Thomas, A. Moulin, G. A. Petsko, W. Fast, and D. Ringe, "Mechanism of the quorum-quenching lactonase (AiiA) from Bacillus thuringiensis. 1. Product-bound structures," *Biochemistry*, vol. 47, no. 29, pp. 7706–7714, 2008. (Cited on page 152.)

[230] Y. Lin, X. Shen, Q. Yuan, and Y. Yan, "Microbial biosynthesis of the anticoagulant precursor 4-hydroxycoumarin," *Nature Communications*, vol. 4, no. May, pp. 1–8, 2013. (Cited on page 155.)

[231] R. Wang, S. Zhao, Z. Wang, and M. A. Koffas, "Recent advances in modular co-culture engineering for synthesis of natural products," *Current Opinion in Biotechnology*, vol. 62, pp. 65–71, 2020. [Online]. Available: https://doi.org/10.1016/j.copbio.2019.09.004 (Cited on page 156.)

[232] D. Yang, S. Y. Park, Y. S. Park, H. Eun, and S. Y. Lee, "Metabolic Engineering of Escherichia coli for Natural Product Biosynthesis," *Trends in Biotechnology*, vol. 38, no. 7, pp. 745–765, 2020. [Online]. Available: https://doi.org/10.1016/j.tibtech.2019.11.007 (Cited on page 156.)

[233] J. A. Jones, V. R. Vernacchio, S. M. Collins, A. N. Shirke, Y. Xiu, J. A. Englaender, and B. F. Cress, "Complete biosynthesis of anthocyanins using E. coli polycultures," *mBio*, vol. 8, no. 3, pp. e00 621–17, 2017. (Cited on page 157.)

[234] V. Ganesan, Z. Li, X. Wang, and H. Zhang, "Heterologous biosynthesis of natural product naringenin by co-culture engineering," *Synthetic and Systems Biotechnology*, vol. 2, no. 3, pp. 236–242, 2017. [Online]. Available: https://doi.org/10.1016/j.synbio.2017.08.003 (Cited on page 157.)

[235] M. A. Lalwani, H. Kawabe, R. L. Mays, S. M. Hoffman, and J. L. Avalos, "Optogenetic Control of Microbial Consortia Populations for Chemical Production," *ACS Synthetic Biology*, vol. 10, no. 8, pp. 2015–2029, 2021. (Cited on page 157.)

[236] S. Y. Kang, O. Choi, J. K. Lee, B. Y. Hwang, T. B. Uhm, and Y. S. Hong, "Artificial biosynthesis of phenylpropanoic acids in a tyrosine overproducing Escherichia coli strain," *Microbial Cell Factories*, vol. 11, pp. 1–9, 2012. (Cited on page 157.)

[237] J. L. Rodrigues, R. G. Araújo, K. L. Prather, L. D. Kluskens, and L. R. Rodrigues, "Heterologous production of caffeic acid from tyrosine in Escherichia coli," *Enzyme and Microbial Technology*, vol. 71, pp. 36–44, 2015. [Online]. Available: http://dx.doi.org/10.1016/j.enzmictec.2015.01.001 (Cited on page 157.)

[238] J. M. Camacho-Zaragoza, G. Hernández-Chávez, F. Moreno-Avitia, R. Ramírez-Iñiguez, A. Martínez, F. Bolívar, and G. Gosset, "Engineering of a microbial coculture of Escherichia coli strains for the biosynthesis of resveratrol," *Microbial Cell Factories*, vol. 15, no. 1, pp. 1–11, 2016. (Cited on page 157.)

[239] H. Zhang, B. Pereira, Z. Li, G. Stephanopoulos, and A. L. Demain, "Engineering Escherichia coli coculture systems for the production of biochemical products," *PNAS*, vol. 112, no. 27, pp. 8266–8271, 2015. (Cited on page 157.)

[240] C. Briat, A. Gupta, and M. Khammash, "Antithetic Integral Feedback Ensures Robust Perfect Adaptation in Noisy Bimolecular Networks," *Cell Systems*, vol. 2, no. 1, 2016. (Cited on page 158.)

[241] A. A. Baetica, Y. P. Leong, and R. M. Murray, "Guidelines for designing the antithetic feedback motif," *Physical Biology*, vol. 17, no. 5, 2020. (Cited on page 158.)

[242] C. Cuba Samaniego and E. Franco, "Ultrasensitive molecular controllers for quasi-integral feedback," *Cell Systems*, vol. 12, no. 3, pp. 272–288.e3, 2021. [Online]. Available: https://doi.org/10.1016/j.cels.2021.01.001 (Cited on page 158.)

[243] I. Golding, J. Paulsson, S. M. Zawilski, and E. C. Cox, "Real-time kinetics of gene activity in individual bacteria," *Cell*, vol. 123, no. 6, pp. 1025–1036, 2005. (Cited on page 158.)

[244] Y. Shimoni, G. Friedlander, G. Hetzroni, G. Niv, S. Altuvia, O. Biham, and H. Margalit, "Regulation of gene expression by small non-coding RNAs: A quantitative view," *Molecular Systems Biology*, vol. 3, no. 138, pp. 1–9, 2007. (Cited on page 158.)

[245] X. Darzacq, Y. Shav-Tal, V. De Turris, Y. Brody, S. M. Shenoy, R. D. Phair, and R. H. Singer, "In vivo dynamics of RNA polymerase II transcription," *Nature Structural and Molecular Biology*, vol. 14, no. 9, pp. 796–806, 2007. (Cited on page 158.)

[246] J. A. Jones and X. Wang, "Use of bacterial co-cultures for the efficient production of chemicals," *Current Opinion in Biotechnology*, vol. 53, pp. 33–38, 2018. [Online]. Available: https://doi.org/10.1016/j.copbio.2017.11.012 (Cited on page 158.)

[247] C. Gao, J. Hou, P. Xu, L. Guo, X. Chen, G. Hu, C. Ye, H. Edwards, J. Chen, W. Chen, and L. Liu, "Programmable biomolecular switches for rewiring flux in Escherichia coli," *Nature Communications*, vol. 10, no. 1, pp. 1–12, 2019. [Online]. Available: http://dx.doi.org/10.1038/s41467-019-11793-7 (Cited on page 158.)

[248] Y. Liu, M. Ding, W. Ling, Y. Yang, X. Zhou, B. Z. Li, T. Chen, Y. Nie, M. Wang, B. Zeng, X. Li, H. Liu, B. Sun, H. Xu, J. Zhang, Y. Jiao, Y. Hou, H. Yang, S. Xiao, Q. Lin, X. He, W. Liao, Z. Jin, Y. Xie, B. Zhang, T. Li, X. Lu, J. Li, F. Zhang, X. L. Wu, H. Song, and Y. J. Yuan, "A three-species microbial consortium for power generation," *Energy and Environmental Science*, vol. 10, no. 7, pp. 1600–1609, 2017. (Cited on page 160.)

[249] T. L. Weiss, E. J. Young, and D. C. Ducat, "A synthetic, light-driven consortium of cyanobacteria and heterotrophic bacteria enables stable polyhydroxybutyrate production," *Metabolic Engineering*, vol. 44, no. September, pp. 236–245, 2017. [Online]. Available: https://doi.org/10.1016/j.ymben.2017.10.009 (Cited on page 160.)

[250] G. M. Taylor, P. M. Mordaka, and J. T. Heap, "Start-Stop Assembly : a functionally scarless DNA assembly system optimized for metabolic engineering," *Nucleic Acids Research*, vol. 47, no. 3, 2019. (Cited on pages 173, 187, 199 and 200.)

[251] A. Haldimann and B. L. Wanner, "Conditional-Replication, Integration, Excision, and Retrieval Plasmid-Host Systems for Gene Structure-Function Studies of Bacteria," *Journal of Bacteriology*, vol. 183, no. 21, pp. 6384–6393, 2001. (Cited on pages 173, 175 and 200.)

[252] D. M. Bubnov, T. V. Yuzbashev, T. V. Vybornaya, A. I. Netrusov, and S. P. Sineoky, "Development of new versatile plasmid-based systems for λRed-mediated Escherichia coli genome engineering," *Journal of Microbiological Methods*, vol. 151, no. May, pp. 48–56, 2018. [Online]. Available: https://doi.org/10.1016/j.mimet.2018.06.001 (Cited on page 176.)

[253] Y. J. Chen, P. Liu, A. A. Nielsen, J. A. Brophy, K. Clancy, T. Peterson, and C. A. Voigt, "Characterization of 582 natural and synthetic terminators and quantification of their design constraints," *Nature Methods*, vol. 10, no. 7, pp. 659–664, 2013. (Cited on page 199.)

[254] K. Campbell, L. Herrera-Dominguez, C. Correia-Melo, A. Zelezniak, and M. Ralser, "Biochemical principles enabling metabolic cooperativity and phenotypic heterogeneity at the single cell level," *Current Opinion in Systems Biology*, 2017. [Online]. Available: http://linkinghub.elsevier.com/retrieve/pii/S2452310017301828 (Cited on page 199.)

[255] N. Kylilis, G.-B. Stan, and K. M. Polizzi, "Tools for engineering coordinated system behaviour in synthetic microbial consortia," *bioRxiv*, p. 231597, 2017. [Online]. Available: https://www.biorxiv.org/content/early/2017/12/11/231597?rss=1 (Cited on page 200.)